

# Two Applications of Effective Field Theory: Factorisation of $gg \rightarrow h$ in SCET & Flavour Physics of ALPs

---

Dissertation submitted for the award of the title  
“Doctor of Natural Sciences”  
to the Faculty of Physics, Mathematics and Computer Science of  
Johannes Gutenberg University Mainz

**Marvin SCHNUBEL**  
born in Lebach, Germany

Mainz, May 08, 2023

---

JOHANNES GUTENBERG  
UNIVERSITÄT MAINZ



Johannes Gutenberg University Mainz  
Mainz, Germany

*Two Applications of Effective Field Theory: Factorisation of  $gg \rightarrow h$  in SCET & Flavour Physics of ALPs*, © May 2023

Author:

Marvin SCHNUBEL

Date of submission: May 08, 2023

Date of defence: September 15, 2023

Johannes Gutenberg University Mainz, Germany

For my family

*“Deep in the human unconscious is a pervasive need for a logical universe that makes sense.”*

**Frank Herbert, Dune**

*“«In almost all textbooks, even the best, this principle is presented so that it is impossible to understand.»  
(K. Jacobi, Lectures on Dynamics, 1842 – 1843) I have not chosen to break with tradition.”*

**V. I. Arnold, Mathematical Methods of Classical Mechanics**

*“Effective Field Theory is essentially dimensional analysis and Taylor expansion”*

**Timothy Cohen**

*“Insight must precede application.”*

**Max Planck**

*“It doesn't stop being magic just because you know how it works.”*

**Terry Pratchett**

*“Tudo vale a pena, quando a alma não é pequena”*

**Fernando Pessoa**



# ABSTRACT

---

The Standard Model of Particle Physics has been confirmed by numerous measurements verifying its predictions. However, there are multiple direct and indirect hints pointing towards physics beyond the Standard Model. Two possibilities where new physics could show up are deviations of theory prediction and experiment in high-precision observables or direct detection of new particles, for instance at colliders or in particle transitions forbidden in the Standard Model. In this thesis, we approach both possibilities in two separate projects that are linked in their use of methodology rooted in the framework of effective field theories.

In the first project we study gluon-gluon to Higgs boson fusion via a light quark loop in the context of soft-collinear effective theory (SCET) at next-to-leading order in SCET power counting. Generalising the refactorisation-based subtraction scheme to regulate endpoint divergences to non-abelian final states, we are able to derive a factorisation theorem consisting of convolutions of hard Wilson coefficients and jet and soft functions that is endpoint divergence-free and UV finite. We demonstrate that even though regularisation and renormalisation do not commute in general, all mismatching terms can be absorbed into a redefinition of Wilson coefficients. After deriving the renormalisation group (RG) equations, we solve them iteratively to predict the leading large logarithmic corrections in the three-loop  $gg \rightarrow h$  form factor. Eventually, we solve the RG equations for the leading contribution jet and soft function to RG-improved leading order. This allows us to resum the three leading towers of large logarithms in the form factor to all orders of perturbation theory.

In the second project we investigate how flavour physics experiments can constrain parameter space of axion-like particle (ALP) models. First, we present how couplings at the high-energy scale evolve to low energies. We show that independent of the specific UV coupling, couplings to all Standard Model particles are generated through a series of RG running and matching effects. This also includes effective flavour-changing couplings. Furthermore, we explain how to consistently implement ALPs in the weak chiral and nuclear Lagrangian, thereby freeing the formula for the branching ratio of the important  $K \rightarrow \pi a$  decay from a long-standing inconsistency. We then explore the bounds on ALPs from quark and lepton flavour experiments in four benchmark scenarios, where we assume that only a certain coupling is present at the UV scale, and all other couplings are generated via evolution effects.



## ZUSAMMENFASSUNG

---

Das Standardmodell der Teilchenphysik wurde bereits durch zahlreiche Messungen belegt, die die theoretischen Vorhersagen bestätigen. Es gibt jedoch etliche direkte sowie indirekte Hinweise auf Physik jenseits des Standardmodells. Zwei Möglichkeiten, wo solche neue Physik auftreten könnte, sind Abweichungen von Theorievorhersagen und experimentellen Messungen in Hochpräzisionsobservablen oder direkte Entdeckung neuer Teilchen, zum Beispiel an Beschleunigern oder durch Beobachtung von im Standardmodell verbotenen Teilchenübergängen. In dieser Arbeit beschäftigen wir uns mit beiden Möglichkeiten in zwei verschiedenen Projekten, die durch die Verwendung von Methoden der effektiven Feldtheorien verbunden sind.

Im ersten Projekt untersuchen wir die Fusion zweier Gluonen zu einem Higgs-Boson über eine Schleife aus leichten Quarks im Kontext der soft-kollinearen effektiven Theorie (SCET), ein Prozess in nachführender Ordnung im SCET Powercounting. Durch das Verallgemeinern des refaktorisierungsbasierten Subtraktionsschema zur Regularisierung von Endpunktdivergenzen auf nicht-abelsche externe Felder sind wir in der Lage, ein Faktorisierungstheorem bestehend aus Konvolutionen von Wilson-Koeffizienten und Jet- und soften Funktionen herzuleiten, das sowohl endpunktdivergenzfrei als auch UV-endlich ist. Wir zeigen, dass obwohl Regularisierung und Renormierung im Allgemeinen nicht vertauschbar sind, alle nicht übereinstimmenden Terme durch eine Redefinition der Wilson-Koeffizienten absorbiert werden können. Nachdem wir die Renormierungsgruppengleichungen (RGE) hergeleitet haben, lösen wir sie iterativ, um die größten logarithmischen Korrekturen zum drei-Schleifen Formfaktor vorherzusagen. Wir lösen die RGE der führenden Jet- und soften Funktion in führender Ordnung, was uns erlaubt die drei führenden Terme logarithmischer Korrekturen im Formfaktor für alle Ordnungen der Störungstheorie aufzusummieren.

Im zweiten Projekt untersuchen wir, wie Flavourphysikexperimente den theoretisch erlaubten Parameterbereich von Axion-artigen Teilchen (ALPs) einschränken können. Wir zeigen zunächst, wie sich Kopplungen von einer hohen zu einer niedrigen Energieskala durch RGE-Effekte entwickeln und dass, unabhängig von der UV-Kopplung, Kopplungen an sämtliche Standardmodellteilchen an der Niederenergieskala generiert werden. Dies beinhaltet auch Flavour-verletzende Kopplungen. Außerdem können wir zeigen, wie ALPs konsistent in die schwach-chirale und nukleare Theorie eingebunden werden können. Dabei lösen wir eine seit langem bestehende Inkonsistenz in der Berechnung der wichtigen  $K \rightarrow \pi a$  Amplitude auf. Unsere Ergebnisse werden in vier Referenzszenarien, bei denen wir jeweils angenommen haben, dass nur eine Kopplung an der UV-Skala existiert und alle anderen durch Evolutionseffekte generiert werden, vorgestellt.





## LIST OF PUBLICATIONS

---

This thesis is based on the publications and preprints [1–7] listed below. Here, we give a short summary of each work and highlight the author’s contribution. Preliminary results of [1] were presented at the conference “RADCOR–Loopfest 2021”, and published in the corresponding conference proceeding [2]. Additionally, the works [4–7] contributed to the publication [8], which is listed afterwards. The following articles provide the basis to [Part I: Gluon-gluon to Higgs fusion in SCET](#) of this thesis.

[1] Z. Liu, M. Neubert, M. Schnubel and X. Wang, *Radiative quark jet function with an external gluon*, *JHEP* **02** (2022) 075 [2112.00018]

Radiative jet functions with external gauge fields appear in many factorisation theorems at next-to-leading power in SCET. They are defined in terms of matrix elements of collinear fields with a soft momentum emitted from inside the jet. While the photon case has been studied extensively in previous work, we presented here a detailed study of the radiative jet function with an external gluon. We calculated this jet function at one- and two-loop order, derived its one-loop anomalous dimension and studied its renormalisation-group evolution.

Results from this publication enter chapter 5. While all authors contributed equally to the calculations, the author of this thesis set up the first draft for the publication. The calculations were performed using different gauge choices among the authors. All plots were crafted by the author, while the Feynman diagrams were created by Z.L.L.

[2] M. Schnubel, *The two-loop radiative gluon jet function for  $gg \rightarrow h$  via a light quark loop*, *SciPost Phys. Proc.* **7** (2022) 039 [2110.05322]

Preliminary results of [1] were presented by the author at the conference “RADCOR–Loopfest 2021”, and published in this conference proceeding.

[3] Z. Liu, M. Neubert, M. Schnubel and X. Wang, *Factorization, Renormalization, and Endpoint Divergences at next-to-leading Power in  $gg \rightarrow h$  Production*, *JHEP* **02** (2022) 075 [2112.00018]

We derived the renormalised factorisation amplitude for the fusion process  $gg \rightarrow h$  via light quarks. It is structurally similar to the one obtained previously for the  $h \rightarrow \gamma\gamma$  decay amplitude, but additional challenges arise due to the external coloured states. We generalised the refactorisation-based subtraction scheme to regulate endpoint divergences. Furthermore, we used renormalisation group techniques to predict the leading logarithmic correction in the three-loop amplitude. Additionally, we solved the RG equations for the jet and soft function to RG-improved leading order and resummed the three leading logarithmic towers to all orders of perturbation theory.

This publication is the basis for chapter 5. All authors contributed equally to the calculations. The first draft was set up by the author of this thesis and X.W., the figures were created in collaboration of the author, X.W. and Z.L.L. The author was the main responsible person for the section on resummation and it was checked by the co-authors.

The second part of this thesis, [Part II: Flavour physics of ALPs](#), is based on the works listed below.

[4] M. Bauer, M. Neubert, S. Renner, M. Schnubel and A. Thamm, *Axion-like Particles, Lepton-Flavor Violation and a New Explanation of  $a_\mu$  and  $a_e$* , *Phys. Rev. Lett.* **121** (2020) 211803 [[1908.00008](#)]

We described how ALPs with lepton flavour-violating couplings can be constrained from various experiments. Furthermore, we gave a prospect how flavour-violating ALPs could possibly explain the current tension in the anomalous magnetic moment of the electron and the muon.

This publication includes research carried out in the author's Master thesis. For this reason, we only present the main results in chapter 7, and explicitly state when results were taken from this publication. All authors contributed equally to the text and plots.

[5] M. Bauer, M. Neubert, S. Renner, M. Schnubel and A. Thamm, *The Low-Energy Effective Theory of Axions and ALPs*, *JHEP* **04** (2021) 063 [[2012.12272](#)]

Here we showed how ALP couplings evolve from the high energy scale to low energies by a series of RG running and matching with heavy particles integrated out whenever crossing a particle mass threshold. We demonstrated that independent of the UV coupling, at the low energy scale an effective coupling to all Standard Model particles is generated inevitably, including flavour-violating ones. Furthermore, we repeat this study for an alternate form of the ALP Lagrangian.

This publication is the basis for much of chapter 6. All authors contributed equally to text and calculations.

[6] M. Bauer, M. Neubert, S. Renner, M. Schnubel and A. Thamm, *Consistent Treatment of Axions in the Weak Chiral Lagrangian*, *Phys. Rev. Lett.* **127** (2021) 081803 [[2102.13112](#)]

We showed how to consistently implement ALPs in the weak chiral Lagrangian in a model-independent way. We argued that previous treatments of such processes have used an incorrect representation of the flavour-changing quark currents in the chiral theory. As the most important result, we corrected the  $K \rightarrow \pi a$  decay formula from a long-standing inconsistency.

This publication enters in chapter 6. The text and the computations were first obtained by M.B. and M.N., and were checked by the author and the co-authors. The author checked the derivation of the  $K^- \rightarrow \pi^- a$  amplitude by an independent calculation explicitly.

[7] M. Bauer, M. Neubert, S. Renner, M. Schnubel and A. Thamm, *Flavor probes of axion-like particles*, *JHEP* **09** (2022) 056 [[2110.10698](#)]

We presented an exhaustive study of quark and lepton flavour probes of axions and ALPs. We summarised our former works and showed how flavour experiments constrain UV ALP couplings in benchmark scenarios, where only one specific ALP coupling is present at the high scale, and all other interactions are generated through evolution effects. Furthermore we explained, how ALPs could in principle tackle several low-energy anomalies observed in rare B-meson decays, measurements at the ATOMKI and KTeV experiments, and in the anomalous magnetic moments of the muon and the electron.

This publication yields the basis for chapter 7 of this thesis. All authors contributed equally to the text and calculations. The benchmark plots in chapter 7 are taken from

this publication. The study of ALP effects in low-energy anomalies of this work is not included in this thesis.

If not stated otherwise, the figures presented in this thesis have been created by the author himself. Most figures from the publications listed above that are used in here have been remade for this thesis in order to achieve a uniform layout and colouring scheme.

The works on axion-like particles [4–7] led to a contribution in the following publication

[8] E. Goudzovski et al., *New Physics Searches at Kaon and Hyperon Factories*, [2201.07805]

where searches for new physics in Kaon experiments have been studied extensively.



# ACRONYMS AND ABBREVIATIONS

---

## List of acronyms and abbreviations

<b>ALP</b>	axion-like particle	$\overline{\text{MS}}$	modified minimal subtraction
<b>BSM</b>	beyond the Standard Model, often used synonymously with new physics	<b>NLO</b>	next-to-leading order
<b>Br</b>	branching ratio	<b>NLL</b>	next-to-leading logarithm
<b>CKM</b>	Cabibbo-Kobayashi-Maskawa	<b>NLL'</b>	modified next-to-leading logarithm
<b>CL</b>	confidence level	<b>NLP</b>	next-to-leading power
<b>CMB</b>	cosmic microwave background	<b>NNLO</b>	next-to-next-to-leading order
<b>DM</b>	dark matter	<b>PDF</b>	parton distribution function
<b>EDM</b>	electric dipole moment	<b>pNGB</b>	pseudo-Nambu–Goldstone boson
<b>EFT</b>	Effective Field Theory	<b>PQ</b>	Peccei-Quinn
<b>EW</b>	electro-weak	<b>PMNS</b>	Pontecorvo-Maki-Nakagawa-Sakata
<b>EWSB</b>	electro-weak symmetry breaking	<b>QCD</b>	quantum chromodynamics
<b>FCNC</b>	flavour-changing neutral current	<b>QED</b>	quantum electrodynamics
<b>GIM</b>	Glashow-Iliopolus-Maiani	<b>QFT</b>	quantum field theory
<b>HQET</b>	heavy quark effective theory	<b>RBS</b>	refactorisation-based subtraction scheme
<b>IBP</b>	integration by parts	<b>RG</b>	renormalisation group
<b>IR</b>	infrared	<b>RGE</b>	renormalisation group equation
<b>LCDA</b>	light-cone distribution amplitude	<b>RH</b>	right-handed
<b>LFUV</b>	lepton flavour universality violation	<b>SCET</b>	Soft-Collinear Effective Theory
<b>LFV</b>	lepton flavour violation	<b>SM</b>	Standard Model of Particle Physics
<b>LH</b>	left-handed	<b>SMEFT</b>	SM effective field theory
<b>LL</b>	leading logarithm	<b>UV</b>	ultraviolet
<b>LO</b>	leading order	<b>vev</b>	vacuum expectation value
		$\chi$ <b>PT</b>	chiral perturbation theory

## List of Experiments

### Hadron Colliders and Detectors

- **CERN** Conseil européen pour la recherche nucléaire
  - **ATLAS** A Toroidal LHC Apparatus
  - **CMS** Compact Muon Solenoid
  - **FCC** Future Circular Collider
  - **HL-LHC** High Luminosity LHC
  - **LEP** Large Electron Proton Collider
  - **LHC** Large Hadron Collider
  - **LHCb** LHC beauty
  - **NA62** North Area 62 (fixed target experiment)
- **Fermilab** Fermi National Accelerator Laboratory
  - **Tevatron** Proton-Antiproton Collider
- **FCC** future circular collider

### Lepton Colliders and Flavour Experiments

- **ACME** Advanced Cold Molecule Electron EDM
- **BaBar**  $B$  factory
- **Belle**  $B$  factory
- **COMET** Coherent Muon to Electron Transition
- **Mu2e**  $\mu \rightarrow e$  experiment
- **PSI** Paul Scherrer Institute
  - **MEG**  $\mu \rightarrow e\gamma$  experiment
  - **Mu3e**  $\mu^+ \rightarrow e^+e^-e^+$  experiment

# CONTENTS

---

Abstract . . . . .	v
Zusammenfassung . . . . .	vii
List of Publications . . . . .	ix
Acronyms and Abbreviations . . . . .	xiii
<i>Prologue</i> . . . . .	1
1 Introduction . . . . .	3
2 Theoretical foundation . . . . .	7
2.1 The Standard Model of elementary particle physics . . . . .	7
2.2 Effective field theories . . . . .	11
2.3 Beyond the Standard Model physics . . . . .	14
<i>Part I: Gluon-gluon to Higgs fusion in SCET</i> . . . . .	17
3 A two-fold motivation . . . . .	19
3.1 The need for an EFT approach . . . . .	19
3.2 Motivation from a technical point of view . . . . .	20
3.3 Motivation from a phenomenological point of view . . . . .	20
4 Introduction to SCET . . . . .	21
4.1 Introduction to SCET . . . . .	21
4.2 Resummation . . . . .	25
4.3 SCET at subleading power . . . . .	26
5 Factorisation and resummation of gluon-gluon to Higgs fusion . . . . .	29
5.1 Factorisation of $gg \rightarrow h$ . . . . .	29
5.1.1 Decoupling perturbative and non-perturbative physics . . . . .	30
5.1.2 Derivation of the effective SCET operators . . . . .	31
5.1.3 Bare factorisation theorem and two-loop expressions for the component functions . . . . .	35
5.1.4 Refactorisation theorems and regularisation of endpoint divergences . . . . .	39
5.2 Renormalisation of the factorisation theorem . . . . .	44
5.2.1 Renormalisation of $T_3$ . . . . .	45

5.2.2	Renormalisation of $T_2$ . . . . .	47
5.2.3	Renormalisation of $T_1$ . . . . .	49
5.2.4	Form factor expressions in terms of renormalised quantities . . . . .	54
5.3	RG equations and prediction of large logarithms at higher loops . . . . .	54
5.3.1	Evolution equations for the jet and soft functions . . . . .	54
5.3.2	Evolution equations for the hard matching coefficients . . . . .	55
5.3.3	Evolution equations for the form factor and its three components . . . . .	58
5.3.4	Large logarithms in the three-loop $gg \rightarrow h$ form factor . . . . .	59
5.4	Resummation . . . . .	63
5.4.1	RG-improved LO jet function . . . . .	64
5.4.2	RG-improved LO soft function $S_3$ . . . . .	65
5.4.3	Large logarithms at NLL' in the form factor . . . . .	67
Appendix I . . . . .		73
AI.1	Renormalisation factors . . . . .	73
AI.2	Anomalous dimensions . . . . .	74
AI.2.1	Cusp anomalous dimension . . . . .	74
AI.2.2	Anomalous dimension $\gamma_{gg}$ . . . . .	75
AI.2.3	Anomalous dimensions of component functions . . . . .	75
AI.3	RG functions . . . . .	77
 <i>Part II: Flavour physics of ALPs</i> . . . . .		 79
6	Effective field theory for ALPs . . . . .	81
6.1	Introduction to ALPs . . . . .	81
6.2	The ALP Lagrangian and RG effects at low energies . . . . .	83
6.2.1	RG evolution to the electroweak scale . . . . .	85
6.2.2	Effective ALP Lagrangian at the electroweak scale . . . . .	89
6.2.3	Effective ALP Lagrangian below the electroweak scale . . . . .	90
6.3	ALPs within the weak chiral and nuclear Lagrangian . . . . .	95
6.3.1	Implementing ALPs in the weak chiral Lagrangian . . . . .	95
6.3.2	ALPs in the chiral nuclear Lagrangian . . . . .	101
7	Flavour probes of ALPs . . . . .	107
7.1	Quark flavour probes of ALPs . . . . .	107
7.1.1	ALPs in exotic meson decays . . . . .	108
7.1.2	The rare pion decay $\pi^- \rightarrow ae^- \bar{\nu}_e$ . . . . .	110
7.1.3	Radiative $J/\psi$ and $\Upsilon$ decays . . . . .	112
7.1.4	The chromomagnetic dipole moment of the top-quark . . . . .	113
7.1.5	Flavour physics constraints on select benchmark scenarios . . . . .	114
7.2	Lepton flavour probes of ALPs . . . . .	121
7.2.1	Form factors . . . . .	121
7.2.2	The decay $\mu \rightarrow ea\gamma$ . . . . .	126



7.2.3	$\mu \rightarrow e$ conversion . . . . .	127
7.2.4	Muonium-antimuonium oscillations . . . . .	127
7.2.5	$\mu \rightarrow e\gamma$ and $\mu \rightarrow 3e$ . . . . .	128
7.2.6	Constraints on lepton flavour-violating couplings . . . . .	129
Appendix II . . . . .		133
	AII.1 Measurements and SM predictions for flavour observables . . . . .	133
	AII.2 Expressions for the form factors . . . . .	134
<i>Epilogue</i> . . . . .		137
8	Conclusions and outlook . . . . .	139
a	Appendix . . . . .	143
	A.1 Notations and conventions . . . . .	143
Acknowledgements . . . . .		145
List of Figures . . . . .		147
List of Tables . . . . .		151
BIBLIOGRAPHY . . . . .		154
CURRICULUM VITAE . . . . .		177





*Prologue*



## INTRODUCTION

---

When Max Planck was about to start his studies of physics, he asked his future advisor Philipp von Jolly about the prospects of the field. Von Jolly told him «in this field, almost everything has already been discovered, and all that remains is to fill a few holes», to which Planck replied that he did not wish to discover something new, only to understand the fundamentals [9]. Later, he went on to revolutionise physics as the originator of quantum physics. This concept was the beginning of a development that, for the branch of particle physics, eventually led to the Standard Model of Particle Physics (SM). It is among the best understood theories of nature, and describes the properties and interactions of the very building blocks of matter with incredible precision. The validity of its predictions has been tested with countless experiments. As the most recent example, the scalar Higgs boson [10–15] was discovered at the LHC in 2012 [16, 17], which was the last elementary particle missing in the SM.

With this well-established theory at hand, one might be tempted to say that in today’s particle physics, there are only “a few holes” left to fill. For various reasons, most physicists refrain from doing so. Most of the problems present within the Standard Model call for a generalised theory. However, because of its success of predicting many observables correctly, theorists generally prefer not to abandon the SM all at once. Most theories trying to tackle one of the SM problems therefore extend it by new symmetries and particles. Moreover, we do not know where physics beyond the Standard Model (BSM), often used synonymously with new physics, could show up first. Thus, one option is to look for deviations of high-precision calculations of SM predictions and experimental measurements. Both branches that could possibly lead to the discovery of new physics – high precision calculations and explicit BSM models – often make use of the methodology of Effective Field Theories (EFTs).

The basic concept of effective theories is that one should in principle be able to disentangle the dynamics of different scales involved in a process as soon as this scale separation is large enough. Effects from physics at high scales should be very suppressed if a certain process of interest only features low-energetic particles and momenta otherwise. On the other hand, low-energy processes should only give perturbative fluctuations to very high-energetic systems. A prime example for a problem involving multiple scales is the creation of Higgs bosons at the Large Hadron Collider (LHC). With a mass of  $m_h = 125.25$  GeV [18] it is produced mainly via the gluon-gluon fusion channel [19]. Since free gluons cannot exist in nature, they must be extracted from protons, which are collided with a centre-of-mass energy of 13 TeV [20]. The energy and momentum distribution of the gluons inside

of the proton, however, are described non-perturbatively with parton distribution functions (PDFs) at energies below the QCD factorisation scale  $\Lambda_{\text{QCD}} \approx 300 \text{ MeV}$ . The only feasible way to obtain high-precision predictions is to describe the physics at these vastly different energy scales with different effective theories, where certain assumptions can be made for each sector.

Historically speaking, EFTs have been used to gain knowledge about physics at energies that were still out of reach for experiments at that time. For instance, Fermi’s theory of the weak interaction could describe nucleon  $\beta$ -decay with high precision, even long before the underlying gauge principle was discovered [21]. Again, the reason was a large scale separation. The  $W$ -boson with a mass  $m_W = 80.38 \text{ GeV}$  is much heavier than the typical energy of the  $\beta$ -decay electrons  $E_e \sim \mathcal{O}(1 \text{ MeV})$ , hence the process including a  $W$ -boson exchange can be approximated by a contact interaction.

In the same sense that Fermi’s theory effectively describes the weak interaction, many models for BSM physics aim to describe the effects of new physics at high energy scales without knowing the exact dynamics. A great number of these models are motivated by so-called anomalies – observables where the theoretical SM prediction and the experimental measurement do not agree – in the hope that they are residual effects of yet unknown high-energy physics. Since only a few models really influence the dynamics of just one problem or anomaly, we emphasise that it is most important to always check that a solution to a certain problem is not already ruled out by other experiments.

Even though the concept of EFTs has been used for a long time and Fermi’s interaction theory celebrates its 90th birthday in 2023, effective (field) theories are an active field of research. Apart from the countless applications of EFTs in the field of particle physics, EFT methods can also be transferred to other problems in physics. For instance, a common way to calculate the gravitational wave signature of inspiralling finite-sized objects is to employ so-called non-relativistic general relativity (NRGR) [22–24]. Another famous example is the Bardeen–Cooper–Schrieffer (BCS) theory used in condensed matter research, yielding the first microscopic explanation for superconductivity [25, 26]. Even more surprisingly, the EFT methodology has seen application outside of physics, too. In [27], the authors established an effective theory to describe how a deep neural network manages to detect patterns and derive rules from training data, thus gaining insights how the machine actually “learns”.

This thesis is structured as follows: In chapter 2, we first briefly review the Standard Model and its properties. Furthermore, we give an introduction to effective field theories and present motivations for beyond the Standard Model physics. In [Part I: Gluon-gluon to Higgs fusion in SCET](#), we apply the EFT Soft-Collinear Effective Theory (SCET) to the process of Higgs production via a gluon pair and a virtual light quark loop. As for this theory, we first describe the initial problem in chapter 3 and give an introduction to SCET in chapter 4. In chapter 5 we present our main results with the derivation of a renormalised factorisation theorem, deriving the RG equations, and eventually solving them to resum large logarithms in the form factor expression to an unprecedented high accuracy. Thereby we generalise the refactorisation-based subtraction scheme (RBS) introduced in [28, 29] to

non-abelian final states. Additional information is collected in appendix [AI](#). The second part of this thesis [Part II: Flavour physics of ALPs](#) is dedicated to the question how flavour physics experiments can yield constraints on axion-like particle models. We first describe the general set-up of the effective theory and how high-energy couplings evolve down to the low-energy scale of experiments in chapter [6](#). In chapter [7](#) we present the derived constraints from various flavour experiments, in both the quark and the lepton sector. The appendix [AII](#) collects additional information about the relevant experimental measurements. In chapter [8](#), we conclude and summarise the results obtained for this thesis.





## THEORETICAL FOUNDATION

---

Both research projects that make up this thesis, “[Gluon-gluon to Higgs fusion in SCET](#)” and “[Flavour physics of ALPs](#)”, are rooted within the theoretical framework of Effective Field Theories (EFTs) that are derived from the Standard Model of Particle Physics (SM) and extensions thereof. In this chapter, we want to give a brief introduction to the SM, how to derive EFTs from the SM in general and universal properties of EFTs. Furthermore we will tackle what the currently unanswered questions of the SM are, giving a motivation for beyond the Standard Model (BSM) physics. An introduction to the specific effective theories that are used is given within each of the two parts, respectively. As usually in high-energy particle physics, we tacitly adopt several conventions. They are summarised in appendix [A](#).

### 2.1 The Standard Model of elementary particle physics

The Standard Model was developed in the 60’s and 70’s of the last century in multiple works, see for example [\[30–40\]](#). For a pedagogical and exhaustive introduction to the SM, we refer to the standard literature such as [\[41–44\]](#).

The SM describes almost all properties of all known subatomic elementary particles as well as their strong, weak and electromagnetic interactions as a quantum field theory (QFT). Hitherto, it has not been possible to derive a consistent quantum theory of the fourth force, gravity. The fundamental basis of the SM as a renormalisable QFT is the concept of local gauge symmetry groups, where the SM gauge group is

$$SU(3)_c \times SU(2)_L \times U(1)_Y. \quad (2.1)$$

Here,  $SU(3)_c$  is the special unitary group describing the strong interactions, and the gauge group  $SU(2)_L \times U(1)_Y$  describes the unified electroweak interactions corresponding to the weak isospin and hypercharge, respectively.

The matter content of the SM consists of three families of fermions, the strong and electroweak gauge bosons, and the Higgs boson – the particle in the SM with the most recent experimental verification [\[16,17\]](#). The fermions can further be split into two groups, namely those that interact through the strong force, called quarks, and those that do not, named leptons. All fermions are charged under the SM symmetries [\(2.1\)](#), and we give their charges in table [2.1](#). As a chiral field theory, left- and right-handed fermions transform differently

under weak gauge transformations. The quarks form left-handed doublets, and up and down-type right-handed singlets. The leptons also form left-handed doublets, but only the charged leptons can be grouped in a right-handed singlet, too. As will be explained later, this is the reason that neutrinos are massless in the SM.

Fields	Representation	electric charge
Left-handed quark doublets $\begin{pmatrix} u_L \\ d_L \end{pmatrix}, \begin{pmatrix} c_L \\ s_L \end{pmatrix}, \begin{pmatrix} t_L \\ b_L \end{pmatrix}$	$(\mathbf{3}, \mathbf{2}, \frac{1}{6})$	$\begin{pmatrix} 2/3 \\ -1/3 \end{pmatrix}$
Right-handed up-type quarks: $u_R, c_R, t_R$	$(\mathbf{3}, \mathbf{1}, \frac{2}{3})$	$2/3$
Right-handed down-type quarks: $d_R, s_R, b_R$	$(\mathbf{3}, \mathbf{1}, -\frac{1}{3})$	$-1/3$
Left-handed lepton doublets $\begin{pmatrix} e_L \\ \nu_e \end{pmatrix}, \begin{pmatrix} \mu_L \\ \nu_\mu \end{pmatrix}, \begin{pmatrix} \tau_L \\ \nu_\tau \end{pmatrix}$	$(\mathbf{1}, \mathbf{2}, -\frac{1}{2})$	$\begin{pmatrix} -1 \\ 0 \end{pmatrix}$
Right-handed leptons: $e_R, \mu_R, \tau_R$	$(\mathbf{1}, \mathbf{1}, -1)$	$-1$

Table 2.1: The fermions of the SM and their representations under the SM gauge group  $SU(3)_c \times SU(2)_L \times U(1)_Y$ .

As it turns out, the quarks and strong gauge bosons (called gluons) are the constituents of protons and neutrons, and therefore also of all atomic nuclei. The strong interactions among those quarks lead to so-called confinement. That means that no free coloured particles can be observed in nature, and instead all quarks and gluons are confined to bound states that carry no colour charge. The bosons of the SM are the force carriers, and thus mediate interactions between the fermions.

All fields and their interactions can be neatly combined in the SM Lagrangian, which can be written as

$$\mathcal{L}_{\text{SM}} = \mathcal{L}_\psi + \mathcal{L}_V + \mathcal{L}_H + \mathcal{L}_{\text{Yuk}}. \quad (2.2)$$

Here,  $\mathcal{L}_\psi$  contains the kinetic terms of fermion fields including their interactions with the gauge bosons,  $\mathcal{L}_V$  the kinetic and self-interaction terms of the gauge bosons,  $\mathcal{L}_H$  the kinetic and potential terms of the Higgs boson including self interactions, and  $\mathcal{L}_{\text{Yuk}}$  the interaction terms of the Higgs boson with the fermions. The gauge group of the SM completely dictates the Lagrangian structure, and no gauge symmetry violating term is allowed. Additionally, the SM features multiple accidental symmetries, namely baryon number and the individual lepton numbers as global symmetries. However, it is thought that effects of quantum gravity will eventually break those<sup>1</sup>.

This formulation of the SM is valid at energies higher than the electroweak scale  $\Lambda_{\text{EW}} = 246 \text{ GeV}$ . Below that scale, the mechanism known as Higgs mechanism occurs that leads to the fermions and weak gauge bosons acquiring masses [10–15]. We will explain below, how this happens in detail.

The Higgs field transforms as  $(\mathbf{1}, \mathbf{2}, 1/2)$  under the SM gauge group, and its Lagrangian term is given by

$$\mathcal{L}_H = (D_\mu \phi)^\dagger (D^\mu \phi) + \mu^2 \phi^\dagger \phi - \lambda (\phi^\dagger \phi)^2, \quad (2.3)$$

<sup>1</sup> Moreover, many BSM scenarios feature explicit breaking of the accidental symmetries.

where

$$\phi = \begin{pmatrix} \phi^+ \\ \phi_0 \end{pmatrix} \quad (2.4)$$

is the Higgs fields,  $\lambda$  the dimensionless quartic coupling, and  $\mu$  with  $\mu^2 < 0$  has the dimensions of a mass. The Higgs potential consists of the last two terms of (2.3) and is often referred to as a “champagne-bottle” potential, because of their resemblance when the former is plotted as a 3D graph with the imaginary and real part of the Higgs field serving as coordinate axes. The potential obeys a rotational symmetry. When the Higgs field acquires a vacuum expectation value (vev),

$$\langle \phi \rangle = \frac{1}{\sqrt{2}} \begin{pmatrix} 0 \\ v \end{pmatrix}, \quad (2.5)$$

this symmetry is not respected by the specific ground state. This is known as *spontaneous symmetry breaking*, and is not specific to the SM, but also happens in other QFTs. For the SM, the gauge group  $SU(2)_L \times U(1)_Y$  is broken, and only the subgroup of electromagnetic symmetry  $U(1)_{\text{em}}$  remains. With the help of a global transformation, the vev can be rotated into the neutral component, such that the Higgs field reads

$$\phi = \begin{pmatrix} \phi^+ \\ \frac{1}{\sqrt{2}} (v + h + i\tilde{\phi}_0) \end{pmatrix}, \quad (2.6)$$

where  $\phi^+$  and  $\tilde{\phi}_0$  are the charged and neutral would-be Goldstone bosons, and  $h$  is the physical Higgs boson. The three would-be Goldstones provide the longitudinal degrees of freedom for the electroweak gauge bosons. Expanding around the vev leads to the transformation  $W_1, W_2, W_3, B_0 \rightarrow W^\pm, Z^0, \gamma$ , where the charged  $W$ -bosons and the neutral  $Z$  bosons now acquire a mass, whereas the photon  $\gamma$  remains massless as the force carrier of the remaining unbroken electromagnetic gauge group. One usually says that the Goldstone bosons are therefore “eaten” by the weak gauge bosons. Both the  $Z$  and the photon can be written as linear combinations of  $W_3$  and  $B_0$ , and the  $W^\pm$  are combinations of  $W_1$  and  $W_2$ .

In addition to giving masses to the weak gauge bosons, the Higgs mechanism also yields masses for the fermions. In eq. (2.2) the Yukawa interaction term  $\mathcal{L}_{\text{Yuk}}$  is of the form

$$\mathcal{L}_{\text{Yuk}} = - (Y_u)_{ij} \bar{Q}_L^i \tilde{\phi} w_R^j - (Y_d)_{ij} \bar{Q}_L^i \phi d_R^j - (Y_L)_{ij} \bar{L}_L^i \tilde{\phi} e_R^j, \quad (2.7)$$

where  $\tilde{\phi} = i\sigma_2 \phi^*$  and  $\sigma_2$  is the second Pauli matrix. After electro-weak symmetry breaking (EWSB), we expand the Higgs fields around its vev and find

$$\mathcal{L}_{\text{Yuk}} = - (M_u)_{ij} \bar{u}_L^i u_R^j - (M_d)_{ij} \bar{d}_L^i d_R^j - (M_e)_{ij} \bar{e}_L^i e_R^j, \quad (2.8)$$

where  $M_f = Y_f v / \sqrt{2}$  are the mass matrices. These can be diagonalised by individually rotating the left and right-handed fields according to

$$f_{L,R}^i = \left( U_{L,R}^f \right)^{ij} f_{L,R}^j, \quad (2.9)$$

and  $U_{L,R}$  are unitary rotations. This has strong implications for the fermion interactions with the gauge bosons. The fermion term in the SM Lagrangian features current terms of the form

$$\mathcal{L}_\psi \supset \bar{\psi} \not{D} \psi, \quad (2.10)$$

with  $\psi$  denoting the fermion fields and  $D_\mu$  is the covariant derivative, containing the gauge fields. All current terms remain unchanged under the  $U_{L,R}$  transformations with the exception of the charged current  $j_W^\mu$ . For this we obtain

$$j_W^\mu = \frac{1}{\sqrt{2}} \bar{u}_L^i \gamma^\mu d_L^i \rightarrow \frac{1}{\sqrt{2}} \bar{u}_L^i \gamma^\mu \underbrace{\left( U_u^\dagger U_d \right)^{ij}}_{=V^{ij}} d_L^j \quad (2.11)$$

with the primed quark fields denoting the fields in the mass basis and  $V^{ij}$  is the Cabibbo-Kobayashi-Maskawa (CKM) matrix [45, 46]. The off-diagonal entries of the CKM matrix mediate quark flavour-changing effects, i.e. interactions between quarks that belong to different families. At tree-level, flavour-changing neutral currents (FCNCs) are forbidden. Via the Glashow-Iliopolus-Maiani (GIM) mechanism, FCNCs are suppressed even at loop-level in the SM [47, 48]. Since there are no right-handed partners to the purely left-handed neutrinos, they remain massless in the SM.

In interactions where only the lightest quarks, the up, down and strange-quark, contribute, it is often useful to employ chiral perturbation theory ( $\chi$ PT). When the masses of these quarks are taken to be zero, the Lagrangian features an additional chiral  $SU(3)_L \times SU(3)_R$  symmetry. The quark condensate now breaks this symmetry softly, and only the subgroup  $SU(3)_V$ , where  $V$  stands for vector, is unbroken. Moreover, the quark masses are tiny but non-vanishing, so the chiral symmetry is only approximately installed. From Goldstone's theorem we therefore expect  $N^2 - 1 = 9 - 1 = 8$  light pseudo-Nambu-Goldstone bosons (pNGBs), one for each broken generator of the  $SU(3)$  symmetry [49, 50]. They are the three pions  $\pi^\pm, \pi^0$ , the four kaons  $K^\pm, K^0, \bar{K}^0$ , and the eta meson  $\eta^0$ .

A peculiarity of QFTs is that the coupling constants are actually *not* constant, but they depend on the energy scale  $\mu$  where they are evaluated. This scale dependence is governed by the renormalisation group equations (RGEs), which take the form

$$\frac{d}{d \ln \mu} \alpha(\mu) = \beta(\alpha(\mu)), \quad (2.12)$$

with  $\alpha$  a generic coupling constant. For quantum electrodynamics (QED), the beta function  $\beta(\alpha(\mu))$  is positive, meaning that with higher energies, the coupling constant gets larger. Eventually, it will get so large that it diverges and perturbation theory will break down. This point is known as the Landau pole  $\Lambda_L$ . Since it is in the vicinity of  $\Lambda_L \approx 10^{31}$  TeV, it

is far beyond any observable physics in the near future, and is usually not regarded as a problem. Still, several extensions of the SM can take the Landau pole further down to lower energy scales, and its existence can generally be regarded as sign of incompleteness of the theory [51]. In the case of quantum chromodynamics (QCD), the situation is different, since the beta function is negative. Hence for higher energies, the coupling gets weaker, leading to the so-called *asymptotic freedom*. This means that quarks and gluons can move almost freely at high energies, or when they are in close vicinity, respectively. For energies below the QCD scale  $\Lambda_{\text{QCD}} \approx 300 \text{ MeV}$  [52], perturbation theory cannot be applied any more, because the strong coupling constant is too large. This also explains the phenomenon of confinement mentioned earlier. Here, non-perturbative theories must take over, such as lattice QCD [53].

## 2.2 Effective field theories

Though in principle it is possible to perform many computations with the Lagrangian formulation of the SM, in practice it is often way more useful to switch to an alternative formulation instead. These *effective (field) theories* are often valid only in certain limits. They work best, when there is a large hierarchy between the energy scale of interest for the process and the scale of the underlying dynamics. Furthermore, they are generally not renormalisable by a finite number of counterterms, like the SM is. However, they are renormalisable by a finite number order by order in perturbation theory. With  $\chi\text{PT}$ , we have already seen the basis for such an EFT, since it was constructed using the limit that the three lightest quarks are essentially massless. Moreover, for energies below the QCD confinement scale, it is often helpful to switch to a version of  $\chi\text{PT}$ , where instead of quarks and gluons the interacting degrees of freedom are mesons instead.

Generally speaking, there are two main types of EFTs: top-down and bottom-up approaches. In the top-down theories the full theory is known, and in a certain limit an effective theory is constructed. An example for such a theory is Soft-Collinear Effective Theory (SCET) that is used in the first project [gluon-gluon to Higgs fusion in SCET](#). For SCET, the full theory it is derived from is QCD, and it is valid in the limit when multiple particles are light, but have a large momentum component into a certain direction. In bottom-up theories the full theory is unknown, and the EFT is constructed by extending a known EFT to higher dimensional operators. With Fermi's theory of the weak interaction and SM effective field theory (SMEFT) we are going to briefly present two prime examples of a top-down and a bottom-up EFT, respectively. The EFT used in the second project, [flavour physics of ALPs](#), cannot easily be put into one of the two categories. It shows characteristics of both approaches, because we construct the Lagrangian in a bottom-up manner, but still apply assumptions from the ultraviolet (UV) completion onto the EFT like in a top-down approach.

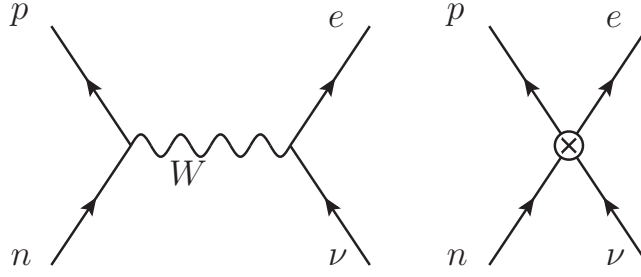


Figure 2.1: Feynman diagrams contributing to the neutron decay  $n \rightarrow p^+ e^- \bar{\nu}_e$  in the Standard Model (left) and in Fermi effective theory (right).

**FERMI THEORY OF WEAK INTERACTIONS** Fermi's theory of nucleon  $\beta$ -decay is historically one of the first applications of EFTs, even though it was only identified as such at a much later stage. It describes the interaction Lagrangian as

$$\mathcal{L}_F = \frac{G_F}{\sqrt{2}} (\bar{p}n \bar{e}\nu + \bar{n}p \bar{\nu}e), \quad (2.13)$$

where  $p, n, e, \nu$  denote the proton, neutron, electron and electron-neutrino, respectively.  $G_F$  is the Fermi constant, and it needs to be extracted from the full theory through a matching calculation. The advantage of working with the Lagrangian (2.13) is that one does neither need to know specific details of weak interactions nor how the proton and neutron are built from quarks to derive decay amplitudes for neutron decay. The disadvantage is then that the Lagrangian is only renormalisable order by order, because the coupling constant has two negative mass dimensions, i.e.  $[G_F] = 1 \text{ eV}^{-2}$ .

The corresponding decay in the full SM is much more involved. In a yet simplified picture, the neutron decay can be seen as an exchange of  $W$ -bosons that changes the neutron into a proton. In figure 2.1 we show the Feynman diagrams for both theories. In the matching computation of Fermi theory onto the SM, we find that the  $W$ -boson mass is much larger than all other scales involved, especially much larger than the momentum transfer  $q$  between the neutron and the proton. Thus we may expand the  $W$ -boson propagator as  $1/(q^2 - m_W^2) = -1/m_W^2 + \mathcal{O}(q^2/m_W^2)$ . This process is known as *integrating out* the heavy particles from the low-energy effective theory. Performing this calculation more carefully, one finds [54]

$$G_F = \frac{\sqrt{2}}{8} \frac{g^2}{m_W^2} = 1.166 \times 10^{-5} \text{ GeV}^{-2}. \quad (2.14)$$

**SMEFT** As will be explained in the next section, it is generally believed that the SM itself is only an effective theory valid at lower energies. At energies somewhere above the TeV scale, new physics is expected to come into play. The effects of the unknown new physics are encrypted in effective higher-dimensional operators built out of SM fields. Here, every operator that respects the SM symmetries is allowed. Sometimes, these new

effects are allowed to break the accidental symmetries of the SM. The SMEFT Lagrangian reads [55–57]

$$\mathcal{L}_{\text{SMEFT}} = \mathcal{L}_{\text{SM}} + \frac{1}{\Lambda_{\text{BSM}}} \sum_i C_i \mathcal{O}_i + \frac{1}{\Lambda_{\text{BSM}}^2} \sum_i C_i \mathcal{O}_i + \mathcal{O}\left(\frac{1}{\Lambda_{\text{BSM}}^3}\right), \quad (2.15)$$

where  $\Lambda_{\text{BSM}}$  is the characteristic scale where new physics comes into play,  $\mathcal{O}_i$  are the operators built out of SM fields, and  $C_i$  are the Wilson coefficients. Without a given UV completion, they cannot be calculated from other theories. Since  $\Lambda_{\text{BSM}}$  is believed to be large, higher dimensional operators become less and less relevant with more suppression factors of  $1/\Lambda_{\text{BSM}}$ . At five spacetime dimensions, i.e. the first expansion term that is added to the SM, only one operator is allowed, if one allows lepton number violation. This operator can explain the smallness of the neutrino masses via the see-saw mechanism [58].

**RENORMALISATION GROUP EQUATIONS** We have already noticed that the coupling constants in the SM obey renormalisation group equations (RGEs) (2.12). We are now going to derive a similar set of equations for a general EFT. We write the (renormalised) amplitude of a given process as the product of Wilson coefficients  $C_i(\mu)$  and operators  $O_i(\mu)$

$$i\mathcal{M} = \sum_i C_i(\mu) O_i(\mu). \quad (2.16)$$

Since all physical observables must be independent of our choice of the renormalisation scale  $\mu$ , the equation

$$\frac{d}{d \ln \mu} i\mathcal{M} = \left( \frac{d}{d \ln \mu} C_i(\mu) \right) O_i(\mu) + C_i(\mu) \frac{d}{d \ln \mu} O_i(\mu) = 0 \quad (2.17)$$

must be fulfilled. The operators span a linearly independent basis, implying that we may write

$$\frac{d}{d \ln \mu} O_i(\mu) = -\gamma_{ij} O_j(\mu), \quad \text{and} \quad \gamma_{ij} = \frac{d}{d \ln \mu} \ln Z_{ij}(\mu), \quad (2.18)$$

where  $Z_{ij}$  is the renormalisation factor. The quantity  $\gamma_{ij}$  is known as the anomalous dimension. Note that it need not be diagonal, thus accounting for operator mixing. Inserting this equation into (2.17), we find a similar relation for the Wilson coefficients

$$\frac{d}{d \ln \mu} C_j(\mu) = \gamma_{ij} C_i(\mu). \quad (2.19)$$

Solving (2.19) and (2.18) then allows for a full control over the scale dependencies of operators and matching coefficients, such that one can compute them at one scale where it is most convenient, and then evolve them to the scale where they eventually need to be evaluated. Note that in general instead of a simple multiplication as in (2.17) in many cases the coefficients and operators need to be convoluted, resulting in the RG equations containing convolution integrals, too.



## 2.3 Beyond the Standard Model physics

Despite its tremendous success and a wonderful agreement of many of its predictions with experimental measurements, there are many direct and indirect hints that the SM is not the end of the quest for a universal description of nature. Here, we collect few of these hints.

- **Neutrino masses** The discovery of neutrino oscillations, i.e. the observation that neutrinos have flavour-changing interactions, was only possible, because at least two of the three neutrino flavours are massive [59,60]. The SM does not provide a mechanism to generate these masses.
- **Quantum gravity** Thus far, it has not been possible to develop a consistent quantum field theory of gravity.
- **Dark matter** First proposed as an answer to the puzzle that galactic rotation curves seem to indicate that there is more matter in a galaxy than is observable, dark matter has since gained much more justification as an explanation for various observations that cannot be explained with modifications of Newtonian gravity [61,62]. Yet, its origin and nature are still unknown. This is a real problem, because it is believed by many physicists that dark matter makes up 27 % of the energy density of the universe, while the Standard Model baryonic matter only contributes 5 % to that budget.
- **Dark energy** To explain the accelerated expansion of the universe, it needs to consist to 68 % of dark energy, an energy form whose nature is still unknown.
- **Baryon asymmetry** In the SM, matter and anti-matter are treated equally except for the different charges. A small phase in the CKM matrix allows for a distinction of the two matter forms, since it introduces CP-violating effects. However, this amount of CP-violation is not enough to explain the observation that almost all observable matter in the universe consists of “normal” matter, and not anti-matter.

Apart from these direct hints for BSM physics, there are several indirect ones, consisting largely of incongruities between the actual observation and our understanding of nature. Many of the following arguments could in principle be swept off the table with the argument “nature is just like that”, but as scientists we usually believe that there must be a deeper meaning or a higher guiding principle behind. In the literature, these problems are therefore often called *naturalness* or *fine-tuning* problems.

- **Hierarchy problem** The hierarchy problem consists of the question why the two fundamental scales of the Higgs mass and the Planck scale are separated by so many orders of magnitude. Since the Higgs boson is an elementary scalar, it receives corrections to its mass from all particles. If there are particles with masses between the Higgs mass and the Planck scale, which is generally believed to be true, their effects must precisely cancel out if there is no mechanism to protect the Higgs mass from such corrections.



- **Strong CP problem** In the Lagrangian of the Standard Model one is allowed to add a CP-violating term proportional to  $\theta G\tilde{G}$ , where  $G$  is the gluon field strength tensor and  $\tilde{G}^{\mu\nu} = \epsilon^{\mu\nu\alpha\beta} G_{\alpha\beta}$  its dual. In contrast to the corresponding expression in QED, it cannot be neglected due to non-perturbative instanton contributions even though it can be written as a total derivative. This term gives rise to a non-vanishing neutron electric dipole moment (EDM). Measurements constrain the coefficient associated with this term to be  $\theta \lesssim 10^{-10}$ , while there is no apparent reason why it should not be of order  $\theta \sim \mathcal{O}(1)$ , like the other free parameters of the SM.
- **Cosmological constant** The cosmological constant problem consists of the discrepancy between the small measured value of the cosmological constant, and therefore the vacuum energy density, and the large theoretical prediction for these effects.

Note that we refrain from mentioning the various anomalies where Standard Model predictions and measurement are in more or less strong disagreement. The reason why we do so is that such discrepancies often vanish as they turn out to be mere statistical fluctuations, misinterpretations, or a misunderstanding, as has been the case with multiple anomalies in the past. However, if these anomalies are found to persist even with improved measurements and theoretical predictions, and reach a statistical significance of more than the usually required five standard deviations, then of course they would be included in the first list of direct evidence for new physics. As an example how several anomalies can give a misleading picture, we briefly present here the case of three anomalies that all seemed to indicate that our understanding of muons is not quite correct: The  $R_{K^{(*)}}$  anomalies, the proton radius puzzle, and the anomalous magnetic moment of the muon. In the past, these anomalies were used as a strong motivation for BSM models that feature lepton flavour universality violation (LFUV). With the most recent developments, this motivation now seems to be significantly weaker.

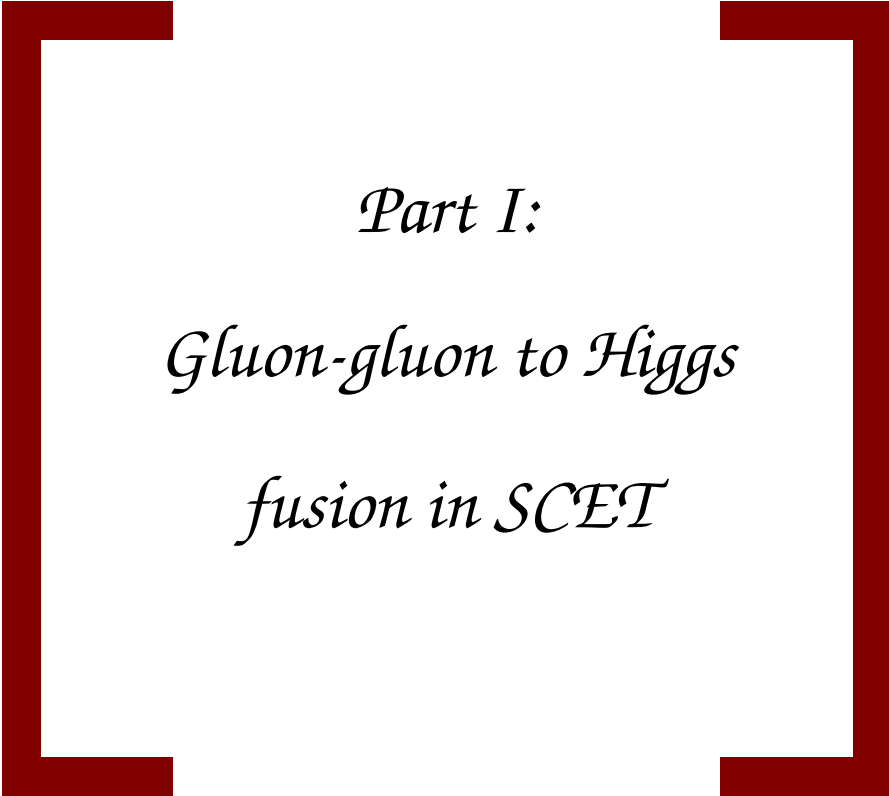
The  $R_K$  and  $R_{K^*}$  measurements are the measurements of the double ratios  $R_K = \text{Br}(B^+ \rightarrow K^+ \mu^+ \mu^-) / \text{Br}(B^+ \rightarrow K^+ e^+ e^-)$  and  $R_{K^*} = \text{Br}(B^0 \rightarrow K^{*0} \mu^+ \mu^-) / \text{Br}(B^0 \rightarrow K^{*0} e^+ e^-)$ . For a long time, the most recent measurement was in disagreement with the SM prediction of about  $\sim 3\sigma$  [63,64]. However, it turned out that previously experimental background was underestimated, and the latest analysis including new experimental data-sets suggests instead a complete agreement of experiment and theory [65].

The proton (charge) radius is defined as the slope of the proton charge form factor at vanishing momentum transfer, and has been a fundamental quantity in nuclear physics. It can be determined with lepton scattering experiments or alternatively by measuring the Lamb shift. Until most recently, all measurements seemed to indicate that whenever the proton radius is measured using muons, the proton seemed to be smaller than when using electrons [66]. New experimental results as well as a re-analysis of old experimental data for scattering experiments instead show agreement of the two approaches [67–71].

The anomalous magnetic moment of the muon  $(g-2)_\mu$  is the deviation of the muon  $g$ -factor from 2. These deviations are due to quantum loop corrections. Here, the situation is exactly the opposite as in the  $R_{K^{(*)}}$  case. New measurements agree with older ones in their respective uncertainty bands, and  $(g-2)_\mu$  is among the most precisely measured quantities

in physics [72,73]. The uncertainty lies in the theory prediction, where the biggest contribution that is not yet well-understood comes from the hadronic vacuum polarisation. It has been calculated using experimental input from LEP measurements in a data-driven approach to yield the theory initiative white paper (TI) prediction [74], and alternatively, with lattice QCD computations by the Budapest, Marseille and Wuppertal (BMW) collaboration [75]. While the TI prediction is in tension with the measurement by  $4.2\sigma$ , the BMW result yields a better agreement with experiments. As long as the discrepancy in the two theory approaches is not understood, it is unclear how meaningful the (possible) deviation from the Standard Model really is.

Most new physics models try to tackle one or several of the problems presented above with a minimal number of new parameters. Since no such model has been found yet to address *all* of these problems, these BSM models are usually regarded as effective theories. In the construction of the Standard Model the importance of symmetries as guiding principles was noticed. Therefore, many new physics scenarios also implement new symmetries that are usually broken spontaneously or directly by low-energy effects. While there are too many BSM models to name them all, we give a few examples in the context of models of axion-like particles (ALPs) in [Part II: Flavour physics of ALPs](#).



*Part I:*  
*Gluon-gluon to Higgs*  
*fusion in SCET*



## A TWO-FOLD MOTIVATION

---

The discovery of the Higgs boson at the LHC in 2012 was a tremendous success for particle physics in general and proved the high predictability of the SM. So far, all measurements concerning the Higgs boson and its properties seem to agree with SM calculations.

At the LHC, Higgs bosons are produced in proton-proton collisions with a centre of mass energy of  $\sqrt{s} = 8\text{--}13.6\text{ TeV}$  in Run 1–3, respectively [20,76]. The main production channel is the fusion of two gluons via a virtual quark loop [19]. The numerically dominant contribution is given by the top-quark, because the amplitude scales with the mass of the loop-quark. It has been studied up to three-loop order in [77] with semi-numerical methods in Higgs effective theory (HEFT). When instead the second-heaviest quark, the bottom (or  $b$ ) quark is included, estimates for its contribution to the amplitude vary in the range between 9–13%, depending on whether one takes the value for the  $b$ -quark pole mass  $m_b^{\text{pole}} \approx 4.8\text{ GeV}$  [18] or the running mass  $m_b(M_h) \approx 2.6\text{ GeV}$  [78]. Analysis of the Run 3 LHC data for the  $gg \rightarrow h$  process will be able to determine the production rate up to this level of precision.

### 3.1 The need for an EFT approach

The computation of the  $gg \rightarrow h$  amplitude is, however, a difficult task. While top-quark loops are dominated by short-distance physics, the numerically subleading contributions from light quarks are sensitive to three very different mass scales  $M_h \gg \sqrt{M_h m_b} \gg m_b$ . Note that in this work we focus on the case of a  $b$ -quark as the light quark. However, our results are also valid for the other light quarks with the obvious substitutions. Using the Feynman diagrammatic approach, one finds that loop corrections involving  $b$ -quarks scale as  $\alpha_s^n \ln^{2n}(-M_h^2/m_b^2)$  at the  $n$ th order. Since this combination is parametrically of order  $\mathcal{O}(1)$ , standard perturbation theory cannot be applied, because corrections from higher loop orders must not be neglected. Hence, all terms must be resummed to all orders of perturbation theory to obtain meaningful results. SCET achieves a factorisation of scales already at the Lagrangian level (at leading order in power counting in small scale ratios), allowing the computation of the individual components at scales where there are no large corrections. It is therefore only natural to apply this EFT to the case at hand.

### 3.2 Motivation from a technical point of view

In [28,29,79–81], SCET has been applied successfully to derive a factorisation theorem for the  $h \rightarrow \gamma\gamma$  decay at next-to-leading power (NLP) in SCET power counting. This factorisation theorem consists of a sum of convolutions over Wilson coefficients with operator matrix elements. It is by now well-known, that at subleading power, scale factorisation is full of complexities. For instance, the factorisation formulae for  $gg \rightarrow h$  and  $h \rightarrow \gamma\gamma$  are plagued by endpoint divergences. These singularities manifest themselves as divergent convolution integrals of component functions of the factorisation theorem. They may be interpreted as a failure of dimensional regularisation and the  $\overline{\text{MS}}$  subtraction scheme, because poles in the dimensional regulator are not removed by renormalising the individual component functions. Naïve scale separation is hence violated. The problem of divergences in the endpoint region is not exclusive to our Higgs production process, but in fact is regularly encountered in NLP problems. Examples include among others the factorisation theorems of Refs. [28,29,80,82–91]. One major novelty in [28,29,80] was the introduction of the refactorisation-based subtraction scheme (RBS). It provided an efficient way to derive an endpoint divergence-free factorisation formula by cleverly rearranging terms and redefining matching coefficients. Showing that the RBS is also applicable in the non-abelian  $gg \rightarrow h$  case will help to establish the procedure as a state-of-the-art method to consistently derive endpoint divergence-free factorisation formulae in SCET. As an affirmation of our methodology, the RBS has already seen use in endpoint factorisation and resummation in gluon thrust [90,92].

### 3.3 Motivation from a phenomenological point of view

Besides its intriguing technical details, the study of  $gg \rightarrow h$  via light quarks is also motivated by phenomenological arguments. As has been already mentioned, the SM predictions and experimental measurements of the Higgs boson’s properties are in good agreement. However, we already know that the SM is only valid as an EFT at low energies, and even then effects remain that are yet inexplicable (see chapters 1 and 2). Since there is no strong hint where new physics could show up first, it is important to pursue research in many different directions and sectors of the SM. The Higgs boson of the SM is an elementary scalar, which already gives rise to certain theoretical problems like the hierarchy problem (see section 2.3). Deviations of Higgs production rates from their theoretical predictions could hint to either previously misunderstood properties of the Higgs itself, or the presence of new particles which couple weakly to SM particles at the given scale and therefore cause minor alterations. Hence, it is of highest importance to verify whether the Higgs boson measurements and its SM predictions truly agree.

## INTRODUCTION TO SCET

---

We find it instructive to first give a brief introduction to SCET as an effective field theory before applying it to the  $gg \rightarrow h$  fusion process. Here, we will establish the language commonly used in the literature and point out typical obstacles one encounters at subleading powers in scale ratios. For an extensive pedagogical introduction to SCET, see Ref. [93].

### 4.1 Introduction to SCET

For a given process, different momentum regions are often of different importance, i.e. contributions from some regions are suppressed by powers of a small expansion parameter  $\lambda$ . The basic concept of SCET is now to identify the leading momentum regions and split up the particle fields according to that identification. For processes where SCET is applicable, the leading regions most often come from hard, (anti-)collinear and soft momenta [94,95]. A hard momentum has large components into every direction; a (anti-)collinear momentum has a large component only into one direction, whereas components anti-parallel or perpendicular are power-suppressed; a soft momentum has power-suppressed components in every direction. The collinear modes also define the directions of light-like reference vectors  $n_i$ . For the case of  $gg \rightarrow h$ , those are the directions of the two final-state gluons. They satisfy  $n_1^2 = n_2^2 = 0$  and  $n_1 \cdot n_2 = 2$ . In the following, we will often use the abbreviations  $n_1 \equiv n$  and  $n_2 \equiv \bar{n}$ . In the Higgs rest frame, we can choose them to be  $n^\mu = (1, 0, 0, 1)$  and  $\bar{n}^\mu = (1, 0, 0, -1)$ . Much of the power of SCET stems from the fact that the separation into hard, collinear and soft modes is, at leading power, already achieved at the Lagrangian level, and interactions between the different sectors can be absorbed into field redefinitions. This allows us to factorise a given process into products or convolutions of hard, collinear, and soft component functions, and compute each of them at their natural scale. One major complexity of SCET at next-to-leading power is the reintroduction of separation-violating interactions, as will be explained further later on.

Often it is not possible to use the coupling constant  $\alpha_s$  as an expansion parameter, since it is accompanied by large logarithms. Instead, the ratio of soft to hard scales is used. For  $gg \rightarrow h$ , we expand in  $\lambda = m_b/M_h \ll 1$ . As usual in SCET, we decompose all momenta into their light-cone components

$$p^\mu = (n_1 \cdot p) \frac{n_2^\mu}{2} + (n_2 \cdot p) \frac{n_1^\mu}{2} + p_\perp^\mu. \quad (4.1)$$

In a short-hand notation, one often writes  $p^\mu = (n_1 \cdot p, n_2 \cdot p, p_\perp) = (p_+, p_-, p_\perp)$ . The hard, collinear and soft momenta then scale as

$$\begin{aligned}
\text{hard} & \quad h : & p^\mu & \sim (1, 1, 1) M_h \\
\text{collinear} & \quad c : & p^\mu & \sim (\lambda^2, 1, \lambda) M_h \\
\text{anti-collinear} & \quad \bar{c} : & p^\mu & \sim (1, \lambda^2, \lambda) M_h \\
\text{soft} & \quad s : & p^\mu & \sim (\lambda, \lambda, \lambda) M_h
\end{aligned} \tag{4.2}$$

The exact scaling of the soft momenta depends on the process. In the literature, one regularly encounters (ultra-)soft scaling  $p^\mu \sim (\lambda^2, \lambda^2, \lambda^2)Q$  or Glauber scaling  $p^\mu \sim (\lambda^2, \lambda^2, \lambda)Q$  besides the soft scaling specified above, where  $Q$  is the hard scale of the given problem. However, all soft scalings have in common that they vanish in the limit  $\lambda \rightarrow 0$ . Similarly, instead of or in addition to collinear momenta, one might face hard-collinear modes that scale as  $p^\mu \sim (\lambda, 1, \lambda^{1/2})Q$  or have other comparable scalings. These modes share the feature that one of the momentum components aligned with the collinear reference vectors is unsuppressed.

In the low-energy effective theory, we eventually integrate out all hard modes from the problem. This will result in a factorisation into a Wilson coefficient and a low-energy effective operator (see chapter 2). After integrating out the hard momenta from a SCET problem, we split the quantum fields into their collinear and soft components

$$\begin{aligned}
\psi(x) &= \psi_c(x) + \psi_s(x) \\
A^\mu(x) &= A_c^\mu(x) + A_s^\mu(x),
\end{aligned} \tag{4.3}$$

with  $\psi$  a fermion field and  $A^\mu$  a gauge boson. Here and below we assume that the fields only have a collinear component. The discussion can be extended to include the anti-collinear case with obvious replacements. The propagator  $\not{p}/p^2$  of the collinear fermion field has a different scaling in each of its light-cone directions. Therefore we further split the fermion field into

$$\psi_c = P_+ \psi_c + P_- \psi_c = \xi_c + \eta_c, \tag{4.4}$$

where

$$P_+ = \frac{\not{p} \not{p}_+}{4}, \quad P_- = \frac{\not{p} \not{p}_-}{4} \tag{4.5}$$

are projection operators fulfilling  $P_\pm^2 = P_\pm$ ,  $P_+ + P_- = \mathbb{1}$  and  $P_+ P_- = P_- P_+ = 0$ . As a consequence,  $P_- \xi_c = P_+ \eta_c = 0$ . The scaling of the various fields can be deduced from their two-point correlation functions. Eventually, one finds

$$\xi_c \sim \lambda, \quad \eta_c \sim \lambda^2, \quad \text{and} \quad \psi_s \sim \lambda^{\frac{3}{2}}. \tag{4.6}$$

The gauge fields scale exactly as their corresponding momentum, i.e. a collinear gauge field scales as a collinear momentum as given in eq. (4.2).



Having all ingredients at hand, we may decompose the SCET-Lagrangian as

$$\mathcal{L}_{\text{SCET}} = \mathcal{L}_c + \mathcal{L}_s + \mathcal{L}_{\text{int}}. \quad (4.7)$$

The soft part is an exact copy of the QCD Lagrangian, where all fields are replaced by their soft counterparts. Using eq. (4.4) and the properties of the projection operators, we can simplify the collinear Lagrangian to

$$\bar{\xi}_c \frac{\not{n}}{2} i \bar{n} \cdot D_c \xi_c + \bar{\xi}_c i \not{D}_{c\perp} \eta_c + \bar{\eta}_c i \not{D}_{c\perp} \xi_c + \bar{\eta}_c \frac{\not{n}}{2} i \bar{n} \cdot D_c \eta_c, \quad (4.8)$$

where  $iD_c^\mu = i\partial^\mu + gA_c^\mu$ . Since  $\eta_c$  is power-suppressed in comparison with  $\xi_c$ , it is most convenient to integrate out the small components from the Lagrangian using their equations of motion<sup>1</sup>. The collinear Lagrangian then simplifies to

$$\mathcal{L}_c = \bar{\xi}_c \frac{\not{n}}{2} \left[ i \bar{n} \cdot D_c + i \not{D}_{c\perp} \frac{1}{i \bar{n} \cdot D} i \not{D}_{c\perp} \right] \xi_c. \quad (4.9)$$

At leading power in SCET all modes are completely decoupled, i.e. there are no interactions between the different sectors. Interactions between soft and (anti-)collinear particles are power-suppressed [96, 97]. Furthermore, interactions of collinear fermions with anti-collinear gauge fields would create hard momenta, and hence are not part of the low-energy theory.

When matching the full theory onto SCET, interactions between collinear and anti-collinear fermions can be mediated through external currents, where the necessary hard momentum transfer is provided by an external gauge field. The problem is that even at leading power insertions of an arbitrary number of derivatives in the direction of the large momentum component (i.e.  $\bar{n} \cdot \partial \xi_c \sim \lambda^0 \xi_c$ ) as well as an arbitrary number of gauge field insertions ( $\bar{n} \cdot A^\mu \sim \lambda^0$ ) is allowed. To account for this fact, we could work with infinitely many operators and Wilson coefficients, one for each power of derivative and/or gauge field insertion. However, there is a more elegant way to deal with this problem: We allow for *non-local* operators in SCET that are smeared along the light-cone direction of the large momentum component.

$$\xi_c(x) \rightarrow \xi_c(x + t\bar{n}) = \sum_{n=0}^{\infty} \frac{t^n}{n!} (\bar{n} \cdot \partial)^n \xi_c(x). \quad (4.10)$$

One problem that arises in this treatment is that with fields at different spacetime points, gauge invariance is not manifest any more. To preserve the gauge symmetry, we must transport the gauge transformation from one spacetime point at  $x$  to the one at  $x + t\bar{n}$ . This can be achieved by using Wilson lines. For example, the bilinear

$$\bar{\xi}_c(x + t\bar{n}) [x + t\bar{n}, x] \frac{\not{n}}{2} \xi_c(x) \quad (4.11)$$

<sup>1</sup> The resulting determinant is independent of the gauge fields and therefore no physical consequence follows from removing  $\eta_c$  [93].

with the Wilson line

$$[x + t\bar{n}, x] = \mathbf{P} \exp \left[ ig \int_0^t ds \bar{n} \cdot A_c(x + t\bar{n}) \right] \quad (4.12)$$

is gauge invariant under the collinear gauge transformation  $V_c(x) = \exp[i\alpha_s^a(x)t^a]$ , since the fields and the Wilson line transform as

$$\begin{aligned} \xi_c(x) &\rightarrow V_c(x)\xi_c(x), \\ [x + t\bar{n}, x] &\rightarrow V_c(x + t\bar{n})[x + t\bar{n}, x]V_c^\dagger(x). \end{aligned} \quad (4.13)$$

The symbol  $\mathbf{P}$  in eq. (4.12) denotes a path ordering of the matrices at different times such that those at later times should be to the left of the ones at earlier times. In SCET, it is often useful to define a Wilson line aligned with  $\bar{n}$  that runs to infinity

$$W_c(x) = [x, x - \infty\bar{n}]. \quad (4.14)$$

The finite segment can then be expressed as

$$[x + t\bar{n}, x] = W_c(x + t\bar{n})W_c^\dagger(x). \quad (4.15)$$

This introduction of the infinite length Wilson line now allows us to define gauge invariant building blocks [97,98]

$$\begin{aligned} \mathcal{X}_c(x) &\equiv W_c^\dagger(x)\xi_c(x) \\ \mathcal{A}_c^\mu &\equiv W_c^\dagger[D_c^\mu W_c]. \end{aligned} \quad (4.16)$$

Hence, the bilinear in eq. (4.11) can be written as

$$\bar{\xi}_c(x + t\bar{n})[x + t\bar{n}, x] \frac{\not{n}}{2} \xi_c(x) = \bar{\mathcal{X}}_c(x + t\bar{n}) \frac{\not{n}}{2} \mathcal{X}_c(x). \quad (4.17)$$

SCET operators can then easily be built out of these building blocks. Eventually, at NLP we will also introduce soft Wilson lines  $S_n$  and  $S_{\bar{n}}$  in the (anti-)collinear direction. They are defined like their collinear counterparts with the replacement  $A_c \rightarrow A_s$ . As an example of a SCET operator built out of building blocks, we may now write down the most general leading-power SCET current operator as

$$J^\mu(x=0) = \int ds \int dt C_V(s, t) \bar{\mathcal{X}}_c(t\bar{n}) \gamma_\perp^\mu \mathcal{X}_{\bar{c}}(sn). \quad (4.18)$$

Here,  $C_V(s, t)$  is the Fourier transform of the hard component function. It corresponds to the integral where all momentum components are of the order of the large scale. Note that in the case of  $x \neq 0$ , a multipole expansion of the fields is needed in order to sustain a consistent power counting [99].

As is common for a non-local EFT, Lorentz invariance is not obviously manifest in SCET. Therefore, we need to require that operators are invariant under the following transformations of the reference vectors  $n$  and  $\bar{n}$  [100]

$$(I) \begin{cases} n^\mu \rightarrow n^\mu + \Delta_\perp^\mu \\ \bar{n}^\mu \rightarrow \bar{n}^\mu \end{cases}, \quad (II) \begin{cases} n^\mu \rightarrow n^\mu \\ \bar{n}^\mu \rightarrow \bar{n}^\mu + \epsilon_\perp^\mu \end{cases}, \quad (III) \begin{cases} n^\mu \rightarrow (1 + \alpha)n^\mu \\ \bar{n}^\mu \rightarrow (1 - \alpha)\bar{n}^\mu \end{cases}. \quad (4.19)$$

The four-vectors  $\Delta_\perp$  and  $\epsilon_\perp$  obey

$$\Delta_\perp \cdot n = \Delta_\perp \cdot \bar{n} = \epsilon_\perp \cdot n = \epsilon_\perp \cdot \bar{n} = 0. \quad (4.20)$$

Furthermore, they must count as  $\mathcal{O}(\lambda)$  or smaller to not disrupt the power counting. There is no such restriction to the parameter  $\alpha$  in (III). The invariance of operators under (I)–(III) is known as *reparametrisation invariance* (RPI), and is a central concept in SCET.

## 4.2 Resummation

As was mentioned earlier, in SCET problems, the strong coupling constant is for usual accompanied by large logarithms. To obtain sensible predictions for observables, it is thus necessary to resum those logarithms to all orders of perturbation theory. To give an example how this procedure works in general, we briefly recapitulate the resummation of the Sudakov form factor in [101]. Its Feynman diagram is given by two (anti-)collinear fermions with incoming momenta  $p$  and  $-k$ , respectively, coupling to a boson with outgoing momentum  $q = p - k$ , which provides the necessary hard momentum transfer. This is a leading order process in SCET, and hence the renormalised form factor can be expressed as

$$F(Q^2, K^2, P^2) = C(Q^2, \mu) \bar{J}(K^2, \mu) J(P^2, \mu) S(\Lambda_s^2, \mu). \quad (4.21)$$

Here,  $Q^2 = -q^2$ ,  $K^2 = -k^2$ ,  $P^2 = -p^2$  and  $\Lambda_s^2 = K^2 P^2 / Q^2$ .  $C(Q^2, \mu)$  is the hard Wilson coefficient,  $J(P^2, \mu)$  and  $\bar{J}(K^2, \mu)$  are the (identical) collinear functions into the two collinear directions, and  $S(\Lambda_s^2, \mu)$  is the soft function. Since the form factor is a gauge-invariant quantity, all dependence on the renormalisation scale  $\mu$  must drop out, eventually. The renormalisation group (RG) equations for the component functions read

$$\begin{aligned} \frac{d}{d \ln \mu} C(Q^2, \mu) &= \left[ C_F \Gamma_{\text{cusp}}(\alpha_s) \ln \left( \frac{Q^2}{\mu^2} \right) + \gamma_C(\alpha_s) \right] C(Q^2, \mu) \\ \frac{d}{d \ln \mu} J(P^2, \mu) &= - \left[ C_F \Gamma_{\text{cusp}}(\alpha_s) \ln \left( \frac{P^2}{\mu^2} \right) + \gamma_J(\alpha_s) \right] J(P^2, \mu) \\ \frac{d}{d \ln \mu} S(\Lambda_s^2, \mu) &= - \left[ C_F \Gamma_{\text{cusp}}(\alpha_s) \ln \left( \frac{\Lambda_s^2}{\mu^2} \right) + \gamma_S(\alpha_s) \right] S(\Lambda_s^2, \mu). \end{aligned} \quad (4.22)$$

The extra logarithmic dependence on  $\mu$  is due to the presence of characteristic Sudakov double-logs in the one-loop amplitude of the form  $\alpha_s^n L^{2n}$  with  $L$  such a large logarithm [93]. The function  $\Gamma_{\text{cusp}}$  is the *cusp anomalous dimension*. The label “cusp” is linked to the

renormalisation of Wilson lines that form a cusp, e.g. a Wilson line that runs along  $\bar{n}^\mu$  from  $-\infty \dots 0$  and back along  $n^\mu$  from  $0 \dots \infty$ . The cusp anomalous dimension is then proportional to the cusp angle at 0 [102–104]. For the cancellation of all  $\mu$ -dependencies to happen for the form factor, it is crucial that the RGEs of all component functions (4.22) feature the same coefficient for the extra logarithmic piece.

The solutions to (4.22) sum up the logarithmic terms to all orders in perturbation theory. As an illustration, we give the solution for the hard coefficient:

$$\begin{aligned} C(Q^2, \mu) &= \exp \left\{ \int_{\mu_h}^{\mu} \left[ C_F \Gamma_{\text{cusp}}(\alpha_s) \ln \left( \frac{Q^2}{\mu'^2} \right) + \gamma_C(\alpha_s) \right] d \ln(\mu') \right\} C(Q^2, \mu_h) \\ &= U(\mu_h, \mu) C(Q^2, \mu_h). \end{aligned} \quad (4.23)$$

In the last line, the function  $U$  can be regarded as an evolution function that runs down the scale from  $\mu_h$  to  $\mu$ . Note that because for the hard function the large logarithm is of the form  $\ln(Q^2/\mu^2)$ , if we choose  $\mu_h \sim Q$ , there are no large logarithms left in this problem. This means, that eq. (4.23) is valid for all values  $\mu$ , where  $\alpha_s(\mu)$  remains perturbative. This is a vast improvement over the expression for the renormalised coefficient, which through its dependence on  $\alpha_s \ln^2(Q^2/\mu^2)$  cannot be used in the regime where  $\mu \gg Q$  or  $\mu \ll Q$ . When evaluating the transfer function  $U$ , one exchanges the logarithmic dependence on the scales for a dependence on coupling constants in practice, eventually reaching

$$U(\mu_h, \mu) = \exp [2C_F S(\mu_h, \mu) - a_{\gamma_C}(\mu_h, \mu)] \left( \frac{Q^2}{\mu_h^2} \right)^{C_F a_{\Gamma_{\text{cusp}}}(\mu_h, \mu)}. \quad (4.24)$$

Here,

$$\begin{aligned} S(\nu, \mu) &= - \int_{\alpha_s(\nu)}^{\alpha_s(\mu)} d\alpha \frac{\Gamma_{\text{cusp}}(\alpha)}{\beta(\alpha)} \int_{\alpha_s(\nu)}^{\alpha} \frac{d\alpha'}{\beta(\alpha')} \\ a_{\gamma_i} &= - \int_{\alpha_s(\nu)}^{\alpha_s(\mu)} d\alpha \frac{\gamma_i(\alpha)}{\beta(\alpha)} \end{aligned} \quad (4.25)$$

with  $i = \{C, \Gamma_{\text{cusp}}\}$  are RG-functions. The solution to the RG equations for the collinear and soft functions take a similar form. The procedure of eliminating large logarithms in favour of coupling constants at different scales is known as *renormalisation group improved perturbation theory*.

### 4.3 SCET at subleading power

At subleading power, SCET is full of complexities. The factorisation theorems consist of sums of convolutions over Wilson coefficients and operator-matrix elements. Additionally, scale separation is not obvious due to the reintroduction of interactions between the different scales. A common feature of NLP SCET problems is the occurrence of endpoint

divergences. They manifest themselves as divergent convolution integrals over individual component functions. Some of these singularities can be regularised using dimensional regularisation, while others still remain. One may hence interpret the presence of endpoint divergences as a failure of dimensional regularisation and the modified minimal subtraction ( $\overline{\text{MS}}$ ) scheme. In general, it is therefore necessary to introduce an additional analytic (or rapidity) regulator that is associated with its own regularisation scale. Eventually, all dependence on rapidity regulators and the regularisation scale cancels among the different terms of the factorisation theorem. However, regularisation of endpoint divergences and renormalisation of UV divergences does not commute, spoiling the naïve scale separation, and preventing the derivation of a well-defined, renormalised factorisation theorem. This provides a bottleneck for all NLP problems.

In [28,80], the RBS has been introduced. It addresses the problem of endpoint divergent terms in a systematic way. Its basis is the observation that the integrands of the divergent integrals in different terms of the factorisation formula become identical in the singular region. With its help, one is able to derive exact  $d$ -dimensional refactorisation conditions, which subsequently allow for a rearrangement of terms in the factorisation theorem that is free of endpoint divergences. The importance of the RBS has also been emphasised in works about gluon thrust at NLP [89,90,92]. Up to this date, it is the only known systematic approach how to deal with endpoint factorisation at subleading power. In this thesis, we will generalise the approach to non-abelian final states.



## FACTORISATION AND RESUMMATION OF GLUON-GLUON TO HIGGS FUSION

---

The foundation of this treatise is the derivation of a renormalised factorisation theorem, the corresponding RG equations and eventually the resummation of the light quark induced Higgs decay  $h \rightarrow \gamma\gamma$  in Refs. [28,29,79–81]. Here, we generalise the method to non-abelian external states, namely the Higgs production process  $gg \rightarrow h$ . Throughout this thesis, we will refer to the former as the “photon” or the “abelian case”, and the latter will be called the “gluon” or “non-abelian case”. The results of this work have already been published in short form in [1,3].

### 5.1 Factorisation of $gg \rightarrow h$

In this section, we apply SCET to disentangle the physics at the different relevant energy scales and obtain a (bare) factorisation theorem for the light quark induced  $gg \rightarrow h$  form factor. The Feynman diagram for the leading order process is shown in figure 5.1. Here and in the following, we will focus on the numerically most important case where the light quark is the  $b$ -quark. We use  $\lambda = m_b/M_h$  as our small expansion parameter. Note that because of the quark loop, the amplitude is proportional to the light quark mass  $\mathcal{M} \sim m_b = \lambda M_h$ . Hence, this is a power-suppressed process.

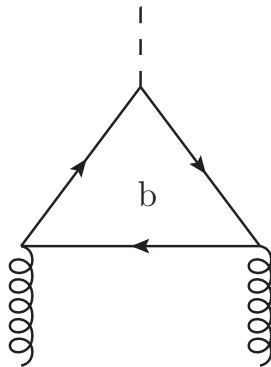


Figure 5.1: Leading order Feynman diagram for the fusion process  $gg \rightarrow h$  via light quarks. The amplitude is proportional to the quark mass, giving a power-suppressed process.

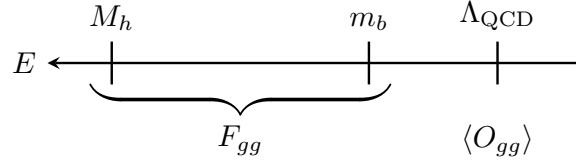


Figure 5.2: Illustration of the matching process for  $gg \rightarrow h$ . The perturbative physics above  $m_b$  are combined in the form factor  $F_{gg}$ , which is calculated using SCET. All non-perturbative effects are incorporated in the operator  $O_{gg}$ , whose matrix element yields the gluon distribution functions in the proton when squared and integrated over phase space.

### 5.1.1 Decoupling perturbative and non-perturbative physics

There are no free gluons in nature, because they carry colour charge and due to confinement all physical states must be colour neutral. Therefore, Higgs bosons are produced at colliders like the LHC from proton-proton collisions, which then provide the necessary gluons. For a full treatment of  $gg \rightarrow h$ , it is therefore crucial to disentangle the perturbative physics of gluon-gluon to Higgs fusion at the parton level and the non-perturbative part of extracting the gluons from the proton. We embody all non-perturbative physics in the EFT called LEFT (low-energy EFT), which is valid below the  $b$ -quark mass scale. The only operator left in LEFT is the two-gluon operator

$$O_{gg} = \frac{1}{g_s^2} \mathcal{G}_n^{\perp\mu,a} \mathcal{G}_{\bar{n}\mu}^{\perp a} \quad (5.1)$$

built out of two collinear gluon fields along the directions  $n$  and  $\bar{n}$ . The perturbative physics above the scale  $m_b$  is captured in the form factor  $F_{gg}$ . At the low scale, we match onto  $O_{gg}$  in LEFT, therefore we write

$$\langle pp | O_{\text{pert}} | h \rangle = F_{gg} \langle pp | O_{gg} | h \rangle, \quad (5.2)$$

where  $O_{\text{pert}}$  is the sum of relevant operators encoding the perturbative physics. In this sense, the form factor is the non-abelian equivalent to the amplitude in  $h \rightarrow \gamma\gamma$ <sup>1</sup>. Since we interpret  $F_{gg}$  as a matching coefficient, it can be calculated using on-shell gluon states. The matching is shown in figure 5.2. The operator  $O_{gg}$  needs to be renormalised. Consequently, its matrix element is scale dependent. This scale dependence will also manifest itself in additional IR-poles that do not cancel out among different terms in the form factor. When the whole amplitude is squared and integrated over phase space, the squared matrix element of  $O_{gg}$  will yield the product of two well-known PDFs of the gluon in the proton.

To compute the perturbative part of  $gg \rightarrow h$  via light quarks at the parton level, we use SCET. In a two-step matching procedure we first match full QCD to an intermediate theory SCET<sub>1</sub> by integrating out hard modes. Further decoupling hard-collinear modes then yields SCET<sub>2</sub>, which is the final theory used to compute  $F_{gg}$ .

<sup>1</sup> In contrast to gluons, free photons exist in nature. Therefore this additional matching step onto low-energy operators is omitted for  $h \rightarrow \gamma\gamma$ .



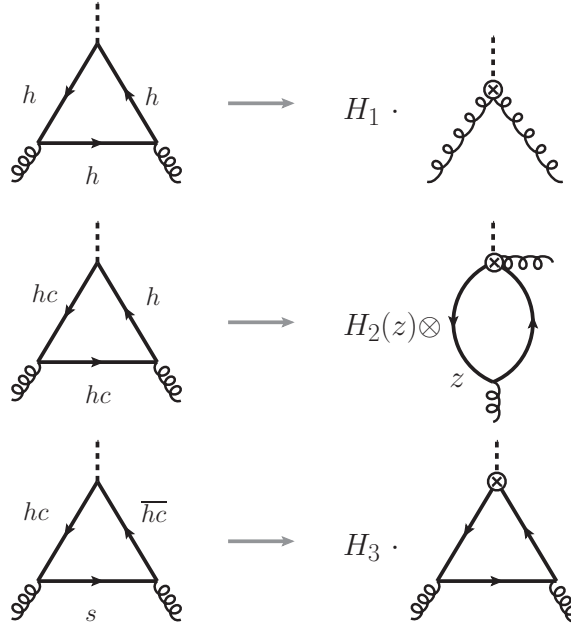


Figure 5.3: Leading momentum regions contributing to the matching of  $\text{SCET}_1$  to QCD in  $gg \rightarrow h$  via light quarks. The symbol  $\otimes$  in the second row denotes a convolution integral over  $z$ .

### 5.1.2 Derivation of the effective $\text{SCET}_1$ operators

We use the method of regions [105–107] to identify the leading contributing momentum modes in the full QCD picture. We find the relevant modes to be in the hard, collinear, anti-collinear and soft sector, obeying the scaling given in eq. (4.2). In an intermediate step, when there are soft exchanges present, we need to include regions with a hard-collinear scaling  $p^\mu \sim (\lambda, 1, \lambda^{1/2})$  and the first two entries exchanged for anti-hard-collinear momenta. The derivation of the QCD  $\rightarrow$   $\text{SCET}_1$  matching is portrayed in figure 5.3. When all loop momenta of the quark loop are of the order of the hard scale, the loop is shrunk to a point-like interaction connecting the Higgs boson directly to two gluon fields along the directions  $n$  and  $\bar{n}$ , yielding the  $\text{SCET}_1$  operator

$$O_1 = \frac{m_b}{g_s^2} h \mathcal{G}_n^{\perp\mu,a} \mathcal{G}_{\bar{n}\mu}^{\perp a}. \quad (5.3)$$

Here,  $h$  denotes the Higgs field. Note that we pulled a factor  $g_s^{-2}$  out in front, because the Feynman rule for the gauge covariant gluon field contains a factor of the strong coupling constant. From here on, fields without arguments are located at the spacetime point  $x = 0$ . The symbol  $\mathcal{G}$  stands for the gauge invariant building block of the collinear gluon field. The second operator arises, when the loop momentum is collinear with one of the gluon directions. The corresponding operator contains a Higgs field, an anti-collinear gluon field in the  $\bar{n}$  direction, and two collinear  $b$ -quark fields, which annihilate to produce the collinear gluon moving along the direction  $n$ .

$$O_2(z) = h \left[ \bar{\chi}_n \gamma_\perp^\mu T^a \frac{\not{n}_1}{2} \delta(z\bar{n}_1 \cdot k_1 + i\bar{n}_1 \cdot \partial) \chi_n \right] \mathcal{G}_{\bar{n}\mu}^{\perp a} \quad (5.4)$$

The variable  $z \in [0, 1]$  denotes the fraction of the  $n$ -collinear momentum  $k_1$  of the gluon that is carried by one of the  $n$ -collinear quarks, denoted by the symbol  $\mathcal{X}$ . Note that there is an equivalent contribution coming from interchanging the collinear  $n$  with the anti-collinear  $\bar{n}$  region, hence giving rise to an additional factor 2 for this contribution to the factorisation theorem. The third operator consists of the time-ordered product of the scalar Higgs current with two insertions of the subleading power SCET Lagrangian, in which hard-collinear fields are coupled to a soft field [108].

$$O_3 = \hat{T} \left\{ h \bar{\mathcal{X}}_n \mathcal{X}_{\bar{n}}, i \int d^D x \mathcal{L}_{q\xi_n}^{(1/2)}(x), i \int d^D x \mathcal{L}_{\xi_{\bar{n}q}}^{(1/2)}(y) \right\} + \text{h.c.} . \quad (5.5)$$

In the matching  $\text{SCET}_1 \rightarrow \text{SCET}_2$ , one integrates out these hard-collinear fields. In practice, for  $O_1$  and  $O_2$ , the hard-collinear fields are simply replaced by their collinear counterparts, whereas  $O_3$  can be further factorised into a double convolution of two jet functions and one soft function, which we are going to demonstrate in the following.

In eq. (5.5), the two subleading power Lagrangian insertions read [108]

$$\begin{aligned} \mathcal{L}_{q\xi_n}^{(1/2)}(x) &= \bar{q}_s(x_-) W_n^\dagger(x) i \not{D}_n^\perp \xi_n(x), \\ \mathcal{L}_{\xi_{\bar{n}q}}^{(1/2)}(y) &= \bar{\xi}_{\bar{n}}(y) \left[ i \not{D}_{\bar{n}}^\perp W_{\bar{n}}(y) \right] q_s(y_+), \end{aligned} \quad (5.6)$$

where the soft quark fields  $q_s$  need to be multipole expanded for consistency [96, 108]. As for momenta, we denote  $x_-^\mu = (\bar{n} \cdot x) \frac{n^\mu}{2}$  for spacetime points, equivalently. Introducing gauge-invariant building blocks, we may transform eq. (5.6) into

$$\begin{aligned} \mathcal{L}_{q\xi_n}^{(1/2)}(x) &= \bar{q}_s(x_-) \mathcal{G}_n^\perp(x) \mathcal{X}_n(x), \\ \mathcal{L}_{\xi_{\bar{n}q}}^{(1/2)}(y) &= \bar{\mathcal{X}}_{\bar{n}}(y) \mathcal{G}_{\bar{n}}^\perp(y) q_s(y_+). \end{aligned} \quad (5.7)$$

Consequently, we find for  $O_3$

$$\begin{aligned} O_3 &= h(0) \int d^D x \int d^D y \hat{T} \left\{ \left[ \mathcal{G}_n^\perp(x) \mathcal{X}_n(x) \right]^{\alpha i} \bar{\mathcal{X}}_n^{\beta j}(0) \right\} \hat{T} \left\{ \mathcal{X}_{\bar{n}}^{\beta k}(0) \left[ \bar{\mathcal{X}}_{\bar{n}}(y) \mathcal{G}_{\bar{n}}^\perp(y) \right]^{\gamma l} \right\} \\ &\times \hat{T} \left\{ \left[ S_n^\dagger(y_+) q_s(y_+) \right]^{\gamma l} \left[ \bar{q}_s(x_-) S_n(x_-) \right]^{\alpha i} \left[ S_n^\dagger(0) S_{\bar{n}}(0) \right]^{jk} \right\} + \text{h.c.}, \end{aligned} \quad (5.8)$$

where greek letters represent Dirac indices and latin letters represent colour indices. The symbol  $S_{n_i}$  denotes the soft Wilson line in the respective direction. The first two time-ordered products can be interpreted as operators matching onto two jet functions into the two collinear directions, i.e.

$$\begin{aligned} &\int d^D x_+ \int d^{D-2} x_\perp \hat{T} \left\{ \left[ \mathcal{G}_n^\perp(x) \mathcal{X}_n(x) \right]^{\alpha i} \bar{\mathcal{X}}_n^{\beta j}(0) \right\} \\ &= 2T_{ij}^a \left[ \gamma_\mu^\perp \not{n} \right]^{\alpha\beta} \int \frac{d\ell_+}{2\pi} e^{-i\ell_+ \cdot x_-} \frac{iJ(\ell_+ \bar{n} \cdot \mathcal{P})}{\ell_+ + i0} \mathcal{G}_{n_\perp}^{\mu,a}(0). \end{aligned} \quad (5.9)$$

Here,  $\bar{n} \cdot \mathcal{P} = -i\bar{n} \cdot \partial$  is a differential operator projecting out the large component of the collinear momentum carried by the gluon field,  $\ell_+$  is the momentum carried away by the

multipole-expanded soft quark. A similar relation holds for the anti-collinear jet function with the obvious replacements. The remaining soft operator is then given by

$$\mathcal{W}_{ab}^{\gamma\alpha}(x_-, y_+) = \hat{T} \left\{ \text{Tr} S_{\bar{n}}(0) T^b S_{\bar{n}}(y_+) q_s^\gamma(y_+) q_s^\alpha(x_-) S_n(x_-) T^a S_n^\dagger(0) \right\}, \quad (5.10)$$

where  $\text{Tr}$  is a trace over colour indices. In the photon case [28], the two colour matrices  $T^{a(b)}$  were absent, which allowed the authors to combine two semi-finite soft Wilson lines that travel from spacetime point 0 to  $\infty$  along  $\bar{n}$  and back to  $y_+$  along the same direction, into one *finite* soft Wilson line

$$S_{\bar{n}}(0) S_{\bar{n}}^\dagger(y_+) = S_{\bar{n}}(0, y_+) = \mathbf{P} \exp \left[ i g_s \int_{y^+}^0 dt \bar{n} \cdot G_s^a(t\bar{n}) T^a \right]. \quad (5.11)$$

For our studies, this is not trivially possible due to insertions of colour matrices at  $y = \infty$ . However, we can use the identity

$$S_{\bar{n}}(x) T^b S_{\bar{n}}^\dagger(x) = (\mathcal{Y}_{\bar{n}}(x))_b^a T^b, \quad (5.12)$$

with  $\mathcal{Y}_{\bar{n}}$  a semi-finite soft Wilson line in the adjoint representation that extends from 0 to infinity along  $\bar{n}$ . In Feynman diagrams, we will draw these soft Wilson lines in the adjoint as red double lines. The soft operator (5.10) can hence be written as

$$\mathcal{W}_{ab}^{\gamma\alpha}(x_-, y_+) = \hat{T} \left\{ \text{Tr}_c (\mathcal{Y}_{\bar{n}}(0))_d^b T^d S_{\bar{n}}(0, y_+) q_s^\gamma(y_+) \bar{q}_s^\alpha(x_-) S_n(x_-, 0) (\mathcal{Y}_n(0))_c^a T^c \right\}. \quad (5.13)$$

To further simplify the calculation, we decompose  $\mathcal{W}$  into the different spinor structures

$$\begin{aligned} \mathcal{W}^{\gamma\alpha}(x_-, y_+) = \int \frac{d^D \ell}{(2\pi)^D} e^{-i\ell \cdot (y_+ - x_-)} \left[ \mathcal{S}_1(\ell) + \not{\ell} \mathcal{S}_2(\ell) + \frac{\not{n} \not{\ell}}{n \cdot \ell} \mathcal{S}_3(\ell) + \frac{\not{\bar{n}} \not{\ell}}{\bar{n} \cdot \ell} \mathcal{S}_4(\ell) \right. \\ \left. + \frac{\not{\ell} \not{n}}{n \cdot \ell} \mathcal{S}_5(\ell) + \frac{\not{\bar{n}} \not{\ell}}{\bar{n} \cdot \ell} \mathcal{S}_6(\ell) + \frac{\not{n} \not{\ell}}{4} \mathcal{S}_7(\ell) + \frac{\not{\bar{n}} \not{\ell} \not{n}}{2} \mathcal{S}_8(\ell) \right]^{\gamma\alpha}. \end{aligned} \quad (5.14)$$

Here, all  $\mathcal{S}_i$  are scalar functions. Eventually, the trace over spinor indices will be taken, leaving only  $\mathcal{S}_1$  to contribute to the final soft function. Moreover, we can integrate out the perpendicular component of the loop momentum by defining

$$\mathcal{S}(\ell_{-l_+}) = \int \frac{d^{D-2} \ell_\perp}{(2\pi)^{D-2}} \mathcal{S}_1(\ell). \quad (5.15)$$

With these simplifications, we can derive the final expression for  $O_3$  as

$$\begin{aligned} O_3 = h(0) \int \frac{d\ell_+}{\ell_+ + i0} \int \frac{d\ell_-}{\ell_- - i0} \int \frac{dx_-}{2\pi} \int \frac{dy_+}{2\pi} e^{-i\ell \cdot (y_+ - x_-)} \text{Tr} \left[ \gamma_\mu^\perp \frac{\not{n}}{2} \frac{\not{\bar{n}}}{2} \gamma_\nu^\perp \mathcal{W}(x_-, y_+) \right] \\ \times J(\ell_+ \bar{n} \cdot \mathcal{P}) \mathcal{G}_{n,\perp}^{a,\mu}(0) J(\ell_- n \cdot \mathcal{P}) \mathcal{G}_{\bar{n},\perp}^{a,\nu}(0) \\ = h(0) \mathcal{G}_{n,\perp}^{a,\mu}(0) \mathcal{G}_{\bar{n},\perp}^{a,\nu}(0) \int_0^\infty \frac{d\ell_+}{\ell_+} \int_0^\infty \frac{d\ell_-}{\ell_-} J(-M_h \ell_+) J(M_h \ell_-) \mathcal{S}_3(\ell_{-l_+}), \end{aligned} \quad (5.16)$$

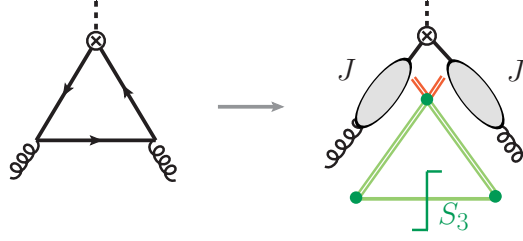


Figure 5.4: Factorisation of  $O_3$  in SCET<sub>2</sub>. In the soft function, green double lines represent soft Wilson lines, red double lines soft Wilson lines in the adjoint representation, and the green single line denotes the soft quark propagator. The rectangular line-shape means that the soft function is defined as the discontinuity of the object shown.

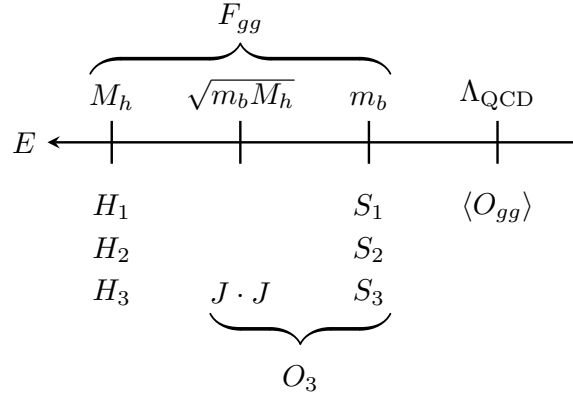


Figure 5.5: Illustration of the relevant energy scales in the  $gg \rightarrow h$  factorisation process. The different objects are shown at their respective scale. At the scale  $m_b$  the perturbative form factor  $F_{gg}$  is matched onto the low-energy effective theory LEFT, where only the operator  $O_{gg}$  consisting of two collinear gluons contributes. The LEFT incorporates all non-perturbative physics.

and

$$S_3(\ell_-\ell_+) = \frac{1}{2\pi i} \left[ \mathcal{S}(\ell_-\ell_+ + i0) - \mathcal{S}(\ell_-\ell_+ - i0) \right], \quad (5.17)$$

is the soft function defined as the discontinuity of  $\mathcal{S}(\ell_+\ell_-)$ . This follows from the analytical structure of the integrand in the first line of eq. (5.16). The jet function depending on  $\ell_-$  ( $\ell_+$ ) has a pole at  $\ell_- = i0$  ( $\ell_+ = i0$ ), and  $\mathcal{S}(\ell_+\ell_-)$  features a cut at  $\ell_+\ell_- = -i0$  that extends to infinity. For  $\ell_+ < 0$  ( $\ell_- < 0$ ), this cut is located above the real axis, allowing us to close the integration contour in the lower half-plane and thus yielding no contribution for the integral. If instead  $\ell_+ > 0$  ( $\ell_- > 0$ ), the discontinuities must be included in the integral, leading to the expression above. The factorisation of  $O_3$  into a convolution of two jet functions and a soft function in SCET<sub>2</sub> is portrayed in figure 5.4.

Having the expressions for all operators in the low-energy effective theory at hand, we may state the matching onto the LEFT (5.2) more precisely as

$$\begin{aligned} \langle pp|O_i|h\rangle &= S_i \langle pp|O_{gg}|0\rangle; \quad i = 1, 2, \\ \langle pp|O_3|h\rangle &= J \otimes J \otimes S_3 \langle pp|O_{gg}|0\rangle. \end{aligned} \quad (5.18)$$

The full matching procedure is shown graphically in figure 5.5.

### 5.1.3 Bare factorisation theorem and two-loop expressions for the component functions

The bare factorisation theorem for the form factor of the  $gg \rightarrow h$  process via light quarks reads

$$F_{gg}(gg \rightarrow h) = H_1^{(0)} S_1^{(0)} + 4 \int_0^1 \frac{dz}{z} \bar{H}_2^{(0)}(z) S_2^{(0)}(z) + H_3^{(0)} \int_0^\infty \frac{d\ell_-}{\ell_-} \int_0^\infty \frac{d\ell_+}{\ell_+} J^{(0)}(M_h \ell_-) J^{(0)}(-M_h \ell_+) S_3^{(0)}(\ell_+ \ell_-), \quad (5.19)$$

where the function  $\bar{H}_2$  is defined via

$$H_2(z) = \frac{\bar{H}_2(z)}{z(1-z)}. \quad (5.20)$$

The pre-factor 4 in the second term is due to a symmetry relating  $z \leftrightarrow 1-z$ , and the fact that there are two equal contributions from the two collinear directions. The factorisation formula (5.19) is problematic, because the second and third term diverge in the limits  $z \rightarrow 0$  and  $\ell_\pm \rightarrow \infty$ , respectively. Before we show how to solve this problem with the RBS, we want to give the expressions for the component functions up to two-loop order.

The hard matching coefficient  $H_1^{(0)}$  is given by

$$H_1^{(0)} = \delta_{ab} T_F \frac{y_{b,0}}{\sqrt{2}} \frac{\alpha_{s,0}}{\pi} \left[ H_{1,0}^{(0)} + \frac{\alpha_{s,0}}{4\pi} H_{1,1}^{(0)} + \dots \right], \quad (5.21)$$

with

$$H_{1,0}^{(0)} = (-M_h^2 - i0)^{-\epsilon} e^{\epsilon\gamma_E} (1-3\epsilon) \frac{2\Gamma(1+\epsilon)\Gamma^2(-\epsilon)}{\Gamma(3-2\epsilon)},$$

$$H_{1,1}^{(0)} = (-M_h^2 - i0)^{-2\epsilon} \left\{ C_F \left[ -\frac{1}{2\epsilon^4} + \frac{3}{2\epsilon^3} - \frac{5\pi^2}{12\epsilon^2} - \frac{1}{\epsilon} \left( \frac{29\zeta_3}{3} + \frac{3\pi^2}{4} + 12 \right) - 72 - \pi^2 - 19\zeta_3 - \frac{3\pi^4}{16} \right] + C_A \left[ -\frac{3}{2\epsilon^4} + \frac{1}{\epsilon^2} \left( 5 + \frac{7\pi^2}{12} \right) + \frac{18\zeta_3 + 14}{\epsilon} + 20 - \frac{2\pi^2}{3} + 18\zeta_3 + \frac{73\pi^4}{240} \right] \right\}. \quad (5.22)$$

Similarly, we find

$$H_2^{(0)}(z) = \frac{y_{b,0}}{\sqrt{2}} \left[ H_{2,0}^{(0)}(z) + \frac{\alpha_{s,0}}{4\pi} H_{2,1}^{(0)}(z) + \dots \right], \quad (5.23)$$

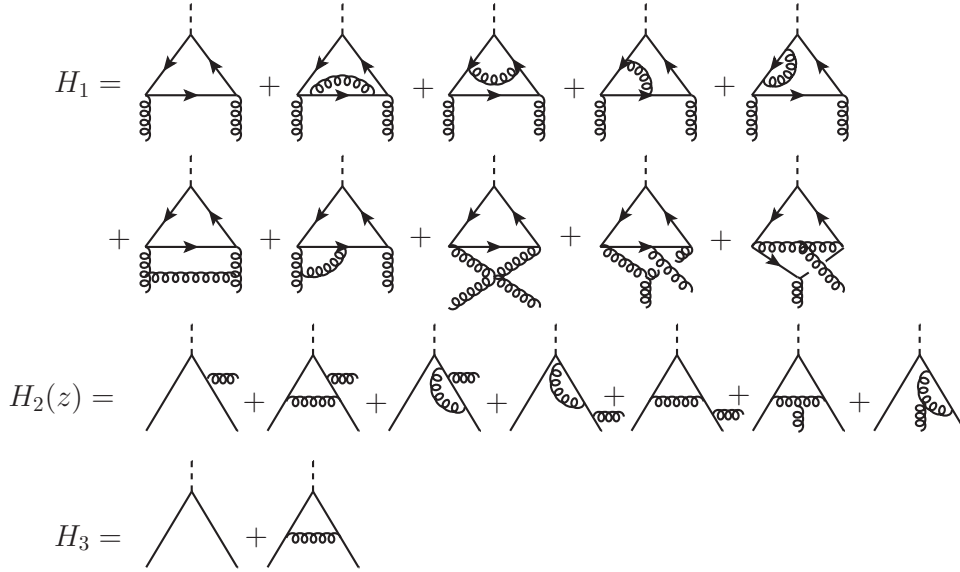


Figure 5.6: Feynman diagrams contributing to the hard matching coefficients  $H_i$ ,  $i = 1, 2, 3$ . Note that we omit mirror diagrams in the rows for  $H_1$  and  $H_2$ .

with

$$\begin{aligned}
 H_{2,0}^{(0)}(z) &= \frac{1}{z} + \frac{1}{1-z}, \\
 H_{2,1}^{(0)}(z) &= (-M_h^2 - i0)^{-\epsilon} e^{\epsilon\gamma_E} \frac{\Gamma(1+\epsilon)\Gamma^2(-\epsilon)}{\Gamma(2-2\epsilon)} \\
 &\quad \times \left\{ C_F \left[ \frac{2-4\epsilon-\epsilon^2}{z^{1+\epsilon}} - \frac{2(1-\epsilon)^2}{z} - 2(1-2\epsilon-\epsilon^2) \frac{1-z^{-\epsilon}}{1-z} \right] \right. \\
 &\quad \left. - C_A \left[ \frac{2-4\epsilon-\epsilon^2}{z^{1+\epsilon}} - \left( 2(1-2\epsilon-\epsilon^2) + \frac{\epsilon^2}{1-\epsilon} \right) \frac{1-z^{-\epsilon}}{1-z} \right] + (z \rightarrow 1-z) \right\}, \tag{5.24}
 \end{aligned}$$

and

$$H_3^{(0)} = -\frac{y_{b,0}}{\sqrt{2}} \left[ 1 - \frac{C_F \alpha_{s,0}}{4\pi} (-M_h^2 - i0)^{-\epsilon} e^{\epsilon\gamma_E} (1-\epsilon)^2 \frac{2\Gamma(1+\epsilon)\Gamma^2(-\epsilon)}{\Gamma(2-2\epsilon)} \right] \tag{5.25}$$

for the hard coefficients of the second and third term of the factorisation theorem. Note that  $H_3$  is the same as in the  $h \rightarrow \gamma\gamma$  process. Feynman diagrams contributing to the three hard matching coefficients are portrayed in figure 5.6. The bare soft function of the first term is  $S_1^{(0)} = m_{b,0}$  and is exact to all orders of perturbation theory. The soft function of the second term reads

$$\begin{aligned}
 S_2^{(0)}(z) &= m_{b,0} T_F \delta_{ab} \frac{\alpha_{s,0}}{4\pi} \left\{ 2e^{\epsilon\gamma_E} (m_{b,0}^2)^{-\epsilon} \Gamma(\epsilon) \right. \\
 &\quad \left. + \frac{\alpha_{s,0}}{4\pi} (m_{b,0}^2)^{-2\epsilon} \left[ C_F K_F(z) + C_A K_A(z) + (z \rightarrow 1-z) \right] \right\}, \tag{5.26}
 \end{aligned}$$

with

$$\begin{aligned}
K_F(z) &= \frac{1}{\epsilon^2} (2L_z + 3) + \frac{1}{\epsilon} \left( L_z^2 - 2L_z L_{\bar{z}} - \frac{1}{2} - \frac{\pi^2}{3} \right) \\
&\quad + 12 \operatorname{Li}_3(z) + 2(1 - 2z - 2L_z) \operatorname{Li}_2(z) + \frac{L_z^3}{3} + 2[z + L_{\bar{z}}] L_z^2 \\
&\quad + \left( 4 \operatorname{Li}_2(\bar{z}) - L_{\bar{z}} - 1 - 3z - \frac{\pi^2}{3} \right) L_z + 3 + \frac{\pi^2}{3} - 8\zeta_3 + \mathcal{O}(\epsilon), \\
K_A(z) &= \frac{-2L_z}{\epsilon^2} + \frac{1}{\epsilon} \left( -L_z^2 + \frac{1}{2} \right) - 8 \operatorname{Li}_3(z) + 2 \operatorname{Li}_2(z)(z - 2L_{\bar{z}}) - \frac{L_z^3}{3} \\
&\quad - 4L_z^2 L_{\bar{z}} - zL_z^2 + \left( 1 + 2z + \frac{\pi^2}{3} \right) L_z + 1 - \frac{\pi^2}{6} + 8\zeta_3 + \mathcal{O}(\epsilon),
\end{aligned} \tag{5.27}$$

and  $L_z = \ln z$  and  $L_{\bar{z}} = \ln(1 - z)$ .

We calculate the jet function of the third term up to two-loop order. This is needed to predict the large logarithms in the three-loop expression for the form factor based on iteratively solving the RG equations later in section 5.3. Up to NNLO, the jet function reads

$$J^{(0)}(p^2) = 1 + \frac{\alpha_{s,0}}{4\pi} (-p^2 - i0)^{-\epsilon} J_1^{(0)} + \left( \frac{\alpha_{s,0}}{4\pi} \right)^2 (-p^2 - i0)^{-2\epsilon} J_2^{(0)}, \tag{5.28}$$

with

$$\begin{aligned}
J_1^{(0)} &= (C_F - C_A) e^{\epsilon\gamma_E} \frac{\Gamma(1 + \epsilon)\Gamma^2(-\epsilon)}{\Gamma(2 - 2\epsilon)} (2 - 4\epsilon - \epsilon^2) \\
J_2^{(0)} &= C_F^2 K_{FF} + C_F C_A K_{FA} + C_A^2 K_{AA} + C_F T_F n_f K_{Fn_f} + C_A T_F n_f K_{An_f},
\end{aligned} \tag{5.29}$$

where

$$\begin{aligned}
K_{FF} &= \frac{2}{\epsilon^4} - \frac{1}{\epsilon^2} \left( 2 + \frac{\pi^2}{3} \right) - \frac{1}{\epsilon} \left( 4 + \frac{\pi^2}{2} + \frac{46\zeta_3}{3} \right) - \frac{13}{2} - \frac{\pi^2}{6} - 39\zeta_3 + \frac{\pi^4}{5} + \mathcal{O}(\epsilon), \\
K_{FA} &= -\frac{4}{\epsilon^4} + \frac{11}{6\epsilon^3} + \frac{1}{\epsilon^2} \left( \frac{139}{18} + \frac{\pi^2}{2} \right) + \frac{1}{\epsilon} \left( \frac{319}{27} - \frac{\pi^2}{18} + \frac{80\zeta_3}{3} \right) \\
&\quad + \frac{1087}{162} - \frac{83\pi^2}{54} + \frac{485\zeta_3}{18} - \frac{49\pi^4}{360} + \mathcal{O}(\epsilon), \\
K_{AA} &= \frac{2}{\epsilon^4} - \frac{11}{6\epsilon^3} - \frac{1}{\epsilon^2} \left( \frac{103}{18} + \frac{\pi^2}{6} \right) - \frac{1}{\epsilon} \left( \frac{413}{54} - \frac{11\pi^2}{18} + \frac{34\zeta_3}{3} \right) \\
&\quad + \frac{100}{81} + \frac{47\pi^2}{27} + \frac{259\zeta_3}{18} - \frac{23\pi^4}{360} + \mathcal{O}(\epsilon), \\
K_{Fn_f} &= -\frac{2}{3\epsilon^3} - \frac{10}{9\epsilon^2} - \frac{1}{\epsilon} \left( \frac{20}{27} - \frac{\pi^2}{9} \right) + \frac{230}{81} + \frac{5\pi^2}{27} + \frac{64\zeta_3}{9} + \mathcal{O}(\epsilon), \\
K_{An_f} &= \frac{2}{3\epsilon^3} + \frac{10}{9\epsilon^2} + \frac{1}{\epsilon} \left( \frac{11}{27} - \frac{2\pi^2}{9} \right) - \frac{491}{81} - \frac{10\pi^2}{27} - \frac{106\zeta_3}{9} + \mathcal{O}(\epsilon),
\end{aligned} \tag{5.30}$$

with  $T_F = \frac{1}{2}$ , and  $n_f$  denotes the number of active quark flavours. The coefficients  $K_{FF}$  and  $K_{Fn_f}$  are identical to the corresponding coefficients in the photon case derived in [81], but for the remaining coefficients no simple relation between the two jet functions can be found past one-loop order.

As has been explained before, the soft function features additional soft Wilson lines in the adjoint representation when compared to its abelian counterpart, giving rise to

“tipi-tent” Feynman diagrams (see figure 5.7). Therefore, one-loop corrections include exchanges of gluons between Wilson lines in the fundamental and adjoint representations. Eventually, the soft function reads

$$S_3^{(0)}(w) = -\frac{T_F \delta_{ab} \alpha_{s,0}}{\pi} m_{b,0} \left[ S_a^{(0)}(w) \theta(w - m_{b,0}^2) + S_b^{(0)}(w) \theta(m_{b,0}^2 - w) \right], \quad (5.31)$$

with

$$\begin{aligned} S_a^{(0)}(w) &= \frac{e^{\epsilon\gamma_E}}{\Gamma(1-\epsilon)} (w - m_{b,0}^2)^{-\epsilon} \left[ 1 + \frac{C_F \alpha_{s,0}}{4\pi} 2e^{\epsilon\gamma_E} \frac{3-2\epsilon}{1-2\epsilon} \Gamma(1+\epsilon) \frac{(m_{b,0}^2)^{1-\epsilon}}{w - m_{b,0}^2} \right] \\ &+ \frac{\alpha_{s,0} C_F}{4\pi} \left\{ (w - m_{b,0}^2)^{-2\epsilon} \left[ -\frac{2}{\epsilon^2} + \frac{6}{\epsilon} + \frac{2}{\epsilon} \ln(1-r) + 12 - \frac{\pi^2}{3} \right. \right. \\ &+ \left. \left. \left( 24 - 3\pi^2 + \frac{4\zeta_3}{3} \right) \epsilon \right] + (m_{b,0}^2)^{-2\epsilon} \left[ -2\text{Li}_2(r) + 2(\ln r + 1) \ln(1-r) \right. \right. \\ &\left. \left. - 3 \ln^2(1-r) \right] \right\} + \frac{\alpha_{s,0} C_A}{4\pi} \left\{ (w - m_{b,0}^2)^{-2\epsilon} \left[ \frac{2}{\epsilon^2} - \frac{\pi^2}{3} - \frac{16}{3} \zeta_3 \epsilon \right] \right. \\ &\left. + (m_{b,0}^2)^{-2\epsilon} \left[ 4\text{Li}_2(r) + 2 \ln^2(1-r) \right] \right\}, \\ S_b^{(0)}(w) &= \left( C_F - \frac{C_A}{2} \right) \frac{\alpha_{s,0}}{4\pi} (m_{b,0}^2)^{-2\epsilon} \left[ -\frac{4}{\epsilon} \ln \left( 1 - \frac{1}{r} \right) + 6 \ln^2 \left( 1 - \frac{1}{r} \right) \right], \end{aligned} \quad (5.32)$$

where  $r = m_{b,0}^2/w$ .

Feynman diagrams for the soft and jet functions are shown in figures 5.7 and 5.8, respectively. For the calculation in practice, we adopt light-cone gauge  $\bar{n} \cdot G_n = 0$  for the computation of  $S_2$  and  $J$ , such that the collinear Wilson lines simplify to  $W_n = 1$ . The smaller number of Feynman diagrams and the absence of ghost contributions allows for a more streamlined computation compared to standard Feynman or general  $R_\xi$  gauges. Nonetheless, we have checked the validity of our calculations in a general covariant gauge. The advantages of light-cone gauge come at the cost of introducing a more complicated propagator for the gluons

$$\frac{i}{l^2 + i0} \left( -g^{\mu\nu} + \frac{\bar{n}^\mu l^\nu + \bar{n}^\nu l^\mu}{\bar{n} \cdot l} \right), \quad (5.33)$$

where we do not adopt the Mandelstam-Leibbrandt prescription to regularise the singularity at  $\bar{n} \cdot l = 0$ , see [109] for further details. The two-loop diagrams of the jet function were computed by using partial-fraction decomposition after applying simplifications to the Dirac and Lorentz structures. Each diagram can then be mapped onto a linear combination of scalar two-loop integrals

$$\int d^d l_1 \int d^d l_2 \frac{1}{\prod_{i=1}^{12} \mathcal{D}_i^{a_i}}, \quad (5.34)$$



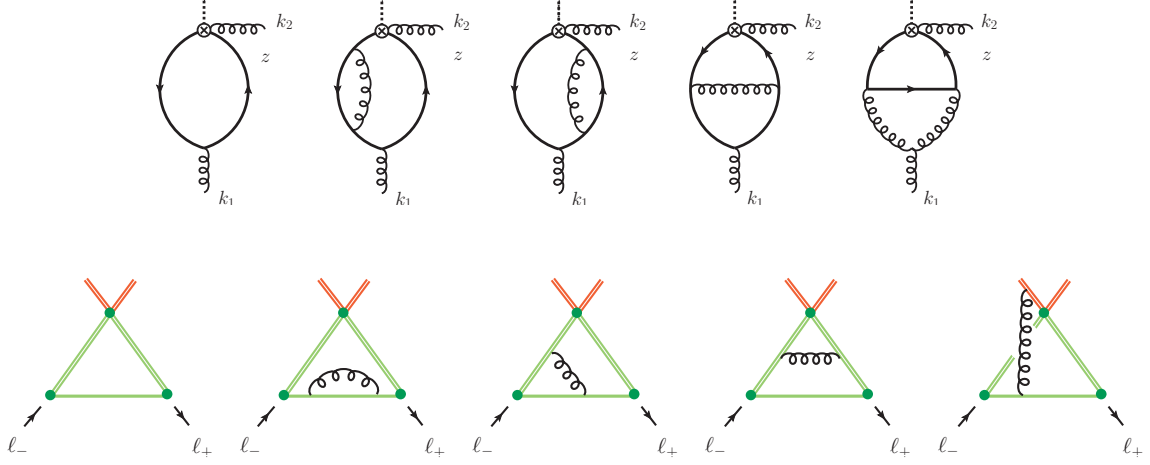


Figure 5.7: Feynman diagrams contributing to the soft functions  $S_2(z)$  (top row) and  $S_3$  (bottom row). The red double lines in  $S_3$  denote soft Wilson lines in the adjoint representation. They are peculiar to the gluon case and lead to “tipi-tent” diagrams.

where the propagators are (omitting the  $-i0$  prescription)

$$\begin{aligned}
 \mathcal{D}_1 &= -l_1^2, & \mathcal{D}_2 &= -l_2^2, & \mathcal{D}_3 &= -(l_1 + l_2)^2, \\
 \mathcal{D}_4 &= -(l_1 + p)^2, & \mathcal{D}_5 &= -(l_2 + p)^2, & \mathcal{D}_6 &= -(l_1 + l_2 + p)^2, \\
 \mathcal{D}_7 &= -(l_1 + p - k)^2, & \mathcal{D}_8 &= -(l_2 + p - k)^2, & \mathcal{D}_9 &= -(l_1 + l_2 + p - k)^2, \\
 \mathcal{D}_{10} &= -\bar{n} \cdot l_1, & \mathcal{D}_{11} &= -\bar{n} \cdot l_2, & \mathcal{D}_{12} &= -\bar{n} \cdot (l_1 + l_2).
 \end{aligned} \tag{5.35}$$

With the help of algebraic relations, we have been able to express all master integrals in terms of integrals encountered in the calculation of the jet function with an external photon [81]. The individual integrals are then either evaluated directly by the method of Feynman parameters or by using dimensional recurrence relations [110,111]. The expansion in  $\epsilon$  was performed using HyperInt [112] and HypExp [113].

#### 5.1.4 Refactorisation theorems and regularisation of endpoint divergences

As has been explained earlier, the bare factorisation theorem (5.19) suffers from endpoint divergences when the integrands of the second and third term approach  $z \rightarrow 0$  and  $l_{\pm} \rightarrow \infty$ , respectively. From the physical point of view, they stem from the region of parameter space where a soft quark becomes collinear or vice versa, hence violating the separation between soft and collinear phase space regions. In principle, one possibility to cure these divergences would be to introduce a new so-called rapidity regulator  $\eta$  related to the rapidity scale  $\nu$  to regularise the singularities. Since regularisation and renormalisation do not commute in general, it is important to first expand in  $\eta$  before expanding in the the dimensional regulator  $\epsilon$ . In the sum of all terms, the dependence of the form factor on the rapidity regulator and scale would cancel among the second and third term. Moreover, this indicates that both terms should have a closely related structure in the sin-

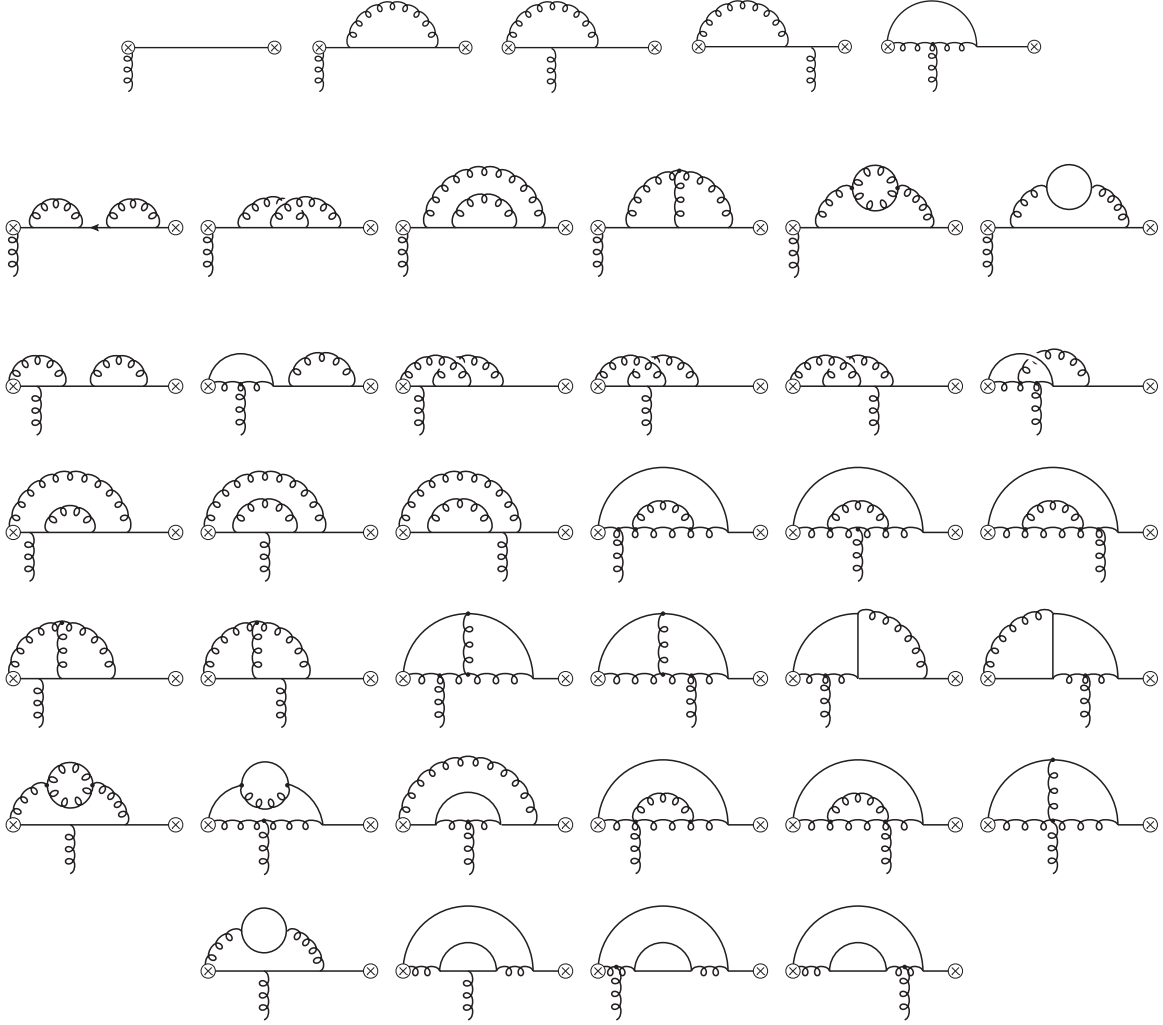


Figure 5.8: Feynman diagrams contributing to the jet function up to two-loop order in light-cone gauge. The left cross corresponds to the spacetime point  $x$ , where the soft momentum  $p_s$  flows out, and the right cross corresponds to the point 0. The fourth diagram in the first row evaluates to zero since it is scaleless. Graphs where the external gluon is emitted off a quark also arise in the calculation of the jet function with an external photon [81] when the radiated gluon is exchanged for a photon.

gular region. Indeed, in [29] two refactorisation conditions were derived, that relate the divergent integrands in the endpoint limit. Following the same arguments, we find

$$\begin{aligned}
 \llbracket \bar{H}_2^{(0)}(z) \rrbracket &= -H_3^{(0)} J^{(0)}(zM_h^2), \\
 \llbracket S_2^{(0)}(z) \rrbracket &= -\frac{1}{2} \int_0^\infty \frac{d\ell_+}{\ell_+} J^{(0)}(-M_h \ell_+) S_3^{(0)}(zM_h \ell_+).
 \end{aligned} \tag{5.36}$$

The symbol  $\llbracket \dots \rrbracket$  signifies that one should only keep the leading terms in the  $z \rightarrow 0$  limit. The situation is portrayed in figure 5.9. In [29], both theorems have been proven to all orders in perturbation theory. An equivalent proof is also possible in the  $gg \rightarrow h$  case. Since it follows the same steps with obvious replacements, we omit to give it here and

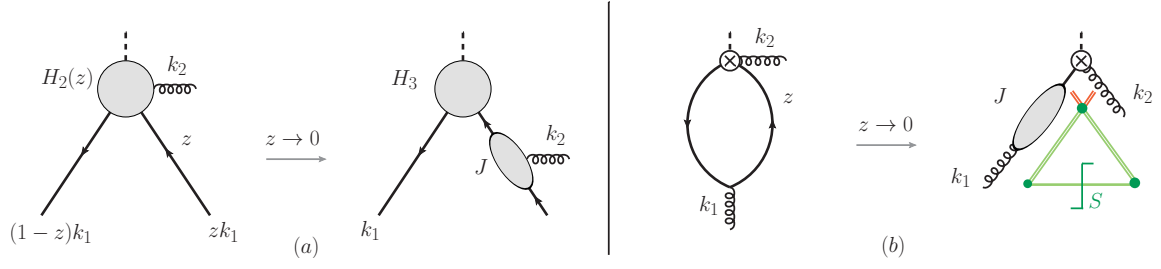


Figure 5.9: Graphical illustration of the refactorisation conditions connecting different objects in the  $gg \rightarrow h$  factorisation formula to all orders in  $\alpha_s$ . The left panel portrays the first equation in (5.36), while the right panel illustrates the second equation.

instead refer to the aforementioned work. Both theorems play a crucial role in deriving the divergence-free factorisation theorem.

With the help of the refactorisation conditions we are now able to derive a version of the factorisation formula that is free of endpoint divergences and UV finite

$$\begin{aligned}
 F_{gg}^{(0)} = & \underbrace{\left( H_1^{(0)} + \Delta H_1^{(0)} \right) S_1}_{T_1^{(0)}} + 4 \int_0^1 \frac{dz}{z} \underbrace{\left( \bar{H}_2^{(0)}(z) S_2^{(0)}(z) - \llbracket \bar{H}_2^{(0)}(z) \rrbracket \llbracket S_2^{(0)}(z) \rrbracket \right)}_{T_2^{(0)}} \\
 & + \underbrace{\lim_{\sigma \rightarrow -1} H_3^{(0)} \int_0^{M_h} \frac{d\ell_-}{\ell_-} \int_0^{\sigma M_h} \frac{d\ell_+}{\ell_+} J^{(0)}(M_h \ell_-) J^{(0)}(-M_h \ell_+) S_3^{(0)}(\ell_- \ell_+) \Big|_{\text{leading power}}}_{T_3^{(0)}}.
 \end{aligned} \tag{5.37}$$

The singularity of the second term is regularised by subtracting the functional behaviour in the problematic region and the third term is regularised by the explicit cutoffs. Note that due to these cutoffs the third term contains some power-suppressed contributions that should be dropped for consistency. Furthermore, the limit in the third term is to be understood in the sense of an analytic continuation, where one evaluates the integral at  $\sigma M_h$  and subsequently follows a path through the complex plane to  $\sigma = -1$ . Removing the divergences in the second term and applying the refactorisation conditions introduces these cutoffs for both convolution integrals in the third term. As shown in figure 5.10, the region  $|\ell_{\pm}| > M_h$  is subtracted twice, hence this  $\infty$ -bin contribution must be added back. Since it only receives contributions above the Higgs mass scale, it is purely hard and can

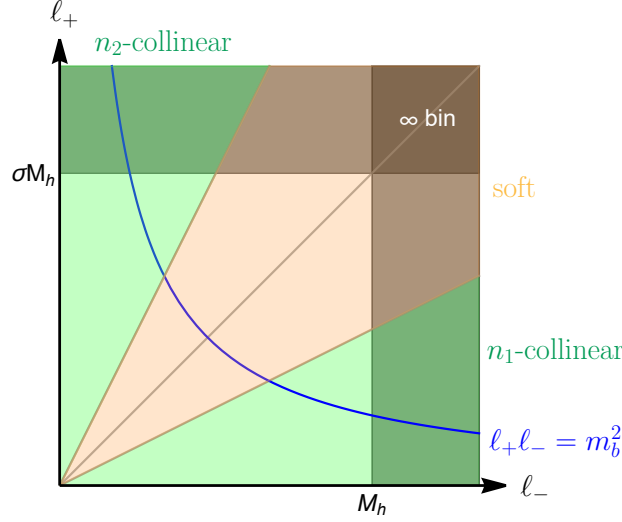


Figure 5.10: Graphical illustration of the impact of the cutoffs on the convolution integrals over  $\ell_+$  and  $\ell_-$  in the last term of the bare factorisation formula (5.36). The “infinity bin” is subtracted twice and must be added back in the form of an extra contribution to the bare Wilson coefficient  $H_1^{(0)}$ .

therefore be seen as an additional input to the hard function  $H_1^{(0)}$ , which is why we call it  $\Delta H_1^{(0)}$ . It is given by

$$\begin{aligned} \Delta H_1^{(0)} &= - \lim_{\sigma \rightarrow -1} H_3 \int_{M_h}^{\infty} \frac{d\ell_-}{\ell_-} \int_{\sigma M_h}^{\infty} \frac{d\ell_+}{\ell_+} J^{(0)}(M_h \ell_-) J^{(0)}(-M_h \ell_+) \frac{S_{\infty}(\ell_+ \ell_-)}{m_b} \\ &= \frac{\alpha_{s,0} T_F \delta_{ab} y_{b,0}}{\pi \sqrt{2}} \left\{ \frac{(-M_h^2)^{-\epsilon} e^{\epsilon \gamma_E}}{\epsilon^2 \Gamma(1-\epsilon)} + \frac{\alpha_{s,0}}{4\pi} (-M_h^2)^{-2\epsilon} e^{2\epsilon \gamma_E} \left[ C_A \frac{\Gamma(-\epsilon) \Gamma(\epsilon) (3-6\epsilon-2\epsilon^2)}{2\epsilon^2 \Gamma(2-2\epsilon)} \right. \right. \\ &\quad \left. \left. + C_F \left( \frac{3\Gamma(\epsilon) \Gamma(-\epsilon)}{\Gamma(2-2\epsilon)} + \frac{(1+\epsilon) \Gamma^2(-\epsilon) + 2\Gamma(-\epsilon) \Gamma(\epsilon) \Gamma(2-2\epsilon)}{2\epsilon^2 \Gamma(1-2\epsilon) \Gamma(2-2\epsilon)} \right) \right] \right\}, \end{aligned} \quad (5.38)$$

and

$$\begin{aligned} S_{\infty}(w) &= - \frac{T_F \delta_{ab} \alpha_{s,0}}{\pi} m_{b,0} \left\{ \frac{e^{\epsilon \gamma_E}}{\Gamma(1-\epsilon)} w^{-\epsilon} + \frac{\alpha_{s,0}}{4\pi} \left[ \left( C_F - \frac{C_A}{2} \right) \frac{4e^{2\epsilon \gamma_E} \Gamma(\epsilon) \Gamma(-\epsilon)}{\Gamma(1-2\epsilon)} \right. \right. \\ &\quad \left. \left. + C_F \frac{2e^{2\epsilon \gamma_E} (1+\epsilon) \Gamma^2(-\epsilon)}{\Gamma(1-2\epsilon) \Gamma(2-2\epsilon)} \right] w^{-2\epsilon} \right\} \theta(w) \end{aligned} \quad (5.39)$$

is the soft function  $S_3(w)$  in the limit where  $w \gg m_b^2$ . This method of removing endpoint divergences by reshuffling terms in the form factor<sup>2</sup> and absorbing the  $\infty$ -bin contributions into hard coefficients is known as refactorisation-based subtraction scheme (RBS) [3].

Note that (5.37) is not infrared (IR) finite because it is calculated using on-shell gluon states. We remove the IR poles by multiplying with the renormalisation factor  $Z_{gg}^{-1}$ , where

<sup>2</sup> The methodology presented here is in fact not limited to  $h \rightarrow GG$ ,  $G = \gamma, g$  processes, but more general. Other instances where it has been used are found in [90,92]

$Z_{gg}$  is the UV renormalisation factor of the two-gluon operator  $O_{gg}$ , defined by  $O_{gg}(\mu) = Z_{gg} O_{gg}^{(0)}$ . In the  $\overline{\text{MS}}$ -scheme, it is given by [114]

$$Z_{gg} = 1 - \frac{\alpha_s(\mu)}{4\pi} \left[ 2C_A \left( \frac{1}{\epsilon^2} - \frac{L_h}{\epsilon} \right) + \frac{\beta_0}{\epsilon} \right] + \mathcal{O}(\alpha_s^2), \quad (5.40)$$

where  $L_h = \ln[(-M_h^2 - i0)/\mu^2]$ .

To show that all UV divergences cancel in the sum of the three terms in (5.37), we first express the bare parameters, i.e. the  $b$ -quark mass, the  $b$ -quark Yukawa coupling and the strong coupling  $\alpha_s$ , in terms of renormalised parameters. The relevant renormalisation conditions are given in appendix A1.1. We use the running parameters  $m_b(\mu)$  and  $y_b(\mu)$  in the overall pre-factor of the form factor. However, in the arguments of logarithms we use the  $b$ -quark pole mass  $m_b$ .

We write the result for the  $gg \rightarrow h$  form factor as

$$Z_{gg}^{-1} F_{gg}^{(0)} = \mathcal{M}_0 Z_{gg}^{-1} \left( T_1^{(0)} + T_2^{(0)} + T_3^{(0)} \right), \quad (5.41)$$

with the overall pre-factor

$$\mathcal{M}_0 = T_F \delta_{ab} \frac{\alpha_s(\mu)}{\pi} \frac{y_b(\mu)}{\sqrt{2}} m_b(\mu). \quad (5.42)$$

The three contributions read

$$\begin{aligned} Z_{gg}^{-1} T_1^{(0)} &= -2 + \frac{\alpha_s(\mu)}{4\pi} \left\{ C_F \left[ -\frac{\pi^2}{3\epsilon^2} + \frac{1}{\epsilon} \left( \frac{2\pi^2 L_h}{3} - 10\zeta_3 \right) - \frac{2\pi^2}{3} L_h^2 + 4(5\zeta_3 + 3) L_h \right. \right. \\ &\quad \left. \left. - 36 - \frac{7\pi^4}{30} \right] + C_A \left[ \frac{\pi^2}{3\epsilon^2} - \frac{1}{\epsilon} \left( \frac{2\pi^2 L_h}{3} - 10\zeta_3 \right) + \left( 2 + \frac{2\pi^2}{3} \right) L_h^2 - 20\zeta_3 L_h \right. \right. \\ &\quad \left. \left. - 12 - \frac{\pi^2}{6} + 18\zeta_3 + \frac{\pi^4}{5} \right] \right\} + \mathcal{O}(\alpha_s^2), \\ Z_{gg}^{-1} T_2^{(0)} &= \frac{\alpha_s(\mu)}{4\pi} \left\{ C_F \left[ \frac{\pi^2}{3\epsilon^2} + \frac{1}{\epsilon} \left( 2\zeta_3 - \frac{2\pi^2 L_h}{3} \right) + \frac{\pi^2}{3} (L_h^2 - L_m^2) + L_h \left( \frac{2\pi^2 L_m}{3} - 4\zeta_3 \right) \right. \right. \\ &\quad \left. \left. + 8\zeta_3 + \frac{13\pi^4}{90} \right] + C_A \left[ -\frac{\pi^2}{3\epsilon^2} + \frac{1}{\epsilon} \left( \frac{2\pi^2 L_h}{3} - 6\zeta_3 \right) - \frac{\pi^2}{3} (L_h^2 - L_m^2) \right. \right. \\ &\quad \left. \left. + L_h \left( 4\zeta_3 - \frac{2\pi^2 L_m}{3} \right) + 8\zeta_3 L_m - \frac{\pi^2}{6} - 6\zeta_3 - \frac{\pi^4}{45} \right] \right\} + \mathcal{O}(\alpha_s^2), \\ Z_{gg}^{-1} T_3^{(0)} &= \frac{L^2}{2} + \frac{\alpha_s(\mu)}{4\pi} \left\{ C_F \left[ \frac{8\zeta_3}{\epsilon} - \frac{L^4}{12} - L^3 + L^2 \left( -3L_m - \frac{\pi^2}{3} + 4 \right) \right. \right. \\ &\quad \left. \left. + \left( 16 - 12L_m + \frac{2\pi^2}{3} \right) L - 16\zeta_3 L_m - 4\zeta_3 - \frac{\pi^4}{9} \right] \right. \\ &\quad \left. + C_A \left[ -\frac{4\zeta_3}{\epsilon} - \frac{5L^4}{12} - L^3 L_m - \frac{L^2 L_m^2}{2} + \left( 1 + \frac{\pi^2}{12} \right) L^2 + 4\zeta_3 (L + 2L_m) \right] \right\} \\ &\quad + \mathcal{O}(\alpha_s^2). \end{aligned} \quad (5.43)$$

The different logarithms appearing in the expressions are

$$L_h = \ln \frac{-M_h^2 - i0}{\mu^2}, \quad L_m = \ln \frac{m_b^2}{\mu^2}, \quad L = L_h - L_m = \ln \frac{-M_h^2 - i0}{m_b^2}, \quad (5.44)$$

with  $m_b$  being the pole mass. It can readily be checked that the remaining  $1/\epsilon$  poles cancel in the sum of the three contributions. Consequently, we find for the full form factor

$$\begin{aligned} Z_{gg}^{-1} F_{gg}^{(0)} = \mathcal{M}_0 & \left\{ -2 + \frac{L^2}{2} + \frac{\alpha_s(\mu)}{4\pi} \left[ C_A \left( -\frac{5L^4}{12} - L^3 L_m - \frac{L^2 L_m^2}{2} + \left( 3 + \frac{5\pi^2}{12} \right) L^2 \right. \right. \right. \\ & \left. \left. + 4LL_m + 2L_m^2 - 12\zeta_3 L - 12 - \frac{\pi^2}{3} + 12\zeta_3 + \frac{8\pi^4}{45} \right) \right. \\ & \left. + C_F \left( -\frac{L^4}{12} - L^3 - 3L_m L^2 + \left( 4 - \frac{2\pi^2}{3} \right) L^2 + \left( 16\zeta_3 + \frac{2\pi^2}{3} + 12 \right) L \right. \right. \\ & \left. \left. + 12L_m - 36 + 4\zeta_3 - \frac{\pi^4}{5} \right) \right] + \mathcal{O}(\alpha_s^2) \left. \right\}. \quad (5.45) \end{aligned}$$

This result agrees with a corresponding expression obtained in [115] after taking into account differences in the IR subtraction schemes. In the limit  $C_A \rightarrow 0$ , and performing some simple replacements in the pre-factor  $\mathcal{M}_0$ , the above result reproduces the two-loop amplitude for  $h \rightarrow \gamma\gamma$  decay obtained in [28].

## 5.2 Renormalisation of the factorisation theorem

In this section, we establish the factorisation formula in terms of renormalised component functions. It is given by

$$\begin{aligned} F_{gg}(\mu) = & \underbrace{\overbrace{H_1(\mu) S_1(\mu)}^{T_1(\mu)}}_{T_1(\mu)} + 4 \underbrace{\int_0^1 \frac{dz}{z} \left( \bar{H}_2(z, \mu) S_2(z, \mu) - \llbracket \bar{H}_2(z, \mu) \rrbracket \llbracket S_2(z, \mu) \rrbracket \right)}_{T_2(\mu)} \\ & + \underbrace{\lim_{\sigma \rightarrow -1} H_3(\mu) \int_0^{M_h} \frac{d\ell_-}{\ell_-} \int_0^{\sigma M_h} \frac{d\ell_+}{\ell_+} J(M_h \ell_-, \mu) J(-M_h \ell_+, \mu) S_3(\ell_- \ell_+, \mu)}_{T_3(\mu)} \Big|_{\text{leading power}}. \quad (5.46) \end{aligned}$$

Its derivation is a highly non-trivial task, since renormalisation does in general not commute with the RBS prescription to remove endpoint divergences. Below, we will show how to manage the calculations to unify both concepts – RBS and renormalisation – and implement them at the same time.

Factorisation in terms of renormalised quantities involves two steps. First, we need to renormalise all component functions separately. In general, the renormalised operator can be obtained from the bare one using

$$O_i(\mu) = Z_{ij} O_j^{(0)}. \quad (5.47)$$

This is technically challenging, because some component functions are instead renormalised in a convolutional sense. Secondly, we need to prove that the subtraction method used to dispose of endpoint divergences between different terms will not generate additional divergences under renormalisation. In the following, we will discuss the renormalisation of the three terms  $T_i$  individually.

### 5.2.1 Renormalisation of $T_3$

We remind the reader that  $T_3$  is the product of  $H_3$  and the time-ordered product of a scalar current and two NLP SCET Lagrangian insertions. The Lagrangian insertions do not need to be renormalised, and the renormalisation of the scalar current  $J_S = h\bar{\chi}_n\chi_{\bar{n}}$  is known from the literature [116]. Its renormalisation factor is given by  $Z_{J_S} = Z_{33}$ , which is known up to three loops. The remaining IR divergences due to the external gluons can be treated using different prescription schemes, including those in references [114, 117], the latter of which is the  $\overline{\text{MS}}$  subtraction scheme which we adopt for our calculation. As a consequence,  $O_3$  is eventually renormalised by

$$O_3(\mu) = Z_{gg}^{-1} Z_{33} O_3, \quad (5.48)$$

where  $Z_{gg}$  is the renormalisation factor of the LEFT operator  $O_{gg}$ . Consequently, the corresponding hard coefficient is renormalised as

$$H_3(\mu) = Z_{33}^{-1} H_3^{(0)} = \frac{y_b(\mu)}{\sqrt{2}} \left[ -1 + \frac{C_F \alpha_s}{4\pi} \left( L_h^2 + 2 - \frac{\pi^2}{6} \right) \right]. \quad (5.49)$$

We collect all trivial renormalisation factors in appendix A1.1. The radiative jet function is renormalised in the convolutional sense by

$$J(p^2, \mu) = \int_0^\infty dx Z_J(p^2, xp^2) J^{(0)}(xp^2). \quad (5.50)$$

Note that different values of  $p^2$  mix under renormalisation. In the photon case, this convolutional renormalisation condition was derived using the fact that the radiative photon jet function appears along the leading-order light-cone distribution amplitude (LCDA) for the factorisation formula of the  $B^- \rightarrow \gamma \ell^- \bar{\nu}$  decay amplitude [118–120]. At the one-loop order, the bare jet function can be obtained from the radiative photon jet function in [28] by a replacement of colour factors  $C_F \rightarrow C_F - C_A$ . Therefore one might expect this relation to hold for the renormalisation factor as well. Since the jet function at leading order is equal

to 1, and the renormalisation factor involves a kernel that integrates to zero when convoluted with constant functions, the question of whether a simple replacement is viable cannot be answered at order  $\mathcal{O}(\alpha_s)$ . However, from the requirement of scale invariance of  $T_3$ , we can extract the correct renormalisation factor and find that the convolution kernel is accompanied by a factor of  $C_F - C_A/2$  instead of  $C_F - C_A$ , such that the renormalisation factor is given by

$$Z_J(y p^2, x p^2) = \left[ 1 + \frac{(C_F - C_A)\alpha_s}{4\pi} \left( -\frac{2}{\epsilon^2} + \frac{2}{\epsilon} \ln \frac{-p^2}{\mu^2} \right) \right] \delta(y - x) + \frac{(C_F - C_A/2)\alpha_s}{2\pi\epsilon} \Gamma(y, x), \quad (5.51)$$

where

$$\Gamma(y, x) = \left[ \frac{\theta(x - y)}{x(x - y)} + \frac{\theta(y - x)}{y(y - x)} \right]_+ \quad (5.52)$$

is the Lange-Neubert kernel as introduced in [120]. The plus-distribution is defined such that when  $\Gamma(x, y)$  is to be integrated with a function  $f(x)$ , one has to replace  $f(x) \rightarrow f(x) - f(y)$  under the integral. With (5.50) and (5.51) we find at next-to-leading order (NLO)

$$J(p^2, \mu) = 1 + \frac{\alpha_s}{4\pi} (C_F - C_A) \left[ \ln^2 \frac{-p^2}{\mu^2} - 1 - \frac{\pi^2}{6} \right] + \mathcal{O}(\alpha_s^2). \quad (5.53)$$

Similarly to the jet function, the soft function is renormalised by a convolution

$$S_3(w, \mu) = \int_0^\infty dw' Z_S(w, w') S_3^{(0)}(w'). \quad (5.54)$$

In the renormalisation of the photon factorisation formula, a conjecture based on the RG evolution of  $T_{3,\gamma}$  was used to derive the soft function renormalisation factor [29]. Iteratively solving the RG equations, the leading logarithmic terms in the three-loop amplitude were then predicted and confirmed against conventional QCD calculations [77]. Later, Bodwin et al. verified the conjecture by a detailed computation from first principles in [121]. Here, we apply the same arguments to derive the following relation of the jet and soft function renormalisation factors

$$Z_S(w, w') = \frac{w}{w'} Z_{33} Z_{gg}^{-1} \int_0^\infty \frac{dx}{x} Z_J^{-1} \left( \frac{M_h w'}{x \ell_+}, \frac{M_h w}{\ell_+} \right) Z_J^{-1} (-x M_h \ell_+, -M_h \ell_+). \quad (5.55)$$

Consequently, we can read off  $Z_S$  as

$$Z_S(w, w') = \delta(w - w') + \frac{\alpha_s}{4\pi} \left\{ \left[ (C_F - C_A) \left( \frac{2}{\epsilon^2} - \frac{2}{\epsilon} \ln \frac{\omega}{\mu^2} \right) - \frac{3C_F - \beta_0}{\epsilon} \right] \delta(w - w') - \frac{4(C_F - C_A/2)}{\epsilon} w \Gamma(w, w') \right\}. \quad (5.56)$$

Through its dependence on the jet function renormalisation factor, in the soft function renormalisation factor the Lange-Neubert kernel is accompanied by a colour factor of



$C_F - C_A/2$  as well. This plays a crucial role even at order  $\mathcal{O}(\alpha_s)$  because the leading order soft function is not a constant – in contrast to the jet function. Since the soft function has support for values below the threshold  $m_b^2$ , the convolution of the kernel with the leading order (LO) function must remove all divergences of the soft function below  $m_b^2$ . Therefore, the colour factor of the convolution kernel must be the same as that of  $S_b$  in (5.32). Using (5.54) and (5.56), we find

$$S_3(w, \mu) = -\frac{T_F \delta_{ab} \alpha_s}{\pi} m_b(\mu) [S_a(w, \mu) \theta(w - m_b^2(\mu)) + S_b(w, \mu) \theta(m_b^2(\mu) - w)], \quad (5.57)$$

with

$$\begin{aligned} S_a(w, \mu) &= 1 + \frac{\alpha_s}{4\pi} \left\{ C_F \left[ -L_w^2 - 6L_w + 12 - \frac{\pi^2}{2} + 2\text{Li}_2\left(\frac{1}{\hat{w}}\right) - 4\ln\left(1 - \frac{1}{\hat{w}}\right) \left(\frac{3}{2}\ln\hat{w} \right. \right. \right. \\ &\quad \left. \left. + \ln\left(1 - \frac{1}{\hat{w}}\right) + L_m + 1\right) \right] + C_A \left[ L_w^2 - \frac{\pi^2}{6} + 2\text{Li}_2\left(\frac{1}{\hat{w}}\right) + 2\ln\left(1 - \frac{1}{\hat{w}}\right) \left(\ln\hat{w} \right. \right. \\ &\quad \left. \left. + \ln\left(1 - \frac{1}{\hat{w}}\right) + L_m\right) \right] \right\}, \\ S_b(w, \mu) &= \frac{\alpha_s}{4\pi} \left( C_F - \frac{C_A}{2} \right) 4\ln(1 - \hat{w}) (\ln(1 - \hat{w}) + L_m), \end{aligned} \quad (5.58)$$

where  $L_w = \ln(w/\mu^2)$  and  $\hat{w} = w/m_b^2$ .

### 5.2.2 Renormalisation of $T_2$

The renormalisation of  $T_2$  is more involved than that of  $T_3$ . Because  $O_2(z, \mu)$  and  $O_1$  share the same final states and same quantum numbers, the corresponding soft functions will inevitably mix under renormalisation. While in principle it is possible to determine the diagonal – i.e., non-mixing – renormalisation factors by studying the UV behaviour of similar diagrams as in  $h \rightarrow \gamma\gamma$ , we instead use the refactorisation theorems (5.36) and consistency conditions.

From the first refactorisation theorem (5.36) we see that  $Z_{33}Z_J^{-1}$  renormalises  $[[\bar{H}_2]]$ . We denote the combination  $Z_{33}Z_J^{-1}$  by  $[[Z_{22}^{-1}]]$  and find that up to order  $\mathcal{O}(\alpha_s)$  it reads

$$\begin{aligned} [[\bar{H}_2(z, \mu)]] &= \int_0^\infty dz' [[Z_{22}^{-1}(z, z')]] [[\bar{H}_2^{(0)}(z')] ] \\ &= 1 + \frac{\alpha_s}{4\pi} \left[ C_F (2L_h L_z + L_z^2 - 3) + C_A \left( -L_h^2 - 2L_h L_z - L_z^2 + 1 + \frac{\pi^2}{6} \right) \right] \\ &\quad + \mathcal{O}(\alpha_s^2). \end{aligned} \quad (5.59)$$

To keep the expressions compact we have abbreviated  $L_z = \ln z$  and  $L_{\bar{z}} = \ln(1 - z)$ . The diagonal renormalisation factor  $Z_{22}^{-1}$ , cannot be directly derived by previous results or refactorisation theorems. However, we can deduce it following the observation that  $[[Z_{22}^{-1}]]$  contains the leading terms of  $Z_{22}^{-1}$  in the  $z \rightarrow 0$  limits, as well as using the requirement

that  $Z_{22}^{-1}$  must be symmetric under the exchange  $z \leftrightarrow 1 - z$ . Based on these two properties, we obtain

$$\begin{aligned}
 Z_{22}^{-1}(z, z') = & \delta(z - z') + \frac{\alpha_s}{4\pi} \left\{ \left[ (C_F - C_A) \frac{2 \ln z + 2 \ln(1 - z) + 3}{\epsilon} \right. \right. \\
 & + C_A \left( \frac{2}{\epsilon^2} - \frac{2L_h - 3}{\epsilon} \right) \left. \right] \delta(z - z') + \frac{2(C_F - C_A/2)}{\epsilon} z(1 - z) \\
 & \times \left[ \frac{1}{z'(1 - z)} \frac{\theta(z' - z)}{(z' - z)} + \frac{1}{z(1 - z')} \frac{\theta(z - z')}{(z - z')} \right]_+ \left. \right\}. \tag{5.60}
 \end{aligned}$$

The renormalised  $\bar{H}_2(z, \mu)$  then reads

$$\begin{aligned}
 \bar{H}_2(z, \mu) = & \int_0^1 dz' Z_{22}^{-1}(z, z') \bar{H}_2^{(0)}(z') \\
 = & 1 + \frac{\alpha_s}{4\pi} \left\{ C_F \left[ 2L_h(L_z + L_{\bar{z}}) + L_z^2 + L_{\bar{z}}^2 - 3 \right] \right. \\
 & \left. + C_A \left[ -L_h^2 - 2L_h(L_z + L_{\bar{z}}) - L_z^2 - L_{\bar{z}}^2 + 1 + \frac{\pi^2}{6} \right] \right\} + \mathcal{O}(\alpha_s^2). \tag{5.61}
 \end{aligned}$$

The full form factor must be multiplied with an additional renormalisation factor  $Z_{gg}^{-1}$ . Therefore in the renormalisation condition for the soft function  $S_2$  this factor also appears. Additionally,  $Z_{22}^{-1}$  depends on the hard scale  $M_h$  via the logarithm  $L_h$ , but the soft function should only depend on the soft scale  $m_b$ . This is indeed the case when we combine the two renormalisation factors

$$\begin{aligned}
 Z_{gg}^{-1} Z_{22}(z, z') = & \delta(z - z') + \frac{\alpha_s}{4\pi} \left\{ -\frac{3C_F - \beta_0 + 2(C_F - C_A)(\ln z + \ln(1 - z))}{\epsilon} \delta(z - z') \right. \\
 & \left. - \frac{2(C_F - C_A/2)}{\epsilon} z(1 - z) \left[ \frac{1}{z'(1 - z)} \frac{\theta(z' - z)}{(z' - z)} + \frac{1}{z(1 - z')} \frac{\theta(z - z')}{(z - z')} \right]_+ \right\}. \tag{5.62}
 \end{aligned}$$

Furthermore, in analogy with the photon case, we find that  $S_1$  and  $S_2$  mix under renormalisation. Hence, the renormalisation condition takes the form

$$S_2(z, \mu) = Z_{gg}^{-1} \left[ \int_0^1 dz' Z_{22}(z, z') S_2^{(0)}(z') + Z_{21}(z) S_1^{(0)} \right], \tag{5.63}$$

with

$$\begin{aligned}
 Z_{gg}^{-1} Z_{21}(z) = & \frac{T_F \delta_{ab} \alpha_s}{2\pi} \left\{ -\frac{1}{\epsilon} + \frac{\alpha_s}{4\pi} \left[ (C_F - C_A) \left( \frac{L_z + L_{\bar{z}}}{\epsilon^2} - \frac{L_z^2 + L_{\bar{z}}^2 - 1}{2\epsilon} \right) \right. \right. \\
 & \left. \left. + C_F \frac{2L_z L_{\bar{z}} - 6 + \pi^2/3}{\epsilon} \right] \right\}. \tag{5.64}
 \end{aligned}$$

For the renormalised soft function, we then obtain (with  $\bar{z} \equiv 1 - z$ )

$$S_2(z, \mu) = \frac{T_F \delta_{ab} \alpha_s}{2\pi} m_b(\mu) \left\{ -L_m + \frac{\alpha_s}{4\pi} \left[ C_F \left( L_m^2 (L_z + L_{\bar{z}} + 3) - L_m \left( L_z^2 + L_{\bar{z}}^2 - 4L_z L_{\bar{z}} + 11 - \frac{2\pi^2}{3} \right) + F(z) + F(\bar{z}) \right) + C_A \left( -L_m^2 (L_z + L_{\bar{z}}) + L_m (L_z^2 + L_{\bar{z}}^2 - 1) + G(z) + G(\bar{z}) \right) \right] + \mathcal{O}(\alpha_s^2) \right\}, \quad (5.65)$$

with

$$\begin{aligned} F(z) &= \frac{L_z^3}{6} + L_z^2 (z - L_{\bar{z}}) - L_z \left( -L_{\bar{z}} + \frac{1+3z}{2} \right) - (4L_z + 2z) \text{Li}_2(z) \\ &\quad + 6 \text{Li}_3(z) + \frac{11}{2} - 4\zeta_3, \\ G(z) &= -\frac{L_z^3}{6} - \frac{z}{2} L_z^2 + \frac{1}{2} (1 + 2z - L_{\bar{z}}) L_z + (2L_z - (1 - z)) \text{Li}_2(z) \\ &\quad - 4 \text{Li}_3(z) + \frac{1}{2} + 4\zeta_3. \end{aligned} \quad (5.66)$$

### 5.2.3 Renormalisation of $T_1$

The renormalisation of the first term  $T_1$  in (5.46) turns out to be the most involved despite its simple definition in terms of bare objects. Especially the hard coefficient of the renormalised operator receives multiple non-trivial contributions. In addition to the renormalised hard matching coefficient itself and the renormalisation of the  $\infty$ -bin subtraction  $\Delta H_1$ , further terms emerge from first renormalising the component function before regularising the endpoint divergences in the terms  $T_2(\mu)$  and  $T_3(\mu)$ , where instead one should renormalise the endpoint divergence-free objects. We will call these additional contributions *mismatch* contributions, because they arise from non-matching limits in the convolution integrals. Since they are of purely hard nature, we will absorb them into a redefinition of the hard function  $H_1(\mu)$ .

Eventually, the renormalisation condition for the hard function  $H_1(\mu)$  is given by

$$\begin{aligned} H_1(\mu) &= Z_{11}^{-1} \left( H_1^{(0)} + \Delta H_1^{(0)} - \delta H_1 - \delta' H_1 \right) \\ &\quad + 4 \int_0^1 \frac{dz}{z} \left( \bar{H}_2^{(0)}(z) Z_{21}^{-1}(z) - \llbracket \bar{H}_2^{(0)}(z) \rrbracket \llbracket Z_{21}^{-1}(z) \rrbracket \right). \end{aligned} \quad (5.67)$$

The counterterms  $\delta H_1$  and  $\delta' H_1$  account for the mismatch contributions in  $T_2$  and  $T_3$  [29]. They are a special feature of the process under consideration for which the term  $T_3$  involves a double convolution over jet and soft functions. In other applications of the RBS scheme (see e.g. [90]) such subtractions are not required. Below, we show explicitly, how to derive equation (5.67).

Starting from the basic equation for the renormalisation of the amplitude

$$\begin{aligned} Z_{gg}^{-1}(T_1^{(0)} + T_2^{(0)} + T_3^{(0)}) &= T_1(\mu) + T_2(\mu) + T_3(\mu), \\ \text{with } T_1^{(0)} &= (H_1^{(0)} + \Delta H_1^{(0)})S_1^{(0)}, \quad T_1(\mu) = H_1(\mu)S_1(\mu), \end{aligned} \quad (5.68)$$

we see that  $H_1(\mu)$  receives contributions from  $T_2(\mu) - Z_{gg}^{-1}T_2^{(0)}$  and  $T_3(\mu) - Z_{gg}^{-1}T_3^{(0)}$ . For the second of these two terms, we find, expressing  $T_3(\mu)$  in terms of bare quantities,

$$\begin{aligned} \delta T_3 \equiv T_3(\mu) - Z_{gg}^{-1}T_3^{(0)} &= Z_{33}^{-1}H_3^{(0)} \left( \int_0^{M_h} \frac{d\ell_-}{\ell_-} \int_0^{\sigma M_h} \frac{d\ell_+}{\ell_+} \int_0^\infty d\ell'_- \int_0^\infty d\ell'_+ - \int_0^\infty \frac{d\ell_-}{\ell_-} \int_0^\infty \frac{d\ell_+}{\ell_+} \int_0^{M_h} d\ell'_- \int_0^{\sigma M_h} d\ell'_+ \right) \\ &\times \int_0^\infty dw S_3^{(0)}(w) J^{(0)}(M_h \ell'_-) J^{(0)}(-M_h \ell'_+) Z_J(\ell_-, \ell'_-) Z_J(\ell_+, \ell'_+) Z_S(\ell_- \ell_+, w), \end{aligned} \quad (5.69)$$

where the orthogonality condition (5.55) has been used. This term is non-vanishing because the upper integration limits do not match for the  $\ell_\pm^{(\prime)}$  integrals. Furthermore,  $\delta T_3$  is generally sensitive to the low scale of the process  $m_b$ , though not at the lowest order in perturbation theory. We proceed equally for the mismatch terms in  $T_2$  and define

$$\begin{aligned} \tilde{\delta} T_2 \equiv T_2(\mu) - Z_{gg}^{-1}T_2^{(0)} &= 4 \int_0^1 \frac{dz}{z} \left( \bar{H}_2(z, \mu) Z_{21}(z) - \llbracket \bar{H}_2(z, \mu) \rrbracket \llbracket Z_{21}(z) \rrbracket \right) S_1^{(0)} \\ &- 4 Z_{gg}^{-1} \left( \int_0^1 \frac{dz}{z} \int_0^\infty dz' - \int_0^\infty \frac{dz}{z} \int_0^1 dz' \right) \llbracket \bar{H}_2(z, \mu) \rrbracket \llbracket Z_{22}(z, z') \rrbracket \llbracket S_2^{(0)}(z') \rrbracket. \end{aligned} \quad (5.70)$$

Only the expression in the second line in this equation is of the same nature as  $\delta T_3$ , which is why we will call it  $\delta T_2$ . The first line is related to a mixing contribution, which we will discuss later. Using the refactorisation conditions (5.36), the corresponding relation between renormalisation factors, as well as the orthogonality relation (5.55), we can rewrite

$$\begin{aligned} \delta T_2 &= -4 Z_{gg}^{-1} \left( \int_0^1 \frac{dz}{z} \int_0^\infty dz' - \int_0^\infty \frac{dz}{z} \int_0^1 dz' \right) \llbracket \bar{H}_2^{(0)}(z, \mu) \rrbracket \llbracket Z_{22}(z, z') \rrbracket \llbracket S_2^{(0)}(z') \rrbracket \\ &= \left[ -Z_{33}^{-1} H_3^{(0)} \left( \int_0^{M_h} \frac{d\ell_-}{\ell_-} \int_0^{\sigma M_h} \frac{d\ell_+}{\ell_+} \int_0^\infty d\ell'_- \int_0^\infty d\ell'_+ - \int_0^\infty \frac{d\ell_-}{\ell_-} \int_0^\infty \frac{d\ell_+}{\ell_+} \int_0^{M_h} d\ell'_- \int_0^{\sigma M_h} d\ell'_+ \right) \right. \\ &\quad \left. - Z_{33}^{-1} H_3^{(0)} \left( \int_0^\infty \frac{d\ell_-}{\ell_-} \int_0^{\sigma M_h} \frac{d\ell_+}{\ell_+} \int_0^\infty d\ell'_- \int_0^\infty d\ell'_+ - \int_0^\infty \frac{d\ell_-}{\ell_-} \int_0^\infty \frac{d\ell_+}{\ell_+} \int_0^{M_h} d\ell'_- \int_0^{\sigma M_h} d\ell'_+ \right) \right] \\ &\times \int_0^\infty dw S_3^{(0)}(w) J^{(0)}(M_h \ell'_-) J^{(0)}(-M_h \ell'_+) Z_J(\ell_-, \ell'_-) Z_J(\ell_+, \ell'_+) Z_S(\ell_- \ell_+, w). \end{aligned} \quad (5.71)$$

It is obvious that, in general,  $\delta T_2$  is also sensitive to the low scale. Note, however that the integrands in  $\delta T_2$  (5.71) and  $\delta T_3$  (5.69) are the same. Hence, the sum of those two terms will only alter the respective integration limits. We define  $\delta' H_1 = \delta T_2 + \delta T_3$ , and find

$$\begin{aligned} \delta H'_1 S_1^{(0)} &= -Z_{33}^{-1} H_3^{(0)} \left( \int_{M_h}^{\infty} \frac{d\ell_-}{\ell_-} \int_{\sigma M_h}^{\infty} \frac{d\ell_+}{\ell_+} \int_0^{\infty} d\ell'_- \int_0^{\infty} d\ell'_+ - \int_0^{\infty} \frac{d\ell_-}{\ell_-} \int_0^{\infty} \frac{d\ell_+}{\ell_+} \int_{M_h}^{\infty} d\ell'_- \int_{\sigma M_h}^{\infty} d\ell'_+ \right) \\ &\quad \times \int_0^{\infty} d\omega S_{\infty}^{(0)}(\omega) J^{(0)}(M_h \ell'_-) J^{(0)}(-M_h \ell'_+) Z_J(\ell_-, \ell'_-) Z_J(\ell_+, \ell'_+) Z_S(\ell_- \ell_+, \omega). \end{aligned} \quad (5.72)$$

This replacement simplifies the computation and is justified, because  $\delta H'_1 S_1^{(0)}$  (5.72) is a purely hard contribution, and hence the difference between  $S_{\infty}$  and  $S_3$  is power suppressed in this regime.

The first line in the definition of  $\tilde{\delta T}_2$  (5.70) can be split into a true mixing term dependent only on bare hard functions  $\bar{H}_2$  and  $[\bar{H}_2]$ , and another mismatch contribution. To work out this splitting, we first define the inverse of the off-diagonal renormalisation factor as

$$Z_{21}^{-1}(z) = - \int_0^1 dz' Z_{22}^{-1}(z, z') Z_{21}(z') Z_{11}^{-1} \quad (5.73)$$

in accordance with [29]. Its expression can be found in appendix AI.1. This allows us to rewrite

$$\begin{aligned} \tilde{\delta T}_2 - \delta T_2 &= 4 \int_0^1 \frac{dz}{z} \left( \bar{H}_2(z, \mu) Z_{21}(z) - [\bar{H}_2(z, \mu)] [Z_{21}(z)] \right) S_1^{(0)} \\ &= -4 \int_0^1 \frac{dz}{z} \left[ \bar{H}_2^{(0)}(z) Z_{21}^{-1}(z) - [\bar{H}_2^{(0)}(z)] [Z_{21}^{-1}(z)] \right] S_1(\mu) \\ &\quad - 4 \left( \int_0^{\infty} \frac{dz}{z} \int_0^1 dz' - \int_0^1 \frac{dz}{z} \int_0^{\infty} dz' \right) [\bar{H}_2^{(0)}(z)] [Z_{22}^{-1}(z, z')] [Z_{21}(z')] Z_{11}^{-1} S_1(\mu). \end{aligned} \quad (5.74)$$

This is again a purely hard contribution. Since the first term only depends on bare hard coefficients, it is considered a true mixing effect. On the other hand, the second one is a true mismatch contribution due to an incongruousness of integration limits. Hence, we define

$$-\delta H_1 = -4 \left( \int_0^{\infty} \frac{dz}{z} \int_0^1 dz' - \int_0^1 \frac{dz}{z} \int_0^{\infty} dz' \right) [\bar{H}_2^{(0)}(z)] [Z_{22}^{-1}(z, z')] [Z_{21}(z')]. \quad (5.75)$$

To summarise this discussion, we have seen that since the RBS does not commute with renormalisation, terms arise from the difference of  $T_2(\mu) + T_3(\mu) - Z_{gg}^{-1}(T_2 + T_3)$ , which is not equal to 0. However, these additional contributions, called mismatch terms, are of purely hard nature, and hence they can be absorbed into a redefinition of the renormalised

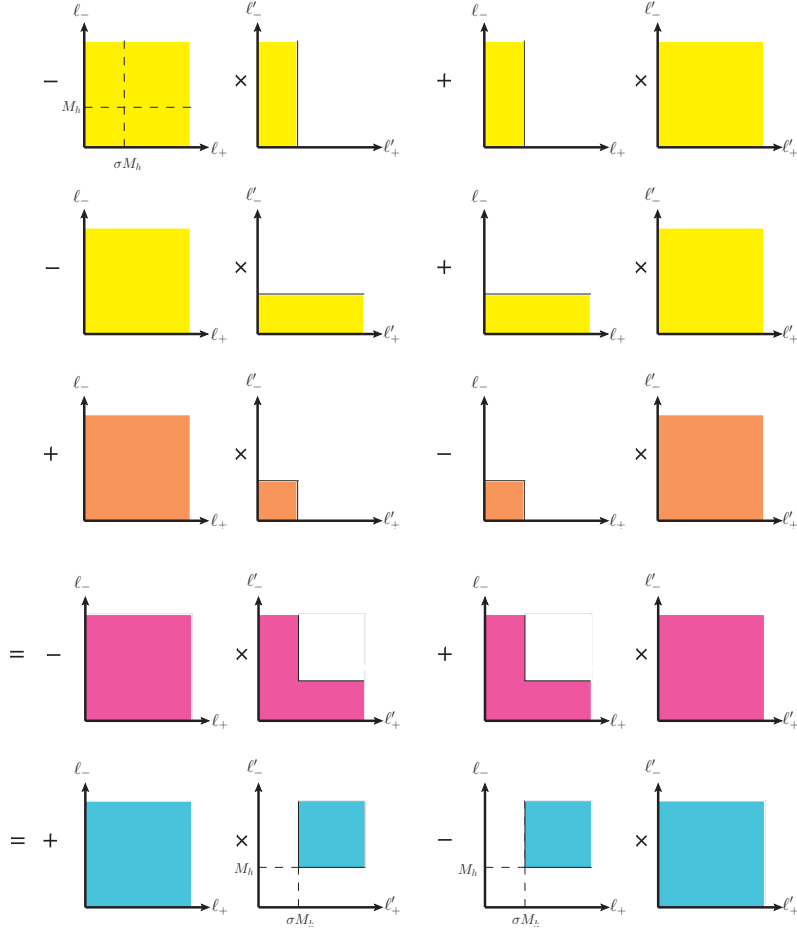


Figure 5.11: The phase space of mismatch in  $T_2$  (yellow) and  $T_3$  (orange). The combination of those two is given by the purple region. It can be flipped into the blue region, which is purely hard.

hard matching  $H_1(\mu)$  (5.67). The mismatch terms are four-fold integrals over soft and jet functions. The situation is shown graphically in figure 5.11. The yellow and orange region corresponds to  $\delta T_2$  and  $\delta T_3$ , respectively. Adding them up, the resulting integration in the purple region can be further flipped into the blue region, because the four-fold integration in the entire region is scaleless.

Going one step further, we note that  $\Delta H_1^{(0)}$  can be written as

$$\begin{aligned}
 Z_{gg}^{-1} \Delta H_1^{(0)} S_1^{(0)} &= -H_3^{(0)} Z_{33}^{-1} \int_{M_h}^{\infty} d\ell_- \int_0^{\infty} \frac{d\ell'_-}{\ell'_-} \int_{\sigma M_h}^{\infty} d\ell_+ \int_0^{\infty} \frac{d\ell'_+}{\ell'_+} \\
 &\quad \times \int_0^{\infty} dw S_3^{(0)}(w) J^{(0)}(-M_h \ell_+) J^{(0)}(M_h \ell_-) \\
 &\quad \times Z_J(M_h \ell'_-, M_h \ell_-) Z_J(-M_h \ell'_+, -M_h \ell_+) Z_S(\ell'_+ \ell'_-, w),
 \end{aligned} \tag{5.76}$$

by the means of the refactorisation conditions (5.36), and thus features the same integrands as the integrals in  $\delta' H_1$ . Comparing the two contributions, we see that  $\Delta H_1$  is exactly

cancelled by the second blue region in figure 5.11. As a result, the renormalised coefficient  $H_1(\mu)$  can be expressed as

$$H_1(\mu) = Z_{11}^{-1} H_1^{(0)} + 4 \int_0^1 \frac{dz}{z} \left( \bar{H}_2^{(\epsilon)}(z, \mu) Z_{21}(z) - \llbracket \bar{H}_2^{(\epsilon)}(z, \mu) \rrbracket \llbracket Z_{21}(z) \rrbracket \right) Z_{11}^{-1} \\ - H_3(\mu) \lim_{\sigma \rightarrow -1} \int_{M_h}^{\infty} \frac{d\ell_-}{\ell_-} \int_{\sigma M_h}^{\infty} \frac{d\ell_+}{\ell_+} J^{(\epsilon)}(M_h \ell_-, \mu) J^{(\epsilon)}(-M_h \ell_+, \mu) \frac{S_3^{(\epsilon)}(\ell_+ \ell_-, \mu)}{S_1(\mu)}, \quad (5.77)$$

where the superscripts “ $(\epsilon)$ ” in  $J$ ,  $S$  and  $\bar{H}_2$  indicate that the full dependence on the dimensional regulator must be kept in place after renormalisation, as explained in [29]. It would seem at first sight that the appearance of the soft and jet functions in the expressions for the subtraction terms (5.69), (5.70) and (5.76) introduces a dependence on the soft and hard-collinear scales in the hard function  $H_1(\mu)$ , which would upset scale factorization. However, this form makes it explicit that  $H_1(\mu)$  only depends on the hard scale  $M_h$  to all orders in  $\alpha_s$ . The explicit result for this function at NLO in perturbation theory is

$$H_1(\mu) = \frac{y_b(\mu) T_F \delta_{ab} \alpha_s}{\sqrt{2} \pi} \left\{ -2 + \frac{\alpha_s}{4\pi} \left[ C_F \left( -\frac{\pi^2}{3} L_h^2 + (12 + 8\zeta_3) L_h - 36 - \frac{2\pi^2}{3} - \frac{11\pi^4}{45} \right) \right. \right. \\ \left. \left. + C_A \left( \left( 2 + \frac{\pi^2}{3} \right) L_h^2 - 12\zeta_3 L_h - 12 + \frac{\pi^2}{6} + 18\zeta_3 + \frac{19\pi^4}{90} \right) \right] + \mathcal{O}(\alpha_s^2) \right\}. \quad (5.78)$$

The soft function  $S_1$  is renormalised multiplicatively. After renormalisation, it is simply given by the running  $b$ -quark mass, such that

$$S_1(\mu) = Z_{gg}^{-1} Z_{11} S_1^{(0)} = Z_m^{-1} S_1^{(0)} = m_b(\mu). \quad (5.79)$$

## 5.2.4 Form factor expressions in terms of renormalised quantities

Having all expressions for the renormalised quantities at hand, we can perform the convolution integrals in (5.46) and obtain explicit expressions for the renormalised terms  $T_i(\mu)$  (with  $i = 1, 2, 3$ ) up to order  $\mathcal{O}(\alpha_s^2)$ . We find

$$\begin{aligned}
T_1(\mu) &= \mathcal{M}_0 \left\{ -2 + \frac{\alpha_s}{4\pi} \left[ C_F \left( -\frac{\pi^2}{3} L_h^2 + (12 + 8\zeta_3) L_h - 36 - \frac{2\pi^2}{3} - \frac{11\pi^4}{45} \right) \right. \right. \\
&\quad \left. \left. + C_A \left( \left( 2 + \frac{\pi^2}{3} \right) L_h^2 - 12\zeta_3 L_h - 12 + \frac{\pi^2}{6} + 18\zeta_3 + \frac{19\pi^4}{90} \right) \right] + \mathcal{O}(\alpha_s^2) \right\}, \\
T_2(\mu) &= \mathcal{M}_0 \frac{\alpha_s}{4\pi} \left[ C_F \left( \frac{2\pi^2}{3} L_h L_m - \frac{\pi^2}{3} L_m^2 + \frac{2\pi^2}{3} + 8\zeta_3 + \frac{7\pi^4}{45} \right) \right. \\
&\quad \left. + C_A \left( -\frac{2\pi^2}{3} L_h L_m + \frac{\pi^2}{3} L_m^2 + 8\zeta_3 L_m - \frac{\pi^2}{2} - 6\zeta_3 - \frac{\pi^4}{30} \right) + \mathcal{O}(\alpha_s^2) \right], \quad (5.80) \\
T_3(\mu) &= \mathcal{M}_0 \left\{ \frac{L^2}{2} + \frac{\alpha_s}{4\pi} \left[ C_F \left( -\frac{L^4}{12} - L^3 - 3L_m L^2 + \left( 4 - \frac{\pi^2}{3} \right) L^2 \right. \right. \right. \\
&\quad \left. \left. + \left( \frac{2\pi^2}{3} + 8\zeta_3 \right) L - 8\zeta_3 L_m - 4\zeta_3 - \frac{\pi^4}{9} \right) \right. \\
&\quad \left. \left. + C_A \left( -\frac{5L^4}{12} - L_m L^3 - \frac{L_m^2 L^2}{2} + \left( 1 + \frac{\pi^2}{12} \right) L^2 + 4\zeta_3 L_m \right) \right] + \mathcal{O}(\alpha_s^2) \right\}.
\end{aligned}$$

Adding up the three terms, we reproduce the result for the renormalised form factor given in (5.45).

## 5.3 RG equations and prediction of large logarithms at higher loops

In this section, we will first derive the RG equations for the individual component functions. Afterwards, we will solve them iteratively to predict the large logarithmic corrections in the three-loop expressions for the component functions. After performing the remaining convolution integrals, we will find the leading large logarithms of the form factor, too.

### 5.3.1 Evolution equations for the jet and soft functions

In general, the anomalous dimensions can be extracted from the renormalisation factors  $Z_{ij}$  defined in (5.47) using the relation

$$\gamma_{ij} = 2\alpha_s \frac{\partial}{\partial \alpha_s} Z_{ij}^{(1)}, \quad (5.81)$$

where  $Z_{ij}^{(1)}$  denotes the coefficient of the single  $1/\epsilon$  pole in  $Z_{ij}$ . For convenience, we collect all anomalous dimensions in appendix A1.2.



The renormalised jet and soft functions satisfy the RG equations

$$\begin{aligned}
\frac{d}{d \ln \mu} S_1(\mu) &= -(\gamma_{11} - \gamma_{gg}) S_1(\mu), \\
\frac{d}{d \ln \mu} S_2(z, \mu) &= - \int_0^1 dz' [\gamma_{22}(z, z') - \gamma_{gg} \delta(z - z')] S_2(z', \mu) - \gamma_{21}(z) S_1(\mu), \\
\frac{d}{d \ln \mu} \llbracket S_2(z, \mu) \rrbracket &= - \int_0^1 dz' [\llbracket \gamma_{22}(z, z') \rrbracket - \gamma_{gg} \delta(z - z')] \llbracket S_2(z', \mu) \rrbracket - \llbracket \gamma_{21}(z) \rrbracket S_1(\mu), \quad (5.82) \\
\frac{d}{d \ln \mu} J(p^2, \mu) &= - \int_0^\infty dx \gamma_J(p^2, xp^2) J(xp^2, \mu), \\
\frac{d}{d \ln \mu} S_3(w, \mu) &= - \int_0^\infty dw' \gamma_S(w, w') S_3(w', \mu).
\end{aligned}$$

Here we find two main differences in comparison with the photon case in [29]. First, the cusp anomalous dimension and the convolution kernel do not share the same colour factor any more, except for  $\gamma_{11}$ . This fact was already noted for the renormalisation factors for the jet and soft function  $S_3$  in (5.51) and, as we will see later, has severe consequences for the solution of the RGEs. Secondly, the renormalised soft functions receive a contribution from the renormalisation factor  $Z_{gg}^{-1}$  to render them independent of the hard scale  $M_h$ . As a result, their evolution equations feature an additional term  $\gamma_{gg}$ . From the renormalised form factor (5.46) and the renormalisation condition for the soft function  $S_3$  we may deduce the non-trivial relation

$$(\gamma_{33} - \gamma_{gg}) \delta(1 - x) = \gamma_J \left( \frac{M_h w}{\ell_+}, x \frac{M_h w}{\ell_+} \right) + \gamma_J(-M_h \ell_+, -x M_h \ell_+) + \gamma_S(w, w/x), \quad (5.83)$$

which holds to all orders in  $\alpha_s$ . Despite appearance, the right-hand side of this formula is independent of  $\ell_+$  and  $w$ .

### 5.3.2 Evolution equations for the hard matching coefficients

The renormalised hard functions obey the RG equations

$$\begin{aligned}
\frac{d}{d \ln \mu} H_3(\mu) &= \gamma_{33} H_3(\mu), \\
\frac{d}{d \ln \mu} H_2(z, \mu) &= \int_0^1 dz' H_2(z', \mu) \gamma_{22}(z', z), \\
\frac{d}{d \ln \mu} \llbracket \bar{H}_2(z, \mu) \rrbracket &= \int_0^\infty dz' \llbracket \bar{H}_2(z', \mu) \rrbracket \frac{z}{z'} \llbracket \gamma_{22}(z', z) \rrbracket.
\end{aligned} \quad (5.84)$$

The RG equation for  $H_1$  is more involved and reads

$$\frac{dH_1(\mu)}{d \ln \mu} = D_{\text{cut}}(\mu) + \gamma_{11} H_1(\mu) + 4 \int_0^1 \frac{dz}{z} \left[ \bar{H}_2(z, \mu) \gamma_{21}(z) - \llbracket \bar{H}_2(z, \mu) \rrbracket \llbracket \gamma_{21}(z) \rrbracket \right], \quad (5.85)$$

with

$$D_{\text{cut}}(\mu) = - \frac{T_F \alpha_s y_b(\mu)}{\pi \sqrt{2}} \left[ \frac{\alpha_s}{4\pi} \left( C_F - \frac{C_A}{2} \right) 16\zeta_3 + \mathcal{O}(\alpha_s^2) \right]. \quad (5.86)$$

Its complicated structure has its roots in the mismatch terms and operator mixings contributing to the renormalised  $H_1(\mu)$  discussed in section 5.2. In the following, we will derive the RGE step by step.

We start with the scale dependence of the amplitude

$$\left(\frac{d}{d \ln \mu} - \gamma_{gg}\right) [T_1(\mu) + T_2(\mu) + T_3(\mu)] = 0. \quad (5.87)$$

Inserting the expressions for the different terms

$$\left(\frac{dH_1(\mu)}{d \ln \mu} - \gamma_{11}H_1(\mu)\right) S_1(\mu) + \left(\frac{d}{d \ln \mu} + \gamma_{gg}\right) [T_2(\mu) + T_3(\mu)] = 0, \quad (5.88)$$

we see that the scale dependence of  $H_1(\mu)$  is related to that of the second and third term of the amplitude. We investigate the scale dependence of  $T_3(\mu)$  first and find

$$\begin{aligned} \frac{dT_3(\mu)}{d \ln \mu} &= -\gamma_{gg}T_3(\mu) + H_3(\mu) \int_0^\infty dx K(x) \\ &\times \left[ \int_{M_h}^{M_h/x} \frac{d\ell_-}{\ell_-} \int_0^{\sigma M_h} \frac{d\ell_+}{\ell_+} J(xM_h\ell_-, \mu) J(-M_h\ell_+, \mu) S(\ell_+\ell_-, \mu) \right. \\ &\left. + \int_0^{M_h} \frac{d\ell_-}{\ell_-} \int_{\sigma M_h}^{\sigma M_h/x} \frac{d\ell_+}{\ell_+} J(M_h\ell_-, \mu) J(-xM_h\ell_+, \mu) S(\ell_+\ell_-, \mu) \right]_{\text{LP}}, \end{aligned} \quad (5.89)$$

where

$$K(x) = \frac{\alpha_s}{\pi} \left(C_F - \frac{C_A}{2}\right) \Gamma(1, x) + \mathcal{O}(\alpha_s^2) \quad (5.90)$$

is the non-local convolution kernel of the soft function  $S_3$  and the jet functions. The contributions of the second and third line in (5.89) are identical after integration. This can easily be seen by changing the integration variables to  $\ell_- \rightarrow \sigma\ell_+$ ,  $\ell_+ \rightarrow \sigma^{-1}\ell_-$ . It is important to remark that this contribution is *not* a purely hard one, but instead explicitly depends on the soft scale  $m_b$  [29, 79]. However, these effects are of higher order than the precision desired for our purposes. Plugging in the expressions, we find

$$\frac{dT_3(\mu)}{d \ln \mu} = \mathcal{M}_0 \left\{ \frac{\alpha_s}{4\pi} \left[ 2L^2 \left( C_A L_h - \frac{\beta_0}{2} \right) + 16\zeta_3 \left( C_F - \frac{C_A}{2} \right) \right] + \mathcal{O}(\alpha_s^2) \right\}. \quad (5.91)$$

The scale dependence of  $T_2$  is more involved due to the subtraction and mixing nature. Applying the RGEs for operators (5.82) and hard functions (5.84), we find

$$\begin{aligned} \frac{dT_2(\mu)}{d \ln \mu} &= \gamma_{gg}T_2(\mu) - 4 \int_0^1 \frac{dz}{z} \left( \bar{H}_2(z, \mu) \gamma_{21}(z) - \llbracket \bar{H}_2(z, \mu) \rrbracket \llbracket \gamma_{21}(z) \rrbracket \right) S_1(\mu) \\ &+ 4 \left[ \int_0^1 dz \int_0^\infty dz' - \int_0^1 dz' \int_0^\infty dz \right] \frac{\llbracket \bar{H}_2(z, \mu) \rrbracket}{z} \llbracket \gamma_{22}(z, z') \rrbracket \llbracket S_2(z', \mu) \rrbracket. \end{aligned} \quad (5.92)$$

Comparing this to the corresponding equation for the photon case, we find there is an additional scale dependence governed by  $\gamma_{gg}$  due to the external gluons, as expected. Note that

$$\llbracket \gamma_{22}(z, z') \rrbracket = -\frac{z}{z'^2} K\left(\frac{z}{z'}\right) + \text{local terms}, \quad (5.93)$$

with  $K(x)$  as defined above. In the second line of (5.92), all integrals involving local terms vanish evidently. Substituting  $x = z/z'$  and using the renormalised version of the first refactorisation theorem (5.36), we are able to rewrite

$$\begin{aligned} \left. \frac{dT_2(\mu)}{d \ln \mu} \right|_{\text{left-over}} &= 4H_3(\mu) \int_0^\infty dx K(x) \int_{M_h}^{M_h/x} \frac{d\ell_-}{\ell_-} J(xM_h\ell_-, \mu) \llbracket S_2(\ell_-/M_h, \mu) \rrbracket \\ &= -4 \int_0^\infty dx K(x) \int_1^{1/x} \frac{dz}{z} \llbracket \bar{H}_2(xz, \mu) \rrbracket \llbracket S_2(z, \mu) \rrbracket. \end{aligned} \quad (5.94)$$

For our next step, a renormalised version of the second refactorisation theorem (5.36) will be helpful. Following the analysis laid out in [29], we obtain

$$\llbracket S_2(z, \mu) \rrbracket = -\frac{1}{2} \int_0^{\sigma M_h} \frac{d\ell_+}{\ell_+} J(-M_h\ell_+, \mu) S(zM_h\ell_+, \mu) \Big|_{\text{LP}} + \Delta_{21}(z, \mu) S_1(\mu), \quad (5.95)$$

with

$$\begin{aligned} \Delta_{21}(z, \mu) &= -\frac{Z_{11}^{-1}}{2} \int_{\sigma M_h}^\infty d\ell_+ \int_0^\infty d\ell'_+ \int_0^\infty d\ell'_- Z_J(\ell'_+, \ell_+) Z_S(\ell_-\ell_+, \ell'_-\ell'_+) J^{(0)}(-M_h\ell'_+) \frac{S_\infty^{(0)}(\ell'_-\ell'_+)}{m_{b,0}} \\ &\quad + \llbracket Z_{21}(z) \rrbracket Z_{11}^{-1}, \end{aligned} \quad (5.96)$$

where  $\ell_- = zM_h$  is implicit. Note that the term involving  $\Delta_{21}(z, \mu)$  is not present in the bare refactorisation theorem. As before, we exchanged the soft function  $S_3$  for its asymptotic counterpart to simplify the computation. Again, this is possible because all integration regions lie in the hard sector. We may interpret  $\Delta_{21}$  as a fairly complex mismatch term. As with many complications in transferring the bare factorisation formula for  $gg \rightarrow h$  to a renormalised one, the source lies within the implemented subtraction scheme to eliminate endpoint divergences. Up to order  $\mathcal{O}(\alpha_s^2)$ , we obtain

$$\begin{aligned} \Delta_{21}(z, \mu) &= \frac{T_F \delta_{ab} \alpha_s}{2\pi} \left\{ -L_h - \ln z + \frac{\alpha_s}{4\pi} \left[ C_F \left( (3 + \ln z) L_h^2 + \left( \ln^2 z + 6 \ln z - 11 + \frac{2\pi^2}{3} \right) L_h \right. \right. \right. \\ &\quad \left. \left. + \frac{\ln^3 z}{6} + 3 \ln^2 z + \left( \frac{2\pi^2}{3} - \frac{23}{2} \right) \ln z + 11 - \pi^2 - 10\zeta_3 \right) \right. \\ &\quad \left. \left. + C_A \left( -\ln z L_h^2 - (1 + \ln^2 z) L_h - \frac{\ln^3 z}{6} - \frac{\ln z}{2} + 1 + 4\zeta_3 \right) \right] \right\}. \end{aligned} \quad (5.97)$$

Setting  $C_A \rightarrow 0$  retrieves the expression for the abelian case in [29]. When plugging in the renormalised refactorisation condition (5.95) into the RGE of  $T_2$  (5.92), we observe that the first term of (5.95) will ultimately cancel out the equivalent contributions in the RGE of  $T_3$ , i.e., the last two lines of (5.89). Combining our findings we obtain

$$\begin{aligned} \frac{d(T_2(\mu) + T_3(\mu))}{d \ln \mu} &= -4 \int_0^1 \frac{dz}{z} \left( \bar{H}_2(z, \mu) \gamma_{21}(z) - [\bar{H}_2(z, \mu)] [\gamma_{21}(z)] \right) S_1(\mu) \\ &\quad - D_{\text{cut}}(\mu) S_1(\mu) - \gamma_{gg}(T_2(\mu) + T_3(\mu)), \end{aligned} \quad (5.98)$$

where

$$\begin{aligned} D_{\text{cut}}(\mu) &= -4H_3(\mu) \int_0^\infty dx K(x) \int_1^{1/x} \frac{dz}{z} J(xz M_h^2, \mu) \Delta_{21}(z, \mu) \\ &= 4 \int_0^\infty dx K(x) \int_1^{1/x} \frac{dz}{z} [\bar{H}_2(xz, \mu)] \Delta_{21}(z, \mu). \end{aligned} \quad (5.99)$$

Here it is explicit that  $D_{\text{cut}}$  depends only on the hard scale  $L_h$ .

At first sight, this function appears as a simple inhomogeneous term in the evolution equation, which would not provide a major obstacle to finding its solution. However, it has been shown in [29] that the quantity  $D_{\text{cut}}$  exhibits single-logarithmic terms in higher orders,  $D_{\text{cut}} \ni \alpha_s (\alpha_s L_h)^n$  for  $n \geq 2$ . With this complication, relation (5.85) establishes a new type of RG equation, which is more complicated than the equations encountered in conventional Sudakov problems. In order to solve this equation, it would be necessary to resum the logarithms contained in  $D_{\text{cut}}$  to all orders.

### 5.3.3 Evolution equations for the form factor and its three components

The renormalised  $gg \rightarrow h$  form factor fulfils the evolution equation

$$\frac{dF_{gg}(\mu)}{d \ln \mu} = \gamma_{gg} F_{gg}(\mu), \quad (5.100)$$

where

$$\gamma_{gg} = \frac{\alpha_s}{4\pi} (4C_A L_h - 2\beta_0) + \mathcal{O}(\alpha_s^2) \quad (5.101)$$

is the anomalous dimension associated with  $Z_{gg}$ . We may also compute the scale dependence of each of the three terms  $T_1(\mu)$ ,  $T_2(\mu)$  and  $T_3(\mu)$  individually, finding

$$\begin{aligned} \frac{dT_1(\mu)}{d \ln \mu} &= \mathcal{M}_0 \left\{ \frac{\alpha_s}{4\pi} \left[ -(C_A - C_F) \frac{4\pi^2}{3} L_h + 8\zeta_3 (3C_A - 2C_F) \right] + \mathcal{O}(\alpha_s^2) \right\}, \\ \frac{dT_2(\mu)}{d \ln \mu} &= \mathcal{M}_0 \left\{ \frac{\alpha_s}{4\pi} \left[ (C_A - C_F) \frac{4\pi^2}{3} L_h - 16\zeta_3 C_A \right] + \mathcal{O}(\alpha_s^2) \right\}, \\ \frac{dT_3(\mu)}{d \ln \mu} &= \mathcal{M}_0 \left\{ \frac{\alpha_s}{4\pi} \left[ 2L^2 \left( C_A L_h - \frac{\beta_0}{2} \right) + 16\zeta_3 \left( C_F - \frac{C_A}{2} \right) \right] + \mathcal{O}(\alpha_s^2) \right\}. \end{aligned} \quad (5.102)$$

### 5.3.4 Large logarithms in the three-loop $gg \rightarrow h$ form factor

Given the RG equations and anomalous dimensions for the ingredients in the factorisation formula, we are able to predict the four leading logarithms in the three-loop expression for the  $gg \rightarrow h$  form factor in analytic form. To this end, we solve the evolution equations iteratively and determine the leading large logarithms in the hard matching coefficients and the soft functions at next-to-next-to-leading order (NNLO) in perturbation theory.

#### 5.3.4.1 Higher-order logarithms in the jet and soft functions

The jet function has been calculated exactly at the two-loop level in (5.28)

The computation of the leading logarithmic behaviour of the soft function  $S_2(z, \mu)$  and the endpoint-region counterpart  $\llbracket S_2(z, \mu) \rrbracket$  requires knowledge of the leading order anomalous dimension. To calculate also sub-leading logarithmic terms would necessitate the anomalous dimension at higher loop order, which is currently unknown. We obtain

$$\begin{aligned} S_2(z, \mu) &= \frac{T_F \delta_{ab} \alpha_s}{2\pi} m_b(\mu) g_{\perp}^{\mu\nu} \left\{ -L_m + \frac{\alpha_s}{4\pi} [\dots] + \left(\frac{\alpha_s}{4\pi}\right)^2 [c_3(z)L_m^3 + \mathcal{O}(L_m^2)] \right\}, \\ \llbracket S_2(z, \mu) \rrbracket &= \frac{T_F \delta_{ab} \alpha_s}{2\pi} m_b(\mu) g_{\perp}^{\mu\nu} \left\{ -L_m + \frac{\alpha_s}{4\pi} [\dots] + \left(\frac{\alpha_s}{4\pi}\right)^2 [d_3(z)L_m^3 + \mathcal{O}(L_m^2)] \right\}, \end{aligned} \quad (5.103)$$

with

$$\begin{aligned} c_3(z) &= -C_F^2 \left[ \frac{2L_z^2}{3} + 4L_z + 3 \right] + C_F C_A \left[ \frac{4L_z^2}{3} + \frac{L_z L_{\bar{z}}}{3} + 4L_z \right] \\ &\quad - C_A^2 \left[ \frac{2L_z^2}{3} + \frac{L_z L_{\bar{z}}}{3} \right] - \beta_0 \left[ \frac{C_F - C_A}{3} L_z + \frac{C_F}{2} \right] + (z \leftrightarrow 1 - z), \\ d_3(z) &= -C_F^2 \frac{2(L_z + 3)^2}{3} + C_F C_A \left[ \frac{4L_z^2}{3} + 4L_z \right] - C_A^2 \frac{2L_z^2}{3} - \beta_0 \left[ \frac{C_F - C_A}{3} L_z + C_F \right]. \end{aligned} \quad (5.104)$$

The soft function  $S_3$  is parametrised as

$$S_3(w, \mu) = -\frac{T_F \delta_{ab} \alpha_s}{\pi} m_b(\mu) [S_a(w, \mu) \theta(w - m_b^2(\mu)) + S_b(w, \mu) \theta(m_b^2(\mu) - w)], \quad (5.105)$$

$$\begin{aligned} S_a(w, \mu) &= 1 + \frac{\alpha_s}{4\pi} [\dots] + \left(\frac{\alpha_s}{4\pi}\right)^2 \left[ r_4 L_w^4 + r_3 L_w^3 + r_2 L_w^2 + r_1 L_w + \mathcal{O}(L_w^0) \right. \\ &\quad \left. + s_{3a}(\hat{w}) L_m^3 + s_{2a}(\hat{w}) L_m^2 + s_{1a}(\hat{w}) L_m + \mathcal{O}(L_m^0) \right], \end{aligned} \quad (5.106)$$

$$S_b(w, \mu) = \frac{\alpha_s}{4\pi} [\dots] + \left(\frac{\alpha_s}{4\pi}\right)^2 \left[ s_{3b}(\hat{w}) L_m^3 + s_{2b}(\hat{w}) L_m^2 + s_{1b}(\hat{w}) L_m + \mathcal{O}(L_m^0) \right].$$

with  $\hat{w} = w/m_b^2$  and the coefficient functions read

$$\begin{aligned}
r_4 &= \frac{(C_F - C_A)^2}{2}, \\
r_3 &= (C_F - C_A) \left( 6C_F + \frac{\beta_0}{3} \right), \\
r_2 &= C_F^2 \left( 6 + \frac{\pi^2}{2} \right) + C_F C_A \frac{140}{9} + C_A^2 \left( \frac{67}{9} - \frac{\pi^2}{2} \right) - \frac{16C_F + 20C_A}{9} T_F n_f, \\
r_1 &= -C_F^2 (75 - 3\pi^2) - C_F C_A \left( \frac{1297}{27} - \frac{29\pi^2}{9} + 14\zeta_3 \right) - C_A^2 \left( \frac{404}{27} - 14\zeta_3 \right) \\
&\quad + C_F T_F n_f \left( \frac{428}{27} - \frac{4\pi^2}{9} \right) + C_A T_F n_f \frac{112}{27},
\end{aligned} \tag{5.107}$$

$$\begin{aligned}
s_{3a}(\hat{w}) &= 4(C_F - C_A) \left( C_F - \frac{C_A}{2} \right) \ln(1 - \hat{w}^{-1}), \\
s_{2a}(\hat{w}) &= 2C_F^2 [\ln(1 - \hat{w}^{-1}) (14 + 10 \ln(1 - \hat{w}^{-1}) + 9 \ln \hat{w}) + 5 \text{Li}_2(\hat{w}^{-1})] \\
&\quad - 2C_F C_A [\ln(1 - \hat{w}^{-1}) (8 + 11 \ln(1 - \hat{w}^{-1}) + 11 \ln \hat{w}) + 7 \text{Li}_2(\hat{w}^{-1})] \\
&\quad + 6C_A^2 [\ln(1 - \hat{w}^{-1}) (\ln(1 - \hat{w}^{-1}) + \ln \hat{w}) + \text{Li}_2(\hat{w}^{-1})] \\
&\quad + 2\beta_0 \left( C_F - \frac{C_A}{2} \right) \ln(1 - \hat{w}^{-1}),
\end{aligned} \tag{5.108}$$

$$\begin{aligned}
s_{3b}(\hat{w}) &= -4(C_F - C_A) \left( C_F - \frac{C_A}{2} \right) \ln(1 - \hat{w}), \\
s_{2b}(\hat{w}) &= - \left( C_F - \frac{C_A}{2} \right) \left[ C_F (\ln(1 - \hat{w}) (24 - 4 \ln \hat{w} + 20 \ln(1 - \hat{w}))) \right. \\
&\quad \left. + 4 \text{Li}_2(\hat{w}) \right] - 12C_A \ln^2(1 - \hat{w}) + 2\beta_0 \ln(1 - \hat{w}).
\end{aligned}$$

Note that since  $s_{3b}(\hat{w}), s_{2b}(\hat{w}) \rightarrow 0$  when  $\hat{w} \rightarrow 0$ , at order  $\mathcal{O}(\alpha_s^3)$  the leading logarithms in the full form factor will not feature contributions from  $S_b(w, \mu)$ .

In order to predict the full logarithmic behaviour of  $S_3$  at three loops, the two-loop anomalous dimension  $\gamma_S$  would be needed. Using eq. (5.83) it can be inferred from the jet function anomalous dimension. Thus we write

$$\begin{aligned}
\gamma_S(w, w') &= - \left[ \left( \Gamma_{\text{cusp}}^F(\alpha_s) - \Gamma_{\text{cusp}}^A(\alpha_s) \right) L_w - \gamma_s(\alpha_s) \right] \delta(w - w') \\
&\quad - 2 \left( \Gamma_{\text{cusp}}^F(\alpha_s) - \frac{\Gamma_{\text{cusp}}^A(\alpha_s)}{2} \right) w \Gamma(w, w') - 2 \left( \frac{\alpha_s}{4\pi} \right)^2 g \left( \frac{\hat{w}}{w} \right) + \mathcal{O}(\alpha_s^3),
\end{aligned} \tag{5.109}$$

where  $\Gamma_{\text{cusp}}^{F/A}$  is the cusp anomalous dimension up to two-loop order in the fundamental/adjoint representation. Here,  $g(x)$  is an unknown non-local kernel function. In the RG equation for the soft function, it will generate a contribution at order  $\mathcal{O}(\alpha_s^3)$  when convoluted with the leading order soft function

$$2 \int_0^\infty dx g(x) \theta(\omega/x - m_b^2) = 2 \int_0^{\hat{\omega}} dx g(x) \equiv G(\hat{\omega}). \tag{5.110}$$

Although the explicit functional form of  $g(x)$  is unknown, its integration over the full space, i.e.,  $G(\infty)$ , has been calculated in [1] by demanding the cancellation of all single  $\epsilon$  poles in two-loop jet function. It reads

$$G(\infty) = C_F^2(4\pi^2 - 16\zeta_3) - C_F C_A \left( \frac{62\pi^2}{9} + 24\zeta_3 \right) - C_A^2 \left( \frac{4}{3} - \frac{22\pi^2}{9} - 40\zeta_3 \right) + C_F T_F n_f \frac{16\pi^2}{9} + C_A T_F n_f \left( \frac{8}{3} - \frac{8\pi^2}{9} \right). \quad (5.111)$$

Knowing  $G(\hat{w})$  only at the limits does not spoil the accuracy of the prediction of the three-loop logarithms in the form factor, since its contributions will only show up at lower logarithmic order.

### 5.3.4.2 Higher-order logarithms in the matching coefficients

The hard function  $H_3(\mu)$  is the same as in the photon case, hence its higher-order logarithmic behaviour can be found in [29]. The hard coefficients  $\bar{H}_2(z, \mu)$  and  $[\bar{H}_2(z, \mu)]$  can be parametrised as

$$\begin{aligned} \bar{H}_2(z, \mu) &= \frac{y_b}{\sqrt{2}} \left\{ 1 + \frac{\alpha_s}{4\pi} [\dots] + \left( \frac{\alpha_s}{4\pi} \right)^2 [a_4 L_h^4 + a_3 L_h^3 + a_2 L_h^2 + \mathcal{O}(L_h)] \right\}, \\ [\bar{H}_2(z, \mu)] &= \frac{y_b}{\sqrt{2}} \left\{ 1 + \frac{\alpha_s}{4\pi} [\dots] + \left( \frac{\alpha_s}{4\pi} \right)^2 [b_4 L_h^4 + b_3 L_h^3 + b_2 L_h^2 + \mathcal{O}(L_h)] \right\}, \end{aligned} \quad (5.112)$$

where we find after solving the evolution equations

$$\begin{aligned} a_4 &= b_4 = \frac{C_A^2}{2}, \\ a_3 &= -2C_A(C_F - C_A)(L_z + L_{\bar{z}}) + \frac{\beta_0 C_A}{3}, \\ b_3 &= -2C_A(C_F - C_A)L_z + \frac{\beta_0 C_A}{3}, \\ a_2 &= (C_F - C_A) \left[ 2(C_F - C_A)(L_z^2 + L_{\bar{z}}^2) - C_A(L_z + L_{\bar{z}})^2 - \beta_0(L_z + L_{\bar{z}}) \right] + C_A \left[ \left( \frac{\pi^2}{6} - \frac{76}{9} \right) C_A + 3C_F + \frac{20}{9} T_F n_f \right], \\ b_2 &= (C_F - C_A) \left[ (2C_F - 3C_A) \ln^2 z - \beta_0 \ln z \right] + C_A \left[ \left( \frac{\pi^2}{6} - \frac{76}{9} \right) C_A + 3C_F + \frac{20}{9} T_F n_f \right]. \end{aligned} \quad (5.113)$$

As a consequence of the complex RG equation for  $H_1(\mu)$ , we can only predict the first two leading logarithms for this hard function. We eventually find

$$H_1(\mu) = \frac{y_b}{\sqrt{2}} \frac{T_F \delta_{ab} \alpha_s}{\pi} \left[ -2 + \frac{\alpha_s}{4\pi} [\dots] + \left( \frac{\alpha_s}{4\pi} \right)^2 [c_4 L_h^4 + c_3 L_h^3 + \mathcal{O}(L_h^2)] \right], \quad (5.114)$$

with

$$\begin{aligned}
c_4 &= -C_A^2 \left(1 + \frac{\pi^2}{3}\right) + C_F C_A \frac{\pi^2}{3}, \\
c_3 &= C_F^2 \left(\frac{2\pi^2}{3} - \frac{16\zeta_3}{3}\right) - C_F C_A \left(12 - \frac{4\pi^2}{27} + \frac{8\zeta_3}{3}\right) - C_A^2 \left(\frac{22}{9} + \frac{22\pi^2}{27} \right. \\
&\quad \left. - 12\zeta_3\right) + C_A T_F n_f \left(\frac{8}{9} + \frac{8\pi^2}{27}\right) - C_F T_F n_f \frac{8\pi^2}{27}.
\end{aligned} \tag{5.115}$$

### 5.3.4.3 Higher order logarithms in the form factor

Eventually, we are able to predict the leading logarithmic corrections to the three-loop form factor from  $\mathcal{O}(\alpha_s^3 L^6)$  to  $\mathcal{O}(\alpha_s^3 L^3)$ . As in the photon case studied in [81], we convert our results to the on-shell scheme. Therefore, we first express the running parameters  $m_b(\mu)$  and  $y_b(\mu)$  in terms of the pole mass  $m_b$ . We then eliminate the remaining scale dependence by taking  $\mu^2 = \hat{\mu}_h^2 \equiv -M_h^2 - i0$ . This greatly simplifies the three-loop expressions. With  $v$  the Higgs field vev, we find

$$\begin{aligned}
F_{gg}(\hat{\mu}_h) &= T_F \delta_{ab} \frac{\alpha_s(\hat{\mu}_h) m_b^2}{\pi v} \left\{ -2 + \frac{L^2}{2} + \frac{\alpha_s(\hat{\mu}_h)}{4\pi} \left[ \frac{C_A - C_F}{12} L^4 - C_F L^3 \right. \right. \\
&\quad + \left( \left(1 + \frac{5\pi^2}{12}\right) C_A - \frac{2\pi^2}{3} C_F \right) L^2 + \left( \left(12 + \frac{2\pi^2}{3} + 16\zeta_3\right) C_F - 12\zeta_3 C_A \right) L \\
&\quad + \left. \left( 4\zeta_3 - \frac{\pi^4}{5} - 20 \right) C_F + \left( 12\zeta_3 + \frac{8\pi^4}{45} - \frac{\pi^2}{3} - 12 \right) C_A \right] \\
&\quad + \left( \frac{\alpha_s(\hat{\mu}_h)}{4\pi} \right)^2 \left[ \frac{(C_A - C_F)^2}{90} L^6 + (C_A - C_F) \left( \frac{\beta_0}{30} - \frac{C_F}{10} \right) L^5 \right. \\
&\quad \left. + d_4^{\text{OS}} L^4 + d_3^{\text{OS}} L^3 + \dots \right] \Big\},
\end{aligned} \tag{5.116}$$

where  $L = \ln[(-M_h^2 - i0)/m_b^2]$ , and

$$\begin{aligned}
d_4^{\text{OS}} &= \left(\frac{3}{2} + \frac{\pi^2}{18}\right) C_F^2 - \left(\frac{191}{54} + \frac{\pi^2}{24}\right) C_F C_A + \left(\frac{85}{108} - \frac{\pi^2}{72}\right) C_A^2 + \frac{32C_F - 5C_A}{27} T_F n_f, \\
d_3^{\text{OS}} &= \left(\frac{20\zeta_3}{3} + \frac{7\pi^2}{9} - \frac{1}{2}\right) C_F^2 - \left(10\zeta_3 + \frac{235}{18} + \frac{43\pi^2}{27}\right) C_F C_A \\
&\quad + \left(\frac{10\zeta_3}{3} + \frac{11\pi^2}{18} + \frac{4}{3}\right) C_A^2 + \left(\frac{22}{9} + \frac{8\pi^2}{27}\right) C_F T_F n_f - \left(\frac{2}{3} + \frac{2\pi^2}{9}\right) C_A T_F n_f.
\end{aligned} \tag{5.117}$$

The coefficients of the colour structures  $C_F^2$  and  $C_F T_F$  agree with the corresponding coefficients in the photon case.



## 5.4 Resummation

In this section, we want to resum the large logarithms in the form factor to all orders in perturbation theory. We therefore need to solve the RG equations for the different hard, jet, and soft functions. Choosing to set the scale where we evaluate our predictions at  $\mu = \mu_h$ , all large logarithms in the evolution of the hard functions vanish, leaving them in the evolution of the jet and soft functions. In this context, the general logarithmic structure reads:

$$\begin{aligned}
 T_1(\mu_h) &= T_F \delta_{ab} \frac{y_b(\mu_h)}{\sqrt{2}} \frac{\alpha_s(\mu_h)}{\pi} m_b(\mu_h) \left[ -2 + \sum_{n \geq 1} \alpha_s(\mu_h)^n a_n \right], \\
 T_2(\mu_h) &= T_F \delta_{ab} \frac{y_b(\mu_h)}{\sqrt{2}} \frac{\alpha_s(\mu_h)}{\pi} m_b(\mu_h) \sum_{n \geq 1} \alpha_s(\mu_h)^n \sum_{i=0}^{n+1} b_{n,i} L^i, \\
 T_3(\mu_h) &= T_F \delta_{ab} \frac{y_b(\mu_h)}{\sqrt{2}} \frac{\alpha_s(\mu_h)}{\pi} m_b(\mu_h) \sum_{n \geq 0} \alpha_s(\mu_h)^n \sum_{i=0}^{2n+2} c_{n,i} L^i,
 \end{aligned} \tag{5.118}$$

where  $a_n$ ,  $c_{n,i}$  and  $b_{n,i}$  are constant numbers. It is obvious that  $T_3$  dominates the logarithmic corrections since it is of Sudakov type. Hence in the following, we will only focus on the third term. The photon case has been resummed to next-to-leading double-logarithmic accuracy (NLL) in [29, 80]. In this paper, we include one more tower of logarithms, i.e. we resum factors of  $\alpha_s^n L^{2n}$ ,  $\alpha_s^n L^{2n-1}$  and  $\alpha_s^n L^{2n-2}$  to all orders of perturbation theory. This is conventionally named modified next-to-leading logarithm (NLL') accuracy.

In the literature, one distinguishes two different schemes for the resummation of large logarithms in Sudakov problems. The so-called ‘‘RG-improved perturbation theory’’ rests on the assumption that  $\alpha_s L = \mathcal{O}(1)$ , where  $L$  is the large logarithm in a given problem. The parametrically leading terms in the *logarithm* of a quantity are then of order  $L(\alpha_s L)^n \sim \alpha_s^{-1}(\alpha_s L)^n$  and are formally larger than  $\mathcal{O}(1)$ . The leading-order approximation (LO) is therefore defined by the simultaneous resummation of all terms of order  $L(\alpha_s L)^n$  and  $(\alpha_s L)^n$  in the logarithm of the quantity; i.e., all such logarithms get exponentiated in the expression for the quantity itself. The NLO approximation resums in addition the terms of order  $\alpha_s(\alpha_s L)^n$  in the exponent, and so on. In the double-logarithmic counting scheme, instead, one assumes that  $\alpha_s L^2 = \mathcal{O}(1)$ . In this case the resummation is performed for the observable itself. In the leading double-logarithmic approximation (LL), all terms of order  $\alpha_s^n L^{2n}$  are resummed. At the next order (NLL), one resums the logarithms of the form  $\alpha_s^n L^{2n-k}$  with  $k = 0, 1$ , and so on. In table 5.1 we summarise the ingredients needed at a given order in the two schemes.  $N^{k+1}$ LL resummations (with  $k \geq 0$ ) are contained in RG-improved perturbation theory at  $N^k$ LO, while  $N^{k+1}$ LL' resummation includes matching corrections at one order higher, however, the same-order anomalous dimensions are used. Hence it is enough to use the RG-improved LO jet and soft functions to account for NLL' corrections from the anomalous dimensions. On top of that, it turns out that only constant terms at NLO in the hard, jet, and soft functions at their respective matching scales contribute to the large logarithms at NLL', which simplifies the calculation a lot.

RG-impr. PT	Log. approx.	$\Gamma_{\text{cusp}, \beta}$	$\gamma$	$H_3, S_3, J$	$\alpha_s^n L^k$
–	LL	LO	–	LO	$k = 2n$
LO	NLL	NLO	LO	LO	$2n - 1 \leq k \leq 2n$
–	NLL'	NLO	LO	NLO	$2n - 2 \leq k \leq 2n$
NLO	NNLL	NNLO	NLO	NLO	$2n - 3 \leq k \leq 2n$

Table 5.1: Naming schemes for logarithmic accuracy in  $T_3(\mu)$ . We list perturbative orders of the cusp anomalous dimension, non-cusp anomalous dimensions  $\gamma$ , QCD  $\beta$  function, and matching corrections from the component functions to obtain resummation at a given logarithmic order.

In the following, we will first derive the RG-improved soft and jet function at LO. Subsequently, we resum the first three towers of large logarithms in the third term of the amplitude. Note that at NLL' accuracy, there are no contributions from the first and second term apart from the fixed  $n = 1$  contribution in the second term, which therefore does not need to be resummed at the given logarithmic order.

### 5.4.1 RG-improved LO jet function

The RG-improved LO jet function can be obtained from the jet function in the photon case in [81] by accounting for the different colour factors. We find

$$\begin{aligned}
J^{\text{RGiLO}}(p^2, \mu) &= e^{-2S_{\Delta\Gamma}(\mu_j, \mu)} \mathcal{J}^{\text{LO}}(\partial_\eta, \mu_j) \left( \frac{-p^2 - i0}{\mu_j^2} \right)^{a_{\Delta\Gamma}(\mu_j, \mu) + \eta} \\
&\times \left[ e^{-2\gamma_E a_{\Delta\Gamma}(\mu_j, \mu)} \frac{\Gamma(1 - a_{\Delta\Gamma}(\mu_j, \mu) - \eta) \Gamma(1 + \eta)}{\Gamma(1 + a_{\Delta\Gamma}(\mu_j, \mu) + \eta) \Gamma(1 - \eta)} \right]^{r_\Gamma} \Big|_{\eta=0}, \tag{5.119}
\end{aligned}$$

where both the Sudakov exponent

$$S_{\Delta\Gamma}(\mu_j, \mu) = \frac{\Delta\Gamma_0}{4\beta_0^2} \left[ \frac{4\pi}{\alpha_s(\mu_j)} \left( 1 - \frac{1}{r} - \ln r \right) + \left( \frac{\Delta\Gamma_1}{\Delta\Gamma_0} - \frac{\beta_1}{\beta_0} \right) (1 - r + \ln r) + \frac{\beta_1}{2\beta_0} \ln^2 r \right], \tag{5.120}$$

with  $r = \alpha_s(\mu)/\alpha_s(\mu_j)$  and  $\Delta\Gamma_0 = 4(C_F - C_A)$ , and the function

$$a_{\Delta\Gamma}(\mu_j, \mu) = \frac{\Delta\Gamma_0}{2\beta_0} \ln \frac{\alpha_s(\mu)}{\alpha_s(\mu_j)} \tag{5.121}$$

are related to the corresponding objects in the photon case by the overall colour factor  $(C_F - C_A)$  (instead of  $C_F$ ). Another important difference is the appearance of the exponent

$$r_\Gamma = \frac{C_F - \frac{1}{2}C_A}{C_F - C_A} = \frac{1}{N_c^2 + 1}, \tag{5.122}$$

which strongly suppresses the deviation of the term shown in the second line of (5.119) from 1. Note that a consistent evaluation of the Sudakov exponent requires the two-loop coefficients of the cusp anomalous dimension and the QCD  $\beta$ -function. The function

$\mathcal{J}_g^{\text{LO}}(\partial_\eta, \mu_j)$  is a differential operator acting on functions of the auxiliary parameter  $\eta$ . It is defined by the identification  $J_g(p^2, \mu_j) \equiv \mathcal{J}_g(L_p, \mu_j)$ . At the matching scale  $\mu_j$  chosen as  $\mu_j^2 \sim p^2$ , the expression for the jet function in (5.53) is free of large logarithms. In fact, at leading order in RG-improved perturbation theory one has  $\mathcal{J}_g^{\text{LO}}(L_p, \mu_j) = 1$ . Using this initial condition, we find the simple result

$$J^{\text{RGi,LO}}(p^2, \mu) = e^{-2S_{\Delta\Gamma}(\mu_j, \mu)} \left( \frac{-p^2 - i0}{\mu_j^2} \right)^{a_{\Delta\Gamma}(\mu_j, \mu)} \left[ e^{-2\gamma_E a_{\Delta\Gamma}(\mu_j, \mu)} \frac{\Gamma(1 - a_{\Delta\Gamma}(\mu_j, \mu))}{\Gamma(1 + a_{\Delta\Gamma}(\mu_j, \mu))} \right]^{r_\Gamma}. \quad (5.123)$$

This formula resums the leading logarithmic corrections to the jet function to all orders of perturbation theory.

### 5.4.2 RG-improved LO soft function $S_3$

The RG-improved LO soft function  $S_3$  can be derived in a similar manner as has been the soft function of  $h \rightarrow \gamma\gamma$  in [79]. Transforming to Laplace space, we find that the ansatz

$$\tilde{S}(\eta, \mu) = \left( \frac{w}{\mu_s^2} \right)^{\eta - a_{\Delta\Gamma}(\mu_s, \mu)} \exp \left[ 2S_{\Delta\Gamma}(\mu_s, \mu) + a_{\gamma_s}(\mu_s, \mu) + 2 \int_{\alpha_s(\mu_s)}^{\alpha_s(\mu)} d\alpha \frac{\Delta'\Gamma(\alpha)}{\beta(\alpha)} \mathcal{F}(\eta - a_{\Delta\Gamma}(\mu_s, \mu_\alpha)) \right], \quad (5.124)$$

provides a solution to the RG equation. Here,  $\Delta'\Gamma = \Gamma_F - \Gamma_A/2$  and  $\Gamma_R$  is the cusp anomalous dimension in the fundamental or adjoint representation, respectively. The RG function  $a_{\gamma_s}$  is defined in analogy to (5.121). The function  $\mathcal{F}$  is defined as

$$\mathcal{F}(x) \equiv \int_0^\infty dw' w \Gamma(w, w') \left( \frac{w'}{w} \right)^x \quad (5.125)$$

and can be expressed as the sum of two harmonic number functions [79]. It has singularities for all values where  $x$  is a positive or negative integer. At RG improved leading order, the third term in the exponential of (5.124) can be simplified to

$$\begin{aligned} \int_{\alpha_s(\mu_s)}^{\alpha_s(\mu)} d\alpha \frac{\Delta'\Gamma(\alpha)}{\beta(\alpha)} \mathcal{F}(\eta - a_{\Delta\Gamma}(\mu_s, \mu_\alpha)) &= r_\Gamma \int_{\alpha_s(\mu_s)}^{\alpha_s(\mu)} d\alpha \frac{\Delta\Gamma(\alpha)}{\beta(\alpha)} \mathcal{F}(\eta - a_{\Delta\Gamma}(\mu_s, \mu_\alpha)) + \mathcal{O}(\alpha_s) \\ &= r_\Gamma \left[ \ln \frac{\Gamma(1 + a_{\Delta\Gamma}^{(0)} - \eta) \Gamma(1 + \eta)}{\Gamma(1 - a_{\Delta\Gamma}^{(0)} + \eta) \Gamma(1 - \eta)} + 2\gamma_E a_{\Delta\Gamma}^{(0)} \right] + \mathcal{O}(\alpha_s), \end{aligned} \quad (5.126)$$

where the superscript (0) in the RG functions denotes that one should take the leading terms of the corresponding function. For the sake of intelligibility, we further suppressed the arguments of the RG functions. Comparing with the photon case, the main difference is that we have  $r_\Gamma = 1/10$  instead of  $r_\Gamma^{h \rightarrow \gamma\gamma} = 1$ . As a consequence, the soft function is not single-valued in the complex plane. Applying the simplification (5.126) and transforming

the ansatz back from Laplace to momentum space, we find for the soft function at leading order

$$S_3^{\text{LO}}(w, \mu) = U_S(w; \mu_s, \mu) \int_0^\infty \frac{dw'}{w'} S^{\text{LO}}(w', \mu_s) \times I_{2,2}^{1,1} \left( \begin{array}{cc} (-a_{\Delta\Gamma}, 1, 2r_\Gamma) & , \quad (1 - a_{\Delta\Gamma}, 1, 2r_\Gamma) \\ (1, 1, 2r_\Gamma) & , \quad (0, 1, 2r_\Gamma) \end{array} \middle| \frac{w'}{w} \right), \quad (5.127)$$

with

$$U_S(w; \mu_s, \mu) = \left( \frac{we^{-4r_\Gamma\gamma_E}}{\mu_s^2} \right)^{-a_{\Delta\Gamma}^{(0)}(\mu_s, \mu)} \exp \left[ 2S_{\Delta\Gamma}^{(0)}(\mu_s, \mu) + a_{\gamma_s}^{(0)}(\mu_s, \mu) \right], \quad (5.128)$$

$$S^{\text{LO}}(w, \mu_s) = -T_F \delta_{ab} \frac{\alpha_s(\mu_s)}{\pi} m_b(\mu_s) \theta(w - m_b^2).$$

Here,  $S^{\text{LO}}(w, \mu_s)$  denotes the soft function at the matching scale  $\mu_s$  at leading order in perturbation theory. The function  $I_{2,2}^{1,1}(\dots|x)$  is a so-called *Rathie-I* function, defined as

$$I_{p,q}^{m,n} \left( \begin{array}{c} (a_1, \alpha_1, A_1), \dots, (a_p, \alpha_p, A_p) \\ (b_1, \beta_1, B_1), \dots, (b_q, \beta_q, B_q) \end{array} \middle| z \right) = \frac{1}{2\pi i} \int_L \phi(s) z^s ds, \quad (5.129)$$

$$\text{with } \phi(s) = \frac{\prod_{j=1}^m \Gamma^{B_j}(b_j - \beta_j s) \prod_{j=1}^n \Gamma^{A_j}(1 - a_j + \alpha_j s)}{\prod_{j=m+1}^q \Gamma^{B_j}(1 - b_j + \beta_j s) \prod_{j=n+1}^p \Gamma^{A_j}(a_j - \alpha_j s)}.$$

Its definition and properties were first presented in [122]. It is a generalisation of the *Meijer-G* function  $G_{p,q}^{m,n}$  and related via

$$G_{p,q}^{m,n} \left( \begin{array}{c} a_1, \dots, a_p \\ b_1, \dots, b_q \end{array} \middle| z \right) = I_{p,q}^{m,n} \left( \begin{array}{c} (a_1, 1, 1), \dots, (a_p, 1, 1) \\ (b_1, 1, 1), \dots, (b_q, 1, 1) \end{array} \middle| z \right). \quad (5.130)$$

So far, it has seen use in wireless communication systems [123, 124] and, most recently, light-ray operators in celestial conformal field theory (CCFT) [125].

Though the analytic solution takes a rather complicated form, the asymptotic behaviour is fairly simple:

$$S_3^{\text{LO}}(w, \mu) = S^{\text{LO}}(w, \mu_s) U_S(w; \mu_s, \mu) \left( \frac{\Gamma(1 + a_{\Delta\Gamma}^{(0)}(\mu_s, \mu))}{\Gamma(1 - a_{\Delta\Gamma}^{(0)}(\mu_s, \mu))} \right)^{2r_\Gamma} + \mathcal{O}(m_b^2/w). \quad (5.131)$$

We have found that only the region above the hyperbola  $\ell_- \ell_+ > m_b^2$  contributes to the NLL' accurate expression. In this context, further corrections from the *Rathie-I* function are not relevant for NLL' resummation, but will come into play in RG-improved perturbation theory. This is however beyond the scope of this thesis.

### 5.4.3 Large logarithms at NLL' in the form factor

The scale dependence of the  $gg \rightarrow h$  form factor is governed by the evolution equation (5.100). It is not scale-invariant due to the external gluon states. At LO in RG-improved perturbation theory, we find [80]

$$F_{gg}^R(\mu) = e^{2S_{\Gamma_A}(\mu_h, \mu)} \frac{\alpha_s(\mu)}{\alpha_s(\mu_h)} F_{gg}^R(\mu_h), \quad (5.132)$$

and  $\Gamma_A$  stands for the cusp anomalous dimension in the adjoint representation. The scale  $\mu_h^2 = -M_h^2 - i0$  is chosen such that there are no large logarithms left in the hard matching coefficients. The derivation of  $F_{gg}^R(\mu_h)$  is highly non-trivial and will be carried out in multiple steps. There are two kinds of contributions. One stems from the RG evolution of the component functions, which is controlled by the respective anomalous dimension. The second one is NLO corrections from these functions at their matching scales.

The contribution from RG evolution is given by taking the RG-improved LO component functions for  $T_3$ ,

$$T_3^{\text{LO}}(\mu_h) = \lim_{\sigma \rightarrow -1} H_3(\mu_h)^{\text{LO}} \int_0^{M_h} \frac{d\ell_-}{\ell_-} \int_0^{\sigma M_h} \frac{d\ell_+}{\ell_+} \times J^{\text{LO}}(-M_h \ell_-, \mu_h) J^{\text{LO}}(M_h \ell_+, \mu_h) S_3^{\text{LO}}(\ell_- \ell_+, \mu_h) \Big|_{\text{leading power}}. \quad (5.133)$$

In principle, the matching scales of the two jet functions could be different, since they depend on different dynamical scales  $\ell_{\pm}$ . They are chosen such that all logarithms are located only in the evolution factors. The LO jet and soft functions have been derived in the previous section.

To extract the first three towers of large logarithms, we only need to enter the regime  $\ell_+ \ell_- \gg m_b^2$ . We may therefore use the asymptotic expression for the soft function  $S_3$  given by (5.131). In the first step, we define the following abbreviations

$$a_s = a_{\Delta\Gamma}^{(0)}(\mu_s, \mu_h), \quad a_- = a_{\Delta\Gamma}^{(0)}(\mu_-, \mu_h), \quad a_+ = a_{\Delta\Gamma}^{(0)}(\mu_+, \mu_h), \quad (5.134)$$

where  $\mu_-$  is the matching scale entering the jet function  $J(-M_h \ell_-, \mu_h)$  while  $\mu_+$  is that entering the jet function  $J(M_h \ell_+, \mu_h)$ . The factors of gamma functions in the RG-improved jet (5.123) and soft (5.127) functions can be further expanded to

$$\left[ e^{4\gamma_E a_s} \frac{\Gamma^2(1 + a_s)}{\Gamma^2(1 - a_s)} e^{2\gamma_E a_-} \frac{\Gamma(1 + a_-)}{\Gamma(1 - a_-)} e^{2\gamma_E a_+} \frac{\Gamma(1 + a_+)}{\Gamma(1 - a_+)} \right]^{r\Gamma} = 1 + \mathcal{O}(a_s^3, a_-^3, a_+^3). \quad (5.135)$$

The jet and soft functions must be free of large logarithms at the matching scales  $\mu_{\pm}$  and  $\mu_s$ . Since these functions are integrated over soft ( $\ell_+ \ell_- \sim m_b^2$ ) and hard ( $\ell_+ \ell_- \sim M_h^2$ ) regions, we must set these matching scales dynamically under the integral. Hence we fix  $\mu_s^2 = \ell_- \ell_+$ ,

$\mu_-^2 = \sigma M_h \ell_-$  and  $\mu_+^2 = M_h \ell_+$ . Additionally, the pre-factor  $\alpha_s(\mu_s)$  entering the soft function (see (5.128)) should be converted into a scheme that only depends on the hard scale

$$\alpha_s(\nu) = \frac{\alpha_s(\mu)}{X} \left[ 1 - \frac{\alpha_s(\mu)}{4\pi} \frac{\beta_1}{\beta_0} \frac{\ln X}{X} + \mathcal{O}(\alpha_s^2) \right], \text{ with } X = 1 - \frac{\alpha_s(\mu)}{4\pi} \beta_0 \ln \frac{\mu^2}{\nu^2}, \quad (5.136)$$

and we abbreviate the logarithms as follows when necessary

$$L_- = \ln \frac{\mu_h^2}{\mu_-^2}, \quad L_+ = \ln \frac{\mu_h^2}{\mu_+^2}, \quad L_s = \ln \frac{\mu_h^2}{\mu_s^2} = L_- + L_+, \quad \text{and } L = \ln \frac{\mu_h^2}{m_b^2}. \quad (5.137)$$

The relevant parameter  $\rho$  in NLL' resummation is defined as

$$\rho = \frac{\alpha_s(\mu_h)}{4\pi} \frac{\Delta\Gamma_0}{2} L^2 = \frac{\alpha_s(\mu_h)}{2\pi} (C_F - C_A) L^2 \sim -1.192 + 0.955 i, \quad (5.138)$$

Substituting  $L_+ = xL$ ,  $L_- = yL$ , we find up to order NLL'

$$\alpha_s(\mu_s) = \alpha_s(\mu_h) \left( 1 + \frac{\rho}{L} \frac{2\beta_0}{\Delta\Gamma_0} (x+y) + \frac{\rho^2}{L^2} \frac{4\beta_0^2}{(\Delta\Gamma_0)^2} (x+y)^2 + \mathcal{O}(L^{-3}) \right). \quad (5.139)$$

Here,  $\beta_0 = \beta_0$  and the colouring is related to a comparison with the resummation of the photon case and will be explained further later on.

As mentioned before, there are also contributions from the NLO corrections at the matching scales. Due to the dynamic scale setting, logarithms at the matching scales vanish. Hence the corrections from the hard and jet functions are given by the constant terms of these functions. For the soft function though, in principle there are some extra functional terms, see (5.58). However, all these terms go to zero when  $\hat{w}$  is large, such that their contributions are not relevant here. We find for the individual corrections from the matching at higher order

$$\begin{aligned} \Delta H_3(\mu_h) &= -\frac{y_b(\mu_h)}{\sqrt{2}} \left( 1 + \left( -2 + \frac{\pi^2}{6} \right) \frac{\rho}{L^2} \frac{2C_F}{\Delta\Gamma_0} \right), \\ \Delta J(\mu_h) &= 1 + \frac{\rho}{2L^2} \left( -1 - \frac{\pi^2}{6} \right), \\ \Delta S_3(\mu_h) &= -T_F \delta_{ab} \frac{\alpha_s}{\pi} m_b(\mu_h) \left( 1 + \frac{\rho}{L^2} \frac{2}{\Delta\Gamma_0} \left[ C_F \left( 12 - \frac{\pi^2}{2} \right) - C_A \frac{\pi^2}{6} \right] \right). \end{aligned} \quad (5.140)$$

Their combined contribution reads

$$\begin{aligned} 1 + \Delta_{\text{matching}} &= \mathcal{M}_0^{-1}(\mu_h) \Delta H_3(\mu_h) (\Delta J(\mu_h))^2 \Delta S_3(\mu_h) \\ &= 1 + \frac{\rho}{L^2} \frac{2}{\Delta\Gamma_0} \left[ C_F \left( 8 - \frac{2\pi^2}{3} \right) + C_A \left( 2 + \frac{\pi^2}{6} \right) \right]. \end{aligned} \quad (5.141)$$

Adding all contributions together,  $T_3(\mu_h)$  reads

$$\begin{aligned}
T_3(\mu_h)|_{\text{NLL}'} &= \mathcal{M}_0(\mu_h) L^2 \int_0^1 dx \int_0^{1-x} dy \left[ 1 + \frac{\rho}{L} \frac{2\beta_0}{\Delta\Gamma_0} (x+y) + \frac{\rho^2}{L^2} \frac{4\beta_0^2}{(\Delta\Gamma_0)^2} (x+y)^2 \right] \\
&\times \{1 + \Delta_{\text{matching}}\} \\
&\times \exp \left[ 2S_{\Delta\Gamma}^{(0)}(\mu_s, \mu_h) - 2S_{\Delta\Gamma}^{(0)}(\mu_-, \mu_h) - 2S_{\Delta\Gamma}^{(0)}(\mu_+, \mu_h) + a_{\gamma_s}^{(0)}(\mu_s, \mu_h) + a_{\gamma_m}^{(0)}(\mu_s, \mu_h) \right]_{\text{NLL}'}, \tag{5.142}
\end{aligned}$$

where the term in square brackets accounts for the contribution from converting the strong coupling constant in the pre-factor, the term in curly braces is generated by corrections to the component functions at the matching scale, and the exponential factor is due to scale evolution. We insert the expressions for the RG functions (see appendix A1.3) and perform all remaining integrals.

Neglecting terms of order  $\mathcal{O}(L^{-3})$  we arrive at

$$\begin{aligned}
T_3(\mu_h)|_{\text{NLL}'} &= \mathcal{M}_0(\mu_h) \frac{L^2}{2} \sum_{n=0}^{\infty} (-\rho)^n \frac{2\Gamma(n+1)}{\Gamma(2n+3)} \left\{ 1 + \frac{1}{L} \left[ \rho \frac{-(\gamma_s^0 + \gamma_m^0) + 2\beta_0}{\Delta\Gamma_0} \frac{2n+2}{2n+3} \right. \right. \\
&\quad \left. \left. - \rho^2 \frac{\beta_0}{\Delta\Gamma_0} \frac{(n+1)^2}{(2n+3)(2n+5)} \right] + \frac{1}{L^2} \left[ \rho \frac{C_F \left(4 - \frac{\pi^2}{3}\right) + C_A \left(1 + \frac{\pi^2}{12}\right)}{C_F - C_A} \right. \right. \\
&\quad \left. \left. + \rho^2 \left( -\frac{\beta_0(\gamma_s^0 + \gamma_m^0)}{(\Delta\Gamma_0)^2} \frac{n+1}{n+2} - \frac{\Delta\Gamma_1}{(\Delta\Gamma_0)^2} \frac{(n+1)^2}{(n+2)(2n+3)} \right. \right. \\
&\quad \left. \left. + \frac{(\gamma_s^0 + \gamma_m^0)^2}{(\Delta\Gamma_0)^2} \frac{n+1}{2(n+2)} - \frac{\beta_0(\gamma_s^0 + \gamma_m^0)}{(\Delta\Gamma_0)^2} \frac{2(n+1)}{n+2} + \frac{\beta_0^2}{(\Delta\Gamma_0)^2} \frac{4(n+1)}{n+2} \right) \right. \\
&\quad \left. \left. + \rho^3 \left( \frac{\beta_0(\gamma_s^0 + \gamma_m^0)}{(\Delta\Gamma_0)^2} \frac{(n+1)^2}{2(n+3)(2n+3)} - \frac{\beta_0^2}{(\Delta\Gamma_0)^2} \frac{(n+1)^2(7n+18)}{6(n+3)(2n+3)(2n+5)} \right. \right. \right. \\
&\quad \left. \left. \left. - \frac{\beta_0^2}{(\Delta\Gamma_0)^2} \frac{(n+1)^2}{(n+3)(2n+3)} \right) + \rho^4 \frac{\beta_0^2}{(\Delta\Gamma_0)^2} \frac{(n+1)^2(n+2)}{8(n+4)(2n+3)(2n+5)} \right] \right\}. \tag{5.143}
\end{aligned}$$

Note that  $\gamma_s^0 = -6C_F + 2\beta_0$ . The first two towers of logarithms (up to order  $\mathcal{O}(L^{-1})$ ) have already been derived in [80, 126]. It is remarkable that the leading logarithm (LL) and next-to-leading logarithm (NLL) term can be retrieved from the corresponding ones in the photon case by a simple replacement of colour factors  $C_F \rightarrow C_F - C_A$ , as was first noted for the LL term in [127]. Furthermore, the NLL corrections have been derived in [128] using non-SCET methods. As a non-trivial cross-check expression (5.143) reproduces correctly the leading logarithms in the three-loop form factor (5.116). In [129], the resummed amplitude for the  $h \rightarrow \gamma\gamma$  process was presented at NLL' accuracy. To compare this with our result (5.143), it is not sufficient to set  $C_A \rightarrow 0$ . The reason for that is that the pre-factor of our  $gg \rightarrow h$  process features a strong coupling constant evaluated at the soft scale which is subject to being converted to an evaluation at the high scale (5.136) and therefore gives rise to additional terms suppressed by one and two factors of  $1/L$ , see (5.139). In contrast, in the  $h \rightarrow \gamma\gamma$  case the pre-factor is  $\alpha_b(\mu_s) = (Q_b e)/(4\pi)$ , which is related to the QED coupling constant at the high scale via  $\alpha_b(\mu_s) = \alpha_b(\mu_h)(1 + \mathcal{O}(\alpha_b(\mu_h)))$ . Since  $\alpha_b \ll \alpha_s$ , these higher terms are neglected consequently. To account for this effect, we must henceforth set

$C_A \rightarrow 0$  and  $\beta_0 \rightarrow 0$  while keeping  $\beta_0 \neq 0$ . Hence, we coloured the corresponding  $\beta_0$ -terms to easily allow comparison between abelian and non-abelian processes.

The series in (5.143) can be cast into more elegant form by executing the infinite sums. We introduce the special functions

$$\begin{aligned} F_1(z) &= {}_2F_2\left(1, 1; \frac{3}{2}, 2; -\frac{z}{4}\right), \\ F_2(z) &= {}_2F_2\left(1, 1; \frac{1}{2}, 2; -\frac{z}{4}\right), \\ D(z) &= e^{-z^2} \int_0^z dx e^{x^2}, \end{aligned} \quad (5.144)$$

where  $F_1(z)$  and  $F_2(z)$  are hypergeometric functions, and  $D(z)$  is a so-called Dawson integral function. We obtain

$$\begin{aligned} T_3(\mu_h)|_{\text{NLL}'} &= \mathcal{M}_0(\mu_h) \frac{L^2}{2} \left\{ F_1(\rho) + \frac{1}{L} \frac{2}{\Delta\Gamma_0} \left[ 4\beta_0 - 3\beta_0 - 2(\gamma_s^0 + \gamma_m^0) \right. \right. \\ &\quad \left. \left. + (-2(4\beta_0 - 3\beta_0) + \rho\beta_0 + 4(\gamma_s^0 + \gamma_m^0)) \frac{D\left(\frac{\sqrt{\rho}}{2}\right)}{\sqrt{\rho}} \right] \right. \\ &+ \frac{1}{L^2} \frac{1}{(\Delta\Gamma_0)^2} \left[ \left( -\frac{\rho^2}{4}\beta_0^2 + \frac{\rho}{6}(24\beta_0^2 - 7\beta_0^2) - 2\rho\beta_0(\gamma_s^0 + \gamma_m^0) \right. \right. \\ &\quad \left. \left. + 18\beta_0^2 + 4\Delta\Gamma_1 \right) \sqrt{\rho} D\left(\frac{\sqrt{\rho}}{2}\right) \right. \\ &\quad \left. + \left( (4 + \rho)\beta_0^2 - 8(\gamma_s^0 + \gamma_m^0)(2\beta_0 - \beta_0) + 4(\gamma_s^0 + \gamma_m^0)^2 \right) \frac{\rho}{4} \right. \\ &\quad \left. - \left( 6\beta_0^2 - 2(\gamma_s^0 + \gamma_m^0)(2\beta_0 - \beta_0) + (\gamma_s^0 + \gamma_m^0)^2 \right) \rho F_2(\rho) \right. \\ &\quad \left. - \left[ 4\beta_0^2 + 2\Delta\Gamma_1 + \frac{C_A\left(\frac{\pi^2}{12} + 1\right) - C_F\left(\frac{\pi^2}{3} - 4\right)}{C_A - C_F} (\Delta\Gamma_0)^2 \right] \rho F_1(\rho) \right] \left. \right\}. \end{aligned} \quad (5.145)$$

For a better intelligibility of the resummed result (5.145), we find it instructive to give the asymptotic behaviour of the special functions. In the limits  $\rho \rightarrow 0, \infty$ , the hypergeometric functions can be expanded as

$$F_1(\rho) = \begin{cases} 1 - \frac{\rho}{12} + \frac{\rho^2}{180} - \frac{\rho^3}{3360} + O(\rho^4), & \rho \rightarrow 0, \\ 2 \frac{\ln(\rho e^{\gamma_E})}{\rho} - \frac{4}{\rho^2} + O(\rho^{-3}), & \rho \rightarrow \infty, \end{cases} \quad (5.146)$$

$$F_2(\rho) = \begin{cases} 1 - \frac{\rho}{4} + \frac{\rho^2}{36} - \frac{\rho^3}{480} + O(\rho^4), & \rho \rightarrow 0, \\ \frac{4 - 2 \ln(\rho e^{\gamma_E})}{\rho} + \frac{12}{\rho^2} + O(\rho^{-3}), & \rho \rightarrow \infty. \end{cases} \quad (5.147)$$



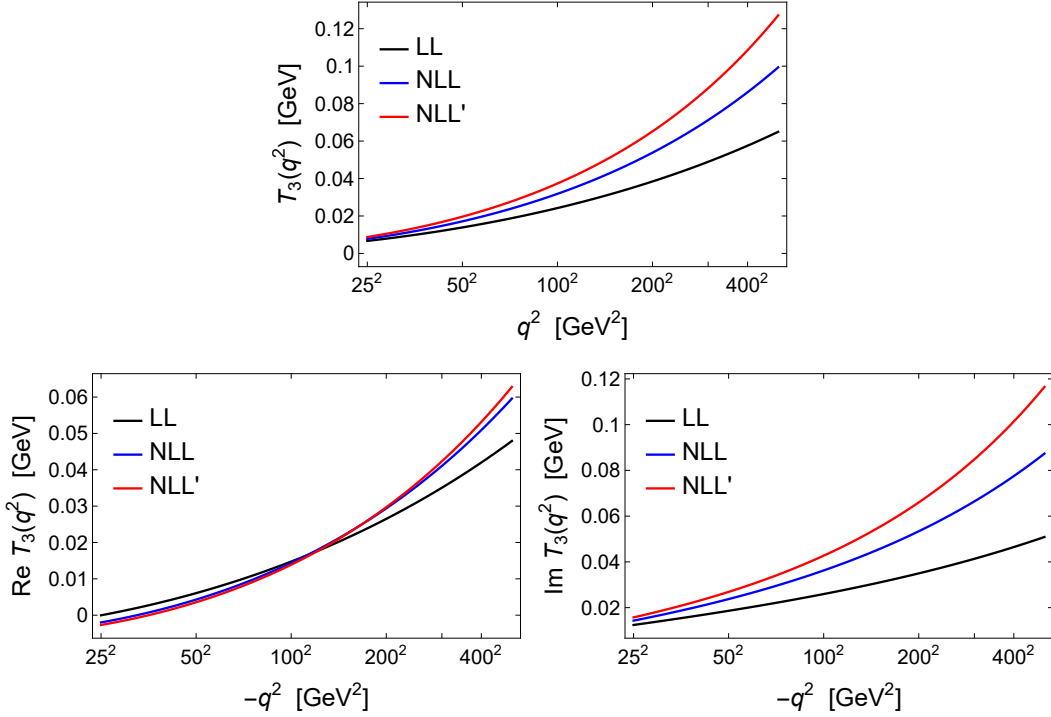


Figure 5.12: Resummed  $T_3$  at LL (black), NLL (blue) and NLL' (red) accuracy. We fix the strong coupling constant at  $\alpha_s(M_h)$  and vary the hard scale  $\mu_h^2 = q^2$  entering the large logarithms  $L$  and expansion parameter  $\rho$ . The upper panel shows  $T_3$  for  $q^2 > 0$ , the lower two panels give the real and imaginary part for  $q^2 < 0$ . NLL(') corrections become increasingly more important for  $q^2$ -values further away from its physical value  $q^2 = -M_h^2$ .

The Dawson function appearing first at NLL obeys the following behaviour

$$D\left(\frac{\sqrt{\rho}}{2}\right) = \begin{cases} \frac{\sqrt{\rho}}{2} \left[ 1 - \frac{\rho}{6} + \frac{\rho^2}{60} - \frac{\rho^3}{840} + \mathcal{O}(\rho^4) \right], & \rho \rightarrow 0, \\ \frac{1}{\sqrt{\rho}} \left[ 1 + \frac{2}{\rho} + \frac{12}{\rho^2} + \mathcal{O}(\rho^{-3}) \right], & \rho \rightarrow \infty. \end{cases} \quad (5.148)$$

In figure 5.12 we show the resummed  $T_3$  at LL (black), NLL (blue) and NLL' (red) accuracy. Here, we fix the strong coupling constant at  $\alpha_s(M_h)$  and vary the hard scale  $\mu_h^2 \equiv q^2$  entering the large logarithms  $L$  and expansion parameter  $\rho$ . We give the plots for both  $q^2 > 0$  (upper panel) and real and imaginary part for  $q^2 < 0$  (lower panels). NLL' corrections become increasingly more significant the further one takes  $q^2$  from its physical value  $q^2 = -M_h^2$  chosen in the resummation.

As explained previously, at NLL' there is one contribution from the second term in the factorisation theorem. However, because  $T_2 \propto \alpha_s^n L^{n+1}$ , only the term for  $n = 1$  is relevant. It reads

$$T_2(\mu_h)|_{\text{NLL}'} = i\mathcal{M}_0(\mu_h) \frac{L^2}{2} \frac{\rho}{L^2} \frac{\pi^2}{3}. \quad (5.149)$$

The full NLL' form factor is then  $F_{gg}(\mu_h)|_{\text{NLL}'} = T_2(\mu_h)|_{\text{NLL}'} + T_3(\mu_h)|_{\text{NLL}'}$ .

## APPENDIX I

---

### AI.1 Renormalisation factors

Here we collect the renormalisation factors of parameters and the different component functions.

The three parameters involved in this process, a) the  $b$  quark mass entering the operators, b) the  $b$  quark Yukawa coupling entering the hard functions, and c) the QCD coupling constant, are renormalised in the  $\overline{\text{MS}}$  subtraction scheme as

$$m_{b,0} = Z_m m_b(\mu), \quad y_{b,0} = \mu^\epsilon Z_y y_b(\mu), \quad \alpha_{s,0} = \mu^{2\epsilon} Z_{\alpha_s} \alpha_s(\mu), \quad (\text{AI.1})$$

with the renormalisation factors

$$Z_y = Z_m = 1 - 3C_F \frac{\alpha_s(\mu)}{4\pi\epsilon} + \mathcal{O}(\alpha_s^2), \quad Z_{\alpha_s} = 1 - \beta_0 \frac{\alpha_s(\mu)}{4\pi\epsilon} + \mathcal{O}(\alpha_s^2). \quad (\text{AI.2})$$

Here  $\beta_0 = \frac{11}{3}C_A - \frac{4}{3}T_F n_f$  is the first coefficient of the QCD  $\beta$ -function, with  $n_f = n_b + n_l = 5$  being the number of active quark flavours. In order to compare our results in different schemes, we need the following relation between the  $b$ -quark pole mass and its running mass [130, 131]:

$$\begin{aligned} \frac{m_b(\mu)}{m_b} &= 1 + \frac{\alpha_s}{4\pi} C_F (-4 + 3L_m) \\ &+ \left(\frac{\alpha_s}{4\pi}\right)^2 \left[ C_F^2 \left( \frac{9L_m^2}{2} - \frac{21L_m}{2} + \frac{7}{8} + (8\ln 2 - 5)\pi^2 - 12\zeta_3 \right) \right. \\ &+ C_F C_A \left( -\frac{11L_m^2}{2} + \frac{185L_m}{6} - \frac{1111}{24} + \frac{4(1 - 3\ln 2)\pi^2}{3} + 6\zeta_3 \right) \\ &\left. + C_F T_F \left( 2n_f L_m^2 - \frac{26n_f}{3} L_m + \frac{(143 - 16\pi^2)n_b}{6} + \frac{(71 + 8\pi^2)n_l}{6} \right) \right], \end{aligned} \quad (\text{AI.3})$$

with  $L_m = \ln(m_b^2/\mu^2)$ .

The hard function  $H_3(\mu)$  (5.49) is renormalised by

$$Z_{33}^{-1} = 1 + \frac{C_F \alpha_s}{4\pi} \left[ \frac{2}{\epsilon^2} - \frac{2}{\epsilon} \left( L_h - \frac{3}{2} \right) \right]. \quad (\text{AI.4})$$

The hard coefficients  $\bar{H}_2(\mu)$  and its endpoint counterpart are renormalised in equation (5.61) and (5.59). The corresponding renormalisation factors are

$$\begin{aligned} Z_{22}^{-1}(z, z') &= \delta(z - z') \\ &+ \frac{\alpha_s}{4\pi} \left\{ \delta(z - z') \left[ (C_F - C_A) \frac{2(L_z + L_{\bar{z}}) + 3}{\epsilon} + C_A \left( \frac{2}{\epsilon^2} - \frac{2L_h - 3}{\epsilon} \right) \right] \right. \\ &\left. + \frac{2(C_F - C_A/2)}{\epsilon} z(1 - z) \left[ \frac{1}{z'(1 - z)} \frac{\theta(z' - z)}{(z' - z)} + \frac{1}{z(1 - z')} \frac{\theta(z - z')}{(z - z')} \right]_+ \right\} \end{aligned} \quad (\text{AI.5})$$

$$\begin{aligned} \llbracket Z_{22}^{-1}(z, z') \rrbracket &= \delta(z - z') + \frac{\alpha_s}{4\pi} \left\{ \delta(z - z') \left[ (C_F - C_A) \frac{2L_z + 3}{\epsilon} + C_A \left( \frac{2}{\epsilon^2} - \frac{2L_h - 3}{\epsilon} \right) \right] \right. \\ &\left. + \frac{(2C_F - C_A)}{\epsilon} z \left[ \frac{\theta(z' - z)}{z'(z' - z)} + \frac{\theta(z - z')}{z(z - z')} \right]_+ \right\}. \end{aligned} \quad (\text{AI.6})$$

At NLO, the renormalisation factor for the soft function  $S_2(z, \mu)$  (5.65) is given by

$$\begin{aligned} Z_{gg}^{-1} Z_{22}(z, z') &= \delta(z - z') + \frac{\alpha_s}{4\pi} \left\{ - \frac{3C_F - \beta_0 + 2(C_F - C_A)(L_z + L_{\bar{z}})}{\epsilon} \delta(z - z') \right. \\ &\left. - \frac{(2C_F - C_A)}{\epsilon} z(1 - z) \left[ \frac{1}{z'(1 - z)} \frac{\theta(z' - z)}{(z' - z)} + \frac{1}{z(1 - z')} \frac{\theta(z - z')}{(z - z')} \right]_+ \right\} \\ Z_{gg}^{-1} Z_{21}(z) &= \frac{T_F \delta_{ab} \alpha_s}{2\pi} \left\{ - \frac{1}{\epsilon} + \frac{\alpha_s}{4\pi} \left[ (C_F - C_A) \left( \frac{L_z + L_{\bar{z}}}{\epsilon^2} - \frac{L_z^2 + L_{\bar{z}}^2 - 1}{2\epsilon} \right) \right. \right. \\ &\left. \left. + C_F \frac{2L_z L_{\bar{z}} - 6 + \pi^2/3}{\epsilon} \right] \right\}. \end{aligned} \quad (\text{AI.7})$$

## AI.2 Anomalous dimensions

### AI.2.1 Cusp anomalous dimension

The cusp anomalous dimension in the fundamental and adjoint representation up to two-loop order is expanded in perturbation theory as

$$\Gamma_{\text{cusp}}^R(\alpha_s) = \Gamma_0^R \frac{\alpha_s}{4\pi} + \Gamma_1^R \left( \frac{\alpha_s}{4\pi} \right)^2 + \dots, \quad (\text{AI.8})$$

where the superscript  $R$  refers to the  $SU(N)$  representation. In the case of QCD, the relevant representations are fundamental ( $R = F$ ) and adjoint ( $R = A$ ). In the  $\overline{\text{MS}}$  renormalisation scheme the expansion coefficients in the respective representation are given by [132]

$$\Gamma_{\text{cusp}}^R(\alpha_s) = 4C_R \left\{ \frac{\alpha_s}{4\pi} + \left( \frac{\alpha_s}{4\pi} \right)^2 \left[ C_A \left( \frac{67}{9} - \frac{\pi^2}{3} \right) - \frac{20}{9} n_f T_F \right] + \dots \right\}, \quad (\text{AI.9})$$

where  $C_R = C_F$  for the fundamental representation while  $C_R = C_A$  for the adjoint representation. We introduce the short-hand notations  $\Delta\Gamma_0$  and  $\Delta\Gamma_1$  which represent the difference of the cusp anomalous dimensions at leading and next-to-leading order

$$\begin{aligned}\Delta\Gamma &= \Delta\Gamma_0 \frac{\alpha_s}{4\pi} + \Delta\Gamma_1 \left(\frac{\alpha_s}{4\pi}\right)^2 \\ &= 4(C_F - C_A) \left\{ \frac{\alpha_s}{4\pi} + \left(\frac{\alpha_s}{4\pi}\right)^2 \left[ C_A \left(\frac{67}{9} - \frac{\pi^2}{3}\right) - \frac{20}{9} n_f T_F \right] + \dots \right\}.\end{aligned}\quad (\text{AI.10})$$

### AI.2.2 Anomalous dimension $\gamma_{gg}$

The anomalous dimension  $\gamma_{gg}$  is associated with the renormalisation factor  $Z_{gg}$  of the two-gluon operator  $O_{gg}$ .<sup>3</sup> To all orders of perturbation theory, it is given by [116]

$$\gamma_{gg} = \Gamma_{\text{cusp}}^A(\alpha_s) L_h + 2\gamma_g = \frac{\alpha_s}{4\pi} (4C_A L_h - 2\beta_0) + \mathcal{O}(\alpha_s^2). \quad (\text{AI.11})$$

Here,  $\gamma_g$  is the anomalous dimension associated with the gluon wave function renormalisation. At two-loop order, it reads [116]

$$\begin{aligned}\gamma_g &= \frac{\alpha_s}{4\pi} (-\beta_0) + \left(\frac{\alpha_s}{4\pi}\right)^2 \left[ \left(-\frac{692}{27} + \frac{11\pi^2}{18} + 2\zeta_3\right) C_A^2 \right. \\ &\quad \left. + \left(\left(\frac{256}{27} - \frac{2\pi^2}{9}\right) C_A + 4C_F\right) T_F n_f \right].\end{aligned}\quad (\text{AI.12})$$

### AI.2.3 Anomalous dimensions of component functions

The renormalisation factor of the soft function  $S_1(\mu)$  is the same as for the quark mass, and so is its anomalous dimension

$$\gamma_{11} - \gamma_{gg} = -\gamma_m = \frac{3C_F\alpha_s}{2\pi} + \mathcal{O}(\alpha_s^2). \quad (\text{AI.13})$$

<sup>3</sup> The two-gluon operator is renormalised by  $\langle O_{gg}(\mu) \rangle = Z_{gg} \langle O_{gg}^{(0)} \rangle$ , hence the renormalised form factor reads  $F_{gg}(\mu) = Z_{gg}^{-1} F_{gg}^{(0)}$ .

The diagonal and off-diagonal elements involved in the RG equation of  $S_2(z, \mu)$  and its endpoint region counterpart are

$$\begin{aligned} \gamma_{22}(z, z') - \gamma_{gg}\delta(z - z') &= -\frac{\alpha_s}{4\pi} \left\{ \left[ 4(C_F - C_A)(L_z + L_{\bar{z}}) + 6C_F - 2\beta_0 \right] \delta(z - z') \right. \\ &\quad \left. + 4 \left( C_F - \frac{C_A}{2} \right) z\bar{z} \left[ \frac{1}{z'\bar{z}} \frac{\theta(z' - z)}{(z' - z)} + \frac{1}{z\bar{z}'} \frac{\theta(z - z')}{(z - z')} \right]_+ \right\}, \\ \llbracket \gamma_{22}(z, z') \rrbracket - \gamma_{gg}\delta(z - z') &= -\frac{\alpha_s}{4\pi} \left\{ \left[ 4(C_F - C_A)L_z + 6C_F - 2\beta_0 \right] \delta(z - z'), \right. \\ &\quad \left. + 4 \left( C_F - \frac{C_A}{2} \right) z \left[ \frac{\theta(z' - z)}{z'(z' - z)} + \frac{\theta(z - z')}{z(z - z')} \right]_+ \right\}, \end{aligned} \quad (\text{AI.14})$$

and

$$\begin{aligned} \gamma_{21}(z) &= \frac{T_F \delta_{ab} \alpha_s}{\pi} \left\{ -1 + \frac{\alpha_s}{4\pi} \left[ (C_F - C_A)(1 - L_z^2 - L_{\bar{z}}^2) \right. \right. \\ &\quad \left. \left. + C_F \left( 4L_z L_{\bar{z}} - 12 + \frac{2\pi^2}{3} \right) \right] \right\}, \\ \llbracket \gamma_{21}(z) \rrbracket &= \frac{T_F \delta_{ab} \alpha_s}{\pi} \left\{ -1 + \frac{\alpha_s}{4\pi} \left[ (C_F - C_A)(1 - L_z^2) + C_F \left( \frac{2\pi^2}{3} - 12 \right) \right] \right\}. \end{aligned} \quad (\text{AI.15})$$

The anomalous dimension for  $H_3(\mu)$  is given by

$$\gamma_{33} = \Gamma_{\text{cusp}}^F(\alpha_s) L_h + \gamma_H(\alpha_s) = \frac{C_F \alpha_s}{\pi} \left( L_h - \frac{3}{2} \right) + \mathcal{O}(\alpha_s^2), \quad (\text{AI.16})$$

where  $\gamma_H = 2\gamma_q$ , and its expression is known up to three loops [116, 133, 134]. The anomalous dimensions for the jet and soft function  $S_3$  in the third term read

$$\begin{aligned} \gamma_J(p^2, xp^2) &= \frac{\alpha_s}{\pi} \left[ (C_F - C_A) L_p \delta(1 - x) + \left( C_F - \frac{C_A}{2} \right) \Gamma(1, x) \right] + \mathcal{O}(\alpha_s^2), \\ \gamma_S(w, w') &= -\frac{\alpha_s}{\pi} \left\{ \left[ (C_F - C_A) L_w + \frac{3C_F - \beta_0}{2} \right] \delta(w - w') \right. \\ &\quad \left. + 2 \left( C_F - \frac{C_A}{2} \right) w \Gamma(w, w') \right\} + \mathcal{O}(\alpha_s^2). \end{aligned} \quad (\text{AI.17})$$

These results satisfy the non-trivial relation (5.83).

### AI.3 RG functions

The RG functions used in section 5.4 are defined as

$$\begin{aligned}
 S_V(\nu, \mu) &= - \int_{\alpha_s(\nu)}^{\alpha_s(\mu)} d\alpha \frac{\gamma_V(\alpha)}{\beta(\alpha)} \int_{\alpha_s(\nu)}^{\alpha} \frac{d\alpha'}{\beta(\alpha')}, \\
 a_V(\nu, \mu) &= - \int_{\alpha_s(\nu)}^{\alpha_s(\mu)} d\alpha \frac{\gamma_V(\alpha)}{\beta(\alpha)},
 \end{aligned}
 \tag{AI.18}$$

with  $\gamma_V$ ,  $V = \Delta\Gamma$ ,  $s$  the respective anomalous dimension. In order to derive the RG-improved soft and jet functions at leading order, we need to solve the integrals up to leading order. We find

$$\begin{aligned}
 a_V^{(0)}(\nu, \mu) &= \frac{\gamma_{V,0}}{2\beta_0} \ln r, \\
 S_V^{(0)}(\nu, \mu) &= \frac{\gamma_{V,0}}{4\beta_0^2} \left[ \frac{4\pi}{\alpha_s(\nu)} \left( 1 - \frac{1}{r} - \ln r \right) + \left( \frac{\gamma_{V,1}}{\gamma_{V,0}} - \frac{\beta_1}{\beta_0} \right) (1 - r + \ln r) + \frac{\beta_1}{2\beta_0} \ln^2 r \right],
 \end{aligned}
 \tag{AI.19}$$

where  $r = \alpha_s(\mu)/\alpha_s(\nu)$ .







*Part II:*

*Flavour physics of ALPs*



## EFFECTIVE FIELD THEORY FOR ALPS

---

### 6.1 Introduction to ALPs

Axion-like particles (ALPs) are among the best motivated extensions of the Standard Model of Particle Physics. They are low-energy remnants of high-energy UV-complete theories. As pseudo-Nambu–Goldstone bosons, they emerge through the spontaneous breaking of a UV  $U(1)$  symmetry. Their name was derived from the QCD axion, a particle that was introduced along with its corresponding spontaneously broken global  $U(1)_{\text{PQ}}$  symmetry by Peccei, Quinn and others to yield a dynamical solution to the strong CP problem [135–138]. The strong CP problem is the question why the parameter associated with a CP violating term in the QCD Lagrangian is experimentally found to be tiny  $\bar{\theta} \leq 10^{-10}$  [139], while theoretically it could be of order  $\mathcal{O}(1)$ . The Peccei-Quinn solution promotes  $\bar{\theta}$  to a quantum field, that dynamically relaxes the effective value to 0. Typical axion models usually feature axions with extremely small masses  $m_a \sim 10^{-5} \text{ eV} - 10^{-3} \text{ eV}$ . Such light-weight models often suffer from the “axion-quality problem” [140–144]: It is a general belief that effects of quantum gravity will eventually break any global symmetry. The breaking of the  $U(1)_{\text{PQ}}$  symmetry will then give rise to higher dimensional operators that introduce corrections to the axion potential, thus reintroducing a non-vanishing CP phase in QCD interactions. A possible work-around is given by heavy axion models, such as [145–150]. Moreover, in most axion models the axion mass and its coupling strength to photons are related. Hence, in probes for axions, the viable region of parameter space of photon coupling versus mass is a relatively thin band. In the literature, two types of axion models have manifested. In KSVZ models the SM fermions are uncharged under the Peccei-Quinn symmetry, hence the axion only couples to gauge bosons [151, 152]. For DFSZ type models, additional axion couplings to SM fermions are present [153, 154].

ALPs generalise the axion concept to different, not necessarily specified  $U(1)$  symmetries that are spontaneously broken. Their mass and general couplings are unrelated and can be seen as free parameters of the theory. As a consequence, ALPs usually do not provide a solution to the strong CP problem. Moreover, if the underlying global symmetry is flavour-dependent, the ALP can acquire flavour-violating couplings to quarks and leptons in the low-energy effective theory. This would provide new sources of flavour and CP violation in addition to the SM Yukawa couplings, and therefore offers a rich phenomenology. Such patterns occur among others in generalised DFSZ models, where the Peccei-Quinn charges of the SM fields are not flavour universal [155–162]. If the  $U(1)_{\text{PQ}}$

is identified with the  $U(1)_{\text{FN}}$  of the Froggatt-Nielsen mechanism to explain the hierarchy in fermion masses, the ALP emerges as the axiflavor or flaxion that has flavour-violating couplings and can simultaneously address the strong CP problem [163, 164]. In even more ambitious approaches, the combined  $U(1)_{\text{PQ/FN}}$  was further identified with the symmetry of the Higgs field [165, 166]. Additionally to the aforementioned properties of the axiflavor, the unified Higgs-axiflavor can further deliver a trigger for electro-weak symmetry breaking (EWSB). In section 6.2 we will show that even flavour-conserving couplings of the ALP in the UV will inevitably generate flavour-changing couplings at low energies through RG running. This fact has also been noted in [167] and was first published in [5]. This is remarkable, because it means that properties of the SM that are not part of the extended model can imprint themselves in the low-energy effective theory, i.e. the SM + ALP. Moreover, it has been shown recently that via RG effects, ALPs can source most dimension-6 SMEFT operators [168]. This can potentially lead to interesting phenomenological implications, reinforcing the importance of studying light new physics models in contrast to heavy new particles.

Apart from their implications on flavour physics phenomenology, ALPs have been shown to be viable cold dark matter candidates [169, 170]. Moreover, they could have triggered phase transitions in the early universe that could in principle be detectable through certain signatures in gravitational waves [171, 172].

In this thesis, we will focus on ALPs within the mass range of a few MeV to a few GeV. Classical axion solutions to the strong CP problem are typically many orders of magnitude lighter. The reason is that as pNGBs, axions should in principle be exactly massless. This masslessness is further protected by a so-called shift symmetry, a remnant of the high energy Peccei-Quinn symmetry. However, QCD instanton effects give rise to a small dynamical mass [152, 173, 174]. We allow for additional sources of shift-symmetry breaking entering in the form of an explicit mass term. In non-abelian extensions of the SM with an enlarged spectrum of coloured particles, dynamically generated breaking terms can occur. Due to the enhancement of the strong coupling constant at higher energies, these effects can be sizeable. Early ideas of introducing extra coloured matter at an intermediate scale either led to new hierarchy problems or spoil the solution of the strong CP problem due to new CP-violating phases [175–180]. Some more recent realisations included mirror copies of the SM, such that the complete particle spectrum inherits an additional  $\mathbb{Z}_2$  symmetry, which is broken. The symmetry-breaking scale of the mirror sector can be larger than the electroweak scale, thereby enhancing significantly the axion mass [145–148, 150]. Another mechanism explored in [181] considers an enlarged colour sector, which solves the strong CP problem via new massless fermions. The spontaneous breaking of the unified colour group  $SU(6) \times SU(3')$  into QCD and another confining group provides a source of naturally large axion mass due to small-size instantons, while automatically ensuring a CP-conserving vacuum. A different approach was presented in [182], where the  $SU(3)_c$  group of the SM is extended to be a diagonal subgroup of a parent  $SU(3) \times SU(3) \times \dots$  group, which is broken at a high scale. All SM quarks are charged under a single  $SU(3)$  factor of the parent group and an axion is introduced for each one, which independently

relaxes the corresponding  $\theta$  angle to 0. This allows each of the axions to have a mass significantly larger than in the QCD axion case. These studies show that in suitable extensions of the SM it is possible to generate a genuine ALP mass term while preserving the solution of the strong CP problem.

In this thesis, we will first introduce the general Lagrangian set-up for an extensive study of flavour observables from ALPs in section 6.2. Furthermore, our study of RG effects will show how any ALP–SM coupling in the UV will inevitably generate couplings to all particles in the low-energy EFT, especially including quark flavour-violating couplings. In more detail, we will demonstrate how ALP couplings evolve from the high scale of Peccei–Quinn (PQ) symmetry breaking to the weak scale, where we integrate out heavy SM fields. From this procedure matching corrections arise, and we give numerical estimates of their strength. Eventually, we study the RG evolution below the weak scale down to hadronic scales where non-perturbative QCD effects come into play. ALP interactions at such low energies are investigated in section 6.3, where we will demonstrate how to consistently implement ALPs into the weak chiral and the nuclear Lagrangian. In sections 7.1 and 7.2 will conduct a comprehensive study of ALP flavour phenomenology in the quark and lepton sector, respectively, and present how flavour observables can be used to constrain ALP models. The results displayed in chapters 6 and 7 have been published in [5–7], and are summarised and adapted for this thesis.

## 6.2 The ALP Lagrangian and RG effects at low energies

We assume the existence of a new pseudoscalar resonance, the ALP  $a$ . Under SM gauge groups, it transforms as a singlet. It is the pseudo-Nambu–Goldstone boson of a spontaneously broken  $U(1)$  symmetry at the UV scale, which we will call the Peccei–Quinn or PQ symmetry. This additional global symmetry is realised at energies above the scale  $\Lambda \gg \Lambda_{\text{EW}}$ , with  $\Lambda_{\text{EW}} = 246 \text{ GeV}$  the electroweak scale. For our purposes we will typically assume  $\Lambda = 4\pi \text{ TeV}$ . The ALP can be regarded as the phase of a complex scalar at high energies. Therefore, at the classical level, its couplings are protected by an approximate shift symmetry  $a \rightarrow a + \text{constant}$ . For a classical QCD axion, this symmetry is exact. However, for the case at hand we allow for an explicit soft breaking of the symmetry by introducing a mass term  $m_{a,0}$  for the ALP. Up to dimension 5, the most general Lagrangian reads [183]

$$\begin{aligned} \mathcal{L}_{\text{eff}}^{D \leq 5} = & \frac{1}{2} (\partial_\mu a)(\partial^\mu a) - \frac{m_{a,0}^2}{2} a^2 + \frac{\partial^\mu a}{f} \sum_F \bar{\psi}_F c_F \gamma_\mu \psi_F + c_\phi \frac{\partial^\mu a}{f} (\phi^\dagger i \overleftrightarrow{D}_\mu \phi) \\ & + c_{GG} \frac{\alpha_s}{4\pi} \frac{a}{f} G_{\mu\nu}^a \tilde{G}^{\mu\nu,a} + c_{WW} \frac{\alpha_2}{4\pi} \frac{a}{f} W_{\mu\nu}^A \tilde{W}^{\mu\nu,A} + c_{BB} \frac{\alpha_1}{4\pi} \frac{a}{f} B_{\mu\nu} \tilde{B}^{\mu\nu}. \end{aligned} \quad (6.1)$$

Here  $G_{\mu\nu}^a$ ,  $W_{\mu\nu}^A$  and  $B_{\mu\nu}$  are the field-strength tensors of  $SU(3)_c$ ,  $SU(2)_L$  and  $U(1)_Y$ ,  $\tilde{B}^{\mu\nu} = \frac{1}{2} \epsilon^{\mu\nu\alpha\beta} B_{\alpha\beta}$  etc. (with  $\epsilon^{0123} = 1$ ) are the dual field-strength tensors, and  $\alpha_s = g_s^2/(4\pi)$ ,  $\alpha_2 = g^2/(4\pi)$  and  $\alpha_1 = g'^2/(4\pi)$  denote the corresponding coupling parameters. The sum in the first line extends over the chiral fermion multiplets  $F$  of the SM, and the Higgs

doublet is denoted by  $\phi$ . The quantities  $c_F$  are  $3 \times 3$  hermitian matrices in generation space.

In the Lagrangian (6.1), the ALP couplings to the SM fermions and the Higgs doublet are obviously shift symmetric. Furthermore, the effects of a shift  $a \rightarrow a + \text{constant}$  for couplings to  $SU(2)_L$  and  $U(1)_Y$  gauge bosons can be removed by field redefinitions. Under a continuous shift, the coupling to the QCD gauge field is not invariant due to instanton effects. However, also in that case, a discrete version is preserved. Note that all couplings to SM fields are suppressed by the large scale  $f$  that is related to the scale of PQ symmetry breaking via  $\Lambda = 4\pi f$ . In the literature for QCD axions, one often eliminates this scale in favour of the axion decay constant  $f_a = -f/(2c_{GG})$ . In good approximation, we may neglect operators that are suppressed by higher powers of  $1/f$ .

The physical ALP mass receives contribution from the explicit soft breaking term as well as from the aforementioned non-perturbative QCD dynamics [152, 173, 174]. It reads

$$m_a^2 = m_{a,0}^2 \left[ 1 + \mathcal{O}\left(\frac{f_\pi^2}{f^2}\right) \right] + c_{GG}^2 \frac{f_\pi^2 m_\pi^2}{f^2} \frac{2m_u m_d}{(m_u + m_d)^2}, \quad (6.2)$$

where  $f_\pi \approx 130.5 \text{ MeV}$  is the pion decay constant, and the corrections to the first term have been calculated in [5]. From this equation it is manifest that there is a direct relation between the ALP coupling to gluons and the effective ALP mass in the limit of vanishing bare ALP mass<sup>1</sup>.

Counting free parameters of the Lagrangian, we find 1 (ALP mass) + 1 (ALP–Higgs coupling) + 3 (ALP–gauge boson couplings) +  $5 \times 9$  (ALP–fermion couplings<sup>2</sup>) = 50 real parameters. Five of them can be removed with the help of the five global symmetries of the individual lepton numbers, baryon number, and hypercharge [183]. We will demonstrate this in detail next. We define  $\mathbf{Q}_{F,\phi}$  as the charge matrix of the fermion  $F$  and the Higgs doublet  $\phi$ , respectively, under one of the global symmetries. For example,  $\mathbf{Q}_d^{(B)} \psi_d = \frac{1}{3} \mathbb{1} \psi_d$  gives the baryon number of the down-type quarks. Then a field redefinition

$$\psi_F \rightarrow \exp\left(ic \frac{a}{f} \mathbf{Q}_F\right) \psi_F, \quad \phi \rightarrow \exp\left(ic \frac{a}{f} \mathbf{Q}_\phi\right) \phi, \quad (6.3)$$

where  $c$  is any real number (but equal for all fields involved in the transformation), will have the following effects on the ALP couplings in the effective Lagrangian (6.1):

$$\begin{aligned} c_F &\rightarrow c_F - c \mathbf{Q}_F, \\ c_\phi &\rightarrow c_\phi - c \mathbf{Q}_\phi, \\ c_{GG} &\rightarrow c_{GG} + \frac{c}{2} \text{Tr}(\mathbf{Q}_u + \mathbf{Q}_d - 2\mathbf{Q}_Q), \\ c_{WW} &\rightarrow c_{WW} - \frac{c}{2} \text{Tr}(3\mathbf{Q}_Q + \mathbf{Q}_L), \\ c_{BB} &\rightarrow c_{BB} + c \text{Tr}\left(\frac{4}{3}\mathbf{Q}_u + \frac{1}{3}\mathbf{Q}_d - \frac{1}{6}\mathbf{Q}_Q + \mathbf{Q}_e - \frac{1}{2}\mathbf{Q}_L\right). \end{aligned} \quad (6.4)$$

<sup>1</sup> Note that this is especially relevant for the QCD axion case.

<sup>2</sup> Each coupling matrix has 9 free entries as it couples to three generations. The five representations are the left-handed quark doublet, the right-handed up- and down-type quark singlets, the left-handed lepton doublet, and the right-handed lepton singlet.

All transformations of this type will leave the coupling combination  $c_{WW} + c_{BB}$  invariant. The observation that both  $c_{WW}$  and  $c_{BB}$  change under transformations proportional to baryon or lepton number reflects the fact that both symmetries are anomalous in the SM. Under the anomaly-free combination  $(B - L)$  all gauge boson couplings remain unchanged. In the literature different choices have been made considering which parameters to remove from the Lagrangian [183–186]. In this work, we refrain from taking a particular choice, thus keeping some parameter redundancies. Though, we remove the ALP–Higgs coupling from the Lagrangian by applying a transformation (6.4) proportional to hypercharge. While the ALP–gauge boson couplings remain unchanged, the ALP–Higgs and –fermion couplings transform as

$$\begin{aligned} c_Q &\rightarrow c_Q - \frac{c}{3} \mathbb{1}, & c_u &\rightarrow c_u - \frac{c}{3} \mathbb{1}, & c_d &\rightarrow c_d - \frac{c}{3} \mathbb{1}, \\ c_{GG} &\rightarrow c_{GG}, & c_{WW} &\rightarrow c_{WW} - \frac{3c}{2}, & c_{BB} &\rightarrow c_{BB} + \frac{3c}{2}. \end{aligned} \quad (6.5)$$

Choosing  $c = 2c_\phi$  then removes the ALP–Higgs coupling. With this choice there are still 4 parameter redundancies remaining. For this reason, physical observables can only depend on certain combinations of couplings that are invariant under all symmetry transformations. In [5], we have shown that these physical ALP couplings can be chosen as

$$\begin{aligned} \tilde{c}_{GG} &= c_{GG} + \frac{1}{2} \text{Tr}(c_u + c_d - 2c_Q), \\ \tilde{c}_{WW} &= c_{WW} - \frac{1}{2} \text{Tr}(3c_Q + c_L), \\ \tilde{c}_{BB} &= c_{BB} + \text{Tr}\left(\frac{4}{3}c_u + \frac{1}{3}c_d - \frac{1}{6}c_Q + c_e - \frac{1}{2}c_L\right), \end{aligned} \quad (6.6)$$

and

$$\begin{aligned} \tilde{Y}_u &= i(Y_u c_u - c_Q Y_u - c_\phi Y_u), \\ \tilde{Y}_d &= i(Y_d c_d - c_Q Y_d + c_\phi Y_d), \\ \tilde{Y}_e &= i(Y_e c_e - c_L Y_e + c_\phi Y_e), \end{aligned} \quad (6.7)$$

where  $Y_F$  are the SM Yukawa matrices. If the effective theory is extended to energies below the weak scale, then the effects of heavy fermions decouple and need to be removed from the above expressions.

### 6.2.1 RG evolution to the electroweak scale

In eq. (6.1), we pulled out a factor  $\alpha_i$ ,  $i = 1, 2, s$  from the ALP coupling to the SM gauge bosons. As a result, these couplings do not run up to two-loop order in gauge couplings [187–189], i.e.

$$\frac{d}{d \ln \mu} c_{VV}(\mu) = 0, \quad V = G, W, B. \quad (6.8)$$

The couplings to fermions, however, receive multiple contributions to their respective RGEs. Representative Feynman diagrams are shown in figure 6.1. Additional to multiplicative contributions from external leg corrections, there are mixings of the left and right-

handed doublet and singlet coefficients  $c_Q$  and  $c_{u,d}$ , and  $c_L$  and  $c_e$ . The results derived here agree with the corresponding terms in [162, 190, 191]. Furthermore, removing the ALP–Higgs coupling can be interpreted as eliminating the corresponding operator from the Lagrangian by re-expressing it in terms of the ALP–fermion interaction terms. However, it is needed as a counterterm for the first diagram in figure 6.1. Its contribution to the RGEs must then be mapped back onto our chosen basis for consistency. In previous studies this operator and its corresponding coupling coefficient were taken as independent and an own RG equation was derived [162, 190]. We want to emphasise here that this leads to ambiguous results and should in general be avoided [192], since it is not possible to distinguish the matrix elements of the ALP–Higgs from the ALP–fermion operators. Additionally, the coefficients  $c_{VV}$  of the ALP–gauge boson interactions mix into the fermion RGEs through the last diagram of figure 6.1. Our findings agree with those of [187, 193], where these structures have been studied for the QCD axion. Due to our choice of normalisation for the bosonic couplings, Feynman diagrams that are essentially two-loop diagrams contribute to the RGEs with the same order of magnitude as one-loop diagrams with corrections from gauge boson interactions, and are henceforth also taken into account. We give an example of such a diagram in figure 6.2. The results for  $SU(3)_c$  gauge bosons have been calculated in [194, 195] first. Here we generalise to the SM gauge group. Combining all effects, we eventually find (with  $q = u, d$ )

$$\begin{aligned}
\frac{d}{d \ln \mu} c_Q(\mu) &= \frac{1}{32\pi^2} \left\{ \mathbf{Y}_u \mathbf{Y}_u^\dagger + \mathbf{Y}_d \mathbf{Y}_d^\dagger, c_Q \right\} - \frac{1}{16\pi^2} \left( \mathbf{Y}_u c_u \mathbf{Y}_u^\dagger + \mathbf{Y}_d c_d \mathbf{Y}_d^\dagger \right) \\
&\quad + \left[ \frac{Q_Q}{8\pi^2} X - \frac{3\alpha_s^2}{4\pi^2} C_F^{(3)} \tilde{c}_{GG} - \frac{3\alpha_2^2}{4\pi^2} C_F^{(2)} \tilde{c}_{WW} - \frac{3\alpha_1^2}{4\pi^2} \mathcal{Y}_Q^2 \tilde{c}_{BB} \right] \mathbb{1}, \\
\frac{d}{d \ln \mu} c_q(\mu) &= \frac{1}{16\pi^2} \left\{ \mathbf{Y}_q \mathbf{Y}_q^\dagger, c_q \right\} - \frac{1}{8\pi^2} \mathbf{Y}_q^\dagger c_Q \mathbf{Y}_q + \left[ \frac{Q_q}{8\pi^2} X + \frac{3\alpha_s^2}{4\pi^2} C_F^{(3)} \tilde{c}_{GG} + \frac{3\alpha_1^2}{4\pi^2} \mathcal{Y}_q^2 \tilde{c}_{BB} \right] \mathbb{1}, \\
\frac{d}{d \ln \mu} c_L(\mu) &= \frac{1}{32\pi^2} \left\{ \mathbf{Y}_e \mathbf{Y}_e^\dagger, c_L \right\} - \frac{1}{16\pi^2} \mathbf{Y}_e c_e \mathbf{Y}_e^\dagger + \left[ \frac{Q_L}{8\pi^2} X - \frac{3\alpha_2^2}{4\pi^2} C_F^{(2)} \tilde{c}_{WW} - \frac{3\alpha_1^2}{4\pi^2} \mathcal{Y}_L^2 \tilde{c}_{BB} \right] \mathbb{1}, \\
\frac{d}{d \ln \mu} c_e(\mu) &= \frac{1}{16\pi^2} \left\{ \mathbf{Y}_e^\dagger \mathbf{Y}_e, c_e \right\} - \frac{1}{8\pi^2} \mathbf{Y}_e c_L \mathbf{Y}_e^\dagger + \left[ \frac{Q_e}{8\pi^2} X - \frac{3\alpha_1^2}{4\pi^2} \mathcal{Y}_e^2 \tilde{c}_{BB} \right] \mathbb{1},
\end{aligned} \tag{6.9}$$

where  $Q_F$  is the charge of the fermions under a transformation proportional to hypercharge as in eq. (6.5),  $C_F^{(N)} = \frac{N^2-1}{2N}$  is the eigenvalue of the quadratic Casimir operator in the fundamental representation of  $SU(N)$ ,  $\mathcal{Y}_F$  is the hypercharge of the fermion multiplet  $F$ , and we have abbreviated

$$X = \text{Tr} \left[ 2c_Q (\mathbf{Y}_u \mathbf{Y}_u^\dagger - \mathbf{Y}_d \mathbf{Y}_d^\dagger) - 3c_u \mathbf{Y}_u^\dagger \mathbf{Y}_u + 3c_d \mathbf{Y}_d^\dagger \mathbf{Y}_d - c_L \mathbf{Y}_e \mathbf{Y}_e^\dagger + c_e \mathbf{Y}_e^\dagger \mathbf{Y}_e \right]. \tag{6.10}$$

Note that we keep the result general by allowing for different choices of  $Q_F$  than the one we will eventually employ. All quantities at the right hand side of eq. (6.9) must be evaluated at the scale  $\mu$ .

Below the weak scale, we ultimately want to integrate out the top quark from our effective theory description. In a first step, we therefore transform all fermion fields into the



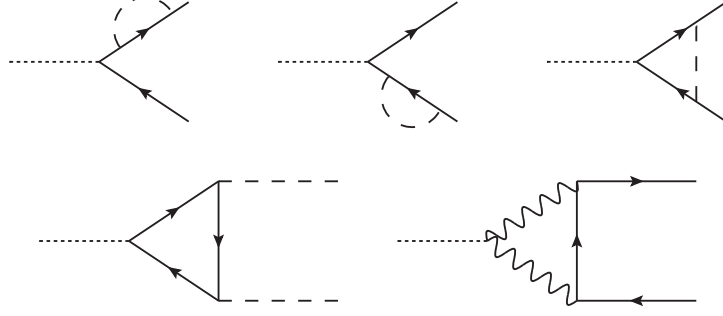


Figure 6.1: One-loop diagrams accounting for operator mixing through Yukawa and gauge interactions. The shortly dashed line represents the ALP, the long dashed one the Higgs.

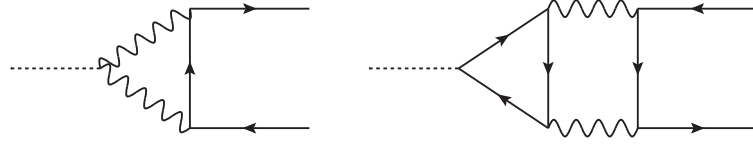


Figure 6.2: Examples of two diagrams that contribute with the same order of magnitude to the RGEs, if the coupling coefficients are taken to be equal.

mass basis by diagonalising the SM Yukawa matrices by means of bi-unitary transformations, such that

$$\begin{aligned}
 U_u^\dagger Y_u W_u &= Y_u^{\text{diag}} = \text{diag}(y_u, y_c, y_t), \\
 U_d^\dagger Y_d W_d &= Y_d^{\text{diag}} = \text{diag}(y_d, y_s, y_b), \\
 U_e^\dagger Y_e W_e &= Y_e^{\text{diag}} = \text{diag}(y_e, y_\mu, y_\tau).
 \end{aligned} \tag{6.11}$$

Redefining the fermion fields as

$$\begin{aligned}
 Q &\rightarrow U_u Q, & u_R &\rightarrow W_u u_R, & d_R &\rightarrow W_d d_R, \\
 L &\rightarrow U_e L, & e_R &\rightarrow W_e e_R,
 \end{aligned} \tag{6.12}$$

then diagonalises the up-sector and the lepton sector, while the down-sector Yukawa matrix is transformed into

$$Y_d \rightarrow U_u^\dagger Y_d W_d = V Y_d^{\text{diag}}, \tag{6.13}$$

and  $V = U_u^\dagger U_d$  is the CKM matrix. In the following, all ALP couplings to fermions  $c_F$  are defined in this basis. Using the fact that all Yukawa couplings are much smaller than the top-Yukawa  $y_t \simeq 1^3$ , the RG equations of eq. (6.9) simplify to

$$\begin{aligned}
\frac{d}{d \ln \mu} [c_Q(\mu)]_{ii} &= -\frac{y_t^2}{8\pi^2} \left( \frac{\delta_{i3}}{2} + 3Q_Q \right) c_{tt} - \frac{\alpha_s^2}{\pi^2} \tilde{c}_{GG} - \frac{9\alpha_2^2}{16\pi^2} \tilde{c}_{WW} - \frac{\alpha_1^2}{48\pi^2} \tilde{c}_{BB} \\
\frac{d}{d \ln \mu} [c_Q(\mu)]_{ij} &= \frac{y_t^2}{32\pi^2} (\delta_{i3} + \delta_{j3}) (c_Q)_{ij}; \quad i \neq j, \\
\frac{d}{d \ln \mu} [c_u(\mu)]_{ii} &= -\frac{y_t^2}{8\pi^2} (\delta_{i3} - 3Q_u) c_{tt} + \frac{\alpha_s^2}{\pi^2} \tilde{c}_{GG} + \frac{\alpha_1^2}{3\pi^2} \tilde{c}_{BB} \\
\frac{d}{d \ln \mu} [c_u(\mu)]_{ij} &= \frac{y_t^2}{16\pi^2} (\delta_{i3} + \delta_{j3}) (c_u)_{ij}; \quad i \neq j, \\
\frac{d}{d \ln \mu} [c_d(\mu)]_{ij} &= \delta_{ij} \left( -\frac{3y_t^2}{8\pi^2} Q_d c_{tt} + \frac{\alpha_s^2}{\pi^2} \tilde{c}_{GG} + \frac{\alpha_1^2}{12\pi^2} \tilde{c}_{BB} \right), \\
\frac{d}{d \ln \mu} [c_L(\mu)]_{ij} &= \delta_{ij} \left( -\frac{3y_t^2}{8\pi^2} Q_L c_{tt} - \frac{9\alpha_2^2}{16\pi^2} \tilde{c}_{WW} - \frac{3\alpha_1^2}{16\pi^2} \tilde{c}_{BB} \right), \\
\frac{d}{d \ln \mu} [c_e(\mu)]_{ij} &= \delta_{ij} \left( -\frac{3y_t^2}{8\pi^2} Q_e c_{tt} + \frac{3\alpha_1^2}{4\pi^2} \tilde{c}_{BB} \right),
\end{aligned} \tag{6.14}$$

where we have defined

$$c_{tt}(\mu) = [c_u(\mu)]_{33} - [c_Q(\mu)]_{33}. \tag{6.15}$$

In the next step, we would in principle solve the RG equations. To keep this treatment compact, we will instead comment on the important measures taken and only give results where appropriate. The full solutions can be found in [5].

The pure ALP–gauge couplings  $c_{VV}$  are scale-independent (6.8). However, this is not true for the physically observable couplings defined in (6.6), since they depend on the fermion couplings as well. In the limit that only the top-Yukawa coupling is taken to be non-vanishing, the four functions  $\tilde{c}_{GG}(\mu)$ ,  $\tilde{c}_{WW}(\mu)$ ,  $\tilde{c}_{BB}(\mu)$  and  $c_{tt}(\mu)$  form a closed set of coupled differential equations. Solving those and plugging them in into the RGEs of the other couplings (6.14), we are able to iteratively solve the equations for all ALP couplings. To give an impression of the strength of the effects of running from the UV scale  $\Lambda = 4\pi f = 4\pi \text{TeV}$  down to the EW scale  $\mu_w = m_t$ , we find numerically for the ALP–top coupling

$$c_{tt}(m_t) \simeq 0.826 c_{tt}(\Lambda) - [6.17 \tilde{c}_{GG}(\Lambda) + 0.23 \tilde{c}_{WW}(\Lambda) + 0.02 \tilde{c}_{BB}(\Lambda)] \times 10^{-3}. \tag{6.16}$$

This is a very important result, because it shows that any ALP coupling in the UV will inevitably generate a coupling to top-quarks at the electro-weak (EW) scale<sup>4</sup>. Moreover, we will see later that this is an even more general result, and in fact any UV ALP coupling

<sup>3</sup> The Yukawa matrices in eq. (6.9) come in pairs, hence the least suppressed terms are those proportional to either the bottom quark or  $\tau$  lepton. Compared with the top Yukawa, these contributions are weaker by factors of  $y_b^2/y_t^2 \sim y_\tau^2/y_t^2 \sim 10^{-4}$ . Note that we include some electroweak contributions of the same order of magnitude as these suppressed terms in the RGE. We do so to keep our treatment as general as possible, because the ALP–gauge boson couplings can be enhanced in some other models.

<sup>4</sup> Note that the  $\tilde{c}_{VV}$  (6.6) also depend on the ALP–fermion couplings, and therefore ALP couplings to *any* SM particle generates an ALP–top coupling.

will generate couplings to *all* SM fermions at the low scale, even such couplings that are flavour-violating.

### 6.2.2 Effective ALP Lagrangian at the electroweak scale

At the weak scale  $\mu_w$ , it is appropriate to express the Lagrangian in terms of fields that are defined in the broken phase after EWSB. Therefore, the Lagrangian reads

$$\begin{aligned} \mathcal{L}_{\text{eff}}(\mu_w) = & \frac{1}{2} (\partial_\mu a)(\partial^\mu a) - \frac{m_{a,0}^2}{2} a^2 + \mathcal{L}_{\text{fermion}}(\mu) + c_{GG} \frac{\alpha_s}{4\pi} \frac{a}{f} G_{\mu\nu}^a \tilde{G}^{\mu\nu,a} + c_{\gamma\gamma} \frac{\alpha}{4\pi} \frac{a}{f} F_{\mu\nu} \tilde{F}^{\mu\nu} \\ & + c_{\gamma Z} \frac{\alpha}{2\pi s_w c_w} \frac{a}{f} F_{\mu\nu} \tilde{Z}^{\mu\nu} + c_{ZZ} \frac{\alpha}{4\pi s_w^2 c_w^2} \frac{a}{f} Z_{\mu\nu} \tilde{Z}^{\mu\nu} + c_{WW} \frac{\alpha}{2\pi s_w^2} \frac{a}{f} W_{\mu\nu}^+ \tilde{W}^{-\mu\nu}, \end{aligned} \quad (6.17)$$

where  $s_w \equiv \sin \theta_W$  and  $c_w \equiv \cos \theta_W$  denote the sine and cosine of the weak mixing angle, and

$$c_{\gamma\gamma} = c_{WW} + c_{BB}, \quad c_{\gamma Z} = c_w^2 c_{WW} - s_w^2 c_{BB}, \quad c_{ZZ} = c_w^4 c_{WW} + s_w^4 c_{BB}. \quad (6.18)$$

To obtain ALP–fermion interactions in the mass basis, we transform the Yukawa couplings according to (6.11). Under these field redefinitions, the flavour matrices transform into new hermitian matrices

$$\begin{aligned} \mathbf{k}_U &= U_u^\dagger \mathbf{c}_Q U_u, & \mathbf{k}_D &= U_d^\dagger \mathbf{c}_Q U_d, & \mathbf{k}_E &= U_e^\dagger \mathbf{c}_L U_e, \\ \mathbf{k}_f &= W_f^\dagger \mathbf{c}_f W_f; & f &= u, d, e. \end{aligned} \quad (6.19)$$

Note that the matrices  $\mathbf{k}_U$  and  $\mathbf{k}_D$  are connected via the CKM matrix  $V$  by

$$\mathbf{k}_D = V^\dagger \mathbf{k}_U V, \quad (6.20)$$

and therefore are not independent. Likewise, the ALP coupling to neutrinos are identical to those to the left-handed charged leptons, i.e.  $\mathbf{k}_\nu = \mathbf{k}_E$ . The ALP–fermion Lagrangian at the EW scale therefore reads

$$\begin{aligned} \mathcal{L}_{\text{fermion}}(\mu) = & \frac{\partial^\mu a}{f} \left[ \bar{u}_L \mathbf{k}_U(\mu) \gamma_\mu u_L + \bar{u}_R \mathbf{k}_u(\mu) \gamma_\mu u_R + \bar{d}_L \mathbf{k}_D(\mu) \gamma_\mu d_L + \bar{d}_R \mathbf{k}_d(\mu) \gamma_\mu d_R \right. \\ & \left. + \bar{\nu}_L \mathbf{k}_\nu(\mu) \gamma_\mu \nu_L + \bar{e}_L \mathbf{k}_E(\mu) \gamma_\mu e_L + \bar{e}_R \mathbf{k}_e(\mu) \gamma_\mu e_R \right]. \end{aligned} \quad (6.21)$$

Since flavour-conserving ALP couplings play a crucial role in our work, we define

$$c_{f_i f_i}(\mu) \equiv [k_f(\mu)]_{ii} - [k_F(\mu)]_{ii}. \quad (6.22)$$

In strong-interaction and electromagnetic processes, the flavour-conserving vector currents are conserved, and hence the corresponding ALP couplings  $[k_f(\mu)]_{ii} + [k_F(\mu)]_{ii}$  are unobservable.<sup>5</sup>

<sup>5</sup> This is no longer true in weak-interaction processes, where *differences* of the vectorial couplings to different quark flavours can appear in predictions for weak decay amplitudes [6].

At the electroweak scale, the physical ALP–gauge boson couplings (6.6) can be rewritten using the ALP–fermion couplings at this scale as

$$\begin{aligned}\tilde{c}_{GG}(\Lambda) &= c_{GG} + \frac{1}{2} \sum_q c_{qq}(\Lambda), \\ \tilde{c}_{WW}(\Lambda) &= c_{WW} - \frac{1}{2} \text{Tr} [3\mathbf{k}_U(\Lambda) + \mathbf{k}_E(\Lambda)], \\ \tilde{c}_{BB}(\Lambda) &= c_{BB} + \sum_f N_c^f Q_f^2 c_{ff}(\Lambda) + \frac{1}{2} \text{Tr} [3\mathbf{k}_U(\Lambda) + \mathbf{k}_E(\Lambda)].\end{aligned}\tag{6.23}$$

Here, the sums run over all fermion flavours,  $N_c^f$  is the number of colour charges of the respective fermion,  $Q_f$  denotes its electric charge in units of the elementary charge  $e$ .

Let us briefly return to the question of parameter redundancies at this point. In the basis where the SM Yukawa matrices are diagonal, the elements of the matrices  $\tilde{\mathbf{Y}}_f$  in (6.7) take the form

$$(\tilde{\mathbf{Y}}_f)_{ij} = i \left[ y_{f_i} [k_f]_{ij} - [k_F]_{ij} y_{f_j} \right],\tag{6.24}$$

where  $y_{f_i}$  denote the eigenvalues of the Yukawa matrices (the physical Yukawa couplings of the quarks and leptons). It follows that  $(\tilde{\mathbf{Y}}_f)_{ii} = i y_{f_i} c_{f_i f_i}$ , which shows that the diagonal ALP–fermion couplings  $c_{f_i f_i}$  in (6.22) are physical parameters. For  $i \neq j$ , one finds that both  $(k_f)_{ij}$  and  $(k_F)_{ij}$  are physical quantities, since for example  $i(\tilde{\mathbf{Y}}_f^\dagger \mathbf{Y}_f + \mathbf{Y}_f^\dagger \tilde{\mathbf{Y}}_f)$  only involves the off-diagonal elements of  $k_f$ . Moreover, from (6.23) one sees that  $\tilde{c}_{GG}$  and  $c_{GG}$  are both unambiguous, because their difference is a linear combination of the physical parameters  $c_{qq}$ . The same statement applies for the combinations  $\tilde{c}_{\gamma\gamma} = \tilde{c}_{WW} + \tilde{c}_{BB}$  and  $c_{\gamma\gamma} = c_{WW} + c_{BB}$ , but not to  $c_{WW}$  and  $c_{BB}$  individually.

### 6.2.3 Effective ALP Lagrangian below the electroweak scale

For ALPs that are lighter than the electroweak scale, we need to evolve their couplings to lower energies. Just below this scale, we integrate out the SM heavy particles — the Higgs boson, the top-quark and the weak gauge bosons  $W^\pm$  and  $Z^0$  — from the theory and match the effective Lagrangian to one where these degrees of freedom are no longer present. We find

$$\begin{aligned}\mathcal{L}_{\text{eff}}^{D \leq 5}(\mu \lesssim \mu_w) &= \frac{1}{2} (\partial_\mu a)(\partial^\mu a) - \frac{m_{a,0}^2}{2} a^2 + \mathcal{L}'_{\text{ferm}}(\mu) \\ &+ c_{GG} \frac{\alpha_s}{4\pi} \frac{a}{f} G_{\mu\nu}^a \tilde{G}^{\mu\nu,a} + c_{\gamma\gamma} \frac{\alpha}{4\pi} \frac{a}{f} F_{\mu\nu} \tilde{F}^{\mu\nu},\end{aligned}\tag{6.25}$$

where  $\mathcal{L}'_{\text{ferm}}$  is given by (6.21) but with the top-quark fields  $t_L$  and  $t_R$  removed. In general, the Wilson coefficients  $c_{GG}$ ,  $c_{\gamma\gamma}$ ,  $\mathbf{k}_F$  and  $\mathbf{k}_f$  in this effective Lagrangian differ from the corresponding coefficients in the effective Lagrangian above the weak scale by calculable matching contributions.

### 6.2.3.1 Matching contributions to ALP couplings at the weak scale

**MATCHING CONTRIBUTIONS TO THE ALP–GAUGE BOSON COUPLINGS** One finds that there are no matching contribution to the ALP–boson couplings  $c_{GG}$  and  $c_{\gamma\gamma}$  if the ALP is much lighter than the weak scale, and therefore terms with a scaling of  $m_a^2/m_{t,W}^2$  can be neglected [196]. Yet, there are corrections to the  $\tilde{c}_{VV}$  couplings in (6.23). Crossing the weak scale and integrating out the top-quark has the effect of removing the top contribution from their expressions. We thus obtain

$$\begin{aligned}\tilde{c}_{GG}(\mu \lesssim \mu_w) &= c_{GG} + \frac{1}{2} \sum_{q \neq t} c_{qq}(\mu), \\ \tilde{c}_{\gamma\gamma}(\mu \lesssim \mu_w) &= c_{\gamma\gamma} + \sum_{f \neq t} N_c^f Q_f^2 c_{ff}(\mu).\end{aligned}\tag{6.26}$$

This procedure repeats itself at lower scales when the respective fermion mass scale is crossed.

**MATCHING CONTRIBUTIONS TO THE ALP–FERMION COUPLINGS** Matching corrections to ALP–fermion couplings at one-loop order arise from diagrams involving one or more heavy gauge bosons in the loop. Representative Feynman diagrams are shown in figure 6.3. Below the EW scale, the top-quark is integrated out already. Therefore we may neglect diagrams where the Higgs boson is involved, since its couplings are proportional to the square of the fermion Yukawa couplings, which are all much smaller than the top-Yukawa. We computed those diagrams in a general  $R_\xi$  gauge, the final result is gauge-independent. Furthermore, the contributions from  $Z$ -bosons and their Goldstones cancel out in the sum of all diagrams. From  $W$ -bosons, a contribution remains when the top-quark is present in the loop. These diagrams source flavour off-diagonal contributions to the left-handed down-type sector ALP couplings  $\mathbf{k}_D(\mu_w)$ . It is most remarkable that flavour-changing ALP interactions are generated in this way, even if the underlying UV theory does not contain new sources of flavour or CP violation beyond those present in the SM. We have neglected the Yukawa couplings of the light quarks and leptons. In this approximation there are no flavour off-diagonal matching contributions in the up-quark

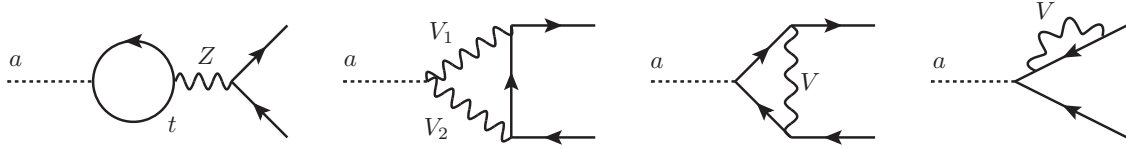


Figure 6.3: Contributions to the matching corrections of the ALP–fermion couplings just below the weak scale. In the second diagram  $(V_1 V_2) = (WW), (ZZ), (Z\gamma)$  or  $(\gamma Z)$ . In the third and fourth diagram  $V = W, Z$ . In the sum of all graphs only the  $W$ -boson graph with internal top-quark loops (and the corresponding diagrams with Goldstone bosons) are non-vanishing. They lead to flavour-changing ALP couplings, even if the underlying UV theory is flavour-conserving.

and lepton sectors. Combining all terms, we find for the matching contributions (with  $F = U, D, E, \nu$  and  $f = u, d, e$ )

$$\begin{aligned}
\Delta \mathbf{k}_F &= \frac{3y_t^2}{8\pi^2} c_{tt} (T_3^f - Q_f s_w^2) \ln \left( \frac{\mu_w^2}{m_t^2} \right) \mathbb{1} \\
&\quad + \frac{3\alpha^2}{8\pi^2} \left[ \frac{c_{WW}}{2s_w^4} \left( \ln \left( \frac{\mu_w^2}{m_W^2} \right) + \frac{1}{2} + \delta_1 \right) + \frac{2c_{\gamma Z}}{s_w^2 c_w^2} Q_f (T_3^f - Q_f s_w^2) \left( \ln \left( \frac{\mu_w^2}{m_Z^2} \right) + \frac{3}{2} + \delta_1 \right) \right. \\
&\quad \left. + \frac{c_{ZZ}}{s_w^4 c_w^4} (T_3^f - Q_f s_w^2)^2 \left( \ln \left( \frac{\mu_w^2}{m_Z^2} \right) + \frac{1}{2} + \delta_1 \right) \right] \mathbb{1} + \delta_{FD} \hat{\Delta} \mathbf{k}_D(\mu_w), \\
\Delta \mathbf{k}_f &= \frac{3y_t^2}{8\pi^2} c_{tt} (-Q_f s_w^2) \ln \left( \frac{\mu_w^2}{m_t^2} \right) \mathbb{1} \\
&\quad + \frac{3\alpha^2}{8\pi^2} Q_f^2 \left[ \frac{2c_{\gamma Z}}{c_w^2} \left( \ln \left( \frac{\mu_w^2}{m_Z^2} \right) + \frac{3}{2} + \delta_1 \right) - \frac{c_{ZZ}}{c_w^4} \left( \ln \left( \frac{\mu_w^2}{m_Z^2} \right) + \frac{1}{2} + \delta_1 \right) \right] \mathbb{1}.
\end{aligned} \tag{6.27}$$

All scale-dependent parameters on the right-hand side of this equation are to be evaluated at the scale  $\mu_w$ . The quantity  $\delta_1 = -\frac{11}{3}$  is a scheme-dependent constant. It stems from the treatment of the Levi-Civita tensor  $\epsilon^{\mu\nu\alpha\beta}$  in  $d$  dimensions. If it is treated as a 4-dimensional object, one obtains  $\delta_1 = 0$  instead. The generated flavour-changing effects read

$$\begin{aligned}
[\hat{\Delta} k_D]_{ij} &= \frac{y_t^2}{16\pi^2} \left\{ V_{mi}^* V_{nj} [k_U(\mu_w)]_{mn} (\delta_{m3} + \delta_{n3}) \left[ -\frac{1}{4} \ln \left( \frac{\mu_w^2}{m_t^2} \right) - \frac{3}{8} + \frac{3}{4} \frac{1-x_t + \ln x_t}{(1-x_t)^2} \right] \right. \\
&\quad + V_{3i}^* V_{3j} [k_U(\mu_w)]_{33} + V_{3i}^* V_{3j} [k_U(\mu_w)]_{33} \left[ \frac{1}{2} \ln \left( \frac{\mu_w^2}{m_t^2} \right) - \frac{1}{4} - \frac{3}{2} \frac{1-x_t + \ln x_t}{(1-x_t)^2} \right] \\
&\quad \left. - \frac{3\alpha}{2\pi s_w^2} c_{WW} V_{3i}^* V_{3j} \frac{1-x_t + x_t \ln x_t}{(1-x_t)^2} \right\},
\end{aligned} \tag{6.28}$$

with  $x_t = m_t^2/m_W^2$ .

### 6.2.3.2 Numerical results for ALP–fermion couplings below the weak scale

The ALP–fermion Lagrangian (6.21) can be re-expressed in terms of vector and axial-vector currents of fermion fields in the mass basis. Since vector currents are conserved below the weak scale, it follows that we can write for the flavour diagonal ALP couplings

$$\mathcal{L}_{\text{fermion}}^{\text{diag}}(\mu) = \frac{\partial^\mu a}{2f} \sum_{f \neq t} c_{ff}(\mu) \bar{f} \gamma_\mu \gamma_5 f, \quad (6.29)$$

where the sum runs over all light fermion mass eigenstates. Applying the equations of motion and the well-known SM anomaly equations, we find that the ALP couples to fermions proportional to their mass. Hence, from now on we neglect interactions between ALPs and neutrinos.

Combining the effects of RG evolution and matching contributions at the weak scale, we obtain numerically for the reference scale  $\Lambda = 4\pi f$ ,  $f = 1 \text{ TeV}$

$$\begin{aligned} c_{uu,cc}(m_t) &\simeq c_{uu,cc}(\Lambda) - 0.116 c_{tt}(\Lambda) - \left[ 6.35 \tilde{c}_{GG}(\Lambda) + 0.19 \tilde{c}_{WW}(\Lambda) + 0.02 \tilde{c}_{BB}(\Lambda) \right] \times 10^{-3}, \\ c_{dd,ss}(m_t) &\simeq c_{dd,ss}(\Lambda) + 0.116 c_{tt}(\Lambda) - \left[ 7.08 \tilde{c}_{GG}(\Lambda) + 0.22 \tilde{c}_{WW}(\Lambda) + 0.005 \tilde{c}_{BB}(\Lambda) \right] \times 10^{-3}, \\ c_{bb}(m_t) &\simeq c_{bb}(\Lambda) + 0.097 c_{tt}(\Lambda) - \left[ 7.02 \tilde{c}_{GG}(\Lambda) + 0.19 \tilde{c}_{WW}(\Lambda) + 0.005 \tilde{c}_{BB}(\Lambda) \right] \times 10^{-3}, \\ c_{e_i e_i}(m_t) &\simeq c_{e_i e_i}(\Lambda) + 0.116 c_{tt}(\Lambda) - \left[ 0.37 \tilde{c}_{GG}(\Lambda) + 0.22 \tilde{c}_{WW}(\Lambda) + 0.05 \tilde{c}_{BB}(\Lambda) \right] \times 10^{-3}. \end{aligned} \quad (6.30)$$

To obtain these solutions, we have solved the RG equations in leading logarithmic approximation, thereby resumming logarithmically enhanced contributions to all loop orders. We use the two-loop expression for the running QCD coupling  $\alpha_s(\mu)$  and one-loop expressions for the running electroweak couplings  $\alpha_1(\mu)$  and  $\alpha_2(\mu)$  as well as for the running top-quark Yukawa coupling.

Applying the same method to the flavour-changing ALP interaction terms, it is evident that both vector and axial-vector currents contribute. We write the corresponding Lagrangian as

$$\begin{aligned} \mathcal{L}_{\text{fermion}}^{\text{FCNC}}(\mu \lesssim \mu_w) &= -\frac{ia}{2f} \sum_f \left[ (m_{f_i} - m_{f_j}) [k_f(\mu) + k_F(\mu)]_{ij} \bar{f}_i f_j \right. \\ &\quad \left. + (m_{f_i} + m_{f_j}) [k_f(\mu) - k_F(\mu)]_{ij} \bar{f}_i \gamma_5 f_j \right]. \end{aligned} \quad (6.31)$$

For all coefficients other than  $k_D$ , flavour-changing effects are inherited from the UV scale, i.e.  $[k_f(\mu_w)]_{ij} = [k_f(\Lambda)]_{ij}$ , with  $f = U, E, u, d, e$ . For the off-diagonal elements of the coefficient  $k_D$  one obtains the more interesting result

$$\begin{aligned} [k_D(\mu_w)]_{ij} &= [k_D(\Lambda)]_{ij} - V_{mi}^* V_{nj} (\delta_{m3} + \delta_{n3} - 2\delta_{m3}\delta_{n3}) \left( 1 - e^{-U(\mu_w, \Lambda)} \right) [k_U(\Lambda)]_{mn} \\ &\quad - \frac{1}{6} V_{3i}^* V_{3j} I_t(\mu_w, \Lambda) + [\hat{\Delta} k_D(\mu_w)]_{ij}, \end{aligned} \quad (6.32)$$

where the evolution functions  $U(\mu_w, \Lambda)$  and  $I_t(\mu_w, \Lambda)$  are defined as

$$U(\mu_w, \Lambda) = - \int_{\Lambda}^{\mu_w} \frac{d\mu}{\mu} \frac{y_t^2(\mu)}{32\pi^2}, \quad I_t(\mu_w, \Lambda) = \int_{\Lambda}^{\mu_w} \frac{d\mu}{\mu} \frac{3y_t^2(\mu)}{8\pi^2} c_{tt}(\mu). \quad (6.33)$$

Explicit analytic expressions for these integrals can be found in eqs. (3.14) and (3.21) of [5], while the matching contribution  $[\hat{\Delta}k_D(\mu_w)]_{ij}$  can be found in eq. (6.28). Via these evolution functions, ALP couplings to any SM field at the UV scale will, at some loop order, produce logarithmically-enhanced contributions to flavour-changing down-type quark couplings below the electroweak scale. We will make use of this important point in section 7.1 to place new constraints on individual ALP couplings defined at the UV scale, by calculating their flavour effects to leading logarithmic approximation via these equations.

### 6.2.3.3 RG evolution below the weak scale

Below the EW scale, the evolution equations take a fairly simple form. Since no Higgs bosons, top-quarks or heavy gauge bosons are present in the theory any more, the only diagrams giving contributions to the RGEs are those shown in figure 6.2, where the gauge bosons are either gluons or photons. We obtain (with  $Q = U, D$  and  $q = u, d$ )

$$\begin{aligned} \frac{d}{d \ln \mu} \mathbf{k}_q(\mu) &= - \frac{d}{d \ln \mu} \mathbf{k}_Q(\mu) = \left( \frac{\alpha_s^2}{\pi^2} \tilde{c}_{GG} + \frac{3\alpha^2}{4\pi^2} Q_q^2 \tilde{c}_{\gamma\gamma} \right) \mathbb{1}, \\ \frac{d}{d \ln \mu} \mathbf{k}_e(\mu) &= - \frac{d}{d \ln \mu} \mathbf{k}_E(\mu) = \frac{3\alpha^2}{4\pi^2} \tilde{c}_{\gamma\gamma} \mathbb{1}. \end{aligned} \quad (6.34)$$

The scale dependence of the gauge boson couplings  $\tilde{c}_{GG}$  and  $\tilde{c}_{\gamma\gamma}$  can be neglected, because it is a two-loop effect. Note that the evolution effects are diagonal in generation space, and hence flavour-changing couplings are scale-independent in the low-energy theory. For flavour-conserving couplings, only the combinations defined in (6.22) are physical. Solving the RGEs (6.34), their scale evolution is given by

$$\begin{aligned} c_{qq}(\mu) &= c_{qq}(\mu_w) - \frac{4\tilde{c}_{GG}(\mu_w)}{\beta_0^{\text{QCD}}} \frac{\alpha_s(\mu) - \alpha_s(\mu_w)}{\pi} - Q_q^2 \frac{3\tilde{c}_{\gamma\gamma}(\mu_w)}{\beta_0^{\text{QED}}} \frac{\alpha(\mu) - \alpha(\mu_w)}{\pi}, \\ c_{\ell\ell}(\mu) &= c_{\ell\ell}(\mu_w) - \frac{3\tilde{c}_{\gamma\gamma}(\mu_w)}{\beta_0^{\text{QED}}} \frac{\alpha(\mu) - \alpha(\mu_w)}{\pi}. \end{aligned} \quad (6.35)$$

In the effective theory below the weak scale the  $\beta$ -function coefficients are

$$\beta_0^{\text{QCD}} = 11 - \frac{2}{3}n_q, \quad \beta_0^{\text{QED}} = -\frac{4}{3} \sum_f N_c^f Q_f^2, \quad (6.36)$$

with  $n_q$  the number of light quark flavours with masses lighter than the scale  $\mu$  and in the second term the sum includes all light fermions with masses below  $\mu$ . According to (6.26),



the gauge boson couplings contain all fermion couplings below the scale where they are evaluated. We generalise this by defining

$$\begin{aligned}\tilde{c}_{GG} &= c_{GG} + \frac{1}{2} \sum_q c_{qq}(\mu) \theta(\mu - m_q), \\ \tilde{c}_{\gamma\gamma} &= c_{\gamma\gamma} + \sum_f N_c^f Q Q_f^2 c_{ff}(\mu) \theta(\mu - m_f).\end{aligned}\tag{6.37}$$

This means that the effective couplings change by a discrete amount whenever a fermion mass threshold is crossed. When this happens, a matching calculation needs to be performed in the usual way. To be more concrete, one evolves the coupling parameters from the weak scale to the scale  $\mu_b \simeq m_b$ . Then one eliminates the  $b$ -quark from the list of light fermions, and subsequently evolves from the  $b$ -quark scale to the scale  $\mu_\tau \simeq m_\tau$ , eliminates the  $\tau$ -lepton, and so on. In each step, the coefficients of the  $\beta$ -functions as well as the values of  $\tilde{c}_{GG}$  and  $\tilde{c}_{\gamma\gamma}$  need to be adjusted. For the diagonal quark couplings for example, we thus obtain for a scale  $\mu$  that is just below the  $b$ -quark mass

$$\begin{aligned}c_{qq}(\mu \lesssim \mu_b) &= c_{qq}(\mu_w) - \frac{4\tilde{c}_{GG}(\mu_w)}{\beta_0^{\text{QCD}}} \frac{\alpha_s(\mu_b) - \alpha_s(\mu_w)}{\pi} - Q_q^2 \frac{3\tilde{c}_{\gamma\gamma}(\mu_w)}{\beta_0^{\text{QED}}} \frac{\alpha(\mu_b) - \alpha(\mu_w)}{\pi} \\ &\quad - \frac{4\tilde{c}_{GG}(\mu_b)}{\beta_0^{\text{QCD}}} \frac{\alpha_s(\mu) - \alpha_s(\mu_b)}{\pi} - Q_q^2 \frac{3\tilde{c}_{\gamma\gamma}(\mu_b)}{\beta_0^{\text{QED}}} \frac{\alpha(\mu) - \alpha(\mu_b)}{\pi}.\end{aligned}\tag{6.38}$$

In the first row, the ALP–boson couplings and the  $\beta$ -functions are evaluated with  $n_q = 5$  active quark flavours, whereas in the second row they are evaluated with  $n_q = 4$ . Numerically, these evolution effects below the weak scale are very small. The evolution of the coefficients from the scale  $\mu_w = m_t$  to the low scale  $\mu_0 = 2 \text{ GeV}$  yields

$$\begin{aligned}c_{qq}(\mu_0) &= c_{qq}(m_t) - \left[ 3.0\tilde{c}_{GG}(\Lambda) - 1.4c_{tt}(\Lambda) - 0.6c_{bb}(\Lambda) \right] \times 10^{-2} \\ &\quad - Q_q^2 \left[ 3.9\tilde{c}_{\gamma\gamma}(\Lambda) - 4.7c_{tt}(\Lambda) - 0.2c_{bb}(\Lambda) \right] \times 10^{-5}, \\ c_{\ell\ell}(\mu_0) &= c_{\ell\ell}(m_t) - \left[ 3.9\tilde{c}_{\gamma\gamma}(\Lambda) - 4.7c_{tt}(\Lambda) - 0.2c_{bb}(\Lambda) \right] \times 10^{-5}.\end{aligned}\tag{6.39}$$

In [197], analogous expressions were derived for the quark coefficients  $c_{qq}$ , but only QCD effects were included. Their results are in agreement with our findings when we ignore terms proportional to the electromagnetic coupling  $\alpha$ . For an ALP lighter than the scale  $\mu_0$ , the interactions with hadrons and photons are affected by non-perturbative hadronic effects. These can be studied in a systematic way using an effective chiral Lagrangian.

## 6.3 ALPs within the weak chiral and nuclear Lagrangian

### 6.3.1 Implementing ALPs in the weak chiral Lagrangian

For energies below the scale  $\mu_0 \approx 2 \text{ GeV}$  it is appropriate to switch the description to a version of chiral perturbation theory ( $\chi$ PT) where the ALP is included, and instead of

interacting with quarks the ALP interacts with the pseudoscalar mesons ( $\pi$ ,  $K$ ,  $\eta$ ). This chiral theory was first introduced in [6, 183, 196, 198]. We start from the Lagrangian (6.25) where the only quark degrees of freedom are the up-, down- and strange-quark. In order to find the bosonised form of this Lagrangian, one eliminates the  $aG\tilde{G}$  term from the Lagrangian in favour of ALP couplings to quark bilinears, whose chiral representation is well-known. This is accomplished with a chiral rotation [183, 199, 200]

$$q(x) \rightarrow \exp \left[ -i \kappa_q \gamma_5 c_{GG} \frac{a(x)}{f} \right] q(x), \quad (6.40)$$

where  $q(x)$  is a 3-component object containing the light-quark fields  $u(x)$ ,  $d(x)$  and  $s(x)$ . The transformation parameters  $\kappa_q$  are hermitian matrices, which we choose to be diagonal in the quark mass basis. Note that in principle one is allowed to add an additional phase term  $-i\delta_q c_{GG} \frac{a(x)}{f}$  in the exponential. Since all dependencies on  $\kappa_q$  and  $\delta_q$  must cancel out for physical observables and the  $\delta_q$ -dependent structure is not needed to redefine or simplify any coupling structures, we refrain from introducing this term here<sup>6</sup>.

Under the chiral rotation (6.40), the path integral measure is not invariant [201]. This generates extra contributions to the ALP–gluon and photon couplings, as well as to the quark mass matrix. Imposing the condition

$$\text{Tr}(\kappa_q) = \kappa_u + \kappa_d + \kappa_s = 1 \quad (6.41)$$

ensures that the ALP–gluon coupling is eliminated from the Lagrangian even with these additional terms. As long as the condition is satisfied, any choice of  $\kappa_q$  leads to an effective chiral Lagrangian describing the same physics. The modified couplings to photons and quarks then read

$$\begin{aligned} \hat{c}_{\gamma\gamma} &= c_{\gamma\gamma} - 2N_c c_{GG} \text{Tr}[\mathbf{Q}^2 \kappa_q], \\ \hat{\mathbf{k}}_Q &= e^{-i\kappa_q c_{GG} \frac{a}{f}} (\mathbf{k}_Q - \kappa_q c_{GG}) e^{i\kappa_q c_{GG} \frac{a}{f}}, \\ \hat{\mathbf{k}}_q &= e^{i\kappa_q c_{GG} \frac{a}{f}} (\mathbf{k}_q + \kappa_q c_{GG}) e^{-i\kappa_q c_{GG} \frac{a}{f}}, \end{aligned} \quad (6.42)$$

where  $\mathbf{Q} = \text{diag}(Q_u, Q_d, Q_s)$  contains the electric charges of the quarks. The matrices  $\mathbf{k}_Q$  and  $\mathbf{k}_q$  have the texture

$$\mathbf{k}_Q = \begin{pmatrix} [k_U]_{11} & 0 & 0 \\ 0 & [k_D]_{11} & [k_D]_{12} \\ 0 & [k_D]_{21} & [k_D]_{22} \end{pmatrix}, \quad \mathbf{k}_q = \begin{pmatrix} [k_u]_{11} & 0 & 0 \\ 0 & [k_d]_{11} & [k_d]_{12} \\ 0 & [k_d]_{21} & [k_d]_{22} \end{pmatrix}, \quad (6.43)$$

where the various entries refer to the ALP–fermion couplings in the mass basis defined in (6.31). We recall that the off-diagonal couplings  $[k_D]_{ij}$  and  $[k_d]_{ij}$  with  $i \neq j$  do not run below the weak scale, and their values are fixed at the scale  $\mu_w$ .

<sup>6</sup> In [6], this term has been included and we refer the interested reader to this work.

The derivative couplings of the ALP to the quarks are implemented by including the ALP in the definition of the covariant derivative [202]

$$iD_\mu \Sigma = i\partial_\mu \Sigma + eA_\mu [\mathbf{Q}, \Sigma] + \frac{\partial_\mu a}{f} (\hat{\mathbf{k}}_Q \Sigma - \Sigma \hat{\mathbf{k}}_q), \quad (6.44)$$

where  $A_\mu$  is the photon field and

$$\Sigma(x) = \exp \left[ \frac{i\sqrt{2}}{f_\pi} \lambda^a \pi^a(x) \right] \quad (6.45)$$

contains the pseudoscalar meson fields. Here,  $\lambda_a$  are the Gell-Mann matrices. The leading order chiral Lagrangian can then be expressed as

$$\begin{aligned} \mathcal{L}_{\text{eff}}^\chi &= \frac{f_\pi^2}{8} \text{Tr} [D^\mu \Sigma (D_\mu \Sigma)^\dagger] + \frac{f_\pi^2}{4} B_0 \text{Tr} [\hat{\mathbf{m}}_q(a) \Sigma^\dagger + \text{h.c.}] \\ &+ \frac{1}{2} \partial^\mu a \partial_\mu a - \frac{m_{a,0}^2}{2} a^2 + \hat{c}_{\gamma\gamma} \frac{\alpha}{4\pi} \frac{a}{f} F_{\mu\nu} \tilde{F}^{\mu\nu}, \end{aligned} \quad (6.46)$$

with  $f_\pi \approx 130.5 \text{ MeV}$  the pion decay constant, and  $B_0 \approx m_\pi^2 / (m_u + m_d)$  is proportional to the quark condensate. Working to lowest order in the chiral expansion, we will consequently neglect effects from  $\pi^0$ - $\eta$ - $\eta'$  mixing. The modified mass matrix is given by

$$\hat{\mathbf{m}}_q(a) = \exp \left( -2i\kappa_q c_{GG} \frac{a}{f} \right) \mathbf{m}_q \quad (6.47)$$

with  $\mathbf{m}_q = \text{diag}(m_u, m_d, m_s)$ .

The Lagrangian of ALP- $\chi$ PT (6.46) has been the basis for numerous studies of low-energy phenomena where ALPs interact with pseudoscalar mesons. For the case of the QCD axion, one finds that QCD dynamics generates a mass for the ALP (see (6.2)), thereby breaking the continuous shift symmetry of the classical Lagrangian to the discrete subgroup  $a \rightarrow a + n\pi f / c_{GG}$ . One also finds that there are mass-mixing and kinetic mixing contributions involving the ALP and the neutral mesons  $\pi^0$  and  $\eta$ , whose explicit form depends on the  $\kappa_q$  parameters. For instance, at leading order in the  $1/f$  expansion one finds for the ALP-pion mixing

$$\pi^0 = \pi_{\text{phys}}^0 + \theta_{a\pi} a_{\text{phys}}, \quad (6.48)$$

with the mixing angle

$$\theta_{a\pi} = \frac{f_\pi}{2\sqrt{2}f} \left[ \frac{m_a^2 (\hat{c}_{uu} - \hat{c}_{dd})}{m_\pi^2 - m_a^2} - \frac{m_\pi^2 \Delta_\kappa}{m_\pi^2 - m_a^2} \right], \quad (6.49)$$

where  $\hat{c}_{qq} = c_{qq} + 2\kappa_q c_{GG}$  and

$$\Delta_\kappa = 4c_{GG} \frac{m_u \kappa_u - m_d \kappa_d}{m_u + m_d}. \quad (6.50)$$

In the literature, one often takes the “default” choice  $\kappa_q = \mathbf{m}_q^{-1}/\text{Tr}(\mathbf{m}_q^{-1})$ , which eliminates the mass mixing contribution  $\Delta_\kappa$  and leaves the kinetic mixing proportional to  $m_a^2$  [183, 197]. The latter can then be neglected for the QCD axion. In [5] we showed that for a non-vanishing ALP mass, the optimal choice is instead

$$\kappa_u = \frac{m_d}{m_u + m_d} + \frac{m_a^2}{m_\pi^2 - m_a^2} \frac{\Delta c_{ud}}{4c_{GG}}, \quad \kappa_d = \frac{m_u}{m_u + m_d} - \frac{m_a^2}{m_\pi^2 - m_a^2} \frac{\Delta c_{ud}}{4c_{GG}}, \quad (6.51)$$

with  $\Delta c_{ud} = c_{uu} - c_{dd} + 2c_{GG} \frac{m_d - m_u}{m_d + m_u}$ , because it eliminates all ALP–pion mixing effects. This equation reduces to the default choice in the limit where  $m_a^2/m_\pi^2 \rightarrow 0$ . However, it is most important to note that through the dependence on the auxiliary  $\kappa_q$  parameters,  $\theta_{a\pi}$  is not a physical quantity, and as such it is unobservable. We therefore refrain from adopting a particular choice for the  $\kappa_q$ .

We will use the chiral Lagrangian (6.46) to study flavour-changing processes such as  $K^- \rightarrow \pi^- a$  and  $\pi^- \rightarrow e^- \bar{\nu}_e a$ , which in the SM are mediated by the weak interactions and low energies are described by 4-fermion operators built out of products of left-handed quark currents. Under a left-handed, flavour off-diagonal rotation  $q_L \rightarrow U_L q_L$ , the meson fields transform as  $\Sigma \rightarrow U_L \Sigma$ . If we treat the modified quark mass matrix and the left-handed ALP couplings as spurions subject to the transformation rules  $\hat{\mathbf{m}}_q(a) \rightarrow U_L \hat{\mathbf{m}}_q(a)$  and  $\hat{\mathbf{k}}_Q \rightarrow U_L \hat{\mathbf{k}}_Q U_L^\dagger$ , the Lagrangian is invariant under  $U_L$  transformations. Applying the Noether procedure, one finds that the chiral representation of the left-handed quark currents  $\bar{q}^i \gamma_\mu P_L q^j$  is given by

$$\begin{aligned} L_\mu^{ji} &= -\frac{i f_\pi^2}{4} e^{i(\kappa_{q_j} - \kappa_{q_i}) c_{GG} \frac{a}{f}} [\Sigma (D_\mu \Sigma)^\dagger]_{ji} \\ &\supset -\frac{i f_\pi^2}{4} \left[ 1 + i(\kappa_{q_j} - \kappa_{q_i}) c_{GG} \frac{a}{f} \right] [\Sigma \partial_\mu \Sigma^\dagger]_{ji} + \frac{f_\pi^2}{4} \frac{\partial^\mu a}{f} [\hat{\mathbf{k}}_Q - \Sigma \hat{\mathbf{k}}_Q \Sigma^\dagger]_{ji}. \end{aligned} \quad (6.52)$$

The derivative ALP couplings in the last term have been omitted in previous treatments of the effective chiral ALP Lagrangian in [183] and all works based on it, but they are crucial to ensure the independence of physical amplitudes from the choice of the auxiliary parameters  $\kappa_q$  [6].

For a consistent analysis of weak-interaction decay processes involving ALPs, it is necessary to include the SM effective weak interactions at low energies. For the leptonic pion decay  $\pi^- \rightarrow e^- \bar{\nu}_e a$  the weak transition is a charged-current process mediated by the effective Lagrangian

$$\mathcal{L}_{u \rightarrow d} = -\frac{4G_F}{\sqrt{2}} V_{ud} L_\mu^{21} \bar{e} \gamma^\mu P_L \nu_e. \quad (6.53)$$

The decay amplitude for this process obtained from the chiral Lagrangian (neglecting contributions suppressed by the electron mass) reads [6, 199]

$$\begin{aligned} i\mathcal{A}(\pi^- \rightarrow e^- \bar{\nu}_e a) &= -\frac{iG_F}{\sqrt{2}} V_{ud} \frac{f_\pi}{2f} \bar{u}_e \gamma_\mu (1 - \gamma_5) v_{\bar{\nu}_e} \\ &\quad \times (p_\pi + p_a)^\mu \left[ 2c_{GG} \frac{m_d - m_u}{m_d + m_u} + [k_u - k_d]_{11} + \frac{m_a^2}{m_\pi^2 - m_a^2} \Delta c_{ud} \right], \end{aligned} \quad (6.54)$$

where  $k_{u,d}$  denotes the ALP couplings to the right-handed up- and down-quark currents, respectively, and

$$\Delta c_{ud} \equiv c_{uu} - c_{dd} + 2c_{GG} \frac{m_d - m_u}{m_d + m_u}. \quad (6.55)$$

All quantities are evaluated at the scale  $\mu_0$ . The leading-order operators mediating flavour-changing non-leptonic meson decays such as  $K^- \rightarrow \pi^- \pi^0$ ,  $K_S \rightarrow \pi^+ \pi^-$  and  $K_S \rightarrow \pi^0 \pi^0$  read [203–205]

$$\mathcal{L}_{s \rightarrow d} = -\frac{4G_F}{\sqrt{2}} V_{ud}^* V_{us} \left( g_8 \mathcal{O}_8 + g_{27}^{1/2} \mathcal{O}_{27}^{1/2} + g_{27}^{3/2} \mathcal{O}_{27}^{3/2} \right), \quad (6.56)$$

where the effective chiral operators are classified according to their transformation properties under  $SU(3)$  and isospin. The  $SU(3)$  octet operator  $\mathcal{O}_8$  mediates weak transitions with isospin change  $\Delta I = \frac{1}{2}$ , while the 27-plet operators  $\mathcal{O}_{27}^{1/2}$  and  $\mathcal{O}_{27}^{3/2}$  mediates transitions with  $\Delta I = \frac{1}{2}$  and  $\Delta I = \frac{3}{2}$ , respectively. These operators can be expressed in terms of products of the left-handed operators  $L_\mu^{ji}$  defined in (6.52). One finds

$$\begin{aligned} \mathcal{O}_8 &= \sum_i L_{3i} L_{i2}, \\ \mathcal{O}_{27}^{1/2} &= L_{32} L_{11} + L_{31} L_{12} + 2L_{32} L_{22} - 3L_{32} L_{33}, \\ \mathcal{O}_{27}^{3/2} &= L_{32} L_{11} + L_{31} L_{12} - L_{32} L_{22}, \end{aligned} \quad (6.57)$$

where contraction over the Lorentz indices is implied. The coefficient of the octet operator,  $|g_8| \approx 5.0$  [206], is larger than the coefficient  $|g_{27}^{3/2}|$  by about a factor of 30, and in the  $SU(3)$  symmetry limit the coefficient  $|g_{27}^{1/2}|$  is smaller than  $|g_{27}^{3/2}|$  by a factor of 5 [207]. The strong dynamical enhancement of  $\Delta I = \frac{1}{2}$  over  $\Delta I = \frac{3}{2}$  transitions is known as the  $\Delta I = \frac{1}{2}$  selection rule, and in our numerical analysis we will only consider the dominant octet contributions to the decay amplitudes.

We have calculated the  $K^- \rightarrow \pi^- a$  and  $\bar{K}^0 \rightarrow \pi^0 a$  decay amplitudes from the Lagrangians (6.46) and (6.56), evaluating the Feynman graphs shown in figure 6.4. The first two diagrams account for the ALP–meson mixing contributions, while the third graph contains the ALP interactions at the weak vertex derived from (6.52). The following two graphs describe ALP emission of an initial or final state meson. They only exist for the case of the charged mesons  $K^-$  and  $\pi^-$  and give non-zero contributions if the ALP has non-universal vector-current interactions with down and strange quarks. The last diagram contains possible flavour-changing ALP–fermion couplings, as parametrised by the off-diagonal elements of the matrices  $k_Q$  and  $k_q$  in 6.31. When all ALP couplings, flavour-conserving and violating ones, are to be taken of the same order of magnitude, the contribution from flavour-violating ones is dominant by far. To simplify the analysis we set  $m_u = m_d \equiv \bar{m}$  in order to eliminate the  $\pi^0$ – $\eta$  mass mixing. The meson masses are then given by  $m_\pi^2 = 2B_0 \bar{m}$ ,  $m_K^2 = B_0(m_s + \bar{m})$ , and  $3m_\eta^2 = 4m_K^2 - m_\pi^2$  with  $B_0 \approx m_\pi^2/(m_u + m_d)$ . Corrections to the

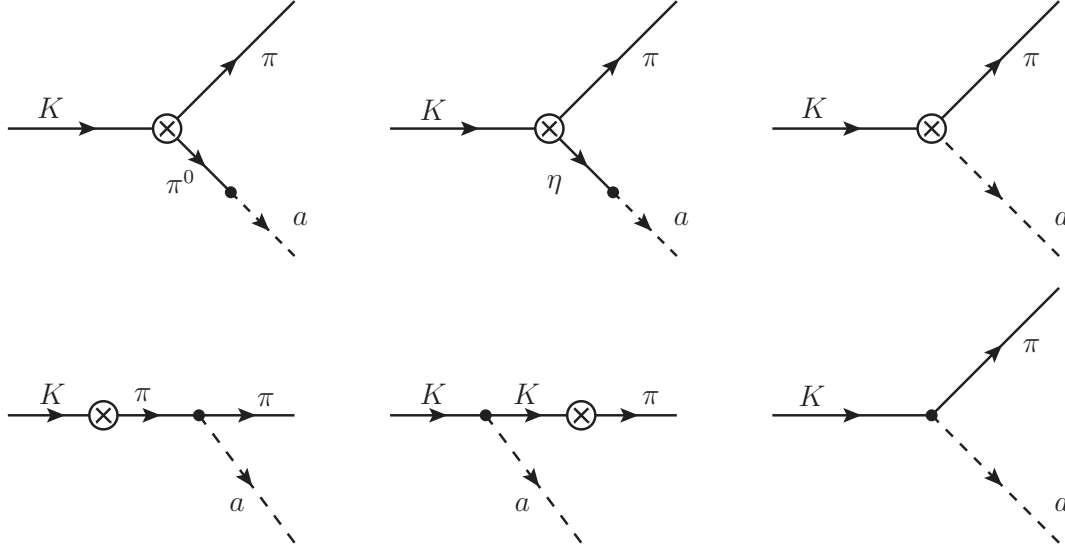


Figure 6.4: Feynman diagrams contributing to the  $K^- \rightarrow \pi^- a$  and  $\bar{K}^0 \rightarrow \pi^0 a$  decay amplitudes at leading order in ALP- $\chi$ PT. The crossed circles denotes weak interaction vertices mediated by the  $SU(3)$  octet operator  $\mathcal{O}_8$ . The dots refer to interactions from Lagrangian (6.46). The first two diagrams in the second row vanish for neutral mesons. If all ALP couplings are assumed to be of the same order, the last diagram with the direct flavour-changing ALP interaction is the most dominant contribution.

decay amplitudes proportional to the mass difference ( $m_u - m_d$ ) are suppressed by a factor  $1/m_s$ , and hence are very small. We then obtain [6]

$$\begin{aligned}
 i\mathcal{A}(K^- \rightarrow \pi^- a) &= \frac{N_8}{4f} \left[ 16c_{GG} \frac{(m_K^2 - m_\pi^2)(m_K^2 - m_a^2)}{4m_K^2 - m_\pi^2 - 3m_a^2} + (2c_{uu} + c_{dd} + c_{ss})(m_K^2 - m_\pi^2) \right. \\
 &\quad - (2c_{uu} + c_{dd} - 3c_{ss})m_a^2 + 6(c_{uu} + c_{dd} - 2c_{ss}) \frac{m_a^2(m_K^2 - m_a^2)}{4m_K^2 - m_\pi^2 - 3m_a^2} \\
 &\quad \left. + ([k_d + k_D]_{11} - [k_d + k_D]_{22})(m_K^2 + m_\pi^2 - m_a^2) \right] \\
 &\quad - \frac{m_K^2 - m_\pi^2}{2f} [k_d + k_D]_{12},
 \end{aligned} \tag{6.58}$$

and

$$\begin{aligned}
 -i\sqrt{2}\mathcal{A}(\bar{K}^0 \rightarrow \pi^0 a) &= \frac{N_8}{4f} \left[ 16c_{GG} \frac{(m_K^2 - m_\pi^2)(m_K^2 - m_a^2)}{4m_K^2 - m_\pi^2 - 3m_a^2} + (3c_{dd} + c_{ss})(m_K^2 - m_\pi^2) \right. \\
 &\quad + (2c_{uu} - c_{dd} - c_{ss})m_a^2 - 2(c_{uu} + c_{dd} - 2c_{ss}) \frac{m_a^2(m_K^2 - m_\pi^2)}{4m_K^2 - m_\pi^2 - 3m_a^2} \\
 &\quad - 2(c_{uu} - c_{dd}) \frac{m_a^2(m_K^2 - m_a^2)}{m_\pi^2 - m_a^2} \\
 &\quad \left. + ([k_d + k_D]_{11} - [k_d + k_D]_{22})(m_K^2 + m_\pi^2 - m_a^2) \right] \\
 &\quad - \frac{m_K^2 - m_\pi^2}{2f} [k_d + k_D]_{12},
 \end{aligned} \tag{6.59}$$

where

$$N_8 = -\frac{G_F}{\sqrt{2}} V_{ud}^* V_{us} g_8 f_\pi^2 \equiv |N_8| e^{i\delta_8}, \quad (6.60)$$

with  $|N_8| \approx 1.53 \times 10^{-7}$ . Here  $\delta_8$  denotes the strong-interaction phase of the phenomenological parameter  $g_8$ , and we adopt the standard phase convention for the CKM matrix, in which the matrix elements  $V_{ud}$  and  $V_{us}$  are real [208]. Note that the flavour-diagonal ALP–fermion couplings  $c_{qq}$  in the above relations are evaluated at the low scale  $\mu_0 \approx 2 \text{ GeV}$ .

In previous literature, crucial terms were omitted in the implementation of the left-handed quark current in the first realisation of ALP– $\chi$ PT in [183], as explained in eq. (6.52). This inconsistency has gone unnoticed ever since, despite a 35 year history of searches for ALPs in kaon decays. We want to briefly examine the impact of this. For the case of the QCD axion ( $m_a^2 \approx 0$ ) without couplings to fermions ( $c_{qq} = 0$ , only  $c_{GG} \neq 0$ ), the authors of [183] obtain (this formula was not shown in the paper, but can be derived from the arguments made and the numerical results presented)

$$i\mathcal{A}(K^- \rightarrow \pi^- a) \approx -\frac{N_8 m_K^2}{4f_a} \frac{m_u}{m_u + m_d}. \quad (6.61)$$

Instead, under the assumptions stated above and exchanging  $f_a = -\frac{f}{2c_{GG}}$ , the correct expression from (6.58) is

$$i\mathcal{A}(K^- \rightarrow \pi^- a) \approx -\frac{N_8 m_K^2}{2f_a}. \quad (6.62)$$

Hence, the amplitude was previously assumed to be smaller by a factor of  $\frac{m_u}{2(m_u+m_d)} \approx 0.16$ , corresponding to an underestimation of the branching ratio by a factor of 37.

### 6.3.2 ALPs in the chiral nuclear Lagrangian

To study ALP couplings to nucleons, we extend the discussion of the previous section to include baryon fields [183, 209–211]. For our purposes it will be sufficient to only include the proton and the neutron as nucleons, hence, we restrict the quark content to up and down-quarks for this discussion. The nucleon spinor field is then  $\psi = (p \quad n)^T$ . The field  $\Sigma$  in (6.45) is given by  $\Sigma = \exp\left[\frac{i\sqrt{2}}{f_\pi} \sigma^a \pi^a\right]$ , where we now only have the Pauli matrices  $\sigma$  in the exponential. In the limit when the up and down quarks have the same masses, and so do the proton and neutron, the Lagrangian features an enhanced chiral symmetry  $SU(2)_L \times SU(2)_R$ . Under such a transformation the meson field transforms as  $\Sigma \rightarrow \mathbf{L}\Sigma\mathbf{R}^\dagger$ . To describe the nucleon–meson interactions, it is convenient to define a field  $\xi$  via  $\xi^2(x) = \Sigma(x)$ , which transforms under the aforementioned symmetry group according to

$$\xi \rightarrow \mathbf{L}\xi\mathbf{U}^\dagger = \mathbf{U}\xi\mathbf{R}^\dagger, \quad \xi^\dagger \rightarrow \mathbf{R}\xi\mathbf{U}^\dagger = \mathbf{U}\xi\mathbf{L}^\dagger, \quad (6.63)$$

which also serves as a definition for the matrix  $\mathbf{U}$  in terms of the left and right transformation matrices  $\mathbf{L}$  and  $\mathbf{R}$  as well as the meson fields. The nucleon fields transform

as  $\psi \rightarrow U\psi$ . Neglecting the electromagnetic interactions for simplicity, we find that the covariant derivative takes the form

$$i\mathcal{D}_\mu\psi = i(\partial_\mu + \Gamma_\mu)\psi \quad (6.64)$$

with the connection

$$\begin{aligned} i\Gamma_\mu &= \frac{1}{2} \left[ \xi \left( i\partial_\mu + \frac{\partial_\mu a}{f} \hat{\mathbf{k}}_q \right) \xi^\dagger + \xi^\dagger \left( i\partial_\mu + \frac{\partial_\mu a}{f} \hat{\mathbf{k}}_Q \right) \xi \right] \\ &\equiv \frac{1}{2} \left[ \xi (i\partial_\mu + \mathbf{r}_\mu) \xi^\dagger + \xi^\dagger (i\partial_\mu + \mathbf{l}_\mu) \xi \right] + v_\mu^{(s)} \mathbb{1}, \end{aligned} \quad (6.65)$$

where  $\hat{\mathbf{k}}_q = \text{diag}(\hat{k}_u, \hat{k}_d)$  and  $\hat{\mathbf{k}}_Q = \text{diag}(\hat{k}_U, \hat{k}_D)$  are diagonal matrices containing the modified ALP–quark couplings defined in (6.42), restricted to the case of two flavours. In the second step we have defined the iso-vector chiral couplings

$$\begin{aligned} \mathbf{r}_\mu &= \frac{\partial_\mu a}{f} \left( \frac{[k_u - k_d]_{11}}{2} + c_{GG} \frac{\kappa_u - \kappa_d}{2} \right) \boldsymbol{\sigma}^3, \\ \mathbf{l}_\mu &= \frac{\partial_\mu a}{f} \left( \frac{[k_U - k_D]_{11}}{2} - c_{GG} \frac{\kappa_u - \kappa_d}{2} \right) \boldsymbol{\sigma}^3, \end{aligned} \quad (6.66)$$

and the iso-scalar vector coupling

$$v_\mu^{(s)} = \frac{\partial_\mu a}{2f} \left( \frac{[k_u + k_d]_{11}}{2} + \frac{[k_U + k_D]_{11}}{2} \right), \quad (6.67)$$

which is invariant under  $SU(2)_L \times SU(2)_R$ .

In the two-flavour  $\chi$ PT where we couple nucleons to pions, one further introduces two hermitian building blocks called vielbeins [212]. They are defined by

$$\xi \left( i\partial_\mu + \frac{\partial_\mu a}{f} \hat{\mathbf{k}}_q \right) \xi^\dagger - \xi^\dagger \left( i\partial_\mu + \frac{\partial_\mu a}{f} \hat{\mathbf{k}}_Q \right) \xi = \mathbf{u}_\mu + \mathbf{u}_\mu^{(s)}, \quad (6.68)$$

with

$$\begin{aligned} \mathbf{u}_\mu &= \xi (i\partial_\mu + \mathbf{r}_\mu) \xi^\dagger - \xi^\dagger (i\partial_\mu + \mathbf{l}_\mu) \xi, \\ \mathbf{u}_\mu^{(s)} &= \frac{\partial_\mu a}{f} \left[ \frac{[k_u + k_d]_{11}}{2} - \frac{[k_U + k_D]_{11}}{2} + c_{GG} (\kappa_u + \kappa_d) \right] \mathbb{1} \equiv 2a_\mu^{(s)} \mathbb{1}. \end{aligned} \quad (6.69)$$

These quantities transform as axial vectors under parity. Note that the iso-scalar axial-vector coupling  $a_\mu^{(s)}$  is invariant under  $SU(2)_L \times SU(2)_R$ . The condition  $\kappa_u + \kappa_d = 1$  is the two-flavour version of (6.41) and ensures that the vielbeins are independent of the auxiliary parameters  $\kappa_q$ .

Up to leading order in the chiral expansion, the chiral Lagrangian including interactions among nucleons, pions and ALPs then takes the form

$$\mathcal{L}_{\pi N} = \bar{\psi} \left( i\not{D} - m_N + \frac{g_A}{2} \gamma^\mu \gamma_5 \mathbf{u}_\mu + \frac{g_0}{2} \gamma^\mu \gamma_5 \mathbf{u}_\mu^{(s)} \right) \psi, \quad (6.70)$$

where  $m_N$  is the nucleon mass. Here,  $g_A$  and  $g_0$  are the coupling strengths to external iso-vector and iso-scalar source terms, respectively. In higher orders, corrections to the



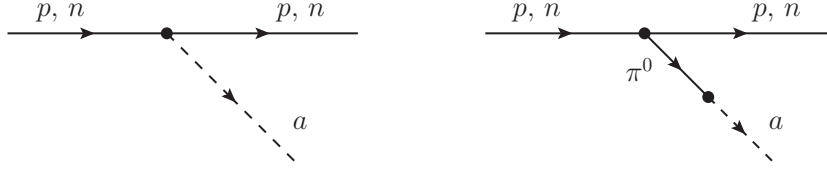


Figure 6.5: Feynman diagrams contributing to the effective ALP–nucleon coupling. The ALP is either radiated off the nucleon directly, or stems from mixing with a radiated neutral pion.

nucleon mass and couplings arise, as well as additional coupling structures. They are studied in [213] and will be omitted in this work.

ALPs can interact with nucleons in two different ways: Either there is a direct interaction vertex between the ALP and two nucleons, or a neutral pion gets radiated off a nucleon at first and subsequently mixes into the ALP. Both possibilities are shown in the Feynman diagrams of figure 6.5. We find for the amplitude in both cases

$$\begin{aligned} i\mathcal{A}(p(k) \rightarrow p(k') + a(q)) &= -\frac{g_{pa}}{4f} \bar{u}_N(k') \not{q} \gamma_5 u_N(k) = \frac{m_N g_{pa}}{2f} \bar{u}_N(k') \gamma_5 u_N(k), \\ i\mathcal{A}(n(k) \rightarrow n(k') + a(q)) &= -\frac{g_{na}}{4f} \bar{u}_N(k') \not{q} \gamma_5 u_N(k) = \frac{m_N g_{na}}{2f} \bar{u}_N(k') \gamma_5 u_N(k), \end{aligned} \quad (6.71)$$

with

$$\begin{aligned} g_{pa} &= g_0 (c_{uu} + c_{dd} + 2c_{GG}) + g_A \frac{m_\pi^2}{m_\pi^2 - m_a^2} \Delta c_{ud}, \\ g_{na} &= g_0 (c_{uu} + c_{dd} + 2c_{GG}) - g_A \frac{m_\pi^2}{m_\pi^2 - m_a^2} \Delta c_{ud}. \end{aligned} \quad (6.72)$$

The quantity  $\Delta c_{ud}$  was already defined in (6.55). We emphasise that the iso-vector current contribution depends on the ALP mass in a non-trivial way, an effect that has not been included in the literature thus far. Note further that the right-hand side of eq. (6.71) does not scale with the nucleon mass despite its appearance in the formulae. The reason is that the spinor product  $\bar{u}_N(k') \gamma_5 u_N(k)$  scales like  $s \cdot (k - k')/m_N$  for  $k \rightarrow k'$ , where  $s$  is the nucleon spin vector.

The coupling constant  $g_A$  can be determined from nucleon  $\beta$  decays and was found to be  $g_A = 1.2754(13)$  [18]. It is not possible to retrieve the parameter  $g_0$  in that way. However, we can take advantage of the fact that the ALP–nucleon coupling can also be inferred directly from the Lagrangian description including quarks and gluons (6.25), instead of taking the detour of a chiral EFT. For the proton one obtains

$$\begin{aligned} \mathcal{A}(p(k) \rightarrow p(k') + a(q)) &= \sum_q \frac{c_{qq}(\mu_0)}{2f} i q_\mu \langle p(k') | \bar{q} \gamma^\mu \gamma_5 q | p(k) \rangle_{\mu_0} \\ &\quad + \frac{c_{GG}}{f} \frac{\alpha_s(\mu_0)}{4\pi} \langle p(k') | G_{\mu\nu}^a \tilde{G}^{\mu\nu,a} | p(k) \rangle_{\mu_0}, \end{aligned} \quad (6.73)$$

where the sum in the first term runs over the (light) quark flavours, and the hadronic matrix elements are renormalised at the scale  $\mu_0$ . An analogous expression holds for the

neutron. When we match these expressions onto (6.71), we can derive the following relations

$$\begin{aligned} \left(g_0 + g_A \frac{m_\pi^2}{m_\pi^2 - q^2}\right) \bar{u}_N(k') \not{q} \gamma_5 u_N(k) &= 2 \langle p(k') | \bar{u} \not{q} \gamma_5 u | p(k) \rangle, \\ \left(g_0 - g_A \frac{m_\pi^2}{m_\pi^2 - q^2}\right) \bar{u}_N(k') \not{q} \gamma_5 u_N(k) &= 2 \langle p(k') | \bar{d} \not{q} \gamma_5 d | p(k) \rangle, \end{aligned} \quad (6.74)$$

where  $q^2 = (k - k')^2$ . A third relation relates the gluon matrix element of the proton to the couplings  $g_A$  and  $g_0$ . We now consider the limit  $q^\mu \rightarrow 0$ , i.e.  $k \rightarrow k'$ , in these relations. Furthermore, we define the nucleon spin vector as

$$s^\mu \equiv \frac{1}{2} \bar{u}_N(k) \gamma^\mu \gamma_5 u_N(k); \quad k \cdot s = 0, \quad (6.75)$$

and introduce the hadronic quantities  $\Delta q$  via [214]

$$\langle p(k) | \bar{q} \gamma^\mu \gamma_5 q | p(k) \rangle \equiv 2 s^\mu \Delta q. \quad (6.76)$$

Combining all expressions, we find the simple equations

$$g_0 + g_A = 2\Delta u, \quad g_0 - g_A = 2\Delta d, \quad (6.77)$$

which are solved by  $g_0 = \Delta u + \Delta d$  and  $g_A = \Delta u - \Delta d$ . The hadronic matrix elements  $\Delta q$  are typically computed using lattice QCD [214]. In the case at hand, we have already integrated out all heavy degrees of freedom, hence we use the the results for  $\Delta q$  obtained by the  $\chi$ QCD collaboration that used  $N_f = 2 + 1^7$  light fermions [215]. They calculated the pion mass to be  $m_\pi = 171$  MeV, what is reasonably close to the physically observed value of  $m_{\pi^0}^{\text{exp}} = 134.98$  MeV. The reported values for the hadronic matrix elements are  $\Delta u = 0.847(18)(32)$  and  $\Delta d = -0.407(16)(18)$ , from which we derive  $g_0 = 0.440(44)$  and  $g_A = 1.254(16)(30)$ , which is in good agreement with the measured value stated above.

Let us now briefly come back to ambiguity concerning the nucleon masses in eq. (6.71). This mass is a large external scale and as such plays no relevant role to the chiral dynamics. The ambiguity can be avoided by matching the ALP–nucleon Lagrangian (6.70) onto a heavy-baryon chiral effective Lagrangian by replacing

$$\psi(x) \rightarrow e^{-im_N v \cdot x} \frac{1 + \not{v}}{2} N(x), \quad (6.78)$$

where  $v^\mu$  is the 4-velocity of the nucleon. Expanding eq. (6.71) to leading order in  $1/m_N$ , we then find

$$\mathcal{L}_{\pi N} \rightarrow \bar{N} \left( i v \cdot \mathbf{D} + g_A S \cdot \mathbf{u} + g_0 S \cdot \mathbf{u}^{(s)} \right) N, \quad (6.79)$$

where  $S^\mu = \frac{i}{2} \sigma^{\mu\nu} \gamma_5 v_\nu$  denotes the Pauli–Lubanski spin operator.

The effective ALP–nucleon couplings in (6.72) depend on the ALP mass, and the corresponding results for the QCD axion are recovered in the limit  $m_a \rightarrow 0$ . For an ALP with a mass not much smaller than the pion mass, this effect can become relevant, especially

---

7 The light fermions are the up and down-quark, and the electron.

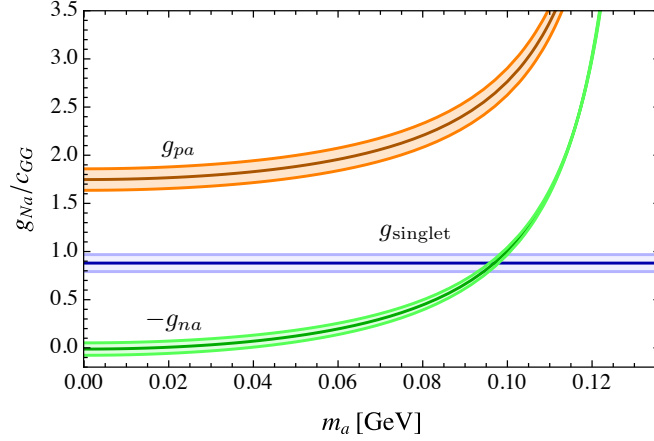


Figure 6.6: Mass dependence of ALP–nucleon couplings for the proton (orange), the neutron (green), and an iso-singlet nucleus with coupling  $g_{\text{singlet}} \equiv (g_{pa} + g_{na})/2$  (blue), in units of the ALP–gluon coupling  $c_{GG}$ . The ALP couplings to quarks are set to zero ( $c_{uu} = c_{dd} = 0$ ). For nuclei with equal numbers of protons and neutrons, the mass dependence cancels out. However, it changes the interaction strength of ALPs with non-singlet nuclei significantly.

in models where the ALP–gluon coupling is much larger than the ALP couplings to the up and down-quarks. For the case where  $c_{uu} = c_{dd} = 0$  at the low scale  $\mu_0$ , we show in figure 6.6 the mass dependence of the effective ALP couplings to the proton, the neutron and an iso-singlet nucleus with equal numbers of protons and neutrons. The mass dependence cancels for iso-singlet nuclei, but can change the ALP interaction strength with non-singlet nuclei significantly. For neutrons the accidental cancellation between the terms proportional to  $c_{GG}$  in the second relation in (6.72) is broken by the mass of the ALP.



## FLAVOUR PROBES OF ALPS

---

In this chapter we will derive constraints on ALP couplings from flavour physics experiments. We split our studies in two parts: First, we investigate flavour experiments in the quark sector. We assume that only one flavour-diagonal or flavour-blind coupling is present in the UV. All other ALP–SM interactions are then generated via evolution and matching effects from high to low energies. Especially flavour-changing ALP couplings are generated through RG-effects, as explained in the previous chapter. In the second section 7.2, we derive bounds coming from searches for rare lepton transitions. Since the lepton numbers are individually conserved in the SM, no lepton flavour-violating couplings are generated in running from the UV to the low energy. Additionally, most observables require a coupling of ALPs to two leptons of the same flavour to be present. Hence, our parameter space is spanned by the ALP mass, the flavour-diagonal couplings, and one flavour-off-diagonal coupling.

### 7.1 Quark flavour probes of ALPs

The focus of this section is on deriving experimental constraints on the ALP couplings from observables sensitive to flavour-changing interactions in the quark sector. Examples for these experiments include searches for rare meson decays like  $K \rightarrow \pi a$  and  $\pi \rightarrow e\bar{\nu}_e a$ , and radiative  $J/\psi$  and  $\Upsilon$  decays. After deriving general expressions for the decay rates and branching ratios, we present our results in four representative benchmark scenarios, where we assume that in the far UV, only a coupling to strong or weak gauge bosons, or a coupling to the left handed quark or lepton doublet is non-zero, respectively. In other words, we study four situations, where one of  $c_{GG}$ ,  $c_{WW}$ ,  $c_Q$ ,  $c_E \neq 0$  and all other coefficients vanish. At the low energy scale, the effective ALP couplings to the other particles are generated through RG effects, as explained in section 6.2.

The results presented in this section have been published in [7] and are summarised for this thesis. In the cited work, we have conducted an exhaustive study of quark flavour probes of ALPs, and presented benchmark scenarios for every UV ALP coupling. Furthermore, we demonstrated how ALPs can possibly explain the (former) low-energy

anomalies of hints for lepton flavour universality violation in  $b \rightarrow s$  transitions<sup>1</sup> [63,64], the ATOMKI anomalies consisting of an excess in excited Helium and Beryllium transitions  ${}^8\text{Be}^* \rightarrow {}^8\text{Be} + e^+e^-$  and  ${}^4\text{He}^* \rightarrow {}^4\text{He} + e^+e^-$  [216–218], as well as the long-standing KTeV anomaly in  $\pi^0 \rightarrow e^+e^-$  [219]. For other works on constraints on ALPs from quark-flavour observables, we refer the reader to [186,190,220–230].

### 7.1.1 ALPs in exotic meson decays

Most stringent bounds on the ALP parameter space can be derived from searches for rare or SM-forbidden two-body meson decays. The reason is that in a decay  $\Pi \rightarrow \tilde{\pi}a$  with  $\Pi$  and  $\tilde{\pi}$  a heavy and light pseudoscalar meson, respectively, the ALP can be produced as an on-shell resonance, hence giving experimentalists a clear decay pattern of a light meson and missing energy and momentum in the opposite direction to look for. We will discuss the decays  $K^- \rightarrow \pi^-a$  and  $K_L \rightarrow \pi^0a$  in detail. Following our layout it is then straightforward to extend the method to  $B \rightarrow \pi a$  and  $D \rightarrow \pi a$  decays.

The kaon decays  $K^- \rightarrow \pi^-a$  and  $K_L \rightarrow \pi^0a$  as two-body decays feature the (for the detector) invisible ALP and diametrically radiated pion as decay products. The pion energy is therefore determined as

$$E_\pi = \frac{m_K^2 + m_\pi^2 - m_a^2}{2m_K} \quad (7.1)$$

in the kaon rest frame. The decay rates for the charged and neutral kaon decays are given by

$$\Gamma(K \rightarrow \pi a) = \frac{1}{16\pi m_K} |\mathcal{A}(K \rightarrow \pi a)|^2 \lambda^{1/2} \left( \frac{m_\pi^2}{m_K^2}, \frac{m_a^2}{m_K^2} \right), \quad (7.2)$$

where

$$\lambda(r_i, r_j) = 1 + r_i^2 + r_j^2 - 2r_i - 2r_j - 2r_i r_j. \quad (7.3)$$

The decay amplitudes have been given in (6.58) and (6.59) for the charged and neutral current, respectively, and they receive contribution from flavour-blind, flavour-conserving and flavour-changing ALP couplings. If a flavour-changing coupling is present at the UV-scale and it is of the same order of magnitude as the flavour-conserving ones, it gives the dominant contribution by many orders of magnitude. This is because FCNCs in the SM are loop and GIM suppressed. The CP-conjugate modes can be obtained by replacing  $[k_d + k_D]_{12} \rightarrow [k_d + k_D]_{21} = [k_d + k_D]_{12}^*$  and changing the overall sign. Furthermore, one should also take the complex conjugate of the product  $V_{ud}^* V_{us}$  of CKM matrix elements in the definition of the quantity  $N_8$ , though this has no effect since these parameters are real in the standard convention for the CKM matrix. The amplitude for the decay  $K_L \rightarrow \pi^0a$ , on

<sup>1</sup> For a long time, the double ratios  $R_K = \text{Br}(B^+ \rightarrow K^+ \mu^+ \mu^-) / \text{Br}(B^+ \rightarrow K^+ e^+ e^-)$  and  $R_{K^*} = \text{Br}(B^0 \rightarrow K^{*0} \mu^+ \mu^-) / \text{Br}(B^0 \rightarrow K^{*0} e^+ e^-)$  were anomalous with respect to the measured value and the SM expectation. They have been a motivation for many BSM models. However, it turned out that previously experimental background was underestimated, and the latest analysis suggests instead a complete agreement of experiment and theory [65].

which constraints can be derived using existing searches for  $K_L \rightarrow \pi^0 \nu \bar{\nu}$  and  $K_L \rightarrow \pi^0 X$ , is then obtained using the relation [231]

$$K_L = \frac{(1 + \epsilon)K^0 + (1 - \epsilon)\bar{K}^0}{\sqrt{2(1 + |\epsilon|^2)}}, \quad (7.4)$$

where  $\epsilon = 2.228(11) \times 10^{-3} e^{i\phi_\epsilon}$  with  $\phi_\epsilon \approx 43.5^\circ$  is the parameter measuring CP violation in  $K^0 - \bar{K}^0$  mixing [208]. One can show that the  $K_L$  decay channel is especially suited to constrain the imaginary part of the flavour-changing coupling  $[k_d + k_D]_{12}$ , whereas the sensitivity to all other couplings is reduced by a factor of  $|\epsilon| \approx 2 \times 10^{-3}$ , when compared with the reach of charged kaon decays.

Note that since the decay rate in (7.2) receives contributions from squaring the amplitudes (6.58) and (6.59), a mixed term involving both flavour-conserving and flavour-changing ALP couplings is in principle sensitive to the strong interaction phase  $\delta_8$ , which cannot be calculated reliably. However, in practice this is not a problem, because the coefficients of the two types of terms differ by many orders of magnitude.

Similarly to ALP production in kaon decays, an ALP can be produced by decays of  $B$  and  $D$  mesons together with pions or kaons. In terms of the flavour-changing ALP couplings, we find the decay rates

$$\begin{aligned} \Gamma(B^- \rightarrow \pi^- a) &= \frac{m_B^3}{64\pi f^2} |[k_D + k_d]_{13}|^2 |F_0^{B \rightarrow \pi}(m_a^2)|^2 \left(1 - \frac{m_\pi^2}{m_B^2}\right)^2 \lambda^{1/2}\left(\frac{m_\pi^2}{m_B^2}, \frac{m_a^2}{m_B^2}\right), \\ \Gamma(\bar{B}^0 \rightarrow \pi^0 a) &= \frac{1}{2} \Gamma(B^- \rightarrow \pi^- a), \\ \Gamma(B^- \rightarrow K^- a) &= \frac{m_B^3}{64\pi f^2} |[k_D + k_d]_{23}|^2 |F_0^{B \rightarrow K}(m_a^2)|^2 \left(1 - \frac{m_K^2}{m_B^2}\right)^2 \lambda^{1/2}\left(\frac{m_K^2}{m_B^2}, \frac{m_a^2}{m_B^2}\right), \\ \Gamma(B^- \rightarrow K^{*-} a) &= \frac{m_B^3}{64\pi f^2} |[k_D - k_d]_{23}|^2 |A_0^{B \rightarrow K^*}(m_a^2)|^2 \lambda^{3/2}\left(\frac{m_K^{*2}}{m_B^2}, \frac{m_a^2}{m_B^2}\right), \\ \Gamma(\bar{B}^0 \rightarrow \bar{K}^{(*)0} a) &= \Gamma(B^- \rightarrow K^{(*)-} a), \\ \Gamma(D^+ \rightarrow \pi^+ a) &= \frac{m_D^3}{64\pi f^2} |[k_U + k_u]_{12}|^2 |F_0^{D \rightarrow \pi}(m_a^2)|^2 \left(1 - \frac{m_\pi^2}{m_D^2}\right)^2 \lambda^{1/2}\left(\frac{m_\pi^2}{m_D^2}, \frac{m_a^2}{m_D^2}\right), \\ \Gamma(D^0 \rightarrow \pi^0 a) &= \frac{1}{2} \Gamma(D^+ \rightarrow \pi^+ a), \\ \Gamma(D_s^+ \rightarrow K^+ a) &= \frac{m_{D_s}^3}{64\pi f^2} |[k_U + k_u]_{12}|^2 |F_0^{D_s \rightarrow K}(m_a^2)|^2 \left(1 - \frac{m_K^2}{m_{D_s}^2}\right)^2 \lambda^{1/2}\left(\frac{m_K^2}{m_{D_s}^2}, \frac{m_a^2}{m_{D_s}^2}\right). \end{aligned} \quad (7.5)$$

For  $B \rightarrow K^* a$  decays the  $K^*$  meson is longitudinally polarised, since the ALP is a pseudo-scalar particle. The quantities  $F_0(q^2)$  and  $A_0(q^2)$  are scalar form factors defined in [232]. We take  $F_0^{B \rightarrow K}(q^2)$  from the lattice average of [214] (based on the calculations of the HPQCD [233] and FNAL/MILC [234] collaborations),  $F_0^{B \rightarrow \pi}(q^2)$  from the FNAL/MILC lattice calculation [235],  $A_0^{B \rightarrow K^*}(q^2)$  from the light-cone QCD sum-rule calculation of [236],  $F_0^{D \rightarrow \pi}(q^2)$  from the ETM lattice calculation of [237], and  $F_0^{D_s \rightarrow K}(q^2)$  from the covariant light-front calculation of [238].

In all of these processes, we have only taken effects from flavour-changing ALP couplings into account, and included the SM weak interactions only to the extent that these contribute to the flavour-changing ALP couplings at low energies. This is justified by the observation we made for  $K \rightarrow \pi a$  decays, that contributions to the amplitude involving the SM weak transition  $s \rightarrow u\bar{d}$  are strongly suppressed. We expect a similar statement to hold for the decays of heavy  $B$  and  $D$  mesons. For example, we expect that subprocesses of the type  $B^- \rightarrow \pi^- \pi^0 \rightarrow \pi^- a$  via ALP–pion mixing give rise to subdominant contributions to the  $B^- \rightarrow \pi^- a$  rate. It would be interesting to work out these effects in greater detail, for instance using the framework of QCD factorisation for non-leptonic  $B$  decays [239, 240].

The bounds we can derive from these rare meson decays are highly dependent on the ALP mass and couplings. While the (effective) flavour-changing couplings allow for these transitions in the first place, the (effective) flavour-conserving ones together with its mass determine the possible decay modes of the ALP. Hence, the effective sensitivity of experiments depends delicately on these parameters. Constraints on a long-lived ALP can be derived from searches for rare decays such as  $K \rightarrow \pi\nu\bar{\nu}$  and  $B \rightarrow K^{(*)}\nu\bar{\nu}$ , whereas bounds on a short-lived ALP can be obtained by recasting searches for meson decays into a final state meson accompanied by a pair of photons or leptons, or by dedicated searches for new light resonances in the final state. An extensive list of experimental searches and the respective limits on the ALP couplings  $[k_d]_{ij}$  and  $[k_D]_{ij}$  with  $ij = 12, 13, 23$  and  $[k_u]_{12}$  and  $[k_U]_{12}$  from exotic decays of kaons,  $B$  mesons and  $D_{(s)}$  mesons are compiled in table 7.1. These experiments probe flavour-changing ALP properties up to new physics scales  $f \lesssim 10^9 \text{ TeV} \times \sqrt{\mathcal{B}}$ , where  $\mathcal{B}$  is the branching ratio of the ALP into the respective signal final state. We emphasise that it is therefore crucial to probe resonances in different channels, even though they all examine the same flavour-changing ALP coupling.

In addition, the lifetime of the ALP changes the strength of experiments through its effect on the fraction of ALPs that escape detection. We define the ALP decay length as

$$\ell_a = c\tau_a = \frac{\hbar c}{\Gamma} \simeq 0.197 \mu\text{m} \frac{1 \text{ eV}}{\Gamma}, \quad (7.6)$$

where  $\Gamma$  is the total decay width. More details about how certain types of experiments depend on the ALP decay length are presented in [7].

### 7.1.2 The rare pion decay $\pi^- \rightarrow ae^-\bar{\nu}_e$

An interesting opportunity to discover ALPs is provided by three-body charged pion decays with leptonic final states. They are insensitive to the flavour-violating couplings of an ALP, because they are mediated by the weak force, and thus probe ALP couplings to gluons and light quarks. As before, these experiments are especially powerful when the ALP can be produced in on-shell resonances, i.e.  $m_a < m_\pi - m_e$ . The amplitude for this



Observable	Mass range [MeV]	ALP decay mode	Constrained coupling $c_{ij}$	Limit (95% CL) on $c_{ij} \cdot \left(\frac{\text{TeV}}{f}\right) \cdot \sqrt{\mathcal{B}}$
$\text{Br}(K^- \rightarrow \pi^- a(\text{inv}))$	$0 < m_a < 261^{(*)}$	long-lived	$ k_D + k_d _{12}$	$1.2 \times 10^{-9}$
$\text{Br}(K_L \rightarrow \pi^0 a(\text{inv}))$	$0 < m_a < 261$	long-lived	$ \text{Im}[[k_D + k_d]_{12}] $	$8.1 \times 10^{-9}$
$\text{Br}(K^- \rightarrow \pi^- \gamma \gamma)$	$m_a < 108$	$\gamma \gamma$	$ k_D + k_d _{12}$	$2.1 \times 10^{-8}$
$\text{Br}(K^- \rightarrow \pi^- \gamma \gamma)$	$220 < m_a < 354$	$\gamma \gamma$	$ k_D + k_d _{12}$	$2.0 \times 10^{-7}$
$\text{Br}(K_L \rightarrow \pi^0 \gamma \gamma)$	$30 < m_a < 110$	$\gamma \gamma$	$ \text{Im}[[k_D + k_d]_{12}] $	$1.3 \times 10^{-8}$
$\text{Br}(K_L \rightarrow \pi^0 \gamma \gamma)$	$m_a < 363^{(\text{**})}$	$\gamma \gamma$	$ \text{Im}[[k_D + k_d]_{12}] $	$1.3 \times 10^{-7}$
$\text{Br}(K^+ \rightarrow \pi^+ a(e^+ e^-))$	$1 < m_a < 100$	$e^+ e^-$	$ k_D + k_d _{12}$	$3.4 \times 10^{-7}$
$\text{Br}(K_L \rightarrow \pi^0 e^+ e^-)$	$140 < m_a < 362$	$e^+ e^-$	$ \text{Im}[[k_D + k_d]_{12}] $	$3.1 \times 10^{-9}$
$\text{Br}(K_L \rightarrow \pi^0 \mu^+ \mu^-)$	$210 < m_a < 350$	$\mu^+ \mu^-$	$ \text{Im}[[k_D + k_d]_{12}] $	$4.0 \times 10^{-9}$
$\text{Br}(B^+ \rightarrow \pi^+ e^+ e^-)$	$140 < m_a < 5140$	$e^+ e^-$	$ k_D + k_d _{13}$	$7.0 \times 10^{-7}$
$\text{Br}(B^+ \rightarrow \pi^+ \mu^+ \mu^-)$	$211 < m_a < 5140^{(\ddagger\ddagger)}$	$\mu^+ \mu^-$	$ k_D + k_d _{13}$	$1.2 \times 10^{-7}$
$\text{Br}(B^- \rightarrow K^- \nu \bar{\nu})$	$0 < m_a < 4785$	long-lived	$ k_D + k_d _{23}$	$6.2 \times 10^{-6}$
$\text{Br}(B \rightarrow K^* \nu \bar{\nu})$	$0 < m_a < 4387$	long-lived	$ k_D - k_d _{23}$	$4.1 \times 10^{-6}$
$d\text{Br}/dq^2(B^0 \rightarrow K^{*0} e^+ e^-)_{[0.0,0.05]}$	$1 < m_a < 224$	$e^+ e^-$	$ k_D - k_d _{23}$	$6.4 \times 10^{-7}$
$d\text{Br}/dq^2(B^0 \rightarrow K^{*0} e^+ e^-)_{[0.05,0.15]}$	$224 < m_a < 387$	$e^+ e^-$	$ k_D - k_d _{23}$	$9.3 \times 10^{-7}$
$\text{Br}(B^- \rightarrow K^- a(\mu^+ \mu^-))$	$250 < m_a < 4700^{(\dagger)}$	$\mu^+ \mu^-$	$ k_D + k_d _{23}$	$4.4 \times 10^{-8}$
$\text{Br}(B^0 \rightarrow K^{*0} a(\mu^+ \mu^-))$	$214 < m_a < 4350^{(\dagger)}$	$\mu^+ \mu^-$	$ k_D - k_d _{23}$	$5.1 \times 10^{-8}$
$\text{Br}(B^- \rightarrow K^- \tau^+ \tau^-)$	$3552 < m_a < 4785$	$\tau^+ \tau^-$	$ k_D + k_d _{23}$	$8.2 \times 10^{-5}$
$\text{Br}(D^0 \rightarrow \pi^0 e^+ e^-)$	$1 < m_a < 1730^{(\ddagger)}$	$e^+ e^-$	$ k_U + k_u _{12}$	$2.8 \times 10^{-5}$
$\text{Br}(D^+ \rightarrow \pi^+ e^+ e^-)$	$200 < m_a < 1730^{(\ddagger\ddagger)}$	$e^+ e^-$	$ k_U + k_u _{12}$	$8.4 \times 10^{-6}$
$\text{Br}(D_s^+ \rightarrow K^+ e^+ e^-)$	$200 < m_a < 1475^{(\text{**})}$	$e^+ e^-$	$ k_U + k_u _{12}$	$2.4 \times 10^{-5}$
$\text{Br}(D^+ \rightarrow \pi^+ \mu^+ \mu^-)$	$250 < m_a < 1730^{(**)}$	$\mu^+ \mu^-$	$ k_U + k_u _{12}$	$2.1 \times 10^{-6}$
$\text{Br}(D_s^+ \rightarrow K^+ \mu^+ \mu^-)$	$200 < m_a < 1475^{(***)}$	$\mu^+ \mu^-$	$ k_U + k_u _{12}$	$5.7 \times 10^{-5}$

Table 7.1: Summary of indicative constraints on quark flavour-violating ALP couplings renormalised at the scale  $\mu_w = m_t$ , derived from measurements of branching fractions (first column) for various decays of kaons and  $B$  mesons in a mass range where an on-shell ALP can be produced. The relevant measurements and SM predictions (where appropriate) are given in AII.3 to AII.8 in appendix AII.1. In each line, the limit cited is the strongest limit found within the mass range probed by the measurement. In the fifth column the symbol  $\mathcal{B}$  denotes the ALP branching ratio to the relevant final state. Asterisks next to the mass range mean that cuts are applied within the mass range to exclude resonance regions, and therefore the corresponding measurement is insensitive to an ALP with mass in the excluded ranges. The excluded regions are as follows. (\*):  $100 \text{ MeV} < m_{\nu\bar{\nu}} < 161 \text{ MeV}$ ; (\*\*):  $525 \text{ MeV} < m_{\mu\mu} < 1250 \text{ MeV}$ ; (\*\*\*) :  $990 \text{ MeV} < m_{\mu\mu} < 1050 \text{ MeV}$ ; (\*\*) :  $950 \text{ MeV} < m_{ee} < 1050 \text{ MeV}$ ; (\*\*) :  $100 \text{ MeV} < m_{\gamma\gamma} < 160 \text{ MeV}$ ; (†):  $935 \text{ MeV} < m_{ee} < 1053 \text{ MeV}$ ; (††):  $8.0 \text{ GeV}^2 < m_{\mu\mu}^2 < 11.0 \text{ GeV}^2$  and  $12.5 \text{ GeV}^2 < m_{\mu\mu}^2 < 15.0 \text{ GeV}^2$ ; (†): various cuts are applied to exclude the regions around the  $J/\psi$ ,  $\psi(2S)$  and  $\psi(3370)$  resonances; (††):  $525 \text{ MeV} < m_{\mu\mu} < 1250 \text{ MeV}$ .

decay is given in (6.54). Neglecting contributions suppressed by  $m_e^2/(m_\pi^2 - m_a^2)$ , one finds the decay rate

$$\Gamma(\pi^- \rightarrow a e^- \bar{\nu}_e) = \frac{G_F^2 |V_{ud}|^2}{24576\pi^3} \frac{f_\pi^2}{f^2} m_\pi^5 g(x_a) \left[ 2c_{GG} \frac{m_d - m_u}{m_d + m_u} + [k_u]_{11} - [k_d]_{11} + \frac{m_a^2}{m_\pi^2 - m_a^2} \Delta c_{ud} \right]^2, \quad (7.7)$$

where  $x_a = m_a^2/m_\pi^2$ , and the phase-space function is given by

$$g(x) = 1 - 8x - 12x^2 \ln x + 8x^3 - x^4. \quad (7.8)$$

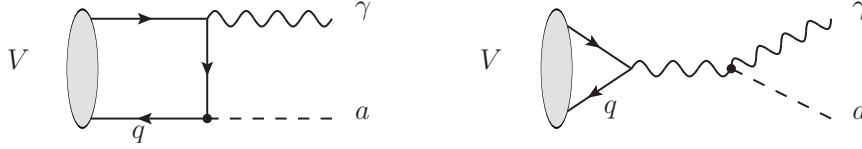


Figure 7.1: Feynman diagrams contributing to the  $V \rightarrow \gamma a$  of the heavy vector mesons  $J/\psi$  and  $\Upsilon$ .

This result agrees with corresponding expressions derived in [241] and [199] (for  $m_a = 0$ ). The PIENU collaboration has recently put a limit on the branching ratio  $\text{Br}(\pi^- \rightarrow a e^- \bar{\nu}_e) < 10^{-6} \text{Br}(\pi^- \rightarrow \mu^- \bar{\nu}_\mu)$  [242].

### 7.1.3 Radiative $J/\psi$ and $\Upsilon$ decays

The decays of the bound charmonium and bottomonium states  $J/\psi$  and  $\Upsilon$  can give rise to interesting constraints to the ALP parameter space. Since no FCNC is involved, there are no constraints on flavour-changing couplings, however, they probe masses and flavour-diagonal couplings in a region that is similar to the one probed by other experiments involving RG induced flavour change. Hence, they can provide complementary searches for our benchmark scenarios. In the literature, these decays have been used to install bounds on ALP couplings to  $b$ -quarks [243–246] and photons [247,248]. The first combined analysis of the contributions from both the ALP–photon coupling and the ALP–quark coupling was performed in [249], neglecting however important QCD corrections. Leading Feynman diagrams are shown in figure 7.1. The decay rate reads

$$\Gamma(V \rightarrow \gamma a) = \frac{m_V f_V^2}{6f^2} Q_q^2 \alpha \left(1 - \frac{m_a^2}{m_V^2}\right) \left| c_{qq}(\mu_q) \left[1 - \frac{2\alpha_s(\mu_q)}{3\pi} a_P(x)\right] - \frac{\alpha}{2\pi} c_{\gamma\gamma} \left(1 - \frac{m_a^2}{m_V^2}\right) \right|^2, \quad (7.9)$$

where  $q = c, b$  as appropriate, and  $\mu_q \sim m_q$  is an appropriate matching scale.

The scale dependence of the coefficients  $c_{bb}$  and  $c_{cc}$  are such that, if  $\Lambda = 4\pi f$  TeV,

$$c_{bb}(m_b) \simeq c_{bb}(\Lambda) + 0.09c_{tt}(\Lambda) - 0.02c_{GG}, \quad (7.10)$$

$$c_{cc}(m_c) \simeq c_{cc}(\Lambda) - 0.13c_{tt}(\Lambda) - 0.04c_{GG}. \quad (7.11)$$

In the strict non-relativistic limit, where each of the two heavy quarks in the quarkonium state carries one half of its momentum, the QCD radiative corrections give rise to [244]

$$a_P(x) = \frac{3-7x}{1-2x} + \frac{1-7x+8x^2}{(1-2x)^2} \ln 2x + 4\sqrt{\frac{1-x}{x}} \arctan \sqrt{\frac{1-x}{x}} + \frac{2(1-2x)}{x} \arctan^2 \sqrt{\frac{1-x}{x}} - \frac{1-4x}{2x} \text{Li}_2(1-2x) - \frac{5-8x}{2x} \frac{\pi^2}{6}, \quad (7.12)$$

where  $x = E_\gamma/E_\gamma^{\text{max}} = 1 - m_a^2/m_V^2$ . This is an increasing function of its argument, which varies between  $a_P(0) = 2$  and  $a_P(1) = \frac{\pi^2}{8} + 2\ln 2 + 4 \approx 6.62$ , thus giving rise to a rather large correction. Note that the contribution proportional to the coefficient  $c_{\gamma\gamma}$  in (7.9) does

not receive any QCD radiative corrections. In the calculation of the decay amplitude we have used the identity

$$\langle 0 | \bar{b} \Gamma b | V(p, \varepsilon) \rangle = \frac{if_V m_V}{2} \text{Tr} \left[ \not{\varepsilon} \Gamma \frac{(1 + \not{v})}{2} \right] \quad (7.13)$$

based on heavy quark effective theory (HQET) [250], where  $v^\mu = p^\mu/m_V$  denotes the 4-velocity of the quarkonium state and  $\varepsilon^\mu$  is its polarisation vector. This identity also serves to define the decay constant  $f_V$ . The  $\mathcal{O}(\alpha_s^0)$  part of our result agrees with [249].

Many experimental results are quoted as a ratio with the SM decay width to electrons, which is given by

$$\Gamma(V \rightarrow e^+ e^-) = \frac{\alpha^2 \pi Q_q^2 f_V^2}{3 m_V} \left[ 1 - \frac{\alpha_s(\mu_q)}{3\pi} \right]. \quad (7.14)$$

Searches have been done in the dimuon final state for radiative  $J/\psi$  decays [251], and in the invisible [252], dimuon [253], ditau [254] and hadronic [255] final states for radiative  $\Upsilon$  decays. The experimental results are collected in tables AII.6, AII.7, and AII.8.

#### 7.1.4 The chromomagnetic dipole moment of the top-quark

The chromomagnetic moment of the top-quark  $\hat{\mu}_t$  is the QCD equivalent to the anomalous magnetic moment ( $g-2$ ) of the leptons. It is defined as the coefficient of the operator [256]

$$\mathcal{L} \supset -\hat{\mu}_t \frac{g_s}{2m_t} \bar{t} \sigma^{\mu\nu} T^a t G_{\mu\nu}^a, \quad (7.15)$$

and was measured by the CMS collaboration to be in the range [257]

$$-0.014 \leq \text{Re}(\hat{\mu}_t) < 0.004. \quad (7.16)$$

Thus, it is in agreement with the assumption of a vanishing chromomagnetic moment. An ALP with couplings to top-quarks (and optionally gluons) generates a contribution via the diagrams shown in figure 7.2 that reads

$$\hat{\mu}_t = \frac{m_t^2}{f^2} \frac{1}{32\pi^2} \left\{ c_{tt}^2 h_1(x_t) + \frac{2\alpha_s}{\pi} c_{tt} c_{GG} \left[ \log \frac{\Lambda^2}{m_t^2} - h_2(x_t) \right] - \frac{25\alpha_s^3}{16\pi^3} c_{GG}^2 \log^2 \frac{\Lambda^2}{m_t^2} \right\}, \quad (7.17)$$

where  $x_t = m_a^2/m_t^2$ . The last term in this equation is found via the RGEs for dimension six operators in the presence of an ALP, see [168]. The explicit functional dependence of the loop functions  $h_{1,2}(x)$  will be given later in section 7.2, but in the limit  $m_a^2/m_t^2 = x \ll 1$ , they satisfy  $h_{1,2}(x) \rightarrow 1$ . The opposite limit of a very heavy ALP, i.e.  $m_a^2/m_t^2 \gg 1$  was studied in [258].

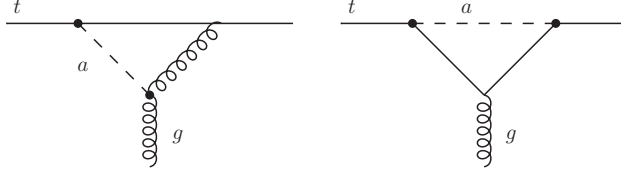


Figure 7.2: Feynman diagrams contributing to the chromomagnetic moment of the top-quark  $\hat{\mu}_t$ . Note that there is a mirrored version of the first diagram, too.

### 7.1.5 Flavour physics constraints on select benchmark scenarios

The phenomenology of ALPs, and with that the constraints we can derive from flavour physics experiments, depends strongly on the UV couplings. In this section we present four benchmark scenarios, where we assume that only one UV coupling of the ALP to a certain type of SM particles is non-vanishing. Those couplings we take to be the coupling to gluons  $c_{GG}$ , to weak  $SU(2)_L$  gauge bosons  $c_{WW}$ , to the left-handed quark doublet  $c_Q$ , and to the left-handed lepton doublet  $c_L$ . All other couplings are then consequently generated through evolution effects according to chapter 6. Especially flavour-changing couplings arise already at tree-level in the effective theory [259]. As shown in table 7.1, these are then highly constrained. From the theory perspective, ALP models with only couplings to gluons are for example the classical KSVZ-type models of QCD axions. In DSFZ-type models, often an additional coupling to fermions is present. The benchmarks for couplings to  $B$ -bosons and the right-handed quark and lepton singlets have been published in [7].

In figure 7.3, we show how the branching ratio of an ALP changes with different UV couplings present. If the ALP only couples to weak gauge bosons, it will mainly decay into a pair of photons for all ALP masses. This is not surprising, because in the low-energy EFT, essentially  $c_{\gamma\gamma} = c_{WW}$  for this case. Similarly, the ALP primarily decays into photons when only a coupling to gluons is present at the high scale. However, when the kinematic possibility to decay into hadrons and quarkonium states is given, the gluon coupling ensures that these instead are the most dominant decay channels. The situation is completely different for couplings to fermions. The ALP decays only into photons in these cases, when there are no other kinematically allowed channels. For quark couplings, it decays into pairs of charged leptons when the respective channel opens up, but as in the gluon coupling case, a very heavy ALP decays into hadrons and mesons. For a UV coupling to leptons, apart from the lightest masses, an ALP predominantly decays into the heaviest charged lepton pair that is lighter than the ALP. Note that for all our scenarios we take a fairly low UV scale of  $\Lambda = 4\pi f = 4\pi \text{TeV}$ . However, we have showed in [5] that changing the scale to  $\Lambda = 10^{12} \text{TeV}$  changes the numerical values for the effective low-energy ALP couplings by less than one order of magnitude. This implies that the derived bounds only depend weakly on the exact UV scale, and hence the exclusion plots presented below are valid for various UV completions to a good approximation.

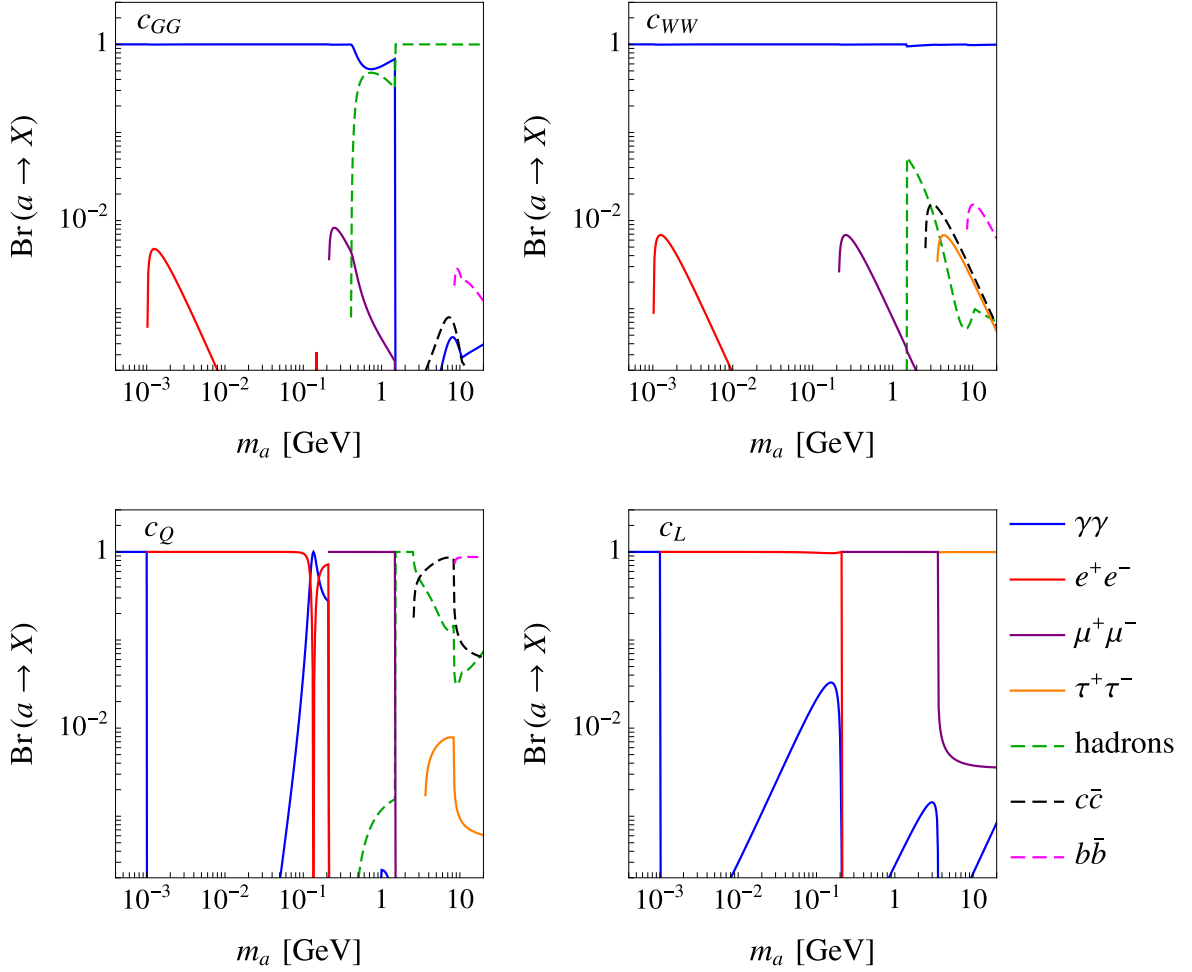


Figure 7.3: Branching ratios of ALPs for our four benchmark scenarios, where the ALP couples only to gluons (top left),  $W$ -bosons (top right), the left-handed quark doublet (bottom left), or the left-handed lepton doublet (bottom right) in the UV. Photon and charged lepton final states are given by solid lines, hadronic final states are indicated with dashed lines.

**CONSTRAINTS ON COUPLINGS TO GLUONS** In the first scenario, only the coupling  $c_{GG}$  is non-zero at the UV scale. The combined constraints are presented in figure 7.4. As shown in figure 7.3, an ALP with such couplings will mainly decay into hadrons for masses above the QCD scale, and to photons below  $m_a < \Lambda_{\text{QCD}}$ . The branching ratio into leptons is subdominant,  $\text{Br}(a \rightarrow \ell^+\ell^-) < 1\%$ . As a result, a light ALP is more likely to decay into photons or escape detection. This follows from the simple estimate of the lifetime as  $\tau_a \propto 1/(c_{GG}^2 m_a^3)$ , which typically exceeds the size of detectors  $\ell_{\text{det}} \approx 10$  m for  $m_a \approx 0.05 c_{GG}^{3/2} \text{GeV}$ .

Consequently, strongest constraints for masses  $m_a < m_\pi$  arise from bounds on  $\text{Br}(K^+ \rightarrow \pi^+ X)$  from NA62, with  $X$  either decaying invisibly or outside of the detector [260]. They are shown in pink. Bounds from the similar decay  $K_L \rightarrow \pi^0 a$  are significantly weaker since the CP conserving part of the amplitude is suppressed by a factor of  $\epsilon \approx 2.3 \times 10^{-3}$ . The reach of the KOTO experiment [261] looking for that decay is coloured in yellow. Other searches for invisible final states lead to weaker constraints, and we show the excluded

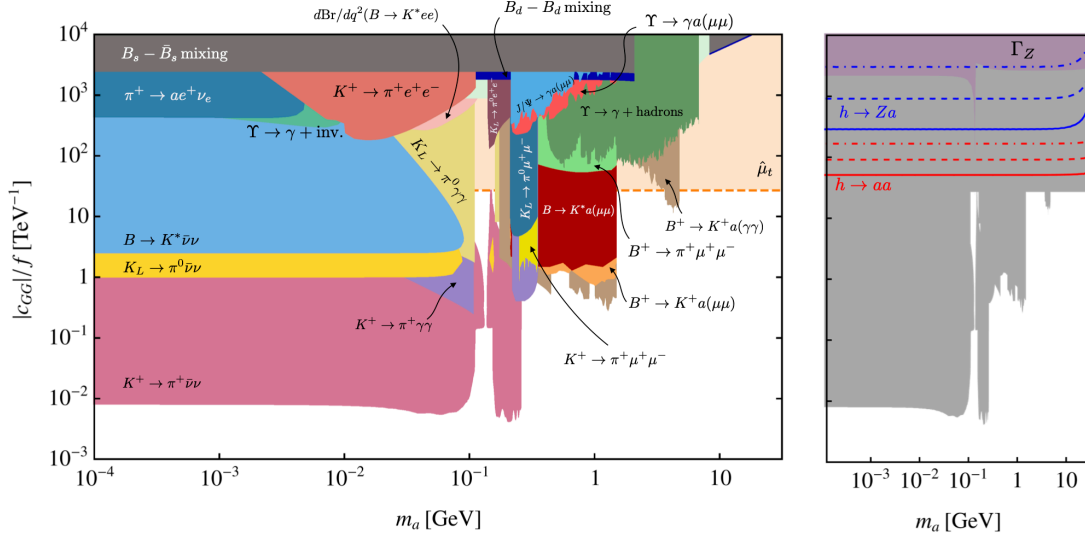


Figure 7.4: Left: Flavour bounds on ALP couplings to gluons with all other Wilson coefficients set to zero at  $\Lambda = 4\pi f$  and  $f = 1$  TeV. Right: Comparison of the same flavour constraints (light grey) with the constraints on  $Z \rightarrow a\gamma$  decays from the LEP measurement of the  $Z$  boson width (violet), contours of constant  $\text{Br}(h \rightarrow aa) = 10^{-1}, 10^{-2}$  and  $10^{-3}$ , depicted as red dotted, dashed and solid lines, and contours of constant  $\text{Br}(h \rightarrow Za) = 10^{-1}, 10^{-2}$  and  $10^{-3}$ , shown as blue dotted, dashed and solid lines, respectively.

parameter space by the measurements of  $B \rightarrow K^* \nu \bar{\nu}$  from Belle [262] in light blue, and  $\pi^+ \rightarrow ae^+ \nu_e$  from the PIENU collaboration in dark blue [242]. For larger ALP masses, decays into photons become relevant and constraints from searches for  $K^+ \rightarrow \pi^+ \gamma \gamma$  and  $K^0 \rightarrow \pi^0 \gamma \gamma$  performed at E949, NA48, NA62 and KTeV exclude the parameter space for larger values of  $c_{GG}/f$  [263–266]. The corresponding parameter space is shown in purple and yellow. These searches provide important constraints even for  $m_a > 2m_e$  when decays to electrons are allowed, because of the dominant ALP branching ratio  $\text{Br}(a \rightarrow \gamma \gamma) > 99\%$  at  $m_a < 3m_\pi$ .

Leptonic final states give much weaker constraints on the ALP parameter space. Yet, LHCb searches for  $B$  decays into kaons with muon final states give the largest bounds onto ALPs with masses  $m_\pi < m_a < m_B$  [267, 268]. Parameter region excluded is shown in red and orange. Pions in the final state reduce the limiting power, and searches have been performed by LHCb in [269] and are shaded green in figure 7.4. For ALPs heavier than the  $B$  mesons, most stringent constraints come from flavour-conserving processes of  $\Upsilon$  decays into a photon and an ALP, followed by a subsequent decay of the ALP into hadrons. This was measured by BaBar [255], and we show the implications in dark green.

Non-resonant ALP contributions to  $B_s - \bar{B}_s$  mixing and  $B_s \rightarrow \mu + \mu^-$  decay lead to very weak constraints. The reason is that with only  $c_{GG}$  present at the UV scale, the induced flavour-changing coupling and the coupling to leptons is rather small. Furthermore, the meson mixing process requires two insertions of flavour change. ALPs that are heavier than the  $\Upsilon$  meson are best constrained by measurements of the chromomagnetic moment of the top-quark, leading to a universal bound of  $c_{GG}/f \gtrsim 30 \text{ TeV}^{-1}$ . Note that this constraint takes the assumption that the ALP only affects the chromomagnetic moment, but has

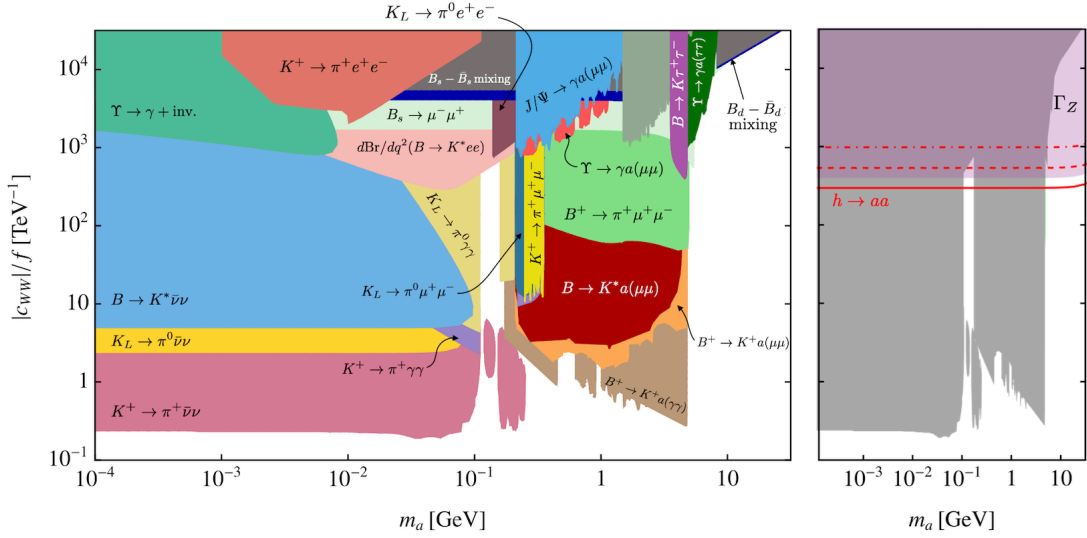


Figure 7.5: Left: Flavour bounds on ALP couplings to  $SU(2)_L$  gauge bosons with all other Wilson coefficients set to zero at  $\Lambda = 4\pi f$  and  $f = 1$  TeV. Right: Comparison of the same flavour constraints (light grey) with the constraints on  $Z \rightarrow a\gamma$  decays from the LEP measurement of the  $Z$  boson width (violet) and contours of constant  $\text{Br}(h \rightarrow aa) = 10^{-1}$ ,  $10^{-2}$  and  $10^{-3}$  depicted as red dotted, dashed and solid lines.

no effect on the underlying  $pp \rightarrow t\bar{t}$  process, otherwise. We consider this approximation appropriate for heavy ALPs, but give the bound as a dashed line to indicate this caveat.

On the right-hand side of figure 7.4, we show how the obtained constraints from flavour physics compare to other bounds from colliders, namely the searches for the Higgs boson decays  $h \rightarrow Za$  and  $h \rightarrow aa$  at the LHC, as well as electroweak precision measurements on the  $Z$  pole from LEP. Excluding the top-chromomagnetic moment constraint, we see that collider searches become relevant for very heavy ALPs. For ALPs in the MeV to GeV mass region, flavour constraints are indeed highly complementary and can reach parameter regions unprobed by colliders. A comparison of the reach of flavour experiments with beam dump and astrophysical searches is difficult, because a gluon coupling necessarily induces a strong ALP–nucleon coupling as well. Henceforth, bounds that rely on the fact that the coupling to photons is the dominant one cannot be directly reliably transferred to bounds on  $c_{GG}$ . An extensive investigation studying limits from astrophysics observables where both the induced photon couplings and a coupling to nucleons is taken into account would thus be highly appreciated.

**CONSTRAINTS ON COUPLINGS TO WEAK GAUGE BOSONS** As in the case with gluon couplings, a coupling to weak gauge bosons results in an ALP decaying into photons with  $\text{Br}(a \rightarrow \gamma\gamma) \approx 100\%$  for all ALP masses. The loop-induced fermion couplings are considerably smaller, and so the ALP is most likely to be long-lived and decay outside of the detector in searches for fermionic final states.

We show the combined exclusion plot for a UV  $c_{WW}$  coupling in figure 7.5. The overall shape of the excluded patches changes only little when compared to the ones when a gluon



coupling is present. Here, we elaborate on the differences. For a high-energy coupling to weak bosons, constraints from the pion decay  $\pi^+ \rightarrow e^+ a \nu_e$  are very weak, since  $c_{WW}$  enters the amplitude only via RG effects. More significant differences lie in the mass region  $m_a > m_K$ . Here, bounds from  $B$  meson decays with leptonic final states are of higher relative importance compared to the gluon exclusion plot. The reason is that the lepton coupling is already induced at the one-loop level when  $W$ -boson couplings are present. Our estimate for searches for  $B^+ \rightarrow K^+ \pi^0 \rightarrow K^+ \gamma \gamma$  at Belle [270] and BaBar [271] results in a constraint  $c_{WW}/f \lesssim 6/\text{TeV}$ . Currently, there is no published search for the decay  $B \rightarrow K^{(*)} \gamma \gamma$ , which would be sensitive to an ALP decaying into photons and could provide an important constraint that would probe the unconstrained parameter space for the mass range  $m_K < m_a < m_B$ . We expect that a dedicated search for resonances in this channel could yield much better sensitivity than this estimate, in particular for ALP masses larger than the pion mass.

ALPs with stronger couplings are also constrained by the measurement of  $B_s \rightarrow \mu^+ \mu^-$ . Radiative  $\Upsilon \rightarrow \gamma \mu^+ \mu^-$ ,  $\Upsilon \rightarrow \gamma \tau^+ \tau^-$  and  $J/\Psi \rightarrow \gamma \mu^+ \mu^-$  decays yield constraints for  $m_a > 2m_\mu$  and  $m_a > 2m_\tau$  respectively, which are of similar strength to the constraint from  $B_s \rightarrow \mu^+ \mu^-$  [251, 254]. Even weaker limits arise from the virtual exchange of ALP in  $B$ -meson mixing, which is suppressed by two flavour-changing vertices.

As before, we compare the derived bounds with those obtained from collider searches. We find that searches for the Higgs boson decay  $h \rightarrow aa$  yields the best limit in the case that the ALP is heavier than the  $B$  mesons. Note also, that the chromomagnetic moment of the top is too weakly constrained to derive meaningful constraints on ALP- $W$ -boson couplings.

In figure 7.6 we compare astrophysical and beam dump bounds on the effective coupling  $c_{\gamma\gamma}^{\text{eff}} = c_{WW}$  to the ones obtained from flavour experiments. They stem from helioscopes CAST [272] and SUMICO [273, 274], cosmological and astrophysical observables [275–281], the supernova SN1987a observation [282–284], collider experiments [196, 252, 285–293] and the beam dump searches in [294–297]. For light ALPs and very small couplings, bounds from astrophysical observables are much stronger than flavour constraints, and for ALPs with masses  $m_a \gtrsim 10 \text{ GeV}$  collider observables are more sensitive. For the case of an ALP with a  $c_{WW}$  coupling, flavour observables, in particular  $B$  meson decays, constrain precisely the ALP masses and couplings in the “gap” for which astrophysical observables and colliders lose sensitivity, because the ALP is too short-lived to be detected in beam-dumps and too light and weakly coupled to be produced and efficiently reconstructed at colliders. This comparison motivates a dedicated search for  $B \rightarrow Ka$  with subsequent  $a \rightarrow \gamma\gamma$  decays, which could provide the most sensitive probe of ALPs in the parameter space unconstrained by either astrophysical, beam dump or collider constraints.

**CONSTRAINTS ON COUPLINGS TO THE QUARK DOUBLET** Universal ALP couplings to quark doublets,  $c_Q(\Lambda) = k_U(\Lambda) = k_D(\Lambda) = c_Q \mathbb{1}$ , lead to ALP decays into charged leptons and hadrons once the respective decay channel is kinematically allowed. We collect bounds from flavour physics on a UV ALP coupling  $c_Q$  in figure 7.7



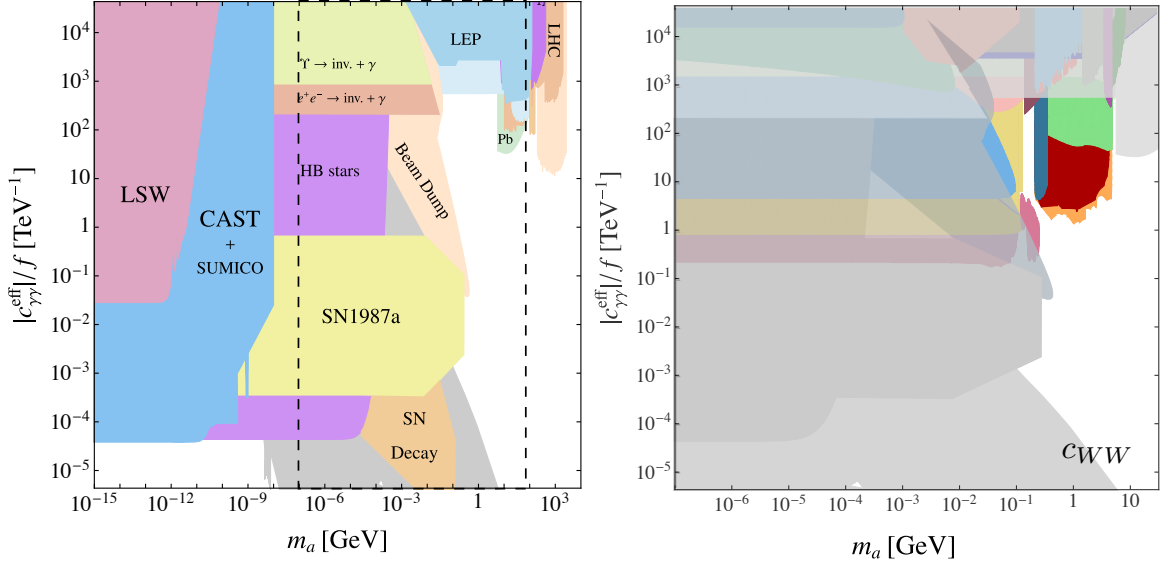


Figure 7.6: Left: Bounds on ALP couplings to photons [196]. The dashed contours indicate the part of the plot shown in various shades of grey in the right panel. Right: In colour, we show flavour bounds on ALPs coupling only to  $SU(2)_L$  gauge bosons (same as in figure 7.5 above). They are compared to the grey astrophysical, beam dump and collider constraints on ALP couplings to photons with  $c_{\gamma\gamma}^{\text{eff}} = c_{WW}$

In this scenario, any isospin violating effect is a consequence of running and matching from  $\Lambda$  to the scale of the measurement. The ALP coupling to photons, when induced by isospin conserving ALP couplings such as  $c_Q$ , is proportional to the isospin breaking term  $(m_d - m_u)/(m_u + m_d) \approx 0.35$  and therefore suppressed compared to a scenario where the ALP has isospin breaking couplings, as in the case for couplings to right-handed quark singlets. The decay width  $\Gamma(a \rightarrow \gamma\gamma)$  is thus suppressed, the ALP branching ratios into leptons are larger and the corresponding constraints from, e.g.,  $K_L \rightarrow \pi^0 e^+ e^-$  are slightly stronger compared to scenarios in which the ALP has isospin breaking couplings in the UV. Since  $c_Q$  couples the ALP to both left-handed up-type and down-type quarks in the UV, constraints from  $J/\Psi$  and  $\Upsilon$  decays are comparable to the  $c_u$  and  $c_d$  scenarios presented in [7].

**CONSTRAINTS ON COUPLINGS TO THE LEPTON DOUBLET** Constraints on ALPs with universal couplings to the lepton doublets are shown in figure 7.8. For this scenario, we set  $c_L = c_L \mathbb{1}$ , with couplings to all other SM fields set to zero at the scale  $\Lambda = 4\pi f$  with  $f = 1$  TeV. Here, the ALP dominantly decay into leptons if kinematically allowed, or into photons if  $m_a < 2m_e$ , as shown in the bottom right panel of figure 7.3. Hadronic ALP decay modes are irrelevant, because ALP couplings to quarks are suppressed by at least two loops. Consequently, only observables searching for invisible, photon, or lepton final states are sensitive to leptonic ALP couplings. ALPs with couplings to lepton doublets induce quark flavour-changing amplitudes at the two-loop level. Due to the normalisation of the ALP gauge boson couplings, this leads to constraints on  $|c_L|/f$  similar in strength to the constraints on  $|c_{WW}|/f$  in figure 7.5. The combined constraints allow values of

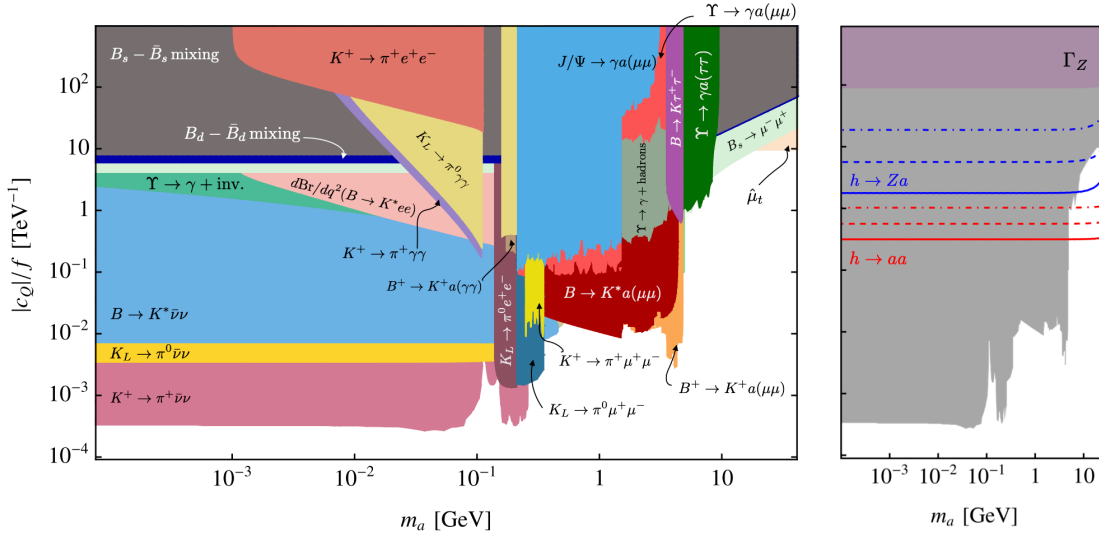


Figure 7.7: Left: Flavour bounds on universal ALP couplings to quark doublets with  $c_Q = c_Q \mathbb{1}$ , and all other Wilson coefficients set to zero at the scale  $\Lambda = 4\pi f$  and  $f = 1$  TeV. Right: Constraints from flavour observables (light grey) are compared to the constraint from  $Z \rightarrow a\gamma$  decays from the LEP measurement of the  $Z$  boson width. Contours of constant  $\text{Br}(h \rightarrow aa) = 10^{-1}, 10^{-2}$  and  $10^{-3}$  are depicted as red dotted, dashed and solid lines, respectively. Contours of constant  $\text{Br}(h \rightarrow Za) = 10^{-1}, 10^{-2}$  and  $10^{-3}$  are shown as blue dotted, dashed and solid lines, respectively.

$|c_L|/f, |c_e|/f < 0.01 \text{ TeV}^{-1}$  for all ALP masses. Exotic Higgs decays are only weakly sensitive to ALP couplings to lepton doublets. The measurement of the  $Z$  decay width does not provide a strong bound, because of the suppressed lepton coupling to  $Z$  bosons.

Finally, we compare the constraints from flavour observables with the constraints from cosmological observables, collider and beam dump searches for ALPs that couple to leptons in figure 7.9. The constraints in the left panel are: Searches by the Edelweiss and Edelweiss III collaborations (dark and light purple respectively) [298, 299] for ALPs produced in the Sun; observations of red giants (red) [277]; searches by the neutrinoless double-beta decay experiment GERDA [300]; searches by dark matter direct detection experiment XMASS (red-brown) [301]<sup>2</sup>; beam dump searches at KEK, SLAC and Fermilab in orange [303], lighter blue, light green [304] and red [294, 305]; SN1987A supernova bounds (dark blue) [306] and a dark photon search at BaBar (green) [307]. Note that the light green beam dump constraint assumes the presence of ALP–muon and ALP–electron couplings while the BaBar bound applies only to ALP–muon couplings. All other constraints have been derived for the ALP–electron coupling. The ALP–tau coupling still remains unconstrained. In this section we assume  $c_{ee} = c_{\mu\mu} = c_{\tau\tau}$  and show the combined experimental constraints in the left panel of figure 7.9. For comparison these constraints are then overlaid with the flavour bounds on ALPs coupling only to  $SU(2)_L$  lepton doublets (as in figure 7.8 above). It can be seen that flavour constraints can provide competitive and complementary constraints on ALP couplings to leptons in the MeV–GeV mass range. Astrophysical constraints dominate at smaller values of  $m_a$ .

<sup>2</sup> Note that this parameter space is also constrained by  $\Delta N_{\text{eff}}$  for ALPs lighter than  $m_a < m_\mu$  [302].

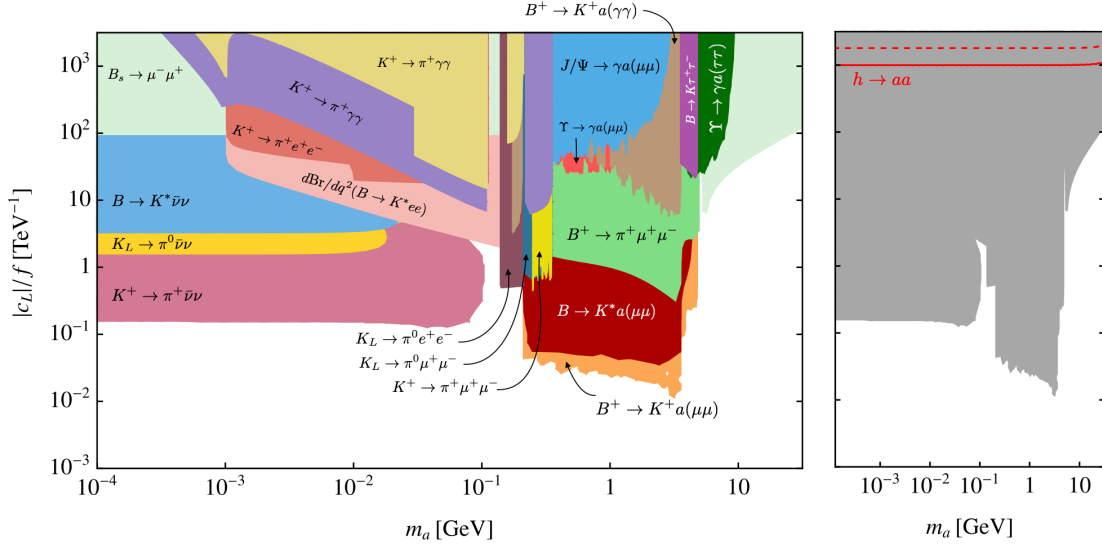


Figure 7.8: Left: Flavour bounds on universal ALP couplings to lepton doublets with  $c_L = c_L \mathbb{1}$ , and all other Wilson coefficients zero at the scale  $\Lambda = 4\pi f$  and  $f = 1$  TeV. Right: Contours of constant  $\text{Br}(h \rightarrow aa) = 10^{-1}, 10^{-2}$  and  $10^{-3}$  are depicted as red dotted, dashed and solid lines, respectively. Contours of constant  $\text{Br}(h \rightarrow Za) = 10^{-1}$  and  $10^{-2}$  are shown as blue dashed and solid lines, respectively.

## 7.2 Lepton flavour probes of ALPs

In contrast to quarks, the numbers of the individual families of leptons are conserved in the SM. Therefore evolution and matching effects will not generate couplings with lepton flavour violation (LFV). However, flavour-change in the uncharged lepton sector has been observed by the discovery of neutrino oscillations. Even when we take these into account, we may still neglect their effects on ALP–lepton couplings, because loops featuring neutrinos are suppressed by factors of  $\Delta m_\nu^2/m_W^2 \approx 10^{-4} \text{ eV}^2/(80 \text{ GeV})^2 \approx 10^{-26}$  [18]. We will therefore assume that additionally to a diagonal coupling to leptons  $c_{\ell\ell}$  a flavour-changing coupling  $c_{ij}$ ,  $i \neq j$ ,  $i, j \in [e, \mu, \tau]$  is present already at the UV scale.

This part of the thesis has already been published in a similar way in [4,7]. Since some computations have been part of the author’s Master thesis, we will just mention the most relevant results from there, and elaborate more on the work that has been added afterwards. For other studies of lepton flavour-changing couplings of ALPs, see [4,226,308–318].

### 7.2.1 Form factors

If the ALP has LFV couplings at tree-level, it follows from eq. (6.31) that these couplings are suppressed by the charged lepton masses. Given the large hierarchy in charged lepton masses, loop-induced contributions to leptonic observables can hence be important if the lepton in the loop is heavier than the external leptons. In lepton flavour-changing decay observables such as  $\mu \rightarrow e\gamma$ ,  $\mu \rightarrow 3e$  or similar tau decays, ALP contributions to electromagnetic form factors may therefore dominate over tree-level ALP-exchange contributions to

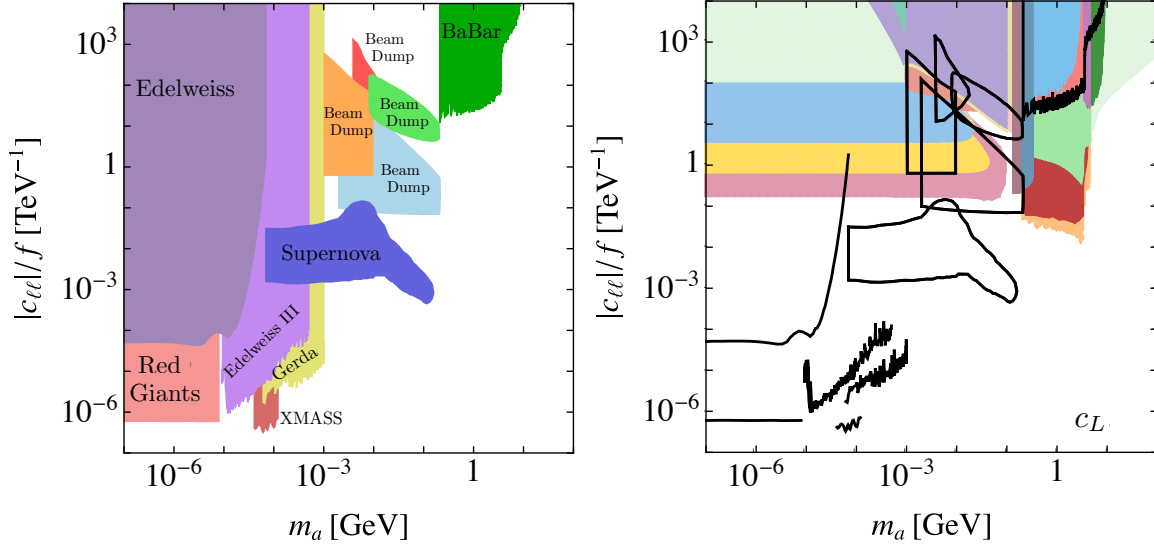


Figure 7.9: Left: Astrophysical, beam dump, and collider constraints on ALP couplings to leptons  $c_{\ell\ell} = c_e - c_L$  (see text for further details). Right: In colour, we show flavour constraints on ALPs coupling to  $SU(2)_L$  lepton doublets, as in figure 7.8 above. For easy comparison, the black contours depict the bounds from the left panel.

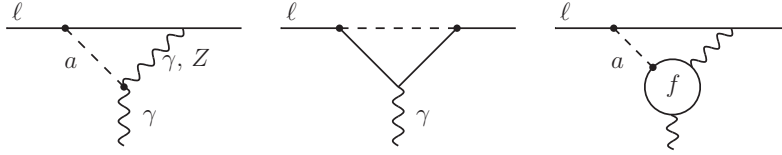


Figure 7.10: Feynman diagrams contributing to LFV electromagnetic form factors. Note that there is a mirrored version of the first diagram, too.

four-fermion operators, for example. Likewise, if an ALP has lepton flavour-violating couplings, it can induce additional mass-enhanced loop contributions to flavour-conserving observables such as anomalous magnetic moments.

Below, we calculate the ALP contributions to the electromagnetic form factors induced by the diagrams shown in figure 7.10. The expressions below cover the general case in which the external leptons may be different from each other as well as from the lepton in the loop. We further give analytical expressions for the corresponding loop functions, in various limits motivated by the phenomenological applications discussed in the remainder of this work. For the case of identical leptons in the initial and final state, we additionally provide a calculation of the two-loop form factor.

If the initial and final state lepton are of different flavour, the ALP-generated contribution to the interaction between the two leptons and a photon is defined such that the matrix element  $\mathcal{M}^\mu \epsilon_\mu(-q)$  for the interaction between leptons and a photon is found by

$$\mathcal{M}^\mu = \bar{u}_j(p_2) \Gamma^\mu u_i(p_1), \quad (7.18)$$

which can be parametrised in terms of form factors  $F_2^{(5),i \rightarrow j}(q^2)$  and  $F_3^{(5),i \rightarrow j}(q^2)$  as follows, where  $p = p_1 + p_2$ , and  $q = p_1 - p_2$  is the *outgoing* photon momentum,

$$\begin{aligned} \bar{\ell}_j(p_2) \Gamma^\mu(p_1, p_2) \ell_i(p_1) = \\ \bar{\ell}_j(p_2) \left[ F_2^{i \rightarrow j}(q^2) (p^\mu - (m_i + m_j) \gamma^\mu) + F_3^{i \rightarrow j}(q^2) \left( q^\mu - \frac{q^2}{m_i - m_j} \gamma^\mu \right) \right. \\ \left. + F_2^{5, i \rightarrow j}(q^2) (p^\mu + (m_i - m_j) \gamma^\mu) \gamma_5 + F_3^{5, i \rightarrow j}(q^2) \left( q^\mu + \frac{q^2}{m_i + m_j} \gamma^\mu \right) \gamma_5 \right] \ell_i(p_1). \end{aligned} \quad (7.19)$$

Here, we used the Ward identities to get rid of the two additional, linearly dependent form factors  $F_1^{(5)}(q^2)$ .

**ONE FLAVOUR-CHANGING COUPLING** If only one flavour-changing coupling is present, the form factor receives contributions from the first two types of diagrams in figure 7.10, where in the centre one either one of the two ALP interactions is flavour-conserving. Denoting the initial state lepton with  $\ell_i$ , the final state lepton with  $\ell_j$ , assuming  $m_i > m_j$  and expanding to leading order in  $m_j/m_i$ , we find

$$\begin{aligned} F_2^{i \rightarrow j}(q^2) = -\frac{m_i e Q_i}{16\pi^2 f^2} \left( [k_E]_{ij} - [k_e]_{ij} \right) \left( \frac{\alpha}{4\pi} c_{\gamma\gamma} g_2(q^2, m_i, m_a) + \frac{1}{4} c_{ii} g_1(q^2, m_i, m_a) \right. \\ \left. + \frac{\alpha}{4\pi} \frac{(4s_w^2 - 1)}{2(s_w c_w)^2} c_{\gamma Z} \left( \log \frac{\Lambda^2}{m_Z^2} + \frac{3}{2} + \delta_2 \right) \right), \end{aligned} \quad (7.20)$$

$$\begin{aligned} F_2^{5, i \rightarrow j}(q^2) = -\frac{m_i e Q_i}{16\pi^2 f^2} \left( [k_E]_{ij} + [k_e]_{ij} \right) \left( \frac{\alpha}{4\pi} c_{\gamma\gamma} g_2(q^2, m_i, m_a) + \frac{1}{4} c_{ii} g_1(q^2, m_i, m_a) \right. \\ \left. + \frac{\alpha}{4\pi} \frac{(4s_w^2 - 1)}{2(s_w c_w)^2} c_{\gamma Z} \left( \log \frac{\Lambda^2}{m_Z^2} + \frac{3}{2} + \delta_2 \right) \right), \end{aligned} \quad (7.21)$$

$$F_3^{i \rightarrow j}(q^2) = -\frac{m_i e Q_i}{16\pi^2 f^2} \left( [k_E]_{ij} - [k_e]_{ij} \right) \left( \frac{\alpha}{4\pi} c_{\gamma\gamma} l_2(q^2, m_i, m_a) + \frac{1}{4} c_{ii} l_1(q^2, m_i, m_a) \right), \quad (7.22)$$

$$F_3^{5, i \rightarrow j}(q^2) = -\frac{m_i e Q_i}{16\pi^2 f^2} \left( [k_E]_{ij} + [k_e]_{ij} \right) \left( \frac{\alpha}{4\pi} c_{\gamma\gamma} l_2(q^2, m_i, m_a) + \frac{1}{4} c_{ii} l_1(q^2, m_i, m_a) \right), \quad (7.23)$$

where the loop functions are given in terms of Feynman integrals in appendix AII.2. For an on-shell photon, as in the case of  $\mu \rightarrow e\gamma$ , the loop functions simplify to

$$g_1(0, m_i, m_a) = 2x_i^{3/2} \sqrt{4 - x_i} \arccos \frac{\sqrt{x_i}}{2} + 1 - 2x_i + \frac{x_i^2(3 - x_i)}{1 - x_i} \log x_i, \quad (7.24)$$

$$g_2(0, m_i, m_a) = 2 \log \frac{\Lambda^2}{m_i^2} + 2\delta_2 + 4 - \frac{x_i^2 \log x_i}{x_i - 1} + (x_i - 1) \log(x_i - 1), \quad (7.25)$$

where we have set the scale  $\mu = \Lambda = 4\pi f$  and  $x_i = m_a^2/m_i^2$ . The scheme dependent constant  $\delta_2$  arises from the treatment of the Levi-Civita symbol in  $d$  dimensions, and for us  $\delta_2 = -3$ . The functions  $l_1$ ,  $g_1$  and  $l_2$  all tend to zero as  $m_a^2/m_i^2 \rightarrow \infty$ , while  $l_2(0, m_i, 0) = 1$  and  $g_1(0, m_i, 0) = 1$ .

**TWO FLAVOUR-CHANGING COUPLINGS** Although generically it is expected that flavour-changing couplings should be suppressed relative to flavour-conserving ones, it

is possible that diagrams containing two flavour-changing couplings may be enhanced by a heavier mass (relative to diagrams with only one flavour-changing coupling) and should therefore be considered. This occurs if the mass of the fermion in the loop is much larger than that of either of the external fermions, for example  $\mu \rightarrow e\gamma$  via an internal  $\tau$ . In this case, the form factor is calculated from the centre diagram in figure 7.10 with  $\ell_k \neq \ell_i \neq \ell_j$ .

Assuming  $m_k > m_i > m_j$  (where  $k$  is the flavour index of the lepton in the loop) and keeping only the leading order contribution in an expansion in  $m_i/m_k$ , the ALP contribution to the electromagnetic form factors is given by

$$F_2^{i \rightarrow j}(q^2) = \frac{m_k e Q_k}{32\pi^2 f^2} \left( [k_e]_{ik} [k_E]_{kj} + [k_E]_{ik} [k_e]_{kj} \right) g_3(q^2, m_k, m_a), \quad (7.26)$$

$$F_2^{5, i \rightarrow j}(q^2) = \frac{m_k e Q_k}{32\pi^2 f^2} \left( [k_e]_{ik} [k_E]_{kj} - [k_E]_{ik} [k_e]_{kj} \right) g_3(q^2, m_k, m_a), \quad (7.27)$$

with

$$g_3(q^2, m_k, m_a) = \frac{1 - 3x_k}{2(x_k - 1)^2} + \frac{x_k^2}{(x_k - 1)^3} \log x_k, \quad (7.28)$$

where  $x_k = m_a^2/m_k^2$ . No terms involving  $q^2$  appear in this function, because  $q^2 \leq m_i^2$ , so these terms are suppressed by a factor proportional to  $q^2/m_k^2 \leq m_i^2/m_k^2$ , and have been dropped, along with terms dependent on  $m_i^2$ . The  $F_3^{(5), i \rightarrow j}(q^2)$  form factors are suppressed by a factor  $\sim m_i^2/m_k^2$  relative to the  $F_2^{(5), i \rightarrow j}(q^2)$  form factors, so we do not quote them here.

**ALP CONTRIBUTIONS TO FLAVOUR-CONSERVING PROCESSES** In principle, the ALP can give rise to electromagnetic dipole moments like the anomalous magnetic moment or electric dipole moment (EDM) of the leptons via all diagrams in figure 7.10. Both flavour-conserving and violating couplings then contribute. Since a thorough discussion of ALP contributions to these dipole moments is beyond the scope of this thesis, we limit ourselves to presenting the expressions for the form factors.

The gauge invariant form factor decomposition of the amplitude is given by

$$\begin{aligned} \bar{\ell}_i(p_2) \Gamma^\mu(p_1, p_2) \ell_i(p_1) = & \bar{\ell}_j(p_2) \left[ F_2^{i \rightarrow i}(q^2) (p^\mu - 2m_i \gamma^\mu) + 2m_i F_3^{i \rightarrow i}(q^2) \gamma^\mu \right. \\ & \left. + F_2^{5, i \rightarrow i}(q^2) p^\mu \gamma_5 + F_3^{5, i \rightarrow i}(q^2) \left( q^\mu + \frac{q^2}{2m_i} \gamma^\mu \right) \gamma_5 \right] \ell_i(p_1). \end{aligned} \quad (7.29)$$

Only the form factor  $F_2$  contributes to the anomalous magnetic moment, and only  $F_2^5$  gives a contribution to the EDM. If only flavour-conserving ALP couplings are present, the form factor  $F_2^5$  vanishes, and  $F_2$  reads

$$\begin{aligned} F_2^{i \rightarrow i}(0) = & \frac{e Q_i m_i}{32\pi^2 f^2} \left\{ c_{ii}^2 h_1(x_i) - \frac{2\alpha}{\pi} c_{ii} \left[ \tilde{c}_{\gamma\gamma} \left( \log \frac{\mu^2}{m_i^2} - h_2(x_i) \right) + \sum_f N_c^f Q_f^2 c_{ff} \int_0^1 dz F(y_z, x_f) \right] \right. \\ & \left. - \frac{\alpha}{2\pi} \frac{1 - 4s_w^2}{s_w c_w} c_{ii} c_{\gamma Z} \left( \log \frac{\mu^2}{m_Z^2} + \delta_2 + \frac{3}{2} \right) \right\} \end{aligned} \quad (7.30)$$

where

$$h_1(x) = 1 + 2x + (1-x)x \log x - 2x(3-x) \sqrt{\frac{x}{4-x}} \arccos \frac{\sqrt{x}}{2}, \quad (7.31)$$

$$h_2(x) = 1 - \frac{x}{3} + x^2 \log x + \frac{x+2}{3} \sqrt{(4-x)x} \arccos \frac{\sqrt{x}}{2} - \delta_2 - 3, \quad (7.32)$$

$$F(y_z, x_f) = \frac{1}{1-y_z} \left[ h_2 \left( \frac{x_f}{y_z} \right) - h_2(x_f) \right]. \quad (7.33)$$

Here we have defined

$$y_z = z(1-z) \frac{m_a^2}{m_f^2}, \quad \tilde{c}_{\gamma\gamma} = c_{\gamma\gamma} + \sum_f N_c^f Q_f^2 c_{ff}. \quad (7.34)$$

In the two limits (a)  $m_a^2 \gg m_\mu^2$  and (b)  $m_f^2 \gg m_a^2, m_\mu^2$ , the integral of  $F(y_z, x_f)$  can be given explicitly

$$\begin{aligned} & \int_0^1 F(y_z, x_f) dz \\ &= \begin{cases} \frac{-4}{\sqrt{x_f(x_f-4)}} \left[ \frac{\pi^2}{12} + \ln^2 \left( \frac{1}{2} (\sqrt{x_f} - \sqrt{x_f-4}) \right) + \text{Li}_2 \left( -\frac{1}{4} (\sqrt{x_f} - \sqrt{x_f-4})^2 \right) \right], & \text{(a)} \\ -\ln \frac{m_f^2}{m_\mu^2} + h_2 \left( \frac{m_a^2}{m_\mu^2} \right) - \frac{7}{2} + \mathcal{O} \left( \frac{m_a^2}{m_f^2}, \frac{m_\mu^2}{m_f^2} \right), & \text{(b)} \end{cases} \end{aligned} \quad (7.35)$$

Our results in these limits agree with the ones presented in [319]<sup>3</sup>.

Flavour-violating ALPs can contribute via the centre diagram of figure 7.10, when the lepton in the loop is of different flavour. The relevant form factors are

$$\begin{aligned} F_2^{i \rightarrow i}(0) &= -\frac{eQ_k m_k}{32\pi^2 f^2} \left\{ \frac{m_i^3}{m_k^3} \left( |[k_E]_{ik}|^2 + |[k_e]_{ik}|^2 \right) \int_0^1 dx \frac{x(1-x)^2}{\Delta_{i \rightarrow i}} \right. \\ &\quad + 2 \text{Re} [[k_E]_{ik}^* [k_e]_{ik}] \int_0^1 dx \frac{(1-x)^2}{\Delta_{i \rightarrow i}} \\ &\quad + 2 \frac{m_i^2}{m_k^2} \text{Re} [[k_E]_{ik}^* [k_e]_{ik}] \int_0^1 dx \frac{(1-x)^2(1-2x)}{\Delta_{i \rightarrow i}} \\ &\quad \left. + \frac{m_i}{m_k} \left( |[k_E]_{ik}|^2 + |[k_e]_{ik}|^2 \right) \int_0^1 dx \frac{(1-x)^2(x-2)}{\Delta_{i \rightarrow i}} \right\}, \end{aligned} \quad (7.36)$$

$$\begin{aligned} F_2^{5, i \rightarrow i}(0) &= -\frac{eQ_k}{16\pi^2 f^2} \left( 1 - \frac{m_i^2}{m_k^2} \right) \left\{ m_i \left( |[k_E]_{ik}|^2 + |[k_e]_{ik}|^2 \right) \right. \\ &\quad \left. + 2im_k \text{Im} [[k_E]_{ik}^* [k_e]_{ik}] \right\} \int_0^1 dx \frac{(1-x)^2}{\Delta_{i \rightarrow i}}, \end{aligned} \quad (7.37)$$

<sup>3</sup> Note that the authors of [319] used dimensional regularisation to perform the two-loop integrals. Therefore they need to add a subtraction term that acts as a counterterm to the occurring divergences. However, this is not needed since all integrals can be evaluated in four dimensions.

where

$$\Delta_{i \rightarrow i} = x \frac{m_a^2}{m_k^2} + x(x-1) \frac{m_i^2}{m_k^2} + (1-x). \quad (7.38)$$

Two interesting limits that are well motivated are the cases where the loop lepton is either much heavier or lighter than the initial and final state ones.

**Limit  $m_k \gg m_i$**  This is the limit where the internal fermion is much heavier than the external fermion, for example in the case of a contribution to the anomalous magnetic moment of the electron via a diagram with an internal muon.

$$F_2^{i \rightarrow i}(0) = -\frac{m_k e Q_k}{32\pi^2 f^2} \text{Re}([k_E]_{ki}^* [k_e]_{ki}) h(x_k) + \mathcal{O}\left(\frac{m_i}{m_k}\right), \quad (7.39)$$

where  $x_k = m_a^2/m_k^2$  and

$$h(x) = \frac{2x^2}{(x-1)^3} \log x - \frac{3x-1}{(x-1)^2}. \quad (7.40)$$

**Limit  $m_k \ll m_i$**  This is the limit where the internal fermion is much lighter than the external fermion, for example in the case of the anomalous magnetic moment of the muon via an internal electron.

$$F_2^{i \rightarrow i}(0) = \frac{m_i e Q_k}{64\pi^2 f^2} \left( |[k_E]_{ki}|^2 + |[k_e]_{ki}|^2 \right) j(x_i) + \mathcal{O}\left(\frac{m_k}{m_i}\right), \quad (7.41)$$

where  $x_i = m_a^2/m_i^2$  and

$$j(x) = 1 + 2x - 2x^2 \log \frac{x}{x-1}. \quad (7.42)$$

## 7.2.2 The decay $\mu \rightarrow ea\gamma$

The decay  $\mu \rightarrow ea\gamma$  can be seen as a  $\mu \rightarrow ea$  decay with additional initial or final state radiation. The process  $\mu \rightarrow ea$  itself can give rise to very meaningful constraints, since in the case that the ALP decays subsequently inside of the detector, it can generate effective  $\mu \rightarrow 3e$ ,  $\mu \rightarrow e\gamma\gamma$  and  $\mu \rightarrow e\gamma^*$  signatures<sup>4</sup>.

The differential decay rate of  $\mu \rightarrow ea\gamma$  is given by

$$d\Gamma(\mu \rightarrow ea\gamma) = \frac{\alpha_{\text{QED}}}{4\pi^2} \frac{1}{32m_\mu} \frac{|[k_E]_{12}|^2 + |[k_e]_{12}|^2}{f^2} \mathcal{F} ds_{12} ds_{23} \quad (7.43)$$

with (in the limit  $m_e^2/m_\mu^2 \rightarrow 0$ )

$$\mathcal{F} = \frac{1}{s_{12}(m_a^2 - s_{12} - s_{23})^2} [m_a^6 - s_{23}^2(s_{12} + s_{23}) - m_a^4(2m_\mu^2 + s_{12} + s_{23}) + 2m_\mu^2(s_{12} + s_{23})(2s_{12} + s_{23}) - 2m_\mu^4(4s_{12} + s_{23}) + m_a^2(2m_\mu^4 + 4m_\mu^2 s_{12} + s_{23}^2)], \quad (7.44)$$

<sup>4</sup>  $\mu \rightarrow e\gamma^*$  is a  $\mu \rightarrow e\gamma\gamma$  decay, where the two photons are so collimated or the ALP decays so close to the detector that it is impossible to resolve the individual photons, and thus they are reconstructed as one instead.



where  $s_{ij} = (p_i + p_j)^2$  and the electron carries momentum  $p_1$ , the photon carries momentum  $p_2$  and the ALP carries momentum  $p_3$ . Up to a prefactor,  $\mathcal{F}$  is the squared matrix element summed over electron spins and photon polarisations and averaged over muon spins. Our findings are in good agreement with [313].

### 7.2.3 $\mu \rightarrow e$ conversion

Experiments searching for  $\mu \rightarrow e$  conversion in the presence of an atomic nucleus have put strong limits on the branching ratio  $\text{Br}(\mu \text{ Au} \rightarrow e \text{ Au}) < 7.0 \times 10^{-13}$ , which was measured by the SINDRUM-II collaboration [320] and looked for conversion in the presence of a gold target. Future experiments aim for increased sensitivity by multiple orders of magnitude, for example Mu2e [321] and COMET [322] which will use aluminium as a stopping target material and hope to reach limits as low as  $\text{Br} \sim \mathcal{O}(10^{-17})$ . We limit ourselves here to the case that only ALP-lepton and/or ALP-photon couplings are present. Then only the Feynman diagrams that are also responsible for  $\mu \rightarrow e\gamma$  will contribute. Using results from [323], we may write

$$\text{Br}(\mu N \rightarrow e N) = \frac{8\alpha_{\text{QED}}^5 m_\mu Z_{\text{eff}}^4 Z F_p^2}{\Gamma_{\text{capt}}} (|F_2(-m_\mu^2) + F_3(-m_\mu^2)| + |F_2^5(-m_\mu^2) + F_3^5(-m_\mu^2)|), \quad (7.45)$$

where  $Z_{\text{eff}}$  is the effective atomic charge,  $F_p^2$  is the nuclear matrix element squared,  $\Gamma_{\text{capt}}$  is the total muon capture rate, and we suppress the  $\mu \rightarrow e$  superscript on the form factors. The numerical values for these quantities for the cases of gold and aluminium can be found in [311, 324, 325]. For heavy ALPs, i.e.,  $m_a > m_\mu$ , the evaluation at  $q^2 = 0$  is a good approximation and simplifies the calculation.

### 7.2.4 Muonium-antimuonium oscillations

Muonium is a hydrogen-like bound state of a negative muon and a positron in the shell ( $\mu^+ e^-$ ). In the presence of flavour-changing couplings, it can oscillate into its anti-particle ( $\mu^- e^+$ ). The ALP can mediate such transitions via both  $s$ - and  $t$ -channel diagrams [308, 312]. In both cases, we have  $s \approx t \approx m_\mu^2$ , where the equality becomes exact in the limit that both the electron mass and the binding energy of muonium are taken to be zero. This means that there are two limits in which the ALP propagators tend to a constant, and so the effects of the ALP can be mapped onto effective four-fermion operators; either  $m_a \ll m_\mu$  or  $m_a \gg m_\mu$ . In the limit  $m_a \ll m_\mu$ ,

$$\mathcal{H}_{\text{eff}}^{m_a \ll m_\mu} = -\frac{1}{4f^2} ([k_e]_{12} + [k_E]_{12})^2 (\bar{\mu}e)(\bar{\mu}e) - \frac{1}{4f^2} ([k_E]_{12} - [k_e]_{12})^2 (\bar{\mu}\gamma^5 e)(\bar{\mu}\gamma^5 e), \quad (7.46)$$

while in the limit  $m_a \gg m_\mu$ :

$$\mathcal{H}_{\text{eff}}^{m_a \gg m_\mu} = \frac{m_\mu^2}{4m_a^2 f^2} ([k_e]_{12} + [k_E]_{12})^2 (\bar{\mu}e)(\bar{\mu}e) + \frac{m_\mu^2}{4m_a^2 f^2} ([k_E]_{12} - [k_e]_{12})^2 (\bar{\mu}\gamma^5 e)(\bar{\mu}\gamma^5 e). \quad (7.47)$$

The muonium-antimuonium transition probability is then given in the  $m_a \ll m_\mu$  limit by [308,312]

$$P^{m_a \ll m_\mu} = \frac{\tau_\mu^2}{2\pi^2 a_B^6} \frac{1}{f^4} \left[ |c_{0,0}|^2 \left| 4[k_E]_{12}[k_e]_{12} - \delta_B ([k_e]_{12} - [k_E]_{12})^2 \right|^2 + |c_{1,0}|^2 \left| 4[k_E]_{12}[k_e]_{12} + \delta_B ([k_e]_{12} - [k_E]_{12})^2 \right|^2 \right], \quad (7.48)$$

and in the  $m_a \gg m_\mu$  limit by

$$P^{m_a \gg m_\mu} = \frac{\tau_\mu^2}{2\pi^2 a_B^6 m_a^4} \frac{m_\mu^4}{f^4} \left[ |c_{0,0}|^2 \left| 4[k_E]_{12}[k_e]_{12} - \delta_B ([k_e]_{12} - [k_E]_{12})^2 \right|^2 + |c_{1,0}|^2 \left| 4[k_E]_{12}[k_e]_{12} + \delta_B ([k_e]_{12} - [k_E]_{12})^2 \right|^2 \right], \quad (7.49)$$

where the muon lifetime  $\tau_\mu = 3.34 \times 10^{18} \text{ GeV}^{-1}$  and the muonium Bohr radius  $a_B = 2.69 \times 10^5 \text{ GeV}^{-1}$ . The population probabilities of the muonium angular momentum states  $c_{J,m_J}$  and the value of  $\delta_B$  depend on the experimental setup. Specifically, we define  $\delta_B$  in terms of the magnetic field  $B$  as  $\delta_B \equiv (1 + X^2)^{-1/2}$ , with  $X$  the dimensionless parameter

$$X = \frac{\mu_B B}{a} \left( g_e + \frac{m_e}{m_\mu} g_\mu \right) \approx 6.24 \frac{B}{\text{Tesla}}, \quad (7.50)$$

where  $\mu_B = e/(2m_e)$  is the Bohr magneton,  $g_e \approx g_\mu \approx 2$  are the magnetic moments of the electron and muon, and  $a \approx 1.864 \times 10^{-5} \text{ meV}$  is the muonium 1S hyperfine splitting.

The strongest constraint on the transition probability has been reported by the MACS collaboration which obtained  $P < 8.3 \times 10^{-11}$  at 90% CL [326]. For the MACS experiment, the population probabilities have been estimated as  $|c_{0,0}|^2 = 0.32$  and  $|c_{1,0}|^2 = 0.18$  and the magnetic field is  $B = 0.1 \text{ T}$ , giving  $\delta_B = 0.85$  [308,327].

### 7.2.5 $\mu \rightarrow e\gamma$ and $\mu \rightarrow 3e$

This subsection has already been included in the author's Master thesis. For the sake of completeness, we repeat the most important results here.

The partial decay width for  $\mu \rightarrow e\gamma$  is given by

$$\Gamma(\mu \rightarrow e\gamma) = \frac{m_\mu^3}{8\pi} \left( 1 - \frac{m_e^2}{m_\mu^2} \right) \left[ |F_2^{\mu \rightarrow e}(0)|^2 + |F_2^{5,\mu \rightarrow e}(0)|^2 \right] \quad (7.51)$$

with

$$F_2^{\mu \rightarrow e}(0) = -\frac{m_\mu e Q_\mu}{16\pi^2 f^2} ([k_E]_{12} - [k_e]_{12}) \left( \frac{1}{4} c_{\mu\mu} g_1(0, m_\mu, m_a) + \frac{\alpha}{4\pi} c_{\gamma\gamma} g_2(0, m_\mu, m_a) \right), \quad (7.52)$$

$$F_2^{5, \mu \rightarrow e}(0) = -\frac{m_\mu e Q_\mu}{16\pi^2 f^2} ([k_E]_{12} + [k_e]_{12}) \left( \frac{1}{4} c_{\mu\mu} g_1(0, m_\mu, m_a) + \frac{\alpha}{4\pi} c_{\gamma\gamma} g_2(0, m_\mu, m_a) \right). \quad (7.53)$$

The differential decay width for the three-body decay  $\mu^+ \rightarrow e^+ e^- e^+$  is given by

$$d\Gamma = \frac{1}{(2\pi)^3} \frac{1}{32m_\mu^2} |\overline{\mathcal{M}}|^2 ds_{12} ds_{23}, \quad (7.54)$$

where  $s_{ij} = (p_i + p_j)^2$  and the two indistinguishable positrons carry momenta  $p_1$  and  $p_2$ , while the momentum of the  $e^-$  is given by  $p_3$ . The squared matrix element summed over electron and positron spins and averaged over muon spin states is given by

$$\begin{aligned} |\overline{\mathcal{M}}|^2 &= (|[k_e]_{12}|^2 + |[k_E]_{12}|^2) |c_{ee}|^2 \frac{m_e^2 m_\mu^2}{f^4} \\ &\times \left\{ \frac{2s_{23}(s_{12} + s_{13})}{|s_{23} - m_a^2 + im_a\Gamma_a|^2} - \frac{s_{13}s_{23}}{\text{Re}[(s_{23} - m_a^2 + im_a\Gamma_a)(s_{13} - m_a^2 - im_a\Gamma_a)]} \right\} \\ &+ 4e^2 \left[ 2(s_{12} + s_{13}) \text{Re} [F_2^*(s_{23})F_3(s_{23}) + F_2^{5*}(s_{23})F_3^5(s_{23})] \right. \\ &+ \frac{1}{s_{23}} (m_\mu^2 (s_{12} + s_{13}) - 2s_{12}s_{13}) (|F_2(s_{23})|^2 + |F_2^5(s_{23})|^2) \\ &+ \frac{1}{m_\mu^2} (s_{23}(s_{12} + s_{13}) + 2s_{12}s_{13}) (|F_3(s_{23})|^2 + |F_3^5(s_{23})|^2) \\ &+ s_{12} (F_2^*(s_{23})F_2(s_{13}) + F_2^{5*}(s_{23})F_2^5(s_{13}) + F_2^*(s_{23})F_3(s_{13}) \\ &+ F_2^{5*}(s_{23})F_3(s_{13}) + F_2^5(s_{13})F_3^{5*}(s_{23}) + F_2(s_{13})F_3^*(s_{23})) \\ &\left. + \frac{s_{12}(s_{13} + s_{23})}{m_\mu^2} (F_3(s_{23})F_3^*(s_{13}) + F_3^5(s_{23})F_3^{5*}(s_{13})) \right] \\ &+ \frac{2es_{23}m_e}{f^2} c_{ee} \text{Re} \left[ \frac{[k_e]_{21} + [k_E]_{21}}{s_{23} - m_a^2 - im_a\Gamma_a} (m_\mu^2 F_2^5(s_{13}) + (s_{12} + s_{13}) F_3^5(s_{13})) \right. \\ &\left. + \frac{[k_e]_{21} - [k_E]_{21}}{s_{23} - m_a^2 - im_a\Gamma_a} (m_\mu^2 F_2(s_{13}) + (s_{12} + s_{13}) F_3(s_{13})) \right] + (1 \leftrightarrow 2). \quad (7.55) \end{aligned}$$

where we have suppressed the  $\mu \rightarrow e$  superscript which should appear on all the form factors. To obtain the full decay rate, the partial decay rate needs to be integrated over the phase space of the Dalitz region [328, 329].

### 7.2.6 Constraints on lepton flavour-violating couplings

The combined excluded regions for ALP-induced  $\mu \rightarrow e$  transitions are presented in figure 7.11. We collect the numerical values for the constraints on the coupling  $c_{e\mu} \equiv$

Observable	Mass Range [MeV]	ALP decay mode	Constrained coupling $c$	Limit (95% CL) one $ c  \cdot \left(\frac{\text{TeV}}{f}\right) \cdot \sqrt{\mathcal{B}}$
$\text{Br}(\mu \rightarrow ea(\text{invisible}))$	$0 < m_a < 13$	Long-lived	$c_{\mu e}^{(\dagger)}$	$7.2 \times 10^{-7}$
$\text{Br}(\mu \rightarrow ea(\text{invisible}))$	$13 < m_a < 80$	Long-lived	$c_{\mu e}^{(\dagger)}$	$5.0 \times 10^{-7}$
$\text{Br}(\mu \rightarrow ea(\text{invisible}))$	$0 < m_a < 10$	Long-lived	$c_{\mu e}^{(\dagger)}$	$2.5 \times 10^{-7}$
$\text{Br}(\mu \rightarrow ea(\text{invisible})\gamma)$	$0 < m_a < 105$	Long-lived	$c_{\mu e}$	$1.0 \times 10^{-5}$
$\text{Br}(\mu \rightarrow e\gamma\gamma)$	$0 < m_a < 105$	$\gamma\gamma$	$c_{\mu e}$	$1.3 \times 10^{-9}$
$\text{Br}(\mu \rightarrow e\gamma_{\text{eff}})$	$0 < m_a < 105$	$\gamma\gamma$	$c_{\mu e}$	$1.0 \times 10^{-10}$
$\text{Br}(\mu \rightarrow 3e)$	$0 < m_a < 105$	$e^+e^-$	$c_{\mu e}$	$1.6 \times 10^{-10}$

Table 7.2: Summary of constraints on the lepton flavour-violating ALP coupling  $c_{e\mu}$  derived from measurements of branching fractions (first column) for various muon decays, in which the lepton can decay to an on-shell ALP. The measurements and SM predictions (where appropriate) are given in AII.9 in appendix AII.1. The limit cited is the strongest limit found within the mass range probed by the measurement. In the fifth column the symbol  $\mathcal{B}$  denotes the ALP branching ratio into the relevant final state. ( $\dagger$ ): these bounds depend on the chirality of the ALP couplings due to the experimental setup, see [313,330,331] for details. Here we assume  $[k_e]_{12} = [k_E]_{12}$  for these.

$(|[k_E]_{21}|^2 + |[k_e]_{21}|)^{1/2}$  in table 7.2. For the flavour-diagonal couplings we make the following assumptions

$$\begin{aligned}
\frac{|c_{ee}|}{f} = \frac{|c_{\mu\mu}|}{f} = \frac{|c_{\tau\tau}|}{f} &\equiv \frac{|c_{\ell\ell}|}{f} = 0, & \text{for } m_a < 2m_e, \\
\frac{|c_{ee}|}{f} = \frac{10^{-3}}{\text{TeV}}, \quad \frac{|c_{\mu\mu}|}{f} = \frac{|c_{\tau\tau}|}{f} &= \frac{1}{\text{TeV}}, & \text{for } 2m_e < m_a < 2m_\mu, \\
\frac{|c_{ee}|}{f} = \frac{|c_{\mu\mu}|}{f} = \frac{|c_{\tau\tau}|}{f} &\equiv \frac{|c_{\ell\ell}|}{f} = \frac{1}{\text{TeV}}, & \text{for } m_a > 2m_\mu
\end{aligned} \tag{7.56}$$

which give the largest flavour-diagonal coupling to leptons that are still allowed from constraints from quark flavour observables in figure 7.8. They are relevant for the branching ratios and decay lengths of the ALP. Our results assume that the coupling  $c_{e\mu}$  dominates over the other flavour-changing ones. However, in the absence of additional assumptions, a UV completion, in which a horizontal global symmetry group is broken to produce a pNGB, could induce all possible flavour off-diagonal couplings to leptons. A discussion of lepton flavour-violating ALP decays in the context of such explicit UV models can be found in [310].

For heavy ALP masses  $m_a > m_\mu$  the most dominant constraints come from searches for  $\mu \rightarrow e\gamma$ , and the three-body decay  $\mu \rightarrow 3e$  is phase space suppressed [332,333]. The situation is completely different for ALPs that are lighter than the muon threshold, for which the ALP can be produced on-shell in muon decays. Constraints from  $\mu \rightarrow ea$  with subsequent decays  $a \rightarrow \gamma\gamma$ ,  $a \rightarrow e^+e^-$  and  $a \rightarrow \text{invisible}$  are shown in orange, purple and red, respectively, and provide stronger constraints than  $\mu \rightarrow e\gamma$  in a mass range of a few  $\text{MeV} < m_a < m_\mu$ . The limits are obtained by SINDRUM for  $\mu \rightarrow 3e$  [334] and LAMPF for  $\mu \rightarrow \gamma\gamma e$  [335].

If the ALP decay is delayed, this parameter space cannot be excluded even if the decay still happens within the detector. A search for resonances in the dataset without the strong cut on the time of detection of the decay products would be sensitive to much smaller ALP masses. This limit on  $\mu \rightarrow e\gamma\gamma$  has been improved recently by [336] and expands the excluded region of our model in the range of  $20 \text{ MeV} < m_a < 35 \text{ MeV}$ . The Collaboration states limits for muon branching ratios for different lifetimes in bins of 1 MeV and we have adapted the appropriate limit by calculating the ALP lifetime in the respective mass region.

Furthermore, a very interesting effect can happen for  $\mu \rightarrow e(a \rightarrow \gamma\gamma)$  decays. When the ALP is boosted a lot or it decays close to the detector, the two photons hit the detector closer than its spatial resolution. Consequently, the two photons cannot be resolved individually, and thus are reconstructed as one, leading to a misinterpretation of the  $\mu \rightarrow e\gamma\gamma$  decay as a  $\mu \rightarrow e\gamma^*$  decay. We present the limits from MEG on  $\mu \rightarrow e\gamma^*$  with a misinterpreted photon in green.

The decay  $a \rightarrow \text{invisible}$  is defined as an ALP leaving the detector before decaying. The corresponding constraint on the ALP-lepton coupling is derived from the limits on the branching ratio of  $\mu \rightarrow ea(\text{invisible})$  obtained by [331] for the case in which  $[k_e]_{12} = [k_E]_{12}$ , and is sensitive to the ALP decay length which is set by the ALP coupling to electrons in this mass range. The parameter space ruled out by the measurement [331] is shown in dark yellow in figure 7.11. For different ALP coupling structures and masses this experiment can be less sensitive than the bound obtained by the TWIST collaboration [330] as emphasised in [313]. For masses  $13 \text{ MeV} < m_a < 80 \text{ MeV}$ , the bound is largely independent of the angular distribution of the electrons, whereas for masses  $m_a > 80 \text{ MeV}$ , the bound depends on whether the decay is (an)isotropic. We show the constraints from [330] in red in figure 7.11.

A slightly weaker constraint is derived from searches for the decay  $\mu \rightarrow ea\gamma$  shown in dark blue. Past searches for this type of decay have been performed with the Crystal Box detector [335]. The experiment required large photon and electron energies of  $E_e > 38 - 43 \text{ MeV}$  and  $E_\gamma > 38 \text{ MeV}$ , respectively. Here, we take the most conservative limits on the energy cuts for our plots. Though theoretically sub-dominant when compared with  $\mu \rightarrow ea$  due to the additional radiation, the angular distribution is less dependent on the chiral structure of the ALP couplings and therefore can be almost competitive in constraining parameter space of ALP couplings and masses. Future searches at the upcoming MEG II experiment could exceed current bounds from TWIST by a factor of 5, assuming optimal conditions and relaxed energy and angular cuts [313].

The lifetime of the ALP strongly affects the reach of the different experiments. The constraint from the measurement of muonium-antimuonium oscillations from the MACS experiment [326] shown in grey is weaker than other constraints throughout the ALP mass range, but relevant for masses  $m_a > m_\mu$ , because it is independent of  $c_{\ell\ell}$ , whereas both the constraints from  $\mu \rightarrow eee$  and  $\mu \rightarrow e\gamma$  vanish for  $c_{ee} \rightarrow 0$  [312]. The bounds obtained from muon to electron conversions in the presence of an atomic nucleus from the SINDRUM-II collaboration [337] are much weaker than those from decay experiments, because we

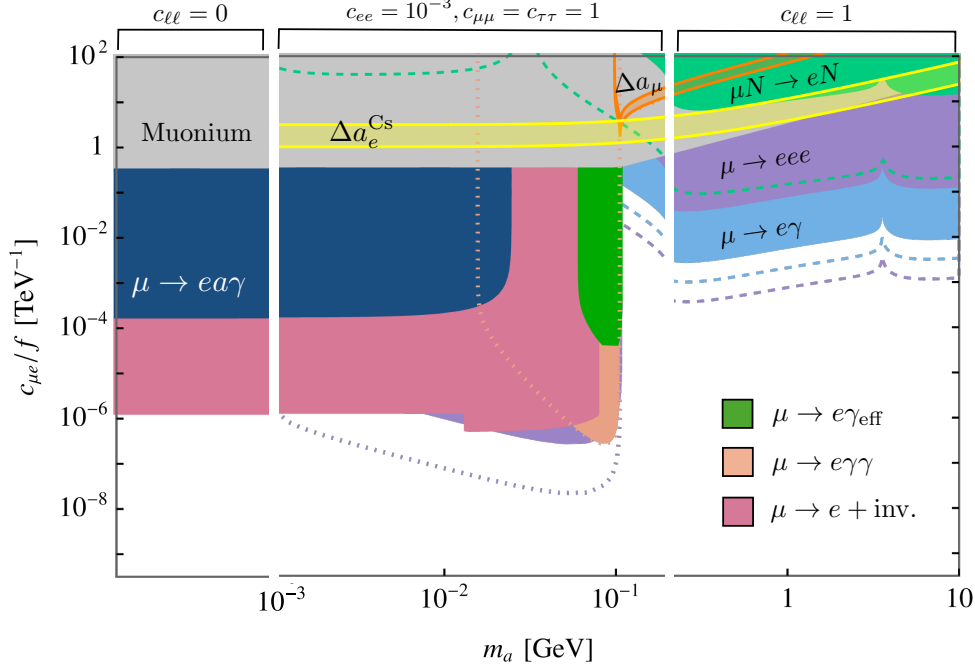


Figure 7.11: Bounds on ALP mediated flavour off-diagonal transitions between muons and electrons with  $c_{\mu e} \equiv \sqrt{|[k_E]_{21}|^2 + |[k_e]_{21}|^2}$ , assuming universal ALP couplings to leptons as indicated above the plot for the different ALP mass regions.

only allow for lepton couplings in our scenario. Hence, the coupling to nucleons must be done through the photon, or is suppressed by multiple loops. Moreover, the form factors contributing to  $\mu \rightarrow e$  conversion also vanish in the limit  $c_{\ell\ell} \rightarrow 0$ . For the ALP couplings considered here, even the significant improvement in sensitivity expected at Mu2e [338] and COMET [339] shown by the green dashed contour cannot compete with the constraints from  $\mu \rightarrow 3e$  and  $\mu \rightarrow e\gamma$ . In addition, we give the optimistic reaches for the upcoming experiments MEG II [340] and Mu3E [341, 342].

The yellow and orange translucent bands give the region where a single flavour-violating ALP coupling could in principle explain the observed anomalies in the anomalous magnetic moment of the electron and the muon, respectively [72–75, 343–347]. However, such an explanation is ruled out by various experiments [4, 7, 309]. For an extensive study how different ALP coupling combinations could still yield a viable explanation for either one of the anomalies and also possibly for both at the same time, we refer the reader to [4, 7, 196, 309, 319, 348–350].

The results for the form factors presented in section 7.2.1 are also valid for LFV tau-lepton transitions. Henceforth, it is straight-forward to extend our analysis to the tau sector, as was done in [7]. Experimental searches have been mainly performed by the  $b$ -factories BaBar and Belle, and upcoming limits are expected from Belle-II and upgrades of LHCb.

## APPENDIX II

### AII.1 Measurements and SM predictions for flavour observables

The measured values and SM predictions for observables used to derive constraints are given in tables AII.3 to AII.9.

Observable	Mass Range [MeV]	Measurement	SM prediction
$\text{Br}(K^+ \rightarrow \pi^+ X)$	$0 < m_X < 261$ (*)	[260] (search)	-
$\text{Br}(K^+ \rightarrow \pi^+ X)$	$110 < m_X < 155$	[351] (search)	-
$\text{Br}(K_L \rightarrow \pi^0 X)$	$0 < m_X < 261$	[261] (search)	-
$\text{Br}(B^+ \rightarrow K^+ \bar{\nu}\nu)$	$0 < m_{\nu\nu} < 4785$	$< 1.6 \times 10^{-5}$ [352]	$(4.0 \pm 0.5) \times 10^{-6}$ [353]
$\text{Br}(B^0 \rightarrow K^{*0} \bar{\nu}\nu)$	$0 < m_{\nu\nu} < 4387$	$< 1.8 \times 10^{-5}$ [262]	$(9.2 \pm 1.0) \times 10^{-6}$ [353]
$\text{Br}(\Upsilon \rightarrow \gamma a(\text{invisible}))$	$m_a < 9200$	[252] (search)	-

Table AII.3: Observables relevant for a long lived ALP. Bounds are at 90% CL. (\*): cuts are applied to exclude the region around  $m_\pi$  ( $100 \text{ MeV} < m_X < 161 \text{ MeV}$ ).

Observable	Mass Range [MeV]	Measurement	SM prediction
$\text{Br}(K^+ \rightarrow \pi^+ \gamma\gamma)$	$m_{\gamma\gamma} < 108$	$< 8.3 \times 10^{-9}$ [263]	$6.1 \times 10^{-9}$ [354]
$\text{Br}(K^+ \rightarrow \pi^+ \gamma\gamma)$	$220 < m_{\gamma\gamma} < 354$	$(9.65 \pm 0.63) \times 10^{-7}$ [264]	$(10.8 \pm 1.7) \times 10^{-7}$ [354]†
$\text{Br}(K_L \rightarrow \pi^0 \gamma\gamma)$	$30 < m_{\gamma\gamma} < 110$	$< 0.6 \times 10^{-8}$ [265]	$(8_{-5}^{+7}) \times 10^{-8}$ [355]*
$\text{Br}(K_L \rightarrow \pi^0 \gamma\gamma)$	$m_{\gamma\gamma} < 363$ (‡)	$(1.29 \pm 0.03 \pm 0.05) \times 10^{-6}$ [266]	$1.12 \times 10^{-6}$ [355]

Table AII.4: Observables with a photon pair in the final state. Bounds are at 90% CL. (‡): cuts are applied to exclude the region around the pion pole ( $100 \text{ MeV} < m_{\gamma\gamma} < 160 \text{ MeV}$ ). (†): calculated from results in the given reference. Error bars estimated from varying parameter  $\hat{c}$  between its quoted errors. (\*) : calculated from results in the given reference. Error bars estimated from varying parameter  $a_V$  between its quoted errors.)

Observable	Mass Range [MeV]	Measurement	SM prediction
$\text{Br}(K^+ \rightarrow \pi^+ a(e^+ e^-))$	$m_a < 100$	$< 8 \times 10^{-7}$ [356]	-
$\text{Br}(K_L \rightarrow \pi^0 e^+ e^-)$	$140 < m_{ee} < 362$	$< 2.8 \times 10^{-10}$ [357]	$(3.1^{+1.2}_{-0.8}) \times 10^{-11}$ [358]
$\text{Br}(B^+ \rightarrow \pi^+ e^+ e^-)$	$140 < m_{ee} < 5140$	$< 8.0 \times 10^{-8}$ [359]	$(2.26^{+0.23}_{-0.19}) \times 10^{-8}$ [360]
$d\text{Br}/dq^2(B^0 \rightarrow K^{*0} e^+ e^-)_{[0.0004, 0.05]}$	$20 < m_{ee} < 224$	$(4.2 \pm 0.5) \times 10^{-6} \text{ GeV}^{-2}$ [361]	$(3.3 \pm 0.7) \times 10^{-6} \text{ GeV}^{-2}$
$d\text{Br}/dq^2(B^0 \rightarrow K^{*0} e^+ e^-)_{[0.05, 0.15]}$	$224 < m_{ee} < 387$	$(2.6 \pm 1.0) \times 10^{-7} \text{ GeV}^{-2}$ [361]	$(3.9 \pm 0.8) \times 10^{-7} \text{ GeV}^{-2}$
$R_{K^*}[0.045, 1.1]$	$212 < m_{ee} < 1049$	$0.66^{+0.11}_{-0.07} \pm 0.03$ [362]	$0.906 \pm 0.028$ [363]
$\text{Br}(D^0 \rightarrow \pi^0 e^+ e^-)$	$m_{ee} < 1730$ (†)	$< 4 \times 10^{-6}$ [364]	$1.9 \times 10^{-9}$ [365]
$\text{Br}(D^+ \rightarrow \pi^+ e^+ e^-)$	$200 < m_{ee} < 1730$ (*)	$< 1.1 \times 10^{-6}$ [366]	$9.4 \times 10^{-9}$ [365]
$\text{Br}(D_s^+ \rightarrow K^+ e^+ e^-)$	$200 < m_{ee} < 1475$ (*)	$< 3.7 \times 10^{-6}$ [366]	$9.0 \times 10^{-10}$ [365]

Table AII.5: Observables with an electron pair in the final state. Bounds are at 90% CL. Here we only include observables for which the electron invariant mass can be below or near the dimuon threshold, on the grounds that above it muonic observables will generically provide stronger bounds. Predictions without accompanying citations have been calculated using flavio [367]. In the measurements of the  $D_{(s)}$  branching ratios, cuts are applied to exclude the region around the  $\phi$  resonance. For the BaBar measurements with a (\*), the excluded region is  $950 \text{ MeV} < m_{ee} < 1050 \text{ MeV}$ , while the BESIII measurement with a (†) excludes the region  $935 \text{ MeV} < m_{ee} < 1053 \text{ MeV}$ . Since the long-distance contributions to these decays peak around this excluded resonance, we take the SM prediction to be only due to the short-distance contributions, as calculated in Ref. [365].

## AII.2 Expressions for the form factors

The loop functions for the form factors in section 7.2.1 are given by the Feynman integrals

$$g_1(q^2, m_i, m_a) = 2 \int_0^1 dx \int_0^{1-x} dy \frac{1-x-yx}{\Delta''_{i \rightarrow j}}, \quad (\text{AII.57})$$

$$g_2(q^2, m_i, m_a) = - \int dx \int_0^{1-x} dy \left[ 4 \log \frac{m_i^2}{\mu^2} + 2 \log \Delta_{i \rightarrow j} + 2 \log \Delta'_{i \rightarrow j} - 4\delta_2 - \left( \frac{x(1-y)}{\Delta'_{i \rightarrow j}} - \frac{yx}{\Delta_{i \rightarrow j}} \right) \right], \quad (\text{AII.58})$$

$$l_1(q^2, m_i, m_a) = 2 \int_0^1 dx \int_0^{1-x} dy \frac{1-x-yx-2y^2}{\Delta''_{i \rightarrow j}}, \quad (\text{AII.59})$$

$$l_2(q^2, m_i, m_a) = \int dx \int_0^{1-x} dy \left( \frac{x(1-y)}{\Delta'_{i \rightarrow j}} - \frac{yx}{\Delta_{i \rightarrow j}} \right), \quad (\text{AII.60})$$

and

$$\Delta_{i \rightarrow j} = y \frac{m_a^2}{m_i^2} - \frac{q^2}{m_i^2} y(1-x-y) - xy, \quad (\text{AII.61})$$

$$\Delta'_{i \rightarrow j} = (1-x-y) \frac{m_a^2}{m_i^2} - \frac{q^2}{m_i^2} y(1-x-y) + x(1-y), \quad (\text{AII.62})$$

$$\Delta''_{i \rightarrow j} = x \frac{m_a^2}{m_i^2} + (1-x-yx) - \frac{q^2}{m_i^2} y(1-x-y). \quad (\text{AII.63})$$



Observable	Mass Range [MeV]	Measurement	SM prediction
$\text{Br}(K_L \rightarrow \pi^0 \mu^+ \mu^-)$	$210 < m_{\mu\mu} < 350$	$< 3.8 \times 10^{-10}$ [368]	$(1.5 \pm 0.3) \times 10^{-11}$ [369]
$\text{Br}(B^+ \rightarrow K^+ a(\mu^+ \mu^-))$	$250 < m_a < 4700$ (†)	[267] (search)	-
$\text{Br}(B^0 \rightarrow K^{*0} a(\mu^+ \mu^-))$	$214 < m_a < 4350$ (†)	[370] (search)	-
$\text{Br}(J/\psi \rightarrow \gamma a(\mu^+ \mu^-))$	$212 < m_{\mu\mu} < 3000$	[251] (search)	-
$\text{Br}(\Upsilon \rightarrow \gamma a(\mu^+ \mu^-))$	$212 < m_{\mu\mu} < 9200$	[253] (search)	-
$\text{Br}(B^+ \rightarrow \pi^+ \mu^+ \mu^-)$	$211 < m_{\mu\mu} < 5140$ (‡)	$(1.83 \pm 0.25) \times 10^{-8}$ [269]	$(2.26_{-0.19}^{+0.23}) \times 10^{-8}$ [360]
$\text{Br}(B_s^0 \rightarrow \mu^+ \mu^-)$	$5320 < m_{\mu\mu} < 6000$	$(2.69_{-0.35}^{+0.37}) \times 10^{-9}$ [371]	$(3.66 \pm 0.14) \times 10^{-9}$ [372]
$\text{Br}(B^0 \rightarrow \mu^+ \mu^-)$	$4900 < m_{\mu\mu} < 6000$	$(0.6_{-0.7}^{+0.7}) \times 10^{-10}$ [371]	$(1.03 \pm 0.05) \times 10^{-10}$ [372]
$\text{Br}(D^+ \rightarrow \pi^+ \mu^+ \mu^-)$	$250 < m_{\mu\mu} < 1730$ (*)	$< 7.3 \times 10^{-8}$ [373]	$9.4 \times 10^{-9}$ [365]
$\text{Br}(D_s^+ \rightarrow K^+ \mu^+ \mu^-)$	$200 < m_{\mu\mu} < 1475$ (**)	$< 21 \times 10^{-6}$ [366]	$9.0 \times 10^{-10}$ [365]

Table AII.6: Observables with a muon pair in the final state. Bounds are at 90% CL. (†): cuts are applied to exclude regions around the  $J/\psi$ ,  $\psi(2S)$  and  $\psi(3370)$  resonances. (‡): cuts are applied to exclude charmonium resonance regions ( $8.0 \text{ GeV}^2 < m_{\mu\mu}^2 < 11.0 \text{ GeV}^2$  and  $12.5 \text{ GeV}^2 < m_{\mu\mu}^2 < 15.0 \text{ GeV}^2$  are excluded).(\*): a large region containing the  $\eta$ ,  $\rho/\omega$  and  $\phi$  resonances is excluded ( $525 \text{ MeV} < m_{\mu\mu} < 1250 \text{ MeV}$ ).(\*\*): cuts are applied to exclude the region around the  $\phi$  resonance ( $990 \text{ MeV} < m_{\mu\mu} < 1050 \text{ MeV}$ ). Since the long-distance contributions to the  $D_{(s)}$  decays peak around the excluded resonance(s), we take the SM prediction to be only due to the short-distance contributions, as calculated in Ref. [365].

Observable	Mass Range [MeV]	Measurement	SM prediction
$\text{Br}(B^+ \rightarrow K^+ \tau^+ \tau^-)$	$3552 < m_{\tau\tau} < 4785$	$< 2.25 \times 10^{-3}$ [374]	-
$\text{Br}(\Upsilon \rightarrow \gamma a(\tau\tau))$	$3500 < m_{\tau\tau} < 9200$	[254] (search)	-

Table AII.7: Observables with a tau pair in the final state. Bounds are at 90% CL.

The scheme dependent constant  $\delta_2$  arises from the treatment of the Levi–Civita symbol in  $d$  dimensions, and for us  $\delta_2 = -3$ .

Observable	Mass Range [MeV]	Measurement	SM prediction
$\text{Br}(\Upsilon \rightarrow \gamma a(\text{hadrons}))$	$290 < m_{\text{hadrons}} < 7100$	[255] (search)	-

Table AII.8: Observables relevant for hadronic decays of the ALP.

Observable	Mass Range [MeV]	Measurement
$\text{Br}(\mu \rightarrow 3e)$	$0 < m_a < 105$	$< 1.0 \times 10^{-12}$ [334]
$\text{Br}(\mu \rightarrow e\gamma)$	-	$< 4.2 \times 10^{-13}$ [340]
$\text{Br}(\mu \rightarrow e\gamma\gamma)$	$0 < m_a < 105$	$< 7.2 \times 10^{-11}$ [335]
$\text{Br}(\mu \rightarrow ea(\text{invisible}))$	$0 < m_a < 13$	$\lesssim 2.1 \times 10^{-5}$ * [330]
$\text{Br}(\mu \rightarrow ea(\text{invisible}))$	$13 < m_a < 80$	$\lesssim 10^{-5}$ * [330]
$\text{Br}(\mu \rightarrow ea(\text{invisible}))$	$0 < m_a < 10$	$\lesssim 2.6 \times 10^{-6}$ * [331]
$\text{Br}(\mu \rightarrow e\gamma a(\text{invisible}))$	$0 < m_a < 105$	$< 1.1 \times 10^{-9}$ [335]
$\text{Br}(\mu N \rightarrow eN)$	-	$< 7.0 \times 10^{-13}$ [337]
$\text{Br}(\tau \rightarrow ea(\text{invisible}))$	$0 < m_a < 1600$	$< 2.7 \times 10^{-3}$ [375]
$\text{Br}(\tau \rightarrow \mu a(\text{invisible}))$	$0 < m_a < 1600$	$< 5 \times 10^{-3}$ [375]
$\text{Br}(\tau \rightarrow 3\mu)$	$211 < m_a < 1671$	$< 2.1 \times 10^{-8}$ [376]
$\text{Br}(\tau \rightarrow 3e)$	$200 < m_a < 1776$	$< 2.7 \times 10^{-8}$ [376]
$\text{Br}(\tau^- \rightarrow \mu^- e^+ e^-)$	$200 < m_a < 1776$	$< 1.8 \times 10^{-8}$ [376]
$\text{Br}(\tau^- \rightarrow e^- \mu^+ \mu^-)$	$211 < m_a < 1776$	$< 2.7 \times 10^{-8}$ [376]
$\text{Br}(\tau \rightarrow \mu\gamma)$	-	$< 4.4 \times 10^{-8}$ [377]
$\text{Br}(\tau \rightarrow e\gamma)$	-	$< 3.3 \times 10^{-8}$ [377]

Table AII.9: Lepton flavour-violating observables. Where a mass range for  $m_a$  is given, the range refers to masses that are consistent with the experimental cuts and for which the decay can proceed via a resonant ALP. For some of the observables (for example  $\mu \rightarrow 3e$ ), an ALP lying outside of this mass range may still be constrained by the experiment, if it can mediate the decay off-shell. Where the mass range is left blank, the measurement can never involve a resonant ALP. \*: for the  $\mu \rightarrow ea(\text{invisible})$  searches, the precise bound depends on the chirality of the ALP couplings due to the experimental setup and the bounds quoted here are assuming vectorial couplings, see [313, 330, 331] for details.

Decay	Experiment	Initial state	Time cut (ns)
$\mu \rightarrow 3e$	SINDRUM [334]	at rest	0.8
$\mu \rightarrow e\gamma\gamma$	Crystal Box [335]	at rest	2.5
$\mu \rightarrow e\gamma$	MEG [340]	at rest	0.7
$\mu \rightarrow e\gamma a(\text{invisible})$	Crystal Box [335]	at rest	1.5

Table AII.10: Cuts on the decay time of the ALP that should be applied in various LFV experiments.

A large, dark red, stylized bracket structure that frames the central text. It consists of two vertical bars, one on the left and one on the right, with horizontal caps at the top and bottom, resembling a pair of square brackets.

*Epilogue*



## CONCLUSIONS AND OUTLOOK

---

The present thesis demonstrated how the concepts and notions of the methodology known as effective field theories can be used to deepen our knowledge of the Standard Model and its properties on the one hand, and how to gain meaningful insights from proposed models beyond the SM on the other hand. We applied the EFT machinery to two specific, yet different projects: high-precision calculations in Higgs production with SCET and flavour physics probes of axion-like particles. Both topics are state-of-the-art research areas where we could significantly enhance our understanding of the principles behind.

In the first part, “[gluon-gluon to Higgs fusion](#)”, we applied the soft-collinear effective theory to the power-suppressed process of gluon-gluon to Higgs fusion via a light quark loop. Since gluon-gluon fusion is the dominant production channel for Higgs bosons at the LHC, and light quarks are estimated to contribute with  $\sim 15\%$  to the total cross section, it is of utmost importance to understand the exact dynamics of the process. This is highly non-trivial, because the appearance of large logarithms spoils the convergence of the perturbation series in the strong coupling constant. Hence, one must resum these large logarithmic corrections to all orders of perturbation theory. Additionally, conventional QCD methods fail to resum more than the leading double-logarithmic corrections, necessitating advanced computational methods.

In this regard, SCET allows us to significantly improve the theory predictions. We successfully applied the SCET methods to  $gg \rightarrow h$  fusion and were able to derive a factorisation theorem. Since we deal with a power-suppressed process, we expectedly encountered endpoint divergences. By generalising the refactorisation-based subtraction scheme introduced in [28, 29] to non-abelian final states, we were able to re-organise the factorisation formula in a way that is free of divergences in section 5.1. In section 5.2, we derived the factorisation formula in terms of renormalised parameters and component functions. This is a crucial achievement because in general renormalisation and regularisation of endpoint divergences do not commute. We demonstrated that all mismatching terms are only dependent on the hard scale of the problem, thus they can be absorbed into a redefinition of the renormalised hard matching coefficient  $H_1(\mu)$ . Having all renormalisation factors at hand, we derived the renormalisation group equations for all component functions in section 5.3. Solving them iteratively then allowed us to predict the leading logarithmic terms in the three-loop amplitude. Eventually, we solved the RG equations for the jet function  $J$  and the soft function  $S_3$  to RG-improved leading order. With this we were able to derive the resummed expression for the third term of the factorisation formula  $T_3$  to modified next-to-leading logarithmic accuracy, i.e. to resum the three leading towers of logarithms

to all orders of perturbation theory. Note that apart from a single constant term from the second term  $T_2$ , the first and second term yield suppressed contributions up to the given precision. As mentioned before, conventional methods can only predict the leading tower of logarithms. The first subleading term can also be retrieved from the expression for the  $h \rightarrow \gamma\gamma$  amplitude by a replacement of colour factors [80]. It must be stressed, however, that in this reference, too, SCET was used to derive the expressions. The result presented in this thesis characterises the prediction for the resummed, light-quark induced  $gg \rightarrow h$  form factor with the highest precision so far.

Apart from its great phenomenological impact for the prediction of Higgs production rates, this thesis also serves the purpose of establishing our methodology of refactorisation-based subtractions for regularising endpoint divergences. Such divergences appear in various subleading power SCET processes, and to this day our method is the only known way to consistently remove them. As an affirmation, most recent works about endpoint factorisation and resummation in gluon thrust made use of this method [90,92].

One minor blemish of the RBS that we were hitherto unable to eliminate is the fact that due to the various contributions the RG equation for the hard coefficient  $H_1$  takes a complicated form that is not of Sudakov type. That prevents us from solving it. On that account we solve the RGEs for the jet and soft functions instead, and evolve all component functions up to the hard scale, where no large logarithms are left in the hard coefficients. However, the solutions are complicated, for instance the RG-improved soft function  $S_3$  involves a *Rathie-I* function, a generalisation of the Meijer-G function that itself is a generalisation of hypergeometric functions. Consequently, we are only able to derive the RG-improved leading order expressions. For a full resummation of  $gg \rightarrow h$  via light quarks it would therefore be necessary to find means to solve the RGEs for the hard coefficients.

In the second part of this thesis, “[flavour physics of ALPs](#)”, we explored how flavour physics experiments can be used to constrain parameter space of axion-like particles. At first we derived how couplings in a general UV theory of axions and ALPs evolve to the low-energy scale via a sequence of running from a higher energy to a lower one, and matching the theory at the mass thresholds where heavy particles need to be integrated out of the theory. We discovered that independent from the specific UV coupling, at the low-energy scale couplings to all SM particles are generated. Moreover, quark flavour-changing ALP couplings are generated regardless of the underlying UV theory. In section 6.3 we showed how to consistently implement ALP interactions in the weak chiral and nuclear Lagrangian, thereby correcting the prediction for the important  $K \rightarrow \pi a$  decay amplitude, which was based on an inconsistent equation in a seminal paper [183]. The inconsistency has gone unnoticed ever since and resulted in an underestimation of the branching ratio by a factor  $\approx 37$ . For ALPs in the context of the nuclear chiral Lagrangian with two quark flavours we demonstrated how the ALP-mass dependence of the ALP-nucleon coupling drops out for iso-singlet nuclei, i.e. nuclei with the same amount of protons and neutrons.

Chapter 7 was dedicated to study constraints on ALP-models from flavour physics. In section 7.1 we investigated constraints from quark flavour experiments using the model established in the previous section. Probes included exotic meson decays, rare pion de-

cays, the flavour-conserving decays of  $J/\psi$  and  $\Upsilon$  mesons and the chromomagnetic dipole moment of the top-quark. We presented our results in four benchmark scenarios assuming that the ALP couples only to gluons, weak gauge bosons, left-handed quarks or left-handed leptons in the UV, respectively. Since flavour off-diagonal ALP couplings are highly constrained already, we assumed that they are only generated via running and matching from the high scale. Furthermore, we compared our obtained flavour bounds with limits from collider and astrophysical searches. We found that flavour observables can neatly fill in blank space of the allowed ALP parameter space that has previously been inaccessible by other experiments, and therefore provide important complementary bounds. Most interestingly, we established that quark flavour observables can give constraints to UV ALP–lepton couplings that are even stronger than dedicated ALP–lepton searches from beam dump and astrophysics experiments. In section 7.2 we studied probes of ALPs with lepton flavour observables. Since the Standard Model conserves each lepton number individually, no flavour changing coupling arises from evolution effects. The induced effect from neutrino oscillations is greatly suppressed by factors of  $\Delta m_\nu^2/m_W^2 \approx 10^{-27}$ . We therefore derived constraints on UV flavour-violating couplings. Observables studied included rare lepton decays like  $\mu \rightarrow ea\gamma$ ,  $\mu \rightarrow e$  conversion in the presence of an atomic nucleus, and muonium oscillations. In addition, we showed the reach of future experiments. Strongest bounds are obtained when the ALP is produced on-shell and can subsequently decay outside of the detector giving rise to missing energy signatures, or decay into pairs of photons or leptons, which then overcome the phase space suppression of three-body decays and yield stronger limits than for instance the  $\mu \rightarrow e\gamma$  bound. In this thesis we focussed on electron–muon flavour-changing ALPs, but the results can easily be transferred to couplings involving tau-leptons, as was presented in [7]. For future research it will be interesting to see whether flavour physics can also give significant constraints to other BSM models than axions and ALPs, especially if they feature a comparably rich generation mechanism of couplings to SM particles via evolution effects.



In this thesis we have taken important steps on the long way to find a more universal theory for the fundamental building blocks of nature than the Standard Model. For this purpose we employed state-of-the-art methods of effective field theory. While there are still a lot of “holes to fill”, we think that effective theories in general and this work in particular represent an important contribution to the general effort of improving our understanding of the properties of the smallest particles. In this spirit, we would like to conclude with a quote from Max Planck: «When you change the way you look at things, the things you look at change.»





# A

## APPENDIX

---

### A.1 Notations and conventions

In this section we want to briefly summarise the notations and conventions used in this document. They are often tacitly accepted in works in the field of high energy physics, but sometimes differ from conventions in other fields.

In this thesis, we use natural units for the reduced Planck constant and the speed of light, i.e. we set

$$\hbar = c = 1, \quad \text{where } \hbar = \frac{h}{2\pi}. \quad (\text{A.1})$$

As a result, all other SI units can be expressed in terms of energies. Greek indices denote spacetime coordinates, and we commonly use Latin letters as colour or flavour-space indices. The symbol  $\epsilon^{\mu\nu\alpha\beta}$  stands for the totally anti-symmetric Levi-Civita tensor, and we adopt the prescription  $\epsilon^{0123} = 1$ . In addition, we employ the Einstein sum convention, i.e. we sum over every repeated spacetime index.

Let  $A$  be a generally complex matrix,  $A^T$  its transpose, and  $A^*$  its complex conjugate. The hermitian conjugate matrix is then  $A^\dagger = (A^*)^T$ . Whenever the expression “+h.c.” appears in a formula, it means that the hermitian conjugate of the preceding quantity is to be added.

For the metric tensor we adopt the “mostly  $-$ ” or time-like convention, i.e.

$$g^{\mu\nu} = \begin{pmatrix} 1 & 0 & 0 & 0 \\ 0 & -1 & 0 & 0 \\ 0 & 0 & -1 & 0 \\ 0 & 0 & 0 & -1 \end{pmatrix}. \quad (\text{A.2})$$

As usual,  $\gamma^\mu$  represents the gamma-matrices fulfilling the anti-commutation relation

$$\{\gamma^\mu, \gamma^\nu\} = \gamma^\mu\gamma^\nu + \gamma^\nu\gamma^\mu = 2g^{\mu\nu}. \quad (\text{A.3})$$

We furthermore define a fifth  $\gamma$ -matrix  $\gamma^5 = i\gamma^0\gamma^1\gamma^2\gamma^3$  and  $\sigma^{\mu\nu} = \frac{i}{2}[\gamma^\mu, \gamma^\nu]$ .

When integrals in loop calculations diverge, we choose to regularise them with dimensional regularisation, i.e. we perform the integral in  $D = 4 - 2\epsilon$  spacetime dimensions. We furthermore adopt the modified minimal subtraction scheme if not stated otherwise.

For the first part of this thesis [Part I: Gluon-gluon to Higgs fusion in SCET](#), we used the position space formulation of SCET. The original papers [94,95] used a hybrid momentum-position space formulation instead known as label formalism. Here, momenta are split into a large constant momentum component and a small perturbation, which shows SCET's lineage from HQET. Label formalism is still used in recent work on the subject, and no clear advantages result from using one or the other [93].

## ACKNOWLEDGEMENTS

---

The acknowledgements have been removed from the electronic publication of this dissertation for privacy reasons.



## LIST OF FIGURES

---

Figure 2.1	Feynman diagrams contributing to the neutron decay $n \rightarrow p^+ e^- \bar{\nu}_e$ in the Standard Model (left) and in Fermi effective theory (right). . .	12
Figure 5.1	Leading order Feynman diagram for the fusion process $gg \rightarrow h$ via light quarks. The amplitude is proportional to the quark mass, giving a power-suppressed process. . . . .	29
Figure 5.2	Illustration of the matching process for $gg \rightarrow h$ . The perturbative physics above $m_b$ are combined in the form factor $F_{gg}$ , which is calculated using SCET. All non-perturbative effects are incorporated in the operator $O_{gg}$ , whose matrix element yields the gluon distribution functions in the proton when squared and integrated over phase space. . . . .	30
Figure 5.3	Leading momentum regions contributing to the matching of SCET <sub>1</sub> to QCD in $gg \rightarrow h$ via light quarks. The symbol $\otimes$ in the second row denotes a convolution integral over $z$ . . . . .	31
Figure 5.4	Factorisation of $O_3$ in SCET <sub>2</sub> . In the soft function, green double lines represent soft Wilson lines, red double lines soft Wilson lines in the adjoint representation, and the green single line denotes the soft quark propagator. The rectangular line-shape means that the soft function is defined as the discontinuity of the object shown. . . . .	34
Figure 5.5	Illustration of the relevant energy scales in the $gg \rightarrow h$ factorisation process. The different objects are shown at their respective scale. At the scale $m_b$ the perturbative form factor $F_{gg}$ is matched onto the low-energy effective theory LEFT, where only the operator $O_{gg}$ consisting of two collinear gluons contributes. The LEFT incorporates all non-perturbative physics. . . . .	34
Figure 5.6	Feynman diagrams contributing to the hard matching coefficients $H_i$ , $i = 1, 2, 3$ . Note that we omit mirror diagrams in the rows for $H_1$ and $H_2$ . . . . .	36
Figure 5.7	Feynman diagrams contributing to the soft functions $S_2(z)$ (top row) and $S_3$ (bottom row). The red double lines in $S_3$ denote soft Wilson lines in the adjoint representation. They are peculiar to the gluon case and lead to “tipi-tent” diagrams. . . . .	39

Figure 5.8 Feynman diagrams contributing to the jet function up to two-loop order in light-cone gauge. The left cross corresponds to the space-time point  $x$ , where the soft momentum  $p_s$  flows out, and the right cross corresponds to the point 0. The fourth diagram in the first row evaluates to zero since it is scaleless. Graphs where the external gluon is emitted off a quark also arise in the calculation of the jet function with an external photon [81] when the radiated gluon is exchanged for a photon. . . . . 40

Figure 5.9 Graphical illustration of the refactorisation conditions connecting different objects in the  $gg \rightarrow h$  factorisation formula to all orders in  $\alpha_s$ . The left panel portrays the first equation in (5.36), while the right panel illustrates the second equation. . . . . 41

Figure 5.10 Graphical illustration of the impact of the cutoffs on the convolution integrals over  $\ell_+$  and  $\ell_-$  in the last term of the bare factorisation formula (5.36). The “infinity bin” is subtracted twice and must be added back in the form of an extra contribution to the bare Wilson coefficient  $H_1^{(0)}$ . . . . . 42

Figure 5.11 The phase space of mismatch in  $T_2$  (yellow) and  $T_3$  (orange). The combination of those two is given by the purple region. It can be flipped into the blue region, which is purely hard. . . . . 52

Figure 5.12 Resummed  $T_3$  at LL (black), NLL (blue) and NLL' (red) accuracy. We fix the strong coupling constant at  $\alpha_s(M_h)$  and vary the hard scale  $\mu_h^2 = q^2$  entering the large logarithms  $L$  and expansion parameter  $\rho$ . The upper panel shows  $T_3$  for  $q^2 > 0$ , the lower two panels give the real and imaginary part for  $q^2 < 0$ . NLL(') corrections become increasingly more important for  $q^2$ -values further away from its physical value  $q^2 = -M_h^2$ . . . . . 71

Figure 6.1 One-loop diagrams accounting for operator mixing through Yukawa and gauge interactions. The shortly dashed line represents the ALP, the long dashed one the Higgs. . . . . 87

Figure 6.2 Examples of two diagrams that contribute with the same order of magnitude to the RGEs, if the coupling coefficients are taken to be equal. . . . . 87

Figure 6.3 Contributions to the matching corrections of the ALP–fermion couplings just below the weak scale. In the second diagram  $(V_1 V_2) = (WW), (ZZ), (Z\gamma)$  or  $(\gamma Z)$ . In the third and fourth diagram  $V = W, Z$ . In the sum of all graphs only the  $W$ -boson graph with internal top-quark loops (and the corresponding diagrams with Goldstone bosons) are non-vanishing. They lead to flavour-changing ALP couplings, even if the underlying UV theory is flavour-conserving. . . . . 92

Figure 6.4	Feynman diagrams contributing to the $K^- \rightarrow \pi^- a$ and $\bar{K}^0 \rightarrow \pi^0 a$ decay amplitudes at leading order in ALP- $\chi$ PT. The crossed circles denotes weak interaction vertices mediated by the $SU(3)$ octet operator $\mathcal{O}_8$ . The dots refer to interactions from Lagrangian (6.46). The first two diagrams in the second row vanish for neutral mesons. If all ALP couplings are assumed to be of the same order, the last diagram with the direct flavour-changing ALP interaction is the most dominant contribution. . . . .	100
Figure 6.5	Feynman diagrams contributing to the effective ALP-nucleon coupling. The ALP is either radiated off the nucleon directly, or stems from mixing with a radiated neutral pion. . . . .	103
Figure 6.6	Mass dependence of ALP-nucleon couplings for the proton (orange), the neutron (green), and an iso-singlet nucleus with coupling $g_{\text{singlet}} \equiv (g_{pa} + g_{na})/2$ (blue), in units of the ALP-gluon coupling $c_{GG}$ . The ALP couplings to quarks are set to zero ( $c_{uu} = c_{dd} = 0$ ). For nuclei with equal numbers of protons and neutrons, the mass dependence cancels out. However, it changes the interaction strength of ALPs with non-singlet nuclei significantly. . . . .	105
Figure 7.1	Feynman diagrams contributing to the $V \rightarrow \gamma a$ of the heavy vector mesons $J/\psi$ and $\Upsilon$ . . . . .	112
Figure 7.2	Feynman diagrams contributing to the chromomagnetic moment of the top-quark $\hat{\mu}_t$ . Note that there is a mirrored version of the first diagram, too. . . . .	114
Figure 7.3	Branching ratios of ALPs for our four benchmark scenarios, where the ALP couples only to gluons (top left), $W$ -bosons (top right), the left-handed quark doublet (bottom left), or the left-handed lepton doublet (bottom right) in the UV. Photon and charged lepton final states are given by solid lines, hadronic final states are indicated with dashed lines. . . . .	115
Figure 7.4	Left: Flavour bounds on ALP couplings to gluons with all other Wilson coefficients set to zero at $\Lambda = 4\pi f$ and $f = 1$ TeV. Right: Comparison of the same flavour constraints (light grey) with the constraints on $Z \rightarrow a\gamma$ decays from the LEP measurement of the $Z$ boson width (violet), contours of constant $\text{Br}(h \rightarrow aa) = 10^{-1}, 10^{-2}$ and $10^{-3}$ , depicted as red dotted, dashed and solid lines, and contours of constant $\text{Br}(h \rightarrow Za) = 10^{-1}, 10^{-2}$ and $10^{-3}$ , shown as blue dotted, dashed and solid lines, respectively. . . . .	116

Figure 7.5	Left: Flavour bounds on ALP couplings to $SU(2)_L$ gauge bosons with all other Wilson coefficients set to zero at $\Lambda = 4\pi f$ and $f = 1$ TeV. Right: Comparison of the same flavour constraints (light grey) with the constraints on $Z \rightarrow a\gamma$ decays from the LEP measurement of the $Z$ boson width (violet) and contours of constant $\text{Br}(h \rightarrow aa) = 10^{-1}, 10^{-2}$ and $10^{-3}$ depicted as red dotted, dashed and solid lines.	117
Figure 7.6	Left: Bounds on ALP couplings to photons [196]. The dashed contours indicate the part of the plot shown in various shades of grey in the right panel. Right: In colour, we show flavour bounds on ALPs coupling only to $SU(2)_L$ gauge bosons (same as in figure 7.5 above). They are compared to the grey astrophysical, beam dump and collider constraints on ALP couplings to photons with $c_{\gamma\gamma}^{\text{eff}} = c_{WW}$ . . .	119
Figure 7.7	Left: Flavour bounds on universal ALP couplings to quark doublets with $c_Q = c_Q \mathbb{1}$ , and all other Wilson coefficients set to zero at the scale $\Lambda = 4\pi f$ and $f = 1$ TeV. Right: Constraints from flavour observables (light grey) are compared to the constraint from $Z \rightarrow a\gamma$ decays from the LEP measurement of the $Z$ boson width. Contours of constant $\text{Br}(h \rightarrow aa) = 10^{-1}, 10^{-2}$ and $10^{-3}$ are depicted as red dotted, dashed and solid lines, respectively. Contours of constant $\text{Br}(h \rightarrow Za) = 10^{-1}, 10^{-2}$ and $10^{-3}$ are shown as blue dotted, dashed and solid lines, respectively. . . . .	120
Figure 7.8	Left: Flavour bounds on universal ALP couplings to lepton doublets with $c_L = c_L \mathbb{1}$ , and all other Wilson coefficients zero at the scale $\Lambda = 4\pi f$ and $f = 1$ TeV. Right: Contours of constant $\text{Br}(h \rightarrow aa) = 10^{-1}, 10^{-2}$ and $10^{-3}$ are depicted as red dotted, dashed and solid lines, respectively. Contours of constant $\text{Br}(h \rightarrow Za) = 10^{-1}$ and $10^{-2}$ are shown as blue dashed and solid lines, respectively. . . . .	121
Figure 7.9	Left: Astrophysical, beam dump, and collider constraints on ALP couplings to leptons $c_{\ell\ell} = c_e - c_L$ (see text for further details). Right: In colour, we show flavour constraints on ALPs coupling to $SU(2)_L$ lepton doublets, as in figure 7.8 above. For easy comparison, the black contours depict the bounds from the left panel. . . . .	122
Figure 7.10	Feynman diagrams contributing to LFV electromagnetic form factors. Note that there is a mirrored version of the first diagram, too. . . . .	122
Figure 7.11	Bounds on ALP mediated flavour off-diagonal transitions between muons and electrons with $c_{\mu e} \equiv \sqrt{ [k_E]_{21} ^2 +  [k_e]_{21} ^2}$ , assuming universal ALP couplings to leptons as indicated above the plot for the different ALP mass regions. . . . .	132



## LIST OF TABLES

---

Table 2.1	The fermions of the SM and their representations under the SM gauge group $SU(3)_c \times SU(2)_L \times U(1)_Y$ . . . . .	8
Table 5.1	Naming schemes for logarithmic accuracy in $T_3(\mu)$ . We list perturbative orders of the cusp anomalous dimension, non-cusp anomalous dimensions $\gamma$ , QCD $\beta$ function, and matching corrections from the component functions to obtain resummation at a given logarithmic order. . . . .	64
Table 7.1	Summary of indicative constraints on quark flavour-violating ALP couplings renormalised at the scale $\mu_w = m_t$ , derived from measurements of branching fractions (first column) for various decays of kaons and $B$ mesons in a mass range where an on-shell ALP can be produced. The relevant measurements and SM predictions (where appropriate) are given in <a href="#">AII.3</a> to <a href="#">AII.8</a> in appendix <a href="#">AII.1</a> . In each line, the limit cited is the strongest limit found within the mass range probed by the measurement. In the fifth column the symbol $\mathcal{B}$ denotes the ALP branching ratio to the relevant final state. Asterisks next to the mass range mean that cuts are applied within the mass range to exclude resonance regions, and therefore the corresponding measurement is insensitive to an ALP with mass in the excluded ranges. The excluded regions are as follows. (*): $100 \text{ MeV} < m_{\nu\bar{\nu}} < 161 \text{ MeV}$ ; (**): $525 \text{ MeV} < m_{\mu\mu} < 1250 \text{ MeV}$ ; (***) : $990 \text{ MeV} < m_{\mu\mu} < 1050 \text{ MeV}$ ; (✱): $950 \text{ MeV} < m_{ee} < 1050 \text{ MeV}$ ; (✱✱): $100 \text{ MeV} < m_{\gamma\gamma} < 160 \text{ MeV}$ ; (‡): $935 \text{ MeV} < m_{ee} < 1053 \text{ MeV}$ ; (‡‡): $8.0 \text{ GeV}^2 < m_{\mu\mu}^2 < 11.0 \text{ GeV}^2$ and $12.5 \text{ GeV}^2 < m_{\mu\mu}^2 < 15.0 \text{ GeV}^2$ ; (†): various cuts are applied to exclude the regions around the $J/\psi$ , $\psi(2S)$ and $\psi(3370)$ resonances; (††): $525 \text{ MeV} < m_{\mu\mu} < 1250 \text{ MeV}$ . . . . .	111
Table 7.2	Summary of constraints on the lepton flavour-violating ALP coupling $c_{e\mu}$ derived from measurements of branching fractions (first column) for various muon decays, in which the lepton can decay to an on-shell ALP. The measurements and SM predictions (where appropriate) are given in <a href="#">AII.9</a> in appendix <a href="#">AII.1</a> . The limit cited is the strongest limit found within the mass range probed by the measurement. In the fifth column the symbol $\mathcal{B}$ denotes the ALP branching ratio into the relevant final state. (†): these bounds depend on the chirality of the ALP couplings due to the experimental setup, see [ <a href="#">313</a> , <a href="#">330</a> , <a href="#">331</a> ] for details. Here we assume $[k_e]_{12} = [k_E]_{12}$ for these. . . . .	130

Table AII.3	Observables relevant for a long lived ALP. Bounds are at 90% CL. (*) : cuts are applied to exclude the region around $m_\pi$ ( $100 \text{ MeV} < m_X < 161 \text{ MeV}$ ). . . . .	133
Table AII.4	Observables with a photon pair in the final state. Bounds are at 90% CL. (‡) : cuts are applied to exclude the region around the pion pole ( $100 \text{ MeV} < m_{\gamma\gamma} < 160 \text{ MeV}$ ). († : calculated from results in the given reference. Error bars estimated from varying parameter $\hat{c}$ between its quoted errors.) (* : calculated from results in the given reference. Error bars estimated from varying parameter $a_V$ between its quoted errors.) . . . . .	133
Table AII.5	Observables with an electron pair in the final state. Bounds are at 90% CL. Here we only include observables for which the electron invariant mass can be below or near the dimuon threshold, on the grounds that above it muonic observables will generically provide stronger bounds. Predictions without accompanying citations have been calculated using flavio [367]. In the measurements of the $D_{(s)}$ branching ratios, cuts are applied to exclude the region around the $\phi$ resonance. For the BaBar measurements with a (*), the excluded region is $950 \text{ MeV} < m_{ee} < 1050 \text{ MeV}$ , while the BESIII measurement with a (†) excludes the region $935 \text{ MeV} < m_{ee} < 1053 \text{ MeV}$ . Since the long-distance contributions to these decays peak around this excluded resonance, we take the SM prediction to be only due to the short-distance contributions, as calculated in Ref. [365]. . . . .	134
Table AII.6	Observables with a muon pair in the final state. Bounds are at 90% CL. (†) : cuts are applied to exclude regions around the $J/\psi$ , $\psi(2S)$ and $\psi(3370)$ resonances. (‡) : cuts are applied to exclude charmonium resonance regions ( $8.0 \text{ GeV}^2 < m_{\mu\mu}^2 < 11.0 \text{ GeV}^2$ and $12.5 \text{ GeV}^2 < m_{\mu\mu}^2 < 15.0 \text{ GeV}^2$ are excluded).(*) : a large region containing the $\eta$ , $\rho/\omega$ and $\phi$ resonances is excluded ( $525 \text{ MeV} < m_{\mu\mu} < 1250 \text{ MeV}$ ).(**) : cuts are applied to exclude the region around the $\phi$ resonance ( $990 \text{ MeV} < m_{\mu\mu} < 1050 \text{ MeV}$ ). Since the long-distance contributions to the $D_{(s)}$ decays peak around the excluded resonance(s), we take the SM prediction to be only due to the short-distance contributions, as calculated in Ref. [365]. . . . .	135
Table AII.7	Observables with a tau pair in the final state. Bounds are at 90% CL.	135
Table AII.8	Observables relevant for hadronic decays of the ALP. . . . .	136

Table AII.9	<p>Lepton flavour-violating observables. Where a mass range for <math>m_a</math> is given, the range refers to masses that are consistent with the experimental cuts and for which the decay can proceed via a resonant ALP. For some of the observables (for example <math>\mu \rightarrow 3e</math>), an ALP lying outside of this mass range may still be constrained by the experiment, if it can mediate the decay off-shell. Where the mass range is left blank, the measurement can never involve a resonant ALP. *: for the <math>\mu \rightarrow ea</math>(invisible) searches, the precise bound depends on the chirality of the ALP couplings due to the experimental setup and the bounds quoted here are assuming vectorial couplings, see [313,330,331] for details. . . . .</p>	136
Table AII.10	<p>Cuts on the decay time of the ALP that should be applied in various LFV experiments. . . . .</p>	136



## BIBLIOGRAPHY

---

- [1] Z. L. Liu, M. Neubert, M. Schnubel and X. Wang, *Radiative quark jet function with an external gluon*, *JHEP* **02** (2022) 075, [[2112.00018](#)].
- [2] M. Schnubel, *The two-loop radiative gluon jet function for  $gg \rightarrow h$  via a light quark loop*, *SciPost Phys. Proc.* **7** (2022) 039, [[2110.05322](#)].
- [3] Z. L. Liu, M. Neubert, M. Schnubel and X. Wang, *Factorization at Next-to-Leading Power and Endpoint Divergences in  $gg \rightarrow h$  Production*, [[2212.10447](#)].
- [4] M. Bauer, M. Neubert, S. Renner, M. Schnubel and A. Thamm, *Axionlike Particles, Lepton-Flavor Violation, and a New Explanation of  $a_\mu$  and  $a_e$* , *Phys. Rev. Lett.* **124** (2020) 211803, [[1908.00008](#)].
- [5] M. Bauer, M. Neubert, S. Renner, M. Schnubel and A. Thamm, *The Low-Energy Effective Theory of Axions and ALPs*, *JHEP* **04** (2021) 063, [[2012.12272](#)].
- [6] M. Bauer, M. Neubert, S. Renner, M. Schnubel and A. Thamm, *Consistent Treatment of Axions in the Weak Chiral Lagrangian*, *Phys. Rev. Lett.* **127** (2021) 081803, [[2102.13112](#)].
- [7] M. Bauer, M. Neubert, S. Renner, M. Schnubel and A. Thamm, *Flavor probes of axion-like particles*, *JHEP* **09** (2022) 056, [[2110.10698](#)].
- [8] E. Goudzovski et al., *New Physics Searches at Kaon and Hyperon Factories*, [[2201.07805](#)].
- [9] A. Lightman, *The Discoveries : Great Breakthroughs in 20th-Century Science, Including the Original Papers* . Knopf Canada, 2005.
- [10] F. Englert and R. Brout, *Broken Symmetry and the Mass of Gauge Vector Mesons*, *Phys. Rev. Lett.* **13** (1964) 321–323.
- [11] P. W. Higgs, *Broken symmetries, massless particles and gauge fields*, *Phys. Lett.* **12** (1964) 132–133.
- [12] P. W. Higgs, *Broken Symmetries and the Masses of Gauge Bosons*, *Phys. Rev. Lett.* **13** (1964) 508–509.
- [13] G. S. Guralnik, C. R. Hagen and T. W. B. Kibble, *Global Conservation Laws and Massless Particles*, *Phys. Rev. Lett.* **13** (1964) 585–587.
- [14] P. W. Higgs, *Spontaneous Symmetry Breakdown without Massless Bosons*, *Phys. Rev.* **145** (1966) 1156–1163.
- [15] T. W. B. Kibble, *Symmetry breaking in nonAbelian gauge theories*, *Phys. Rev.* **155** (1967) 1554–1561.
- [16] ATLAS collaboration, G. Aad et al., *Observation of a new particle in the search for the Standard Model Higgs boson with the ATLAS detector at the LHC*, *Phys. Lett. B* **716** (2012) 1–29, [[1207.7214](#)].

- [17] CMS collaboration, S. Chatrchyan et al., *Observation of a New Boson at a Mass of 125 GeV with the CMS Experiment at the LHC*, *Phys. Lett. B* **716** (2012) 30–61, [1207.7235].
- [18] PARTICLE DATA GROUP collaboration, R. L. Workman et al., *Review of Particle Physics*, *PTEP* **2022** (2022) 083C01.
- [19] S. Catani, D. de Florian and M. Grazzini, *Universality of nonleading logarithmic contributions in transverse momentum distributions*, *Nucl. Phys. B* **596** (2001) 299–312, [hep-ph/0008184].
- [20] Y. Nakahama and on behalf of the ATLAS Collaboration, *The ATLAS Trigger System: Ready for Run-2*, *Journal of Physics: Conference Series* **664** (dec, 2015) 082037.
- [21] C. N. Yang, *Fermi's beta-decay Theory*, *Asia Pac. Phys. Newslett.* **01** (2012) 27–30.
- [22] W. D. Goldberger and I. Z. Rothstein, *An Effective field theory of gravity for extended objects*, *Phys. Rev. D* **73** (2006) 104029, [hep-th/0409156].
- [23] R. A. Porto, *Post-Newtonian corrections to the motion of spinning bodies in NRGR*, *Phys. Rev. D* **73** (2006) 104031, [gr-qc/0511061].
- [24] B. Kol and M. Smolkin, *Non-Relativistic Gravitation: From Newton to Einstein and Back*, *Class. Quant. Grav.* **25** (2008) 145011, [0712.4116].
- [25] J. Bardeen, L. N. Cooper and J. R. Schrieffer, *Microscopic theory of superconductivity*, *Phys. Rev.* **106** (Apr, 1957) 162–164.
- [26] J. Bardeen, L. N. Cooper and J. R. Schrieffer, *Theory of superconductivity*, *Phys. Rev.* **108** (Dec, 1957) 1175–1204.
- [27] D. A. Roberts, S. Yaida and B. Hanin, *The Principles of Deep Learning Theory*. Cambridge University Press, 2022.
- [28] Z. L. Liu and M. Neubert, *Factorization at subleading power and endpoint-divergent convolutions in  $h \rightarrow \gamma\gamma$  decay*, *JHEP* **04** (2020) 033, [1912.08818].
- [29] Z. L. Liu, B. Mecaj, M. Neubert and X. Wang, *Factorization at subleading power and endpoint divergences in  $h \rightarrow \gamma\gamma$  decay. Part II. Renormalization and scale evolution*, *JHEP* **01** (2021) 077, [2009.06779].
- [30] S. L. Glashow, *Partial Symmetries of Weak Interactions*, *Nucl. Phys.* **22** (1961) 579–588.
- [31] S. Weinberg, *A Model of Leptons*, *Phys. Rev. Lett.* **19** (1967) 1264–1266.
- [32] A. Salam, *Weak and Electromagnetic Interactions*, *Conf. Proc. C* **680519** (1968) 367–377.
- [33] G. 't Hooft and M. J. G. Veltman, *Regularization and Renormalization of Gauge Fields*, *Nucl. Phys. B* **44** (1972) 189–213.
- [34] C.-N. Yang and R. L. Mills, *Conservation of Isotopic Spin and Isotopic Gauge Invariance*, *Phys. Rev.* **96** (1954) 191–195.
- [35] M. Gell-Mann, *A Schematic Model of Baryons and Mesons*, *Phys. Lett.* **8** (1964) 214–215.
- [36] G. Zweig, *An SU(3) model for strong interaction symmetry and its breaking. Version 2*, pp. 22–101. 2, 1964.
- [37] G. Zweig, *An SU(3) model for strong interaction symmetry and its breaking. Version 1*, .

- [38] H. Fritzsch, M. Gell-Mann and H. Leutwyler, *Advantages of the Color Octet Gluon Picture*, *Phys. Lett. B* **47** (1973) 365–368.
- [39] D. J. Gross and F. Wilczek, *Ultraviolet Behavior of Nonabelian Gauge Theories*, *Phys. Rev. Lett.* **30** (1973) 1343–1346.
- [40] H. D. Politzer, *Reliable Perturbative Results for Strong Interactions?*, *Phys. Rev. Lett.* **30** (1973) 1346–1349.
- [41] M. E. Peskin and D. V. Schroeder, *An Introduction to quantum field theory*. Addison-Wesley, Reading, USA, 1995.
- [42] M. D. Schwartz, *Quantum Field Theory and the Standard Model*. Cambridge University Press, 3, 2014.
- [43] S. Weinberg, *The Quantum Theory of Fields*, vol. 1. Cambridge University Press, 1995, [10.1017/CBO9781139644167](https://doi.org/10.1017/CBO9781139644167).
- [44] S. Weinberg, *The Quantum Theory of Fields*, vol. 2. Cambridge University Press, 1996, [10.1017/CBO9781139644174](https://doi.org/10.1017/CBO9781139644174).
- [45] N. Cabibbo, *Unitary Symmetry and Leptonic Decays*, *Phys. Rev. Lett.* **10** (1963) 531–533.
- [46] M. Kobayashi and T. Maskawa, *CP Violation in the Renormalizable Theory of Weak Interaction*, *Prog. Theor. Phys.* **49** (1973) 652–657.
- [47] S. L. Glashow, J. Iliopoulos and L. Maiani, *Weak interactions with lepton-hadron symmetry*, *Phys. Rev. D* **2** (Oct, 1970) 1285–1292.
- [48] B. Björken and S. Glashow, *Elementary particles and su(4)*, *Physics Letters* **11** (1964) 255–257.
- [49] Y. Nambu, *Quasiparticles and Gauge Invariance in the Theory of Superconductivity*, *Phys. Rev.* **117** (1960) 648–663.
- [50] J. Goldstone, *Field Theories with Superconductor Solutions*, *Nuovo Cim.* **19** (1961) 154–164.
- [51] M. Gockeler, R. Horsley, V. Linke, P. E. L. Rakow, G. Schierholz and H. Stuben, *Is there a Landau pole problem in QED?*, *Phys. Rev. Lett.* **80** (1998) 4119–4122, [[hep-th/9712244](https://arxiv.org/abs/hep-th/9712244)].
- [52] ALPHA collaboration, M. Dalla Brida, P. Fritzsche, T. Korzec, A. Ramos, S. Sint and R. Sommer, *Determination of the QCD  $\Lambda$ -parameter and the accuracy of perturbation theory at high energies*, *Phys. Rev. Lett.* **117** (2016) 182001, [[1604.06193](https://arxiv.org/abs/1604.06193)].
- [53] K. G. Wilson, *Confinement of Quarks*, *Phys. Rev. D* **10** (1974) 2445–2459.
- [54] PARTICLE DATA GROUP collaboration, M. Tanabashi et al., *Review of Particle Physics*, *Phys. Rev. D* **98** (2018) 030001.
- [55] B. Grzadkowski, M. Iskrzynski, M. Misiak and J. Rosiek, *Dimension-Six Terms in the Standard Model Lagrangian*, *JHEP* **10** (2010) 085, [[1008.4884](https://arxiv.org/abs/1008.4884)].
- [56] G. Passarino and M. Trott, *The Standard Model Effective Field Theory and Next to Leading Order*, [[1610.08356](https://arxiv.org/abs/1610.08356)].
- [57] I. Brivio and M. Trott, *The Standard Model as an Effective Field Theory*, *Phys. Rept.* **793** (2019) 1–98, [[1706.08945](https://arxiv.org/abs/1706.08945)].



- [58] T. Yanagida, *Horizontal gauge symmetry and masses of neutrinos*, *Conf. Proc. C* **7902131** (1979) 95–99.
- [59] SNO collaboration, Q. R. Ahmad et al., *Direct evidence for neutrino flavor transformation from neutral current interactions in the Sudbury Neutrino Observatory*, *Phys. Rev. Lett.* **89** (2002) 011301, [[nucl-ex/0204008](#)].
- [60] SUPER-KAMIOKANDE collaboration, Y. Fukuda et al., *Evidence for oscillation of atmospheric neutrinos*, *Phys. Rev. Lett.* **81** (1998) 1562–1567, [[hep-ex/9807003](#)].
- [61] G. Bertone, D. Hooper and J. Silk, *Particle dark matter: Evidence, candidates and constraints*, *Phys. Rept.* **405** (2005) 279–390, [[hep-ph/0404175](#)].
- [62] G. Bertone and D. Hooper, *History of dark matter*, *Rev. Mod. Phys.* **90** (2018) 045002, [[1605.04909](#)].
- [63] LHCb collaboration, R. Aaij et al., *Test of lepton universality with  $B^0 \rightarrow K^{*0} \ell^+ \ell^-$  decays*, *JHEP* **08** (2017) 055, [[1705.05802](#)].
- [64] LHCb collaboration, R. Aaij et al., *Test of lepton universality in beauty-quark decays*, *Nature Phys.* **18** (2022) 277–282, [[2103.11769](#)].
- [65] LHCb collaboration, *Measurement of lepton universality parameters in  $B^+ \rightarrow K^+ \ell^+ \ell^-$  and  $B^0 \rightarrow K^{*0} \ell^+ \ell^-$  decays*, [[2212.09153](#)].
- [66] H.-W. Hammer and U.-G. Meißner, *The proton radius: From a puzzle to precision*, *Sci. Bull.* **65** (2020) 257–258, [[1912.03881](#)].
- [67] Y.-H. Lin, H.-W. Hammer and U.-G. Meißner, *New Insights into the Nucleon’s Electromagnetic Structure*, *Phys. Rev. Lett.* **128** (2022) 052002, [[2109.12961](#)].
- [68] M. A. Belushkin, H. W. Hammer and U. G. Meissner, *Dispersion analysis of the nucleon form-factors including meson continua*, *Phys. Rev. C* **75** (2007) 035202, [[hep-ph/0608337](#)].
- [69] N. Bezginov, T. Valdez, M. Horbatsch, A. Marsman, A. C. Vutha and E. A. Hessels, *A measurement of the atomic hydrogen lamb shift and the proton charge radius*, *Science* **365** (2019) 1007–1012, [<https://www.science.org/doi/pdf/10.1126/science.aau7807>].
- [70] X. Yan, D. W. Higinbotham, D. Dutta, H. Gao, A. Gasparian, M. A. Khandaker et al., *Robust extraction of the proton charge radius from electron-proton scattering data*, *Phys. Rev. C* **98** (2018) 025204, [[1803.01629](#)].
- [71] W. Xiong et al., *A small proton charge radius from an electron–proton scattering experiment*, *Nature* **575** (2019) 147–150.
- [72] MUON G-2 collaboration, G. W. Bennett et al., *Final Report of the Muon E821 Anomalous Magnetic Moment Measurement at BNL*, *Phys. Rev.* **D73** (2006) 072003, [[hep-ex/0602035](#)].
- [73] MUON G-2 collaboration, B. Abi et al., *Measurement of the Positive Muon Anomalous Magnetic Moment to 0.46 ppm*, *Phys. Rev. Lett.* **126** (2021) 141801, [[2104.03281](#)].
- [74] T. Aoyama et al., *The anomalous magnetic moment of the muon in the Standard Model*, *Phys. Rept.* **887** (2020) 1–166, [[2006.04822](#)].
- [75] S. Borsanyi et al., *Leading hadronic contribution to the muon magnetic moment from lattice QCD*, *Nature* **593** (2021) 51–55, [[2002.12347](#)].



- [76] CERN, “Run 3 of the large hadron collider.”  
<https://home.cern/press/2022/run-3>, 2022.
- [77] M. L. Czakon and M. Niggetiedt, *Exact quark-mass dependence of the Higgs-gluon form factor at three loops in QCD*, *JHEP* **05** (2020) 149, [2001.03008].
- [78] J. Aparisi et al., *mb at mH: The Running Bottom Quark Mass and the Higgs Boson*, *Phys. Rev. Lett.* **128** (2022) 122001, [2110.10202].
- [79] Z. L. Liu, B. Mecaj, M. Neubert, X. Wang and S. Fleming, *Renormalization and Scale Evolution of the Soft-Quark Soft Function*, *JHEP* **07** (2020) 104, [2005.03013].
- [80] Z. L. Liu, B. Mecaj, M. Neubert and X. Wang, *Factorization at subleading power, Sudakov resummation, and endpoint divergences in soft-collinear effective theory*, *Phys. Rev. D* **104** (2021) 014004, [2009.04456].
- [81] Z. L. Liu and M. Neubert, *Two-Loop Radiative Jet Function for Exclusive B-Meson and Higgs Decays*, *JHEP* **06** (2020) 060, [2003.03393].
- [82] M. A. Ebert, I. Moulton, I. W. Stewart, F. J. Tackmann, G. Vita and H. X. Zhu, *Subleading power rapidity divergences and power corrections for  $q_T$* , *JHEP* **04** (2019) 123, [1812.08189].
- [83] M. Beneke, M. Garny, R. Szafron and J. Wang, *Violation of the Kluberg-Stern-Zuber theorem in SCET*, *JHEP* **09** (2019) 101, [1907.05463].
- [84] I. Moulton, I. W. Stewart and G. Vita, *Subleading Power Factorization with Radiative Functions*, *JHEP* **11** (2019) 153, [1905.07411].
- [85] I. Moulton, I. W. Stewart, G. Vita and H. X. Zhu, *The Soft Quark Sudakov*, *JHEP* **05** (2020) 089, [1910.14038].
- [86] M. Beneke, A. Broggio, S. Jaskiewicz and L. Vernazza, *Threshold factorization of the Drell-Yan process at next-to-leading power*, *JHEP* **07** (2020) 078, [1912.01585].
- [87] I. Moulton, G. Vita and K. Yan, *Subleading power resummation of rapidity logarithms: the energy-energy correlator in  $\mathcal{N} = 4$  SYM*, *JHEP* **07** (2020) 005, [1912.02188].
- [88] J. Wang, *Resummation of double logarithms in loop-induced processes with effective field theory*, [1912.09920].
- [89] M. Beneke, M. Garny, S. Jaskiewicz, R. Szafron, L. Vernazza and J. Wang, *Large- $x$  resummation of off-diagonal deep-inelastic parton scattering from  $d$ -dimensional refactorization*, *JHEP* **10** (2020) 196, [2008.04943].
- [90] M. Beneke, M. Garny, S. Jaskiewicz, J. Strohm, R. Szafron, L. Vernazza et al., *Next-to-leading power endpoint factorization and resummation for off-diagonal “gluon” thrust*, *JHEP* **07** (2022) 144, [2205.04479].
- [91] G. Bell, P. Böer and T. Feldmann, *Muon-electron backward scattering: a prime example for endpoint singularities in SCET*, *JHEP* **09** (2022) 183, [2205.06021].
- [92] M. Beneke, M. Garny, S. Jaskiewicz, J. Strohm, R. Szafron, L. Vernazza et al., *Endpoint factorization and next-to-leading power resummation of gluon thrust*, *PoS LL2022* (2022) 068, [2207.14199].
- [93] T. Becher, A. Broggio and A. Ferroglia, *Introduction to Soft-Collinear Effective Theory*, vol. 896. Springer, 2015, 10.1007/978-3-319-14848-9.

- [94] C. W. Bauer, S. Fleming, D. Pirjol and I. W. Stewart, *An Effective field theory for collinear and soft gluons: Heavy to light decays*, *Phys. Rev. D* **63** (2001) 114020, [[hep-ph/0011336](#)].
- [95] C. W. Bauer, D. Pirjol and I. W. Stewart, *Soft collinear factorization in effective field theory*, *Phys. Rev. D* **65** (2002) 054022, [[hep-ph/0109045](#)].
- [96] M. Beneke and T. Feldmann, *Factorization of heavy to light form-factors in soft collinear effective theory*, *Nucl. Phys. B* **685** (2004) 249–296, [[hep-ph/0311335](#)].
- [97] R. J. Hill and M. Neubert, *Spectator interactions in soft collinear effective theory*, *Nucl. Phys. B* **657** (2003) 229–256, [[hep-ph/0211018](#)].
- [98] C. W. Bauer, S. Fleming, D. Pirjol, I. Z. Rothstein and I. W. Stewart, *Hard scattering factorization from effective field theory*, *Phys. Rev. D* **66** (2002) 014017, [[hep-ph/0202088](#)].
- [99] M. Beneke and T. Feldmann, *Multipole expanded soft collinear effective theory with nonAbelian gauge symmetry*, *Phys. Lett. B* **553** (2003) 267–276, [[hep-ph/0211358](#)].
- [100] A. V. Manohar, T. Mehen, D. Pirjol and I. W. Stewart, *Reparameterization invariance for collinear operators*, *Phys. Lett. B* **539** (2002) 59–66, [[hep-ph/0204229](#)].
- [101] T. Becher, *Soft-Collinear Effective Theory*, [[1803.04310](#)].
- [102] A. M. Polyakov, *Gauge Fields as Rings of Glue*, *Nucl. Phys. B* **164** (1980) 171–188.
- [103] R. A. Brandt, F. Neri and M.-a. Sato, *Renormalization of Loop Functions for All Loops*, *Phys. Rev. D* **24** (1981) 879.
- [104] I. A. Korchemskaya and G. P. Korchemsky, *On lightlike Wilson loops*, *Phys. Lett. B* **287** (1992) 169–175.
- [105] M. Beneke and V. A. Smirnov, *Asymptotic expansion of Feynman integrals near threshold*, *Nucl. Phys. B* **522** (1998) 321–344, [[hep-ph/9711391](#)].
- [106] V. A. Smirnov and E. R. Rakhmetov, *The Strategy of regions for asymptotic expansion of two loop vertex Feynman diagrams*, *Theor. Math. Phys.* **120** (1999) 870–875, [[hep-ph/9812529](#)].
- [107] V. A. Smirnov, *Applied asymptotic expansions in momenta and masses*, *Springer Tracts Mod. Phys.* **177** (2002) 1–262.
- [108] M. Beneke, A. P. Chapovsky, M. Diehl and T. Feldmann, *Soft collinear effective theory and heavy to light currents beyond leading power*, *Nucl. Phys. B* **643** (2002) 431–476, [[hep-ph/0206152](#)].
- [109] T. Becher and G. Bell, *The gluon jet function at two-loop order*, *Phys. Lett. B* **695** (2011) 252–258, [[1008.1936](#)].
- [110] O. V. Tarasov, *A New approach to the momentum expansion of multiloop Feynman diagrams*, *Nucl. Phys. B* **480** (1996) 397–412, [[hep-ph/9606238](#)].
- [111] R. N. Lee, *Space-time dimensionality  $D$  as complex variable: Calculating loop integrals using dimensional recurrence relation and analytical properties with respect to  $D$* , *Nucl. Phys. B* **830** (2010) 474–492, [[0911.0252](#)].
- [112] E. Panzer, *Algorithms for the symbolic integration of hyperlogarithms with applications to Feynman integrals*, *Comput. Phys. Commun.* **188** (2015) 148–166, [[1403.3385](#)].

- [113] T. Huber and D. Maitre, *HypExp: A Mathematica package for expanding hypergeometric functions around integer-valued parameters*, *Comput. Phys. Commun.* **175** (2006) 122–144, [[hep-ph/0507094](#)].
- [114] T. Becher and M. Neubert, *Infrared singularities of scattering amplitudes in perturbative QCD*, *Phys. Rev. Lett.* **102** (2009) 162001, [[0901.0722](#)].
- [115] U. Aglietti, R. Bonciani, G. Degrossi and A. Vicini, *Analytic Results for Virtual QCD Corrections to Higgs Production and Decay*, *JHEP* **01** (2007) 021, [[hep-ph/0611266](#)].
- [116] T. Becher and M. Neubert, *On the Structure of Infrared Singularities of Gauge-Theory Amplitudes*, *JHEP* **06** (2009) 081, [[0903.1126](#)].
- [117] S. Catani, *The Singular behavior of QCD amplitudes at two loop order*, *Phys. Lett. B* **427** (1998) 161–171, [[hep-ph/9802439](#)].
- [118] S. W. Bosch, B. O. Lange, M. Neubert and G. Paz, *Factorization and shape function effects in inclusive B meson decays*, *Nucl. Phys. B* **699** (2004) 335–386, [[hep-ph/0402094](#)].
- [119] A. G. Grozin and M. Neubert, *Asymptotics of heavy meson form-factors*, *Phys. Rev. D* **55** (1997) 272–290, [[hep-ph/9607366](#)].
- [120] B. O. Lange and M. Neubert, *Renormalization group evolution of the B meson light cone distribution amplitude*, *Phys. Rev. Lett.* **91** (2003) 102001, [[hep-ph/0303082](#)].
- [121] G. T. Bodwin, J.-H. Ee, J. Lee and X.-P. Wang, *Analyticity, renormalization, and evolution of the soft-quark function*, *Phys. Rev. D* **104** (2021) 016010, [[2101.04872](#)].
- [122] A. K. Rathie, *A new generalization of generalized hypergeometric functions*, *Le Matematiche* **LII** (1997) 297–310, [[1206.0350](#)].
- [123] I. S. Ansari, F. Yilmaz, M. Alouini and O. Kucur, *New results on the sum of gamma random variates with application to the performance of wireless communication systems over nakagami-m fading channels*, *CoRR* **abs/1202.2576** (2012) , [[1202.2576](#)].
- [124] I. S. Ansari, F. Yilmaz and M. Alouini, *On the sum of squared  $\eta$ - $\mu$ random variates with application to the performance of wireless communication systems*, *CoRR* **abs/1210.0100** (2012) , [[1210.0100](#)].
- [125] S. De, Y. Hu, A. Yellespur Srikant and A. Volovich, *Correlators of four light-ray operators in CCFT*, *JHEP* **10** (2022) 170, [[2206.08875](#)].
- [126] X. Wang, *Next-to-leading power SCET in Higgs amplitudes induced by light quarks*, *SciPost Phys. Proc.* **7** (2022) 040, [[2110.05174](#)].
- [127] T. Liu and A. A. Penin, *High-Energy Limit of QCD beyond the Sudakov Approximation*, *Phys. Rev. Lett.* **119** (2017) 262001, [[1709.01092](#)].
- [128] C. Anastasiou and A. Penin, *Light Quark Mediated Higgs Boson Threshold Production in the Next-to-Leading Logarithmic Approximation*, *JHEP* **07** (2020) 195, [[2004.03602](#)].
- [129] Z. L. Liu, B. Mecaj, M. Neubert and X. Wang, *Resummation of  $h \rightarrow \gamma\gamma$  at NNLL, to be published* .
- [130] K. G. Chetyrkin, *Quark mass anomalous dimension to  $O(\alpha_s^4)$* , *Phys. Lett. B* **404** (1997) 161–165, [[hep-ph/9703278](#)].

- [131] J. A. M. Vermaseren, S. A. Larin and T. van Ritbergen, *The four loop quark mass anomalous dimension and the invariant quark mass*, *Phys. Lett. B* **405** (1997) 327–333, [[hep-ph/9703284](#)].
- [132] G. P. Korchemsky and A. V. Radyushkin, *Renormalization of the Wilson Loops Beyond the Leading Order*, *Nucl. Phys. B* **283** (1987) 342–364.
- [133] S. Moch, J. A. M. Vermaseren and A. Vogt, *The Quark form-factor at higher orders*, *JHEP* **08** (2005) 049, [[hep-ph/0507039](#)].
- [134] T. Becher, M. Neubert and B. D. Pecjak, *Factorization and Momentum-Space Resummation in Deep-Inelastic Scattering*, *JHEP* **01** (2007) 076, [[hep-ph/0607228](#)].
- [135] R. D. Peccei and H. R. Quinn, *CP Conservation in the Presence of Instantons*, *Phys. Rev. Lett.* **38** (1977) 1440–1443.
- [136] R. D. Peccei and H. R. Quinn, *Constraints Imposed by CP Conservation in the Presence of Instantons*, *Phys. Rev.* **D16** (1977) 1791–1797.
- [137] S. Weinberg, *A New Light Boson?*, *Phys. Rev. Lett.* **40** (1978) 223–226.
- [138] F. Wilczek, *Problem of Strong P and T Invariance in the Presence of Instantons*, *Phys. Rev. Lett.* **40** (1978) 279–282.
- [139] C. Abel et al., *Measurement of the Permanent Electric Dipole Moment of the Neutron*, *Phys. Rev. Lett.* **124** (2020) 081803, [[2001.11966](#)].
- [140] H. M. Georgi, L. J. Hall and M. B. Wise, *Grand Unified Models With an Automatic Peccei-Quinn Symmetry*, *Nucl. Phys. B* **192** (1981) 409–416.
- [141] G. Lazarides, C. Panagiotakopoulos and Q. Shafi, *Phenomenology and Cosmology With Superstrings*, *Phys. Rev. Lett.* **56** (1986) 432.
- [142] M. Kamionkowski and J. March-Russell, *Planck scale physics and the Peccei-Quinn mechanism*, *Phys. Lett. B* **282** (1992) 137–141, [[hep-th/9202003](#)].
- [143] R. Holman, S. D. H. Hsu, T. W. Kephart, E. W. Kolb, R. Watkins and L. M. Widrow, *Solutions to the strong CP problem in a world with gravity*, *Phys. Lett. B* **282** (1992) 132–136, [[hep-ph/9203206](#)].
- [144] S. M. Barr and D. Seckel, *Planck scale corrections to axion models*, *Phys. Rev. D* **46** (1992) 539–549.
- [145] V. Rubakov, *Grand unification and heavy axion*, *JETP Lett.* **65** (1997) 621–624, [[hep-ph/9703409](#)].
- [146] Z. Berezhiani, L. Gianfagna and M. Giannotti, *Strong CP problem and mirror world: The Weinberg-Wilczek axion revisited*, *Phys. Lett. B* **500** (2001) 286–296, [[hep-ph/0009290](#)].
- [147] A. Hook, *Anomalous solutions to the strong CP problem*, *Phys. Rev. Lett.* **114** (2015) 141801, [[1411.3325](#)].
- [148] H. Fukuda, K. Harigaya, M. Ibe and T. T. Yanagida, *Model of visible QCD axion*, *Phys. Rev. D* **92** (2015) 015021, [[1504.06084](#)].
- [149] T. Gherghetta, N. Nagata and M. Shifman, *A Visible QCD Axion from an Enlarged Color Group*, *Phys. Rev. D* **93** (2016) 115010, [[1604.01127](#)].

- [150] S. Dimopoulos, A. Hook, J. Huang and G. Marques-Tavares, *A collider observable QCD axion*, *JHEP* **11** (2016) 052, [[1606.03097](#)].
- [151] J. E. Kim, *Weak Interaction Singlet and Strong CP Invariance*, *Phys. Rev. Lett.* **43** (1979) 103.
- [152] M. A. Shifman, A. I. Vainshtein and V. I. Zakharov, *Can Confinement Ensure Natural CP Invariance of Strong Interactions?*, *Nucl. Phys. B* **166** (1980) 493–506.
- [153] M. Dine, W. Fischler and M. Srednicki, *A Simple Solution to the Strong CP Problem with a Harmless Axion*, *Phys. Lett. B* **104** (1981) 199–202.
- [154] A. R. Zhitnitsky, *On Possible Suppression of the Axion Hadron Interactions. (In Russian)*, *Sov. J. Nucl. Phys.* **31** (1980) 260.
- [155] A. Davidson and M. A. H. Vozmediano, *The Horizontal Axion Alternative: The Interplay of Vacuum Structure and Flavor Interactions*, *Nucl. Phys. B* **248** (1984) 647–670.
- [156] R. D. Peccei, T. T. Wu and T. Yanagida, *A VIABLE AXION MODEL*, *Phys. Lett. B* **172** (1986) 435–440.
- [157] L. M. Krauss and F. Wilczek, *A SHORTLIVED AXION VARIANT*, *Phys. Lett. B* **173** (1986) 189–192.
- [158] C. Q. Geng and J. N. Ng, *Flavor Connections and Neutrino Mass Hierarchy Invariant Invisible Axion Models Without Domain Wall Problem*, *Phys. Rev. D* **39** (1989) 1449.
- [159] A. Celis, J. Fuentes-Martin and H. Serodio, *An invisible axion model with controlled FCNCs at tree level*, *Phys. Lett. B* **741** (2015) 117–123, [[1410.6217](#)].
- [160] D. S. M. Alves and N. Weiner, *A viable QCD axion in the MeV mass range*, *JHEP* **07** (2018) 092, [[1710.03764](#)].
- [161] L. Di Luzio, F. Mescia, E. Nardi, P. Panci and R. Ziegler, *Astrophobic Axions*, *Phys. Rev. Lett.* **120** (2018) 261803, [[1712.04940](#)].
- [162] J. M. Camalich, J. Terol-Calvo, L. Tolos and R. Ziegler, *Supernova Constraints on Dark Flavored Sectors*, *Phys. Rev. D* **103** (2021) L121301, [[2012.11632](#)].
- [163] Y. Ema, K. Hamaguchi, T. Moroi and K. Nakayama, *Flaxion: a minimal extension to solve puzzles in the standard model*, *JHEP* **01** (2017) 096, [[1612.05492](#)].
- [164] L. Calibbi, F. Goertz, D. Redigolo, R. Ziegler and J. Zupan, *Minimal axion model from flavor*, *Phys. Rev. D* **95** (2017) 095009, [[1612.08040](#)].
- [165] T. Alanne, S. Blasi and F. Goertz, *Common source for scalars: Flavored axion-Higgs unification*, *Phys. Rev. D* **99** (2019) 015028, [[1807.10156](#)].
- [166] T. Alanne, S. Blasi and F. Goertz, *Axiflavor-Higgs Unification*, in *54th Rencontres de Moriond on Electroweak Interactions and Unified Theories (Moriond EW 2019) La Thuile, Italy, March 16-23, 2019*, 2019, [1905.07285](#).
- [167] M. Chala, G. Guedes, M. Ramos and J. Santiago, *Running in the ALPs*, *Eur. Phys. J. C* **81** (2021) 181, [[2012.09017](#)].
- [168] A. M. Galda, M. Neubert and S. Renner, *ALP — SMEFT interference*, *JHEP* **06** (2021) 135, [[2105.01078](#)].



- [169] A. Ringwald, *Exploring the Role of Axions and Other WISPs in the Dark Universe*, *Phys. Dark Univ.* **1** (2012) 116–135, [1210.5081].
- [170] A. Ringwald, *Alternative dark matter candidates: Axions*, *PoS NOW2016* (2016) 081, [1612.08933].
- [171] C. S. Machado, W. Ratzinger, P. Schwaller and B. A. Stefanek, *Audible Axions*, *JHEP* **01** (2019) 053, [1811.01950].
- [172] C. S. Machado, W. Ratzinger, P. Schwaller and B. A. Stefanek, *Gravitational wave probes of axionlike particles*, *Phys. Rev. D* **102** (2020) 075033, [1912.01007].
- [173] W. A. Bardeen, S. H. H. Tye and J. A. M. Vermaseren, *Phenomenology of the New Light Higgs Boson Search*, *Phys. Lett.* **76B** (1978) 580–584.
- [174] P. Di Vecchia and G. Veneziano, *Chiral Dynamics in the Large  $n$  Limit*, *Nucl. Phys.* **B171** (1980) 253–272.
- [175] B. Holdom and M. E. Peskin, *Raising the Axion Mass*, *Nucl. Phys. B* **208** (1982) 397–412.
- [176] B. Holdom, *Strong QCD at High-energies and a Heavy Axion*, *Phys. Lett. B* **154** (1985) 316.
- [177] M. Dine and N. Seiberg, *String Theory and the Strong CP Problem*, *Nucl. Phys. B* **273** (1986) 109–124.
- [178] J. M. Flynn and L. Randall, *A Computation of the Small Instanton Contribution to the Axion Potential*, *Nucl. Phys. B* **293** (1987) 731–739.
- [179] K. Choi, C. Kim and W. Sze, *Mass Renormalization by Instantons and the Strong CP Problem*, *Phys. Rev. Lett.* **61** (1988) 794.
- [180] K. Choi and H. D. Kim, *Small instanton contribution to the axion potential in supersymmetric models*, *Phys. Rev. D* **59** (1999) 072001, [hep-ph/9809286].
- [181] M. Gaillard, M. Gavela, R. Houtz, P. Quilez and R. Del Rey, *Color unified dynamical axion*, *Eur. Phys. J. C* **78** (2018) 972, [1805.06465].
- [182] P. Agrawal and K. Howe, *Factoring the Strong CP Problem*, *JHEP* **12** (2018) 029, [1710.04213].
- [183] H. Georgi, D. B. Kaplan and L. Randall, *Manifesting the Invisible Axion at Low-energies*, *Phys. Lett. B* **169** (1986) 73–78.
- [184] M. Bauer, M. Neubert and A. Thamm, *The “forgotten” decay  $S \rightarrow Z + h$  as a CP analyzer*, [1607.01016].
- [185] M. Bauer, M. Neubert and A. Thamm, *Analyzing the CP Nature of a New Scalar Particle via  $S \rightarrow Z + h$  Decay*, *Phys. Rev. Lett.* **117** (2016) 181801, [1610.00009].
- [186] J. Martin Camalich, M. Pospelov, P. N. H. Vuong, R. Ziegler and J. Zupan, *Quark Flavor Phenomenology of the QCD Axion*, *Phys. Rev. D* **102** (2020) 015023, [2002.04623].
- [187] K. Chetyrkin, B. A. Kniehl, M. Steinhauser and W. A. Bardeen, *Effective QCD interactions of CP odd Higgs bosons at three loops*, *Nucl. Phys. B* **535** (1998) 3–18, [hep-ph/9807241].

- [188] T. Inami, T. Kubota and Y. Okada, *Effective Gauge Theory and the Effect of Heavy Quarks in Higgs Boson Decays*, *Z. Phys. C* **18** (1983) 69–80.
- [189] B. Grinstein and L. Randall, *The Renormalization of  $g^2$* , *Phys. Lett. B* **217** (1989) 335–340.
- [190] K. Choi, S. H. Im, C. B. Park and S. Yun, *Minimal Flavor Violation with Axion-like Particles*, *JHEP* **11** (2017) 070, [[1708.00021](#)].
- [191] M. Heiles, M. König and M. Neubert, *Effective Field Theory for Heavy Vector Resonances Coupled to the Standard Model*, [[2011.08205](#)].
- [192] E. E. Jenkins, A. V. Manohar and M. Trott, *Renormalization Group Evolution of the Standard Model Dimension Six Operators I: Formalism and  $\lambda$  Dependence*, *JHEP* **10** (2013) 087, [[1308.2627](#)].
- [193] G. Altarelli and G. G. Ross, *The Anomalous Gluon Contribution to Polarized Leptoproduction*, *Phys. Lett. B* **212** (1988) 391–396.
- [194] J. Kodaira, *QCD Higher Order Effects in Polarized Electroproduction: Flavor Singlet Coefficient Functions*, *Nucl. Phys. B* **165** (1980) 129–140.
- [195] S. A. Larin, *The Renormalization of the axial anomaly in dimensional regularization*, *Phys. Lett. B* **303** (1993) 113–118, [[hep-ph/9302240](#)].
- [196] M. Bauer, M. Neubert and A. Thamm, *Collider Probes of Axion-Like Particles*, *JHEP* **12** (2017) 044, [[1708.00443](#)].
- [197] G. Grilli di Cortona, E. Hardy, J. Pardo Vega and G. Villadoro, *The QCD axion, precisely*, *JHEP* **01** (2016) 034, [[1511.02867](#)].
- [198] G. Grilli di Cortona, E. Hardy, J. Pardo Vega and G. Villadoro, *The QCD axion, precisely*, *JHEP* **01** (2016) 034, [[1511.02867](#)].
- [199] W. A. Bardeen, R. D. Peccei and T. Yanagida, *Constraints on variant axion models*, *Nucl. Phys.* **B279** (1987) 401–428.
- [200] M. Srednicki, *Axion Couplings to Matter. 1. CP Conserving Parts*, *Nucl. Phys. B* **260** (1985) 689–700.
- [201] K. Fujikawa, *Path Integral Measure for Gauge Invariant Fermion Theories*, *Phys. Rev. Lett.* **42** (1979) 1195–1198.
- [202] J. Gasser and H. Leutwyler, *Chiral Perturbation Theory: Expansions in the Mass of the Strange Quark*, *Nucl. Phys. B* **250** (1985) 465–516.
- [203] C. W. Bernard, T. Draper, A. Soni, H. D. Politzer and M. B. Wise, *Application of Chiral Perturbation Theory to  $K \rightarrow 2\pi$  Decays*, *Phys. Rev. D* **32** (1985) 2343–2347.
- [204] R. J. Crewther, *Chiral Reduction of  $K \rightarrow 2\pi$  Amplitudes*, *Nucl. Phys. B* **264** (1986) 277–291.
- [205] J. Kambor, J. H. Missimer and D. Wyler, *The Chiral Loop Expansion of the Nonleptonic Weak Interactions of Mesons*, *Nucl. Phys. B* **346** (1990) 17–64.
- [206] V. Cirigliano, G. Ecker, H. Neufeld, A. Pich and J. Portoles, *Kaon Decays in the Standard Model*, *Rev. Mod. Phys.* **84** (2012) 399, [[1107.6001](#)].

- [207] M. Neubert and B. Stech, *A Consistent analysis of the Delta I = 1/2 rule in strange particle decays*, *Phys. Rev. D* **44** (1991) 775–793.
- [208] PARTICLE DATA GROUP collaboration, P. A. Zyla et al., *Review of Particle Physics*, *PTEP* **2020** (2020) 083C01.
- [209] H. Georgi, *Weak Interactions and Modern Particle Theory*. 1984.
- [210] J. Gasser, M. E. Sainio and A. Svarc, *Nucleons with Chiral Loops*, *Nucl. Phys. B* **307** (1988) 779–853.
- [211] S. Scherer, *Introduction to chiral perturbation theory*, *Adv. Nucl. Phys.* **27** (2003) 277, [[hep-ph/0210398](#)].
- [212] G. Ecker, *Chiral perturbation theory*, *Prog. Part. Nucl. Phys.* **35** (1995) 1–80, [[hep-ph/9501357](#)].
- [213] T. Vonk, F.-K. Guo and U.-G. Meißner, *Precision calculation of the axion-nucleon coupling in chiral perturbation theory*, *JHEP* **03** (2020) 138, [[2001.05327](#)].
- [214] FLAVOUR LATTICE AVERAGING GROUP collaboration, S. Aoki et al., *FLAG Review 2019: Flavour Lattice Averaging Group (FLAG)*, *Eur. Phys. J.* **C80** (2020) 113, [[1902.08191](#)].
- [215] J. Liang, Y.-B. Yang, T. Draper, M. Gong and K.-F. Liu, *Quark spins and Anomalous Ward Identity*, *Phys. Rev. D* **98** (2018) 074505, [[1806.08366](#)].
- [216] A. Krasznahorkay et al., *New results on the  $^8\text{Be}$  anomaly*, *J. Phys. Conf. Ser.* **1056** (2018) 012028.
- [217] A. Krasznahorkay et al., *New evidence supporting the existence of the hypothetical X17 particle*, [[1910.10459](#)].
- [218] D. Firak et al., *Confirmation of the existence of the X17 particle*, *EPJ Web Conf.* **232** (2020) 04005.
- [219] KTeV collaboration, E. Abouzaid et al., *Measurement of the Rare Decay  $\pi^0 \rightarrow e^+e^-$* , *Phys. Rev.* **D75** (2007) 012004, [[hep-ex/0610072](#)].
- [220] B. Batell, M. Pospelov and A. Ritz, *Multi-lepton Signatures of a Hidden Sector in Rare B Decays*, *Phys. Rev.* **D83** (2011) 054005, [[0911.4938](#)].
- [221] M. J. Dolan, F. Kahlhoefer, C. McCabe and K. Schmidt-Hoberg, *A taste of dark matter: Flavour constraints on pseudoscalar mediators*, *JHEP* **03** (2015) 171, [[1412.5174](#)].
- [222] E. Izaguirre, T. Lin and B. Shuve, *Searching for Axionlike Particles in Flavor-Changing Neutral Current Processes*, *Phys. Rev. Lett.* **118** (2017) 111802, [[1611.09355](#)].
- [223] F. Arias-Aragon and L. Merlo, *The Minimal Flavour Violating Axion*, *JHEP* **10** (2017) 168, [[1709.07039](#)].
- [224] B. Döbrich, F. Ertas, F. Kahlhoefer and T. Spadaro, *Model-independent bounds on light pseudoscalars from rare B-meson decays*, *Phys. Lett.* **B790** (2019) 537–544, [[1810.11336](#)].
- [225] M. B. Gavela, R. Houtz, P. Quilez, R. Del Rey and O. Sumensari, *Flavor constraints on electroweak ALP couplings*, *Eur. Phys. J.* **C79** (2019) 369, [[1901.02031](#)].
- [226] H. Ishida, S. Matsuzaki and Y. Shigekami, *New perspective in searching for axionlike particles from flavor physics*, *Phys. Rev. D* **103** (2021) 095022, [[2006.02725](#)].



- [227] S. Gori, G. Perez and K. Tobioka, *KOTO vs. NA62 Dark Scalar Searches*, *JHEP* **08** (2020) 110, [[2005.05170](#)].
- [228] S. Chakraborty, M. Kraus, V. Loladze, T. Okui and K. Tobioka, *Heavy QCD axion in  $b \rightarrow s$  transition: Enhanced limits and projections*, *Phys. Rev. D* **104** (2021) 055036, [[2102.04474](#)].
- [229] A. Carmona, C. Scherb and P. Schwaller, *Charming ALPs*, *JHEP* **08** (2021) 121, [[2101.07803](#)].
- [230] E. Bertholet, S. Chakraborty, V. Loladze, T. Okui, A. Soffer and K. Tobioka, *Heavy QCD Axion at Belle II: Displaced and Prompt Signals*, [[2108.10331](#)].
- [231] A. J. Buras, *Weak Hamiltonian, CP violation and rare decays*, in *Les Houches Summer School in Theoretical Physics, Session 68: Probing the Standard Model of Particle Interactions*, pp. 281–539, 6, 1998, [hep-ph/9806471](#).
- [232] M. Wirbel, B. Stech and M. Bauer, *Exclusive Semileptonic Decays of Heavy Mesons*, *Z. Phys. C* **29** (1985) 637.
- [233] HPQCD collaboration, C. Bouchard, G. P. Lepage, C. Monahan, H. Na and J. Shigemitsu, *Rare decay  $B \rightarrow K \ell^+ \ell^-$  form factors from lattice QCD*, *Phys. Rev. D* **88** (2013) 054509, [[1306.2384](#)].
- [234] J. A. Bailey et al.,  *$B \rightarrow K \ell^+ \ell^-$  decay form factors from three-flavor lattice QCD*, *Phys. Rev. D* **93** (2016) 025026, [[1509.06235](#)].
- [235] FERMILAB LATTICE, MILC collaboration, J. A. Bailey et al.,  *$B \rightarrow \pi \ell \ell$  form factors for new-physics searches from lattice QCD*, *Phys. Rev. Lett.* **115** (2015) 152002, [[1507.01618](#)].
- [236] A. Bharucha, D. M. Straub and R. Zwicky,  *$B \rightarrow V \ell^+ \ell^-$  in the Standard Model from light-cone sum rules*, *JHEP* **08** (2016) 098, [[1503.05534](#)].
- [237] ETM collaboration, V. Lubicz, L. Riggio, G. Salerno, S. Simula and C. Tarantino, *Scalar and vector form factors of  $D \rightarrow \pi(K) \ell \nu$  decays with  $N_f = 2 + 1 + 1$  twisted fermions*, *Phys. Rev. D* **96** (2017) 054514, [[1706.03017](#)].
- [238] W. Wang and Y.-L. Shen,  *$D_s \rightarrow K, K^*, \phi$  form factors in the Covariant Light-Front Approach and Exclusive  $D_s$  Decays*, *Phys. Rev. D* **78** (2008) 054002.
- [239] M. Beneke, G. Buchalla, M. Neubert and C. T. Sachrajda, *QCD factorization for  $B \rightarrow \pi \pi$  decays: Strong phases and CP violation in the heavy quark limit*, *Phys. Rev. Lett.* **83** (1999) 1914–1917, [[hep-ph/9905312](#)].
- [240] M. Beneke, G. Buchalla, M. Neubert and C. T. Sachrajda, *QCD factorization in  $B \rightarrow \pi K, \pi \pi$  decays and extraction of Wolfenstein parameters*, *Nucl. Phys. B* **606** (2001) 245–321, [[hep-ph/0104110](#)].
- [241] W. Altmannshofer, S. Gori and D. J. Robinson, *Constraining axionlike particles from rare pion decays*, *Phys. Rev. D* **101** (2020) 075002, [[1909.00005](#)].
- [242] PIENU collaboration, A. Aguilar-Arevalo et al., *Search for three body pion decays  $\pi^+ \rightarrow \ell^+ \nu X$* , *Phys. Rev. D* **103** (2021) 052006, [[2101.07381](#)].
- [243] F. Wilczek, *Decays of Heavy Vector Mesons Into Higgs Particles*, *Phys. Rev. Lett.* **39** (1977) 1304.

- [244] P. Nason, QCD Radiative Corrections to  $\Upsilon$  Decay Into Scalar Plus  $\gamma$  and Pseudoscalar Plus  $\gamma$ , *Phys. Lett.* **B175** (1986) 223–226.
- [245] M. L. Mangano and P. Nason, Radiative quarkonium decays and the NMSSM Higgs interpretation of the hyperCP  $\Sigma^+ \rightarrow p\mu^+\mu^-$  events, *Mod. Phys. Lett.* **A22** (2007) 1373–1380, [0704.1719].
- [246] D. McKeen, Constraining Light Bosons with Radiative Upsilon(1S) Decays, *Phys. Rev.* **D79** (2009) 015007, [0809.4787].
- [247] E. Masso and R. Toldra, On a light spinless particle coupled to photons, *Phys. Rev.* **D52** (1995) 1755–1763, [hep-ph/9503293].
- [248] X. Cid Vidal, A. Mariotti, D. Redigolo, F. Sala and K. Tobioka, New Axion Searches at Flavor Factories, *JHEP* **01** (2019) 113, [1810.09452].
- [249] L. Merlo, F. Pobbe, S. Rigolin and O. Sumensari, Revisiting the production of ALPs at B-factories, *JHEP* **06** (2019) 091, [1905.03259].
- [250] M. Neubert, Heavy quark symmetry, *Phys. Rept.* **245** (1994) 259–396, [hep-ph/9306320].
- [251] BESIII collaboration, M. Ablikim, Search for a light CP-odd Higgs boson in radiative decays of  $J/\psi$ , *Phys. Rev.* **D93** (2016) 052005, [1510.01641].
- [252] BABAR collaboration, P. del Amo Sanchez et al., Search for Production of Invisible Final States in Single-Photon Decays of  $\Upsilon(1S)$ , *Phys. Rev. Lett.* **107** (2011) 021804, [1007.4646].
- [253] BABAR collaboration, J. P. Lees et al., Search for di-muon decays of a low-mass Higgs boson in radiative decays of the  $Y(1S)$ , *Phys. Rev.* **D87** (2013) 031102, [1210.0287].
- [254] BABAR collaboration, J. P. Lees et al., Search for a low-mass scalar Higgs boson decaying to a tau pair in single-photon decays of  $\Upsilon(1S)$ , *Phys. Rev.* **D88** (2013) 071102, [1210.5669].
- [255] BABAR collaboration, J. P. Lees et al., Search for hadronic decays of a light Higgs boson in the radiative decay  $\Upsilon \rightarrow \gamma A^0$ , *Phys. Rev. Lett.* **107** (2011) 221803, [1108.3549].
- [256] D. Buarque Franzosi and C. Zhang, Probing the top-quark chromomagnetic dipole moment at next-to-leading order in QCD, *Phys. Rev. D* **91** (2015) 114010, [1503.08841].
- [257] CMS collaboration, A. M. Sirunyan et al., Measurement of the top quark polarization and  $t\bar{t}$  spin correlations using dilepton final states in proton-proton collisions at  $\sqrt{s} = 13$  TeV, *Phys. Rev. D* **100** (2019) 072002, [1907.03729].
- [258] J. Ebadi, S. Khatibi and M. Mohammadi Najafabadi, New probes for axionlike particles at hadron colliders, *Phys. Rev.* **D100** (2019) 015016, [1901.03061].
- [259] F. Wilczek, Axions and Family Symmetry Breaking, *Phys. Rev. Lett.* **49** (1982) 1549–1552.
- [260] NA62 collaboration, E. Cortina Gil et al., Measurement of the very rare  $K^+ \rightarrow \pi^+\nu\bar{\nu}$  decay, *JHEP* **06** (2021) 093, [2103.15389].
- [261] KOTO collaboration, J. K. Ahn et al., Search for the  $K_L \rightarrow \pi^0\nu\bar{\nu}$  and  $K_L \rightarrow \pi^0 X^0$  decays at the J-PARC KOTO experiment, *Phys. Rev. Lett.* **122** (2019) 021802, [1810.09655].
- [262] BELLE collaboration, J. Grygier et al., Search for  $B \rightarrow h\nu\bar{\nu}$  decays with semileptonic tagging at Belle, *Phys. Rev.* **D96** (2017) 091101, [1702.03224].

- [263] E949 collaboration, A. V. Artamonov et al., *Search for the decay  $K^+ \rightarrow \pi^+ \gamma \gamma$  in the  $\pi^+$  momentum region  $P > 213$  MeV/c*, *Phys. Lett.* **B623** (2005) 192–199, [[hep-ex/0505069](#)].
- [264] NA62 collaboration, C. Lazzeroni et al., *Study of the  $K^\pm \rightarrow \pi^\pm \gamma \gamma$  decay by the NA62 experiment*, *Phys. Lett.* **B732** (2014) 65–74, [[1402.4334](#)].
- [265] NA48 collaboration, A. Lai et al., *Precise measurement of the decay  $K_L \rightarrow \pi^0 \gamma \gamma$* , *Phys. Lett.* **B536** (2002) 229–240, [[hep-ex/0205010](#)].
- [266] KTeV collaboration, E. Abouzaid et al., *Final Results from the KTeV Experiment on the Decay  $K_L \rightarrow \pi^0 \gamma \gamma$* , *Phys. Rev.* **D77** (2008) 112004, [[0805.0031](#)].
- [267] LHCb collaboration, R. Aaij et al., *Search for long-lived scalar particles in  $B^+ \rightarrow K^+ \chi(\mu^+ \mu^-)$  decays*, *Phys. Rev.* **D95** (2017) 071101, [[1612.07818](#)].
- [268] LHCb collaboration, R. Aaij et al., *Search for hidden-sector bosons in  $B^0 \rightarrow K^{*0} \mu^+ \mu^-$  decays*, *Phys. Rev. Lett.* **115** (2015) 161802, [[1508.04094](#)].
- [269] LHCb collaboration, R. Aaij et al., *First measurement of the differential branching fraction and CP asymmetry of the  $B^\pm \rightarrow \pi^\pm \mu^+ \mu^-$  decay*, *JHEP* **10** (2015) 034, [[1509.00414](#)].
- [270] BELLE collaboration, Y. T. Duh et al., *Measurements of branching fractions and direct CP asymmetries for  $B \rightarrow K\pi$ ,  $B \rightarrow \pi\pi$  and  $B \rightarrow KK$  decays*, *Phys. Rev.* **D87** (2013) 031103, [[1210.1348](#)].
- [271] BABAR collaboration, J. P. Lees et al., *Measurement of CP Asymmetries and Branching Fractions in Charmless Two-Body B-Meson Decays to Pions and Kaons*, *Phys. Rev.* **D87** (2013) 052009, [[1206.3525](#)].
- [272] CAST collaboration, E. Arik et al., *Probing eV-scale axions with CAST*, *JCAP* **02** (2009) 008, [[0810.4482](#)].
- [273] Y. Inoue, Y. Akimoto, R. Ohta, T. Mizumoto, A. Yamamoto and M. Minowa, *Search for solar axions with mass around 1 eV using coherent conversion of axions into photons*, *Phys. Lett. B* **668** (2008) 93–97, [[0806.2230](#)].
- [274] P. W. Graham, I. G. Irastorza, S. K. Lamoreaux, A. Lindner and K. A. van Bibber, *Experimental Searches for the Axion and Axion-Like Particles*, *Ann. Rev. Nucl. Part. Sci.* **65** (2015) 485–514, [[1602.00039](#)].
- [275] G. G. Raffelt, *Astrophysical axion bounds diminished by screening effects*, *Phys. Rev.* **D33** (1986) 897.
- [276] G. G. Raffelt and D. S. P. Dearborn, *Bounds on Hadronic Axions From Stellar Evolution*, *Phys. Rev.* **D36** (1987) 2211.
- [277] G. G. Raffelt, *Astrophysical axion bounds*, *Lect. Notes Phys.* **741** (2008) 51–71, [[hep-ph/0611350](#)].
- [278] D. Cadamuro and J. Redondo, *Cosmological bounds on pseudo Nambu-Goldstone bosons*, *JCAP* **02** (2012) 032, [[1110.2895](#)].
- [279] M. Millea, L. Knox and B. Fields, *New Bounds for Axions and Axion-Like Particles with keV-GeV Masses*, *Phys. Rev. D* **92** (2015) 023010, [[1501.04097](#)].
- [280] F. Ertas and F. Kahlhoefer, *On the interplay between astrophysical and laboratory probes of MeV-scale axion-like particles*, *JHEP* **07** (2020) 050, [[2004.01193](#)].

- [281] P. F. Depta, M. Hufnagel and K. Schmidt-Hoberg, *Robust cosmological constraints on axion-like particles*, *JCAP* **05** (2020) 009, [[2002.08370](#)].
- [282] A. Payez, C. Evoli, T. Fischer, M. Giannotti, A. Mirizzi and A. Ringwald, *Revisiting the SN1987A gamma-ray limit on ultralight axion-like particles*, *JCAP* **1502** (2015) 006, [[1410.3747](#)].
- [283] J. Jaeckel, P. C. Malta and J. Redondo, *Decay photons from the axionlike particles burst of type II supernovae*, *Phys. Rev.* **D98** (2018) 055032, [[1702.02964](#)].
- [284] A. Caputo, G. Raffelt and E. Vitagliano, *Muonic boson limits: Supernova redux*, *Phys. Rev. D* **105** (2022) 035022, [[2109.03244](#)].
- [285] CLEO collaboration, R. Balest et al., *Upsilon (1s)  $\rightarrow$  gamma + noninteracting particles*, *Phys. Rev. D* **51** (1995) 2053–2060.
- [286] K. Mimasu and V. Sanz, *ALPs at Colliders*, *JHEP* **06** (2015) 173, [[1409.4792](#)].
- [287] J. Jaeckel and M. Spannowsky, *Probing MeV to 90 GeV axion-like particles with LEP and LHC*, *Phys. Lett.* **B753** (2016) 482–487, [[1509.00476](#)].
- [288] M. Casolino, T. Farooque, A. Juste, T. Liu and M. Spannowsky, *Probing a light CP-odd scalar in di-top-associated production at the LHC*, *Eur. Phys. J. C* **75** (2015) 498, [[1507.07004](#)].
- [289] S. Knapen, T. Lin, H. K. Lou and T. Melia, *Searching for Axionlike Particles with Ultraperipheral Heavy-Ion Collisions*, *Phys. Rev. Lett.* **118** (2017) 171801, [[1607.06083](#)].
- [290] U. Haisch and J. F. Kamenik, *Searching for new spin-0 resonances at LHCb*, *Phys. Rev. D* **93** (2016) 055047, [[1601.05110](#)].
- [291] I. Brivio, M. B. Gavela, L. Merlo, K. Mimasu, J. M. No, R. del Rey et al., *ALPs Effective Field Theory and Collider Signatures*, *Eur. Phys. J. C* **77** (2017) 572, [[1701.05379](#)].
- [292] U. Haisch, J. F. Kamenik, A. Malinauskas and M. Spira, *Collider constraints on light pseudoscalars*, *JHEP* **03** (2018) 178, [[1802.02156](#)].
- [293] D. Buarque Franzosi, G. Cacciapaglia, X. Cid Vidal, G. Ferretti, T. Flacke and C. Vázquez Sierra, *Exploring new possibilities to discover a light pseudo-scalar at LHCb*, [[2106.12615](#)].
- [294] E. M. Riordan et al., *A Search for Short Lived Axions in an Electron Beam Dump Experiment*, *Phys. Rev. Lett.* **59** (1987) 755.
- [295] J. D. Bjorken, S. Ecklund, W. R. Nelson, A. Abashian, C. Church, B. Lu et al., *Search for Neutral Metastable Penetrating Particles Produced in the SLAC Beam Dump*, *Phys. Rev. D* **38** (1988) 3375.
- [296] S. Alekhin et al., *A facility to Search for Hidden Particles at the CERN SPS: the SHiP physics case*, *Rept. Prog. Phys.* **79** (2016) 124201, [[1504.04855](#)].
- [297] B. Döbrich, J. Jaeckel, F. Kahlhoefer, A. Ringwald and K. Schmidt-Hoberg, *ALPtraum: ALP production in proton beam dump experiments*, *JHEP* **02** (2016) 018, [[1512.03069](#)].
- [298] E. Armengaud et al., *Axion searches with the EDELWEISS-II experiment*, *JCAP* **11** (2013) 067, [[1307.1488](#)].

- [299] EDELWEISS collaboration, E. Armengaud et al., *Searches for electron interactions induced by new physics in the EDELWEISS-III Germanium bolometers*, *Phys. Rev. D* **98** (2018) 082004, [[1808.02340](#)].
- [300] GERDA collaboration, M. Agostini et al., *First Search for Bosonic Superweakly Interacting Massive Particles with Masses up to 1 MeV/c<sup>2</sup> with GERDA*, *Phys. Rev. Lett.* **125** (2020) 011801, [[2005.14184](#)].
- [301] XMASS collaboration, K. Abe et al., *Search for dark matter in the form of hidden photons and axion-like particles in the XMASS detector*, *Phys. Lett. B* **787** (2018) 153–158, [[1807.08516](#)].
- [302] D. Ghosh and D. Sachdeva, *Constraints on Axion-Lepton coupling from Big Bang Nucleosynthesis*, *JCAP* **10** (2020) 060, [[2007.01873](#)].
- [303] A. Konaka et al., *Search for Neutral Particles in Electron Beam Dump Experiment*, *Phys. Rev. Lett.* **57** (1986) 659.
- [304] R. Essig, R. Harnik, J. Kaplan and N. Toro, *Discovering New Light States at Neutrino Experiments*, *Phys. Rev. D* **82** (2010) 113008, [[1008.0636](#)].
- [305] A. Bross, M. Crisler, S. H. Pordes, J. Volk, S. Errede and J. Wrbanek, *A Search for Shortlived Particles Produced in an Electron Beam Dump*, *Phys. Rev. Lett.* **67** (1991) 2942–2945.
- [306] G. Lucente and P. Carenza, *Supernova bound on Axion-Like Particles coupled with electrons*, [[2107.12393](#)].
- [307] BABAR collaboration, J. P. Lees et al., *Search for a Dark Photon in  $e^+e^-$  Collisions at BaBar*, *Phys. Rev. Lett.* **113** (2014) 201801, [[1406.2980](#)].
- [308] W.-S. Hou and G.-G. Wong,  *$\mu^+ e^- \leftrightarrow \mu^- e^+$  transitions via neutral scalar bosons*, *Phys. Rev. D* **53** (1996) 1537–1541, [[hep-ph/9504311](#)].
- [309] W. J. Marciano, A. Masiero, P. Paradisi and M. Passera, *Contributions of axionlike particles to lepton dipole moments*, *Phys. Rev. D* **94** (2016) 115033, [[1607.01022](#)].
- [310] F. Bjrkeroth, E. J. Chun and S. F. King, *Flavourful Axion Phenomenology*, *JHEP* **08** (2018) 117, [[1806.00660](#)].
- [311] C. Cornella, P. Paradisi and O. Sumensari, *Hunting for ALPs with Lepton Flavor Violation*, *JHEP* **01** (2020) 158, [[1911.06279](#)].
- [312] M. Endo, S. Iguro and T. Kitahara, *Probing  $e\mu$  flavor-violating ALP at Belle II*, *JHEP* **06** (2020) 040, [[2002.05948](#)].
- [313] L. Calibbi, D. Redigolo, R. Ziegler and J. Zupan, *Looking forward to Lepton-flavor-violating ALPs*, [[2006.04795](#)].
- [314] Q. Bonnefoy, P. Cox, E. Dudas, T. Gherghetta and M. D. Nguyen, *Flavoured Warped Axion*, *JHEP* **04** (2021) 084, [[2012.09728](#)].
- [315] P. Escribano and A. Vicente, *Ultralight scalars in leptonic observables*, *JHEP* **03** (2021) 240, [[2008.01099](#)].
- [316] L. Di Luzio, R. Gröber and P. Paradisi, *Hunting for the CP violating ALP*, [[2010.13760](#)].



- [317] K. Ma, *Polarization Effects in Lepton Flavor Violated Decays Induced by Axion-Like Particles*, [[2104.11162](#)].
- [318] J. Heeck and W. Rodejohann, *Lepton flavor violation with displaced vertices*, *Phys. Lett. B* **776** (2018) 385–390, [[1710.02062](#)].
- [319] M. A. Buen-Abad, J. Fan, M. Reece and C. Sun, *Challenges for an axion explanation of the muon  $g - 2$  measurement*, *JHEP* **09** (2021) 101, [[2104.03267](#)].
- [320] SINDRUM II collaboration, W. H. Bertl et al., *A Search for muon to electron conversion in muonic gold*, *Eur. Phys. J. C* **47** (2006) 337–346.
- [321] Mu2E collaboration, L. Bartoszek et al., *Mu2e Technical Design Report*, [[1501.05241](#)].
- [322] COMET collaboration, R. Abramishvili et al., *COMET Phase-I Technical Design Report*, *PTEP* **2020** (2020) 033C01, [[1812.09018](#)].
- [323] Y. Kuno and Y. Okada, *Muon decay and physics beyond the standard model*, *Rev. Mod. Phys.* **73** (2001) 151–202, [[hep-ph/9909265](#)].
- [324] V. Cirigliano, R. Kitano, Y. Okada and P. Tuzon, *On the model discriminating power of  $\mu \rightarrow e$  conversion in nuclei*, *Phys. Rev. D* **80** (2009) 013002, [[0904.0957](#)].
- [325] R. Kitano, M. Koike and Y. Okada, *Detailed calculation of lepton flavor violating muon electron conversion rate for various nuclei*, *Phys. Rev. D* **66** (2002) 096002, [[hep-ph/0203110](#)].
- [326] L. Willmann et al., *New bounds from searching for muonium to anti-muonium conversion*, *Phys. Rev. Lett.* **82** (1999) 49–52, [[hep-ex/9807011](#)].
- [327] K. Horikawa and K. Sasaki, *Muonium - anti-muonium conversion in models with dilepton gauge bosons*, *Phys. Rev.* **D53** (1996) 560–563, [[hep-ph/9504218](#)].
- [328] R. H. Dalitz, *Decay of tau mesons of known charge*, *Phys. Rev.* **94** (1954) 1046–1051.
- [329] M. Michel, F. Feldbauer, K. Götzen, P. Jasinski, A. Karavdina, K. Peters et al., *ComPWA: A common amplitude analysis framework for PANDA*, *J. Phys. Conf. Ser.* **513** (2014) 022025.
- [330] TWIST collaboration, R. Bayes et al., *Search for two body muon decay signals*, *Phys. Rev.* **D91** (2015) 052020, [[1409.0638](#)].
- [331] A. Jodidio et al., *Search for Right-Handed Currents in Muon Decay*, *Phys. Rev. D* **34** (1986) 1967.
- [332] M. Bauer, T. Schell and T. Plehn, *Hunting the Flavon*, *Phys. Rev.* **D94** (2016) 056003, [[1603.06950](#)].
- [333] A. Blondel et al., *Research Proposal for an Experiment to Search for the Decay  $\mu \rightarrow eee$* , [[1301.6113](#)].
- [334] SINDRUM collaboration, U. Bellgardt et al., *Search for the Decay  $\mu^+ \rightarrow e^+e^+e^-$* , *Nucl. Phys.* **B299** (1988) 1–6.
- [335] R. D. Bolton et al., *Search for Rare Muon Decays with the Crystal Box Detector*, *Phys. Rev.* **D38** (1988) 2077.

- [336] MEG collaboration, A. M. Baldini et al., *Search for lepton flavour violating muon decay mediated by a new light particle in the MEG experiment*, *Eur. Phys. J. C* **80** (2020) 858, [2005.00339].
- [337] SINDRUM II collaboration, W. H. Bertl et al., *A Search for muon to electron conversion in muonic gold*, *Eur. Phys. J. C* **47** (2006) 337–346.
- [338] Mu2E collaboration, L. Bartoszek et al., *Mu2e Technical Design Report*, [1501.05241].
- [339] COMET collaboration, R. Abramishvili et al., *COMET Phase-I Technical Design Report*, *PTEP* **2020** (2020) 033C01, [1812.09018].
- [340] MEG collaboration, A. M. Baldini et al., *Search for the lepton flavour violating decay  $\mu^+ \rightarrow e^+ \gamma$  with the full dataset of the MEG experiment*, *Eur. Phys. J. C* **76** (2016) 434, [1605.05081].
- [341] A.-K. Perrevoort, *Sensitivity Studies on New Physics in the Mu3e Experiment and Development of Firmware for the Front-End of the Mu3e Pixel Detector*, Ph.D. thesis, U. Heidelberg (main), 2018. 10.11588/heidok.00024585.
- [342] Mu3E collaboration, A.-K. Perrevoort, *The Rare and Forbidden: Testing Physics Beyond the Standard Model with Mu3e*, *SciPost Phys. Proc.* **1** (2019) 052, [1812.00741].
- [343] D. Hanneke, S. Fogwell and G. Gabrielse, *New Measurement of the Electron Magnetic Moment and the Fine Structure Constant*, *Phys. Rev. Lett.* **100** (2008) 120801, [0801.1134].
- [344] D. Hanneke, S. F. Hoogerheide and G. Gabrielse, *Cavity Control of a Single-Electron Quantum Cyclotron: Measuring the Electron Magnetic Moment*, *Phys. Rev. A* **83** (2011) 052122, [1009.4831].
- [345] T. Aoyama, T. Kinoshita and M. Nio, *Revised and Improved Value of the QED Tenth-Order Electron Anomalous Magnetic Moment*, *Phys. Rev. D* **97** (2018) 036001, [1712.06060].
- [346] R. H. Parker, C. Yu, W. Zhong, B. Estey and H. Müller, *Measurement of the fine-structure constant as a test of the Standard Model*, *Science* **360** (2018) 191, [1812.04130].
- [347] L. Morel, Z. Yao, P. Cladé and S. Guellati-Khélifa, *Determination of the fine-structure constant with an accuracy of 81 parts per trillion*, *Nature* **588** (2020) 61–65.
- [348] J. P. Leveille, *The Second Order Weak Correction to (G-2) of the Muon in Arbitrary Gauge Models*, *Nucl. Phys.* **B137** (1978) 63–76.
- [349] H. E. Haber, G. L. Kane and T. Sterling, *The Fermion Mass Scale and Possible Effects of Higgs Bosons on Experimental Observables*, *Nucl. Phys.* **B161** (1979) 493–532.
- [350] D. Chang, W.-F. Chang, C.-H. Chou and W.-Y. Keung, *Large two loop contributions to g-2 from a generic pseudoscalar boson*, *Phys. Rev.* **D63** (2001) 091301, [hep-ph/0009292].
- [351] NA62 collaboration, E. Cortina Gil et al., *Search for  $\pi^0$  decays to invisible particles*, *JHEP* **02** (2021) 201, [2010.07644].
- [352] BABAR collaboration, J. P. Lees et al., *Search for  $B \rightarrow K^{(*)} \nu \bar{\nu}$  and invisible quarkonium decays*, *Phys. Rev.* **D87** (2013) 112005, [1303.7465].

- [353] A. J. Buras, J. Girrbach-Noe, C. Niehoff and D. M. Straub,  $B \rightarrow K^{(*)}\nu\bar{\nu}$  decays in the Standard Model and beyond, *JHEP* **02** (2015) 184, [[1409.4557](#)].
- [354] J.-M. Gerard, C. Smith and S. Trine, Radiative kaon decays and the penguin contribution to the Delta I = 1/2 rule, *Nucl. Phys.* **B730** (2005) 1–36, [[hep-ph/0508189](#)].
- [355] G. D’Ambrosio and J. Portoles, Vector meson exchange contributions to  $K \rightarrow \pi\gamma\gamma$  and  $K_L \rightarrow \gamma\ell^+\ell^-$ , *Nucl. Phys.* **B492** (1997) 417–454, [[hep-ph/9610244](#)].
- [356] N. J. Baker et al., Search for Shortlived Neutral Particles Emitted in  $K^+$  Decay, *Phys. Rev. Lett.* **59** (1987) 2832–2835.
- [357] KTeV collaboration, A. Alavi-Harati et al., Search for the rare decay  $K_L \rightarrow \pi^0 e^+ e^-$ , *Phys. Rev. Lett.* **93** (2004) 021805, [[hep-ex/0309072](#)].
- [358] G. Buchalla, G. D’Ambrosio and G. Isidori, Extracting short distance physics from  $K(L, S) \rightarrow \pi^0 e^+ e^-$  decays, *Nucl. Phys.* **B672** (2003) 387–408, [[hep-ph/0308008](#)].
- [359] BELLE collaboration, J.-T. Wei et al., Search for  $B \rightarrow \pi l + l^-$  Decays at Belle, *Phys. Rev. D* **78** (2008) 011101, [[0804.3656](#)].
- [360] Z.-H. Li, Z.-G. Si, Y. Wang and N. Zhu,  $B \rightarrow \pi\ell^+\ell^-$  decays revisited in the standard model, [[1411.0466](#)].
- [361] LHCb collaboration, R. Aaij et al., Angular analysis of the  $B^0 \rightarrow K^{*0} e^+ e^-$  decay in the low- $q^2$  region, *JHEP* **04** (2015) 064, [[1501.03038](#)].
- [362] LHCb collaboration, R. Aaij et al., Test of lepton universality using  $B^+ \rightarrow K^+ \ell^+ \ell^-$  decays, *Phys. Rev. Lett.* **113** (2014) 151601, [[1406.6482](#)].
- [363] M. Bordone, G. Isidori and A. Pattori, On the Standard Model predictions for  $R_K$  and  $R_{K^*}$ , *Eur. Phys. J.* **C76** (2016) 440, [[1605.07633](#)].
- [364] BESIII collaboration, M. Ablikim et al., Search for the rare decays  $D \rightarrow h(h')e^+e^-$ , *Phys. Rev. D* **97** (2018) 072015, [[1802.09752](#)].
- [365] S. Fajfer, S. Prelovsek and P. Singer, Rare charm meson decays  $D \rightarrow P\ell^+\ell^-$  and  $c \rightarrow u\ell^+\ell^-$  in SM and MSSM, *Phys. Rev. D* **64** (2001) 114009, [[hep-ph/0106333](#)].
- [366] BABAR collaboration, J. Lees et al., Searches for Rare or Forbidden Semileptonic Charm Decays, *Phys. Rev. D* **84** (2011) 072006, [[1107.4465](#)].
- [367] D. Straub, P. Stangl, Christoph Niehoff, E. Gurler, wzeren, J. Kumar et al., *flav-io/flavio v0.28*, Apr., 2018. [10.5281/zenodo.1218732](#).
- [368] KTeV collaboration, A. Alavi-Harati et al., Search for the Decay  $K_L \rightarrow \pi^0 \mu^+ \mu^-$ , *Phys. Rev. Lett.* **84** (2000) 5279–5282, [[hep-ex/0001006](#)].
- [369] G. Isidori, C. Smith and R. Unterdorfer, The Rare decay  $K_L \rightarrow \pi^0 \mu^+ \mu^-$  within the SM, *Eur. Phys. J.* **C36** (2004) 57–66, [[hep-ph/0404127](#)].
- [370] LHCb collaboration, R. Aaij et al., Search for hidden-sector bosons in  $B^0 \rightarrow K^{*0} \mu^+ \mu^-$  decays, *Phys. Rev. Lett.* **115** (2015) 161802, [[1508.04094](#)].
- [371] ATLAS collaboration, Combination of the ATLAS, CMS and LHCb results on the  $B_{(s)}^0 \rightarrow \mu^+ \mu^-$  decays., tech. rep., CERN, Geneva, Aug, 2020.
- [372] M. Beneke, C. Bobeth and R. Szafron, Power-enhanced leading-logarithmic QED corrections to  $B_q \rightarrow \mu^+ \mu^-$ , *JHEP* **10** (2019) 232, [[1908.07011](#)].



- [373] LHCb collaboration, R. Aaij et al., *Search for  $D^{+}(s)$  to  $\pi^{+} \mu^{+} \mu^{-}$  and  $D^{+}(s)$  to  $\pi^{-} \mu^{+} \mu^{+}$  decays*, *Phys. Lett. B* **724** (2013) 203–212, [1304.6365].
- [374] BABAR collaboration, J. P. Lees et al., *Search for  $B^{+} \rightarrow K^{+} \tau^{+} \tau^{-}$  at the BaBar experiment*, *Phys. Rev. Lett.* **118** (2017) 031802, [1605.09637].
- [375] ARGUS collaboration, H. Albrecht et al., *A Search for lepton flavor violating decays  $\tau \rightarrow e\alpha, \tau \rightarrow \mu\alpha$* , *Z. Phys.* **C68** (1995) 25–28.
- [376] K. Hayasaka et al., *Search for Lepton Flavor Violating Tau Decays into Three Leptons with 719 Million Produced  $\tau^{+} \tau^{-}$  Pairs*, *Phys. Lett.* **B687** (2010) 139–143, [1001.3221].
- [377] BABAR collaboration, B. Aubert et al., *Searches for Lepton Flavor Violation in the Decays  $\tau^{\pm} \rightarrow e^{\pm} \gamma$  and  $\tau^{\pm} \rightarrow \mu^{\pm} \gamma$* , *Phys. Rev. Lett.* **104** (2010) 021802, [0908.2381].
- [378] D. Binosi and L. Theussl, *JaxoDraw: A Graphical user interface for drawing Feynman diagrams*, *Comput. Phys. Commun.* **161** (2004) 76–86, [hep-ph/0309015].
- [379] D. Binosi, J. Collins, C. Kaufhold and L. Theussl, *JaxoDraw: A Graphical user interface for drawing Feynman diagrams. Version 2.0 release notes*, *Comput. Phys. Commun.* **180** (2009) 1709–1715, [0811.4113].
- [380] R. Mertig, M. Bohm and A. Denner, *FEYN CALC: Computer algebraic calculation of Feynman amplitudes*, *Comput. Phys. Commun.* **64** (1991) 345–359.
- [381] V. Shtabovenko, R. Mertig and F. Orellana, *New Developments in FeynCalc 9.0*, *Comput. Phys. Commun.* **207** (2016) 432–444, [1601.01167].
- [382] V. Shtabovenko, R. Mertig and F. Orellana, *FeynCalc 9.3: New features and improvements*, *Comput. Phys. Commun.* **256** (2020) 107478, [2001.04407].
- [383] P. Maierhöfer, J. Usovitsch and P. Uwer, *Kira—A Feynman integral reduction program*, *Comput. Phys. Commun.* **230** (2018) 99–112, [1705.05610].
- [384] A. V. Smirnov, *Algorithm FIRE – Feynman Integral REDuction*, *JHEP* **10** (2008) 107, [0807.3243].
- [385] A. V. Smirnov and V. A. Smirnov, *FIRE4, LiteRed and accompanying tools to solve integration by parts relations*, *Comput. Phys. Commun.* **184** (2013) 2820–2827, [1302.5885].
- [386] A. V. Smirnov, *FIRE5: a C++ implementation of Feynman Integral REDuction*, *Comput. Phys. Commun.* **189** (2015) 182–191, [1408.2372].
- [387] A. V. Smirnov and F. S. Chuharev, *FIRE6: Feynman Integral REDuction with Modular Arithmetic*, *Comput. Phys. Commun.* **247** (2020) 106877, [1901.07808].
- [388] K. G. Chetyrkin, J. H. Kuhn and M. Steinhauser, *RunDec: A Mathematica package for running and decoupling of the strong coupling and quark masses*, *Comput. Phys. Commun.* **133** (2000) 43–65, [hep-ph/0004189].







## PUBLICATIONS

---

- [1] Z. L. Liu, M. Neubert, M. Schnubel and X. Wang, *Factorization at Next-to-Leading Power and Endpoint Divergences in  $gg \rightarrow h$  Production*, [2212.10447].
- [2] E. Goudzovski et al., *New Physics Searches at Kaon and Hyperon Factories*, [2201.07805].
- [3] Z. L. Liu, M. Neubert, M. Schnubel and X. Wang, *Radiative quark jet function with an external gluon*, *JHEP* **02** (2022) 075, [2112.00018].
- [4] M. Bauer, M. Neubert, S. Renner, M. Schnubel and A. Thamm, *Flavor probes of axion-like particles*, *JHEP* **09** (2022) 056, [2110.10698].
- [5] M. Schnubel, *The two-loop radiative gluon jet function for  $gg \rightarrow h$  via a light quark loop*, *SciPost Phys. Proc.* **7** (2022) 039, [2110.05322].
- [6] M. Bauer, M. Neubert, S. Renner, M. Schnubel and A. Thamm, *Consistent Treatment of Axions in the Weak Chiral Lagrangian*, *Phys. Rev. Lett.* **127** (2021) 081803, [2102.13112].
- [7] M. Bauer, M. Neubert, S. Renner, M. Schnubel and A. Thamm, *The Low-Energy Effective Theory of Axions and ALPs*, *JHEP* **04** (2021) 063, [2012.12272].
- [8] M. Bauer, M. Neubert, S. Renner, M. Schnubel and A. Thamm, *Axionlike Particles, Lepton-Flavor Violation, and a New Explanation of  $a_\mu$  and  $a_e$* , *Phys. Rev. Lett.* **124** (2020) 211803, [1908.00008].



## Colophon

This document was authored using TeXstudio<sup>1</sup> and typeset based on a modified version of the La Trobe PhD Thesis Template<sup>2</sup>, which itself is a customisation of the classicthesis<sup>3</sup> L<sup>A</sup>T<sub>E</sub>X template. Feynman diagrams were drawn with JaxoDraw<sup>4</sup> [378,379]. The computations were partially performed using Mathematica<sup>5</sup>. Important Mathematica packages and tools include MaTeX<sup>6</sup>, FeynCalc<sup>7</sup> [380–382], Kira<sup>8</sup> [383], FIRE and LiteRed<sup>9</sup> [384–387] and RunDec<sup>10</sup> [388].

- 
- 1 <https://www.texstudio.org>
  - 2 <https://github.com/bashimao/ltu-thesis>
  - 3 <https://bitbucket.org/amiede/classicthesis>
  - 4 <https://jaxodraw.sourceforge.io/>
  - 5 <https://www.wolfram.com/mathematica/>
  - 6 <http://szhorvat.net/pelican/latex-typesetting-in-mathematica.html>
  - 7 <https://feyncalc.github.io/>
  - 8 <https://gitlab.com/kira-pyred/kira>
  - 9 <https://www.ttp.kit.edu/~asmirnov/FIRE.htm>
  - 10 <http://sfb-tr9.ttp.kit.edu/software/html/rundec.html>